

# Comparison and discrimination of energetic materials via multiple analytical techniques and chemometrics

by

Roy Osamu Yutaka Lehmann

Thesis

Submitted to Flinders University for the degree of

**Doctor of Philosophy (Chemistry)** 

College of Science and Engineering

January 2021

# Contents

Contents	l
Figures	v
Tables	xiii
Equations	xvi
Abbreviations	xvii
Summary	xxi
Declaration	xxiii
Acknowledgements	xxiv
1. Introduction	1
1.1 Intelligence	2
1.2 Chemometrics	4
1.3 Energetic Materials	7
1.3.1 Urea Nitrate/ Uronium Nitrate (UN)	9
1.3.2 Ammonium Nitrate (AN)	10
1.3.3 1,3,5-Trinitro-1,3,5-triazacyclohexane (RDX)	12
1.3.4 1,3,5,7-Tetranitro-1,3,5,7-tetraazacyclooctane (HMX)	15
1.3.5 Erythritol Tetranitrate (ETN)	16
1.3.6 Potassium Chlorate (KClO <sub>3</sub> )	17
1.4 Analytical Techniques	20
1.4.1 Isotope Ratio Mass Spectrometry (IR-MS)	20
1.4.3 Inductively Coupled Plasma Mass Spectrometry (ICP-MS)	24
1.4.4 Raman Spectroscopy (Raman)	27

	1.4.5 Infrared (IR) Spectroscopy	29
	1.4.6 Terahertz/Far-Infrared Spectroscopy (THz/Far-IR)	30
2.	Method Development	32
	2.1 Synthesis	32
	2.1.1 Potassium Chlorate (KClO <sub>3</sub> )	32
	2.1.2 Erythritol Tetranitrate (ETN)	40
	2.2 Analytical Techniques	42
	2.2.1 Isotope Ratio Mass Spectroscopy (IR-MS)	42
	2.2.2 Inductively Coupled Plasma Mass Spectrometry (ICP-MS)	43
	2.2.3 Infrared Spectroscopy (IR)	49
	2.2.4 Raman Spectroscopy (Raman)	51
	2.2.5 Terahertz/Far-Infrared Spectroscopy (THz/Far-IR)	52
3.	Initial Development of Data Analysis and Fusion Methodology	55
	3.1 Background	55
	3.2 IR-MS Data of AN and CAN Samples	55
	3.3 ICP-MS Data of AN and CAN Samples	56
	3.4 Chemometric Analysis of AN/CAN Datasets	57
	3.1 Exploratory Multivariate Data Analysis of Raw Data	57
	3.2 Data Analysis Following Removal of Outliers in Raw Data	70
	3.3 Analysis of Logarithmically Transformed Data	77
	3.4 Analysis after Logarithmic Transformation and Outlier Removal	83
	3.5 Conclusions	90
4.	Analysis of Potassium Chlorate Samples	91
	4.1 ICP-MS of Potassium Chlorate	91
	4.1.1 Exploratory Multivariate Analysis of ICP-MS Data	95

	4.1.2 Trace Element Profile Retention Using Electrochemical Synthesis	109
	4.1.3 Sample Digest Solution Aging Study	110
	4.2 IR Spectroscopy of Potassium Chlorate	113
	4.2.1 Exploratory Multivariate Analysis of FT-IR Data	120
	4.3 Raman Spectroscopy of Potassium Chlorate	142
	4.4 Combined IR and ICP-MS Data for Potassium Chlorate	148
	4.5 Conclusions	153
5.	Analysis of Erythritol Tetranitrate Samples	155
	5.1 IR-MS of ETN	155
	5.1.1 Carbon IR-MS Analysis	156
	5.1.2 Nitrogen IR-MS Analysis	157
	5.1.3 Combined IR-MS Analysis	159
	5.2 ICP-MS of ETN	160
	5.2.1 Exploratory Multivariate Data Analysis	162
	5.3 IR Spectrometry of ETN Samples	173
	5.3.1 Exploratory Multivariate Data Analysis	176
	5.4 Raman Spectroscopy of ETN	181
	5.5 Combined IR-MS and ICP-MS data for ETN	183
	5.6 Chapter Conclusions	188
6.	THz/Far-IR Spectroscopic Analysis of Explosives	190
	6.1 Analysis of Pelletised Explosives	190
	6.2 Analysis of Samples Through Packaging Materials	194
	6.3 ATR THz/Far-IR Spectroscopy	197
	6.4 Full Range Infrared Spectra	199
	6.5. Chanter Conclusions	201

7.	Conclusions and Future Directions	203
8.	References	206

# Figures

Figure 1.1: A) PCA data treatment. B) LDA data treatment	5
Figure 1.2: Dendrogram of 9 samples showing 2 distinct clusters and samples with close relation	
Figure 1.3: Urea nitrate chemical structure	
Figure 1.4: Reaction scheme for urea nitrate production from urea and nitric acid	9
Figure 1.5: Ammonium nitrate chemical structure	11
Figure 1.6: Reaction Scheme for Ammonium nitrate production from ammonia and nitric acid.	11
Figure 1.7: RDX chemical structure	13
Figure 1.8: Chemical structure of HMX	15
Figure 1.9: Chemical structure of erythritol tetranitrate	16
Figure 1.10: Reaction Scheme for ETN production from erythritol with either potassium nitronitric acid with sulfuric acid.	
Figure 1.11: Chemical structure of potassium chlorate.	18
Figure 1.12: Schematic diagram of the separation and collection of ions within a magnetic field	d. <sup>92</sup> 22
Figure 1.13: Schematic of a general sample introduction device	24
Figure 1.14: Thermo Scientific FirstDefender Portable Handheld Raman Spectrometer. 106	28
Figure 2.1: Spectra comparison between commercial KClO <sub>3</sub> (blue) to LITE salt precursor KClO <sub>3</sub> (g	
Figure 2.2: Spectra comparison between successful pool chlorine $KClO_3$ (blue) to a partially successful green)	
Figure 2.3: Schematic of the basic electrochemical cell constructed for the synthesis of pota	assium
chlorate from sodium chloride solution (left) and DC power supply used (right)	37
Figure 2.4: Filtered solution post electrolysis	37
Figure 2.5: Final filtered product potassium chlorate	38

Figure 2.6: Schematic of the Perkin Elmer NexION 350D	43
Figure 2.7: An example of significant matrix effects within a batch (left) and of accepta effects (right)	
Figure 3.1: IR-MS data plotted as carbon delta values vs nitrogen delta values	56
Figure 3.2: Example of ICP-MS data depicted in the form of radar plots for discriminatin samples.	_
Figure 3.3: Scree plot for the raw data PCA	60
Figure 3.4: Bar chart of raw data for elements contributing to PC1-7. Red boxes highlight samples	_
Figure 3.5: PC1/PC2 score plot for all samples.	67
Figure 3.6: PC2/PC3 score plot for all samples.	68
Figure 3.7: PC1/PC3 score plot for all samples.	68
Figure 3.8: PC1/PC2 score plot after outlier omission	69
Figure 3.9: PC2/PC3 score plot after outlier omission	69
Figure 3.10: PC1/PC3 score plot after outlier omission	70
Figure 3.11: Scree plot for the PCA after outlier removal	71
Figure 3.12: PC1/PC2 score plot for all samples.	74
Figure 3.13: PC1/PC3 score plot for all samples.	75
Figure 3.14: PC2/PC3 score plot for all samples.	76
Figure 3.15: Scree plot for PCA of log transformed data	78
Figure 3.16: Coefficient/loading breakdown for the first 7 PCs	80
Figure 3.17: PC2/PC1 score plot for all samples after logarithmic transformation	
Figure 3.18: PC3/PC1 score plot for all samples after logarithmic transformation	
Figure 3.19: PC3/PC2 score plot for all samples after logarithmic transformation	
Figure 3.20: Scree plot for the log transformed data set PCA	84

Figure 3.21: Score plot of PC2 vs PC1 for log transformed ICP-MS data	87
Figure 3.22: Score plot of PC3 vs PC1 for log transformed ICP-MS data	87
Figure 3.23: Score plot of PC3 vs PC2 for log transformed ICP-MS data	88
Figure 3.24: Bar chart for Na, Mg, Al, Ca and Pb ICP-MS analysis of AN.	89
Figure 4.1: Resultant dendrogram from the hierarchical cluster analysis of potassium chlorate data.	
Figure 4.2: Scree plot for the PCA of KClO <sub>3</sub> ICP-MS dataset	98
Figure 4.3: Score plot of PC1 from the PCA of ICP-MS data for $KClO_3$ samples and precursors.	101
Figure 4.4: Score plot of PC2 from the PCA of ICP-MS data for KClO₃ samples and precursors.	101
Figure 4.5: Score plot of PC3 from the PCA of ICP-MS data for $KClO_3$ samples and precursors.	102
Figure 4.6: Bar charts for the ICP-MS analysis of A) magnesium, B) aluminium and C) calcium of the KClO3 samples and precursors.	
Figure 4.7: Bar chart for the ICP-MS analysis of iron content for KClO₃ samples and precursors	s106
Figure 4.8: PC1/PC2 score plot for KClO₃ samples and precursors	107
Figure 4.9: PC1/PC3 score plot for KClO₃ samples and precursors	108
Figure 4.10: IR spectrum of potassium chlorate sample DSTG1.	113
Figure 4.11: Raw IR spectra of all potassium chlorate samples.	115
Figure 4.12: IR spectra of all potassium chlorate samples normalised to the major peak at 93	
Figure 4.13: IR spectrum of cyanuric acid	117
Figure 4.14: IR spectrum of potassium chlorate made using Sigma-Aldrich calcium hypochlorhydrochloric acid	
Figure 4.15: IR spectrum of isolated insoluble material from calcium hypochlorite solution	119
Figure 4.16: IR spectrum of prepared calcium hydroxide.	119
Figure 4.17: IR spectra of KClO <sub>3</sub> samples after initial pre-processing of data	122

Figure 4.18: Resultant dendrogram from the hierarchical cluster analysis of potassium chlorate IF spectra124
Figure 4.19: Scree plot for the PCA of pre-processed KClO <sub>3</sub> IR data125
Figure 4.20: Spectrum loadings for A) PC1, B) PC2, C) PC3 and D) PC4 of the KClO $_3$ FT-IR dataset127
Figure 4.21: Loadings breakdown for first 4 PCs (20% offset between each) highlighting the focus
Figure 4.22: One dimensional score plots for A) PC1, B) PC2, C) PC3 and D) PC4 of the normalised $KClO_3$ FT-IR dataset
Figure 4.23: Two-dimensional score plot of PC1/PC2 of the normalised KClO₃ FT-IR dataset131
Figure 4.24: Two-dimensional score plot of PC1/PC3 of the normalised KClO $_3$ FT-IR dataset132
Figure 4.25: Three-dimensional plot of PC1, PC2 and PC3 of the normalised KClO₃ FT-IR dataset133
Figure 4.26: Manual baseline correction base points marked on KClO3 1 spectrum
Figure 4.27: Spectra of KClO $_3$ samples after 6 base point baseline correction followed by normalisation to the major peak at 930 cm $^{-1}$ (ATR region removed).
Figure 4.28: Hierarchical cluster analysis of potassium chlorate IR spectra after 6-point baseline correction and normalisation.
Figure 4.29: Scree plot for the PCA of KClO₃ IR baseline corrected and normalised data137
Figure 4.30: Spectrum loadings for A) PC1, B) PC2, C) PC3 and D) PC4 of the KClO $_3$ FT-IR dataset afte baseline correction and normalisation
Figure 4.31: One dimensional score plots for A) PC1, B) PC2, C) PC3 and D) PC4 of the baseline corrected and normalised KClO $_3$ FT-IR dataset.
Figure 4.32: Two dimensional plot of PC1/PC2 of the baseline corrected and normalised KClO $_3$ FT-IF dataset
Figure 4.33: Raman spectrum of potassium chlorate sample DSTG1
Figure 4.34: Normalised Raman spectra for all KClO <sub>3</sub> samples (excluding poor quality spectra

Figure 4.35: Resultant dendrogram from the hierarchical cluster analysis of normalised potassiur
chlorate Raman spectra14
Figure 4.36: Scree plot for the PCA of normalised KClO $_3$ Raman data14
Figure 4.37: Spectrum loadings for A) PC1, B) PC2, C) PC3 and D) PC4 of the normalised KClO $_3$ Rama
dataset14
Figure 4.38: Score plots of A) PC2 vs PC1 and B) PC3 vs PC2 of normalised KClO₃ Raman dataset14
Figure 4.39: Score plot of PC1 for the combined raw FT-IR and log transformed ICP-MS datasets of
KClO <sub>3</sub> samples14
Figure 4.40: PC1 coefficient plot for the combined raw FTIR and log transformed ICP-MS datasets of
KClO₃ samples15
Figure 4.41: PC1 coefficient plot for the combined scaled FT-IR and log transformed ICP-MS dataset
of KClO <sub>3</sub> samples15
Figure 4.42: Score plot of PC1 for the combined scaled FT-IR and log transformed ICP-MS datasets of
KClO₃ samples15
Figure 4.43: PC2 coefficient plot for the combined scaled FT-IR and log transformed ICP-MS dataset
of KClO <sub>3</sub> samples15
Figure 4.44: Scree plot for the PCA of combined scaled FT-IR and log transformed ICP-MS datasets on the KClO3 samples
Figure 5.1: Carbon isotope ratios for all ETN samples and erythritol precursors
Figure 5.2: Nitrogen isotope ratio for all ETN samples and potassium nitrates
Figure 5.3: Mean carbon isotope ratio against mean nitrogen isotope ratio for all ETN samples15
Figure 5.4: Resultant dendrogram from the hierarchical cluster analysis of erythritol tetranitrate ICF
MS data16
Figure 5.5: Scree plot for the PCA of ETN ICP-MS dataset16
Figure 5.6: Score plot of PC1 from the PCA of ICP-MS data for ETN samples and precursors16
Figure 5.7: Score plot of PC2 from the PCA of ICP-MS data for ETN samples and precursors16

Figure 5.8: Bar charts for the ICP-MS analysis of A) calcium and B) potassium content for ETN samples and precursors
Figure 5.9: Bar charts for the ICP-MS analysis of A) strontium and B) magnesium content for ETN samples and precursors
Figure 5.10: Two-dimensional score plot of PC1 and PC2 for the PCA of ICP-MS data for ETN samples
Figure 5.11: ATR IR spectrum of ETN sample BCH1-25
Figure 5.12: Baseline corrected and normalised infrared spectra of all erythritol tetranitrate samples
Figure 5.13: Baseline corrected and normalised IR spectra of ETN samples with outlier sample and ATR region removed
Figure 5.14: Resultant dendrogram from the hierarchical cluster analysis of IR data from erythrito tetranitrate samples.
Figure 5.15: Comparative plotting of the pre-processed IR spectra of the most different ETN samples according to HCA
Figure 5.16: Scree plot for the PCA of the pre-processed ETN IR dataset178
Figure 5.17: Spectrum loadings for A) PC1 B) PC2 C) PC3 and D) PC4 for the pre-processed ETN IF dataset
Figure 5.18: One dimensional score plots for A) PC1 B) PC2 C) PC3 and D) PC4 for the pre-processed ETN IR dataset
Figure 5.19: Raman spectra of three ETN samples made via differing synthesis methods (offset for clarity) showing all peaks are common
Figure 5.20: Scree plot for the PCA of the combined IR-MS and ICP-MS dataset for ETN186
Figure 5.21: Two-dimensional score plot of PC1 and PC2 for the combined IR-MS and ICP-MS datase for ETN (with chemist identity tag)
Figure 5.22: Two-dimensional score plot of PC1 and PC2 for the combined IR-MS and ICP-MS datase for ETN (with synthesis method tag)

Figure 5.23: Two-dimensional score plot of PC1 and PC2 for the combined IR-MS and ICP-MS dataset
for ETN (with chemist and synthesis method tags)188
Figure 6.1: THz/Far-IR spectrum of a polyethylene pellet showing great transparency in the frequency range of 30-1000 cm <sup>-1</sup> 190
Figure 6.2: THz/Far-IR spectrum of a paraffin wax pellet showing great transparency in the frequency range of 30-1000 cm <sup>-1</sup> 191
Figure 6.3: THz/Far-IR spectrum of potassium chlorate (25% in PE) in the frequency range of 30-650 cm <sup>-1</sup>
Figure 6.4: THz/Far-IR spectrum of nitrourea (25% in PE) in the frequency range of 30-650 cm <sup>-1</sup> 192
Figure 6.5: THz/Far-IR spectrum of RDX (50% in PE) in the frequency range of 30-650 cm <sup>-1</sup> 193
Figure 6.6: THz/Far-IR spectrum of HMX (50% in PE) in the frequency range of 30-650 cm <sup>-1</sup> 193
Figure 6.7: THz/Far-IR spectrum of PETN (50% in PE) in the frequency range of 30-650 cm <sup>-1</sup> 193
Figure 6.8: THz/Far-IR spectrum of a red Zip-Lock bag between the frequency range of 30-650 cm <sup>-1</sup> showing very little absorbance and clear oscillation195
Figure 6.9: THz/Far-IR spectrum of an overhead projector slide between the frequency range of 30-650 cm <sup>-1</sup> showing strong absorbances at 380, 438 and 507 cm <sup>-1</sup> 195
Figure 6.10: THz/Far-IR spectrum of a Post-It note between the frequency range of 30-650 cm $^{-1}$ showing a sloping absorption, peaks at 104, 173 and 234 cm $^{-1}$ and saturation beyond 300 cm $^{-1}$ 196
Figure 6.11: THz/Far-IR spectra of a PETN sample, purple postage bag and a combination of the two with and without air between them196
Figure 6.12: ATR THz/Far-IR spectrum of KClO <sub>3</sub> (bleach precursor) in the frequency range of 0-650 cm <sup>-1</sup>
Figure 6.13: ATR THz/Far-IR spectrum of KClO $_3$ (pool chlorine precursor) in the frequency range of 0-650 cm $^{-1}$
Figure 6.14: ATR THz/Far-IR spectrum of PETN in the frequency range of 0-650 cm <sup>-1</sup> 198
Figure 6.15: ATR THz/Far-IR spectrum of HMX in the frequency range of 0-650 cm <sup>-1</sup> 198
Figure 6.16: ATR THz/Far-IR spectrum of RDX (Type I) in the frequency range of 0-650 cm <sup>-1</sup> 199

Figure 6.17: ATR THz/Far-IR spectrum of RDX (Type II) in the frequency range of 0-650 cm <sup>-1</sup>	199
Figure 6.18: Combined THz/Far-IR and FTIR ATR spectrum of KClO <sub>3</sub> (bleach precursor)	200
Figure 6.19: Combined THz/Far-IR and FTIR ATR spectrum of PETN	200
Figure 6.20: Combined THz/Far-IR and FTIR ATR spectrum of HMX.	200
Figure 6.21: Combined THz/Far-IR and FTIR ATR spectrum of RDX (type I)	201

# **Tables**

Table 1.1: Relative abundances of isotopes which may be analysed using IR-MS. <sup>88</sup>	21
Table 2.1: Sample matrix for KClO <sub>3</sub> samples made using the bleach method	39
Table 2.2: Sample matrix for KClO <sub>3</sub> samples made using the pool chlorine method	39
Table 2.3: Sample matrix for KClO₃ samples made using the electrolysis method	40
Table 2.4: Nitric acid precursors	41
Table 2.5: Sample matrix for ETN samples produced via the acetyl nitrate nitration method	41
Table 2.6: Sample matrix for ETN samples produced via the mixed acid nitration method	41
Table 2.7: Sample matrix for ETN samples produced via the nitrate salt nitration method	41
Table 2.8: Nexion ICP-MS tuning specifications	44
Table 2.9: Operating conditions for the ICP-MS instrument	44
Table 2.10: Sample introduction parameters for the peristaltic pump	45
Table 2.11: Results of preparing a blank in a randomly selected 15 mL vial showing its lack of suit	ability
for ultra-trace elemental analysis	45
Table 2.12: Range of elements selected for ICP-MS analysis for both KClO₃ and ETN samples	46
Table 3.1: Latent variable table	59
Table 3.2: Raw coefficient values to 1 decimal place	60
Table 3.3: Coefficient table colour coded to highlight major contributors	62
Table 3.4: Correlation coefficient raw table	65
Table 3.5: Correlation coefficient colour coded table	66
Table 3.6: Latent variable table.	71
Table 3.7: Coefficient table colour coded (figures included for magnitude)	72
Table 3.8: Correlation coefficient colour coded table for outlier removed data analysis	73
Table 3.9: Latent variable table.	78
Table 3.10: Coefficient table for the first 7 PCs	79

Table 3.11: Correlation coefficient colour coded table for log transformed raw data analysis81
Table 3.12: Latent variable table for the log transformed data set PCA84
Table 3.13: Coefficients for the log transformed data set PCA85
Table 3.14: Correlation coefficient colour coded86
Table 4.1: Typical quantification limits for elements analysed in the ICP-MS of potassium chlorate
Table 4.2: Example of calibration data for elements selected in the ICP-MS analysis of potassium
Table 4.3: Percent coefficient of variation analysis of random triplicates94
Table 4.4: Sample correlation to number identifiers in HCA dendrogram in Figure 4.197
Table 4.5: Variance retention table for the PCA of KClO $_3$ ICP-MS data98
Table 4.6: Coefficient table for the first eight PCs of potassium chlorate ICP-MS data99
Table 4.7: Correlation coefficients for the PCA of potassium chlorate ICP-MS data100
Table 4.8: ICP-MS data for potassium chlorate samples produced via the electrolysis method109
Table 4.9: Change (in percentage) of ICP-MS results for KClO₃ digestion solutions stored for 9 months
Table 4.10: Sample correlation to number identifiers in HCA dendrogram123
Table 4.11: Variance retention table125
Table 4.12: Loading factors for principal components 1-4
Table 4.13: Manual baseline correction base points selection
Table 4.14: Sample correlation to number identifiers in HCA dendrogram136
Table 4.15: Variance retention table137
Table 4.16: Sample correlation to number identifiers in HCA dendrogram in Figure 4.33145
Table 4.17: Variance retention of the PCA of normalised KClO $_3$ Raman data146
Table 4.18: Variance retention table for the PCA of combined scaled FT-IR and log transformed ICP  MS datasets of KCIO <sub>3</sub> samples

Table 5.1: Typical quantification limits for elements analysed in the ICP-MS of erythritol tetranitrate
samples
Table 5.2: Example of calibration data for elements selected in the ICP-MS analysis of potassium
chlorate160
Table 5.3: Percent coefficient of variation analysis of random triplicates161
Table 5.4: Sample correlation to number identifiers in HCA dendrogram in Figure 5.4162
Table 5.5: Variance retention table for the PCA of ETN ICP-MS dataset164
Table 5.6: Coefficient table for the first 8 PCs of the ETN ICP-MS dataset165
Table 5.7: Correlation coefficients for the PCA of the ETN ICP-MS dataset165
Table 5.8: Summary of variables for the high and low PC1 score clusters of ETN samples in Figure 5.6.
Table 5.9: Polynomial baseline correction points for ETN FT-IR spectra174
Table 5.10: Sample correlation to number identifiers in HCA dendrogram176
Table 5.11: Variance retention table for the PCA of the pre-processed ETN IR dataset178
Table 5.12: Coefficient table of the first 4 PCs for the direct combination of the ETN IR-MS and ICP-
MS datasets
Table 5.13: Coefficient table of the first 6 PCs for the log transformed combined ETN IR-MS and ICP-
MS datasets184
Table 5.14: Coefficient table of the first 5 PCs for the combination of the ETN IR-MS (scaled) and log
transformed ICP-MS datasets
Table 6.1: Summary of THz/Far-IR absorbance results for various materials194

# **Equations**

Equation 1.1: Reaction equation for the Schiessler-Ross method for manufacture of RDX13
Equation 1.2: Woolwich method for the production of RDX
Equation 1.3: Bachmann method for the production of RDX
Equation 1.4: Reaction equation of overall Liebig process for the production of $KClO_3$ 18
Equation 1.5: Reaction equation for the disproportionation stage of KClO $_3$ synthesis from household bleach
Equation 1.6: Reaction equation for the metathesis stage of KClO $_3$ synthesis from household bleach
Equation 1.7: Reaction equation for the disproportionation stage of KClO $_3$ synthesis from poor chlorine
Equation 1.8: Reaction equation for the metathesis stage of KClO $_3$ synthesis from pool chlorine19
Equation 1.9: Reaction equation for the electrolysis stage of KClO $_3$ synthesis from sodium chloride
Equation 1.10: Reaction equation for the metathesis stage of KClO $_3$ synthesis from sodium chloride
Equation 1.11: Reaction Equation for the Electrolytic synthesis of KClO <sub>3</sub> directly from potassium chloride
Equation 1.12: Equation for the calculation of isotope ratio values23
Equation 1.13: Equation for the calculation of delta values23
Equation 5.1: Mixed acid nitration of erythritol to produce ETN155
Equation 5.2: Acetyl nitrate nitration of erythritol to produce ETN155
Equation 5.3: Nitrate salt (potassium/ammonium/calcium nitrate) nitration of erythritol to produce

# **Abbreviations**

%CV	Percent Coefficient of Variation
%RSD	Percent Relative Standard Deviation
(aq)	Aqueous Phase
(1)	Liquid Phase
(s)	Solid Phase
Ac	Acetyl
Ag	Silver
Al	Aluminium
AN	Ammonium Nitrate
ANFO	Ammonium Nitrate Fuel Oil
ANSTO	Australian Nuclear Science and Technology Organisation
Ar	Argon
As	Arsenic
ATR	Attenuated Total Reflectance
AU	Arbitrary Units
В	Boron
Ва	Barium
Ве	Beryllium
С	Carbon
Ca	Calcium
CAN	Calcium Ammonium Nitrate
Cd	Cadmium
CE	Capillary Electrophoresis
Ce	Cerium
CEEM	Centre of Expertise in Energetic Materials (Flinders University and DST Group)
CF-IR-MS	Continuous Flow Isotope Ratio Mass Spectrometry
C-IR-MS	Carbon Isotope Ratio Mass Spectrometry
Cl	Chlorine
cm <sup>-1</sup>	Wavenumbers
Со	Cobalt
COAG	Council of Australian Governments
cps	Counts per Second
Cr	Chromium
Cu	Copper
CV	Coefficient of Variation

DC	Direct Current	
DST Group	Defence Science and Technology Group (Part of the Australia's Department of Defence)	
DPT	Dinitropentamethylenetetramine	
e <sup>-</sup>	Electron	
EA	Elemental Analyser	
EM(s)	Energetic Material(s)	
ETN	Erythritol Tetranitrate	
eV	Electron Volts	
Far-IR	Far-Infrared	
Fe	Iron	
FIR-MS	International Forensic Isotope Ratio Mass Spectrometry Network	
FT-IR	Fourier-Transform Infrared Spectroscopy	
g	Grams	
GC-IR-MS	Gas Chromatography Isotope Ratio Mass Spectrometry	
GC-MS	Gas Chromatography Mass Spectrometry	
Ge	Germanium	
GHz	Gigahertz	
GRNN	Generalised Regression Neural Network	
Н	Hydrogen	
HCA	Hierarchical Cluster Analysis	
Не	Helium	
HME(s)	Home Made Explosive(s)	
HMTD	Hexamethylene Triperoxide Diamine	
HMX	1,3,5,7-Tetranitro-1,3,5,7-tetraazacyclooctane	
HUMINT	Human Intelligence	
I.D.	Identification	
IC	Ion Chromatography	
ICP-MS	Inductively Coupled Plasma Mass Spectrometry	
IED(s)	Improvised Explosive Device(s)	
IR	Infrared Spectroscopy	
IR-MS	Isotope Ratio Mass Spectrometry	
K (element)	Potassium	
K (temperature)	Kelvin	
KCIO <sub>3</sub>	Potassium Chlorate	
KED	Kinetic Energy Discrimination	
kg	Kilogram	
LA-ICP-MS	Laser Ablation Inductively Coupled Plasma Mass Spectrometry	
Li	Lithium	

LOD Limit of	Detection
LOQ Limit of	Quantification
m/z Mass to	Charge Ratio
MASINT Measure	ement and Signature Intelligence
Mg Magnes	ium
mg Milligrar	n
mins Minutes	
Mn Mangan	ese
Mo Molybde	enum
N Nitroger	1
Na Sodium	
NaN Not a Nu	umber
Ni Nickel	
N-IR-MS Nitroger	Isotope Ratio Mass Spectrometry
NMR Nuclear	Magnetic Resonance Spectroscopy
NU Nitroure	ea
O Oxygen	
OSINT Open So	ource Intelligence
P Phospho	prus
Pb Lead	
Pb(N <sub>3</sub> ) <sub>2</sub> Lead Azi	de
PC(s) Principa	l Component(s)
PCA Principa	l Component Analysis
PETN Pentaer	ythritol Tetranitrate
PLS-DA Partial L	east Squares Discriminant Analysis
ppb Parts Pe	r Billion (μg/L)
ppm Parts Pe	r Million (mg/L)
ppt Parts Pe	r Trillion (ng/L)
Pt Platinun	1
R Karl Pea	rson's Coefficient of Correlation
RDX 1,3,5-Tri	nitro-1,3,5-triazacyclohexane
RF Radio Fr	equency
RSD Relative	Standard Deviation
Ru Rutheni	um
S Sulphur	
S&TI Scientifi	c and Technical Intelligence
Sb Antimor	ny
Sc Scandiu	m
Se Seleniur	n

Sr	Strontium
SSAN	Security Sensitive Ammonium Nitrate
STDDEV	Standard Deviation
TATP	Triacetone Triperoxide
TDS	Time Domain Spectroscopy
TECHINT	Technological Intelligence
THz	Terahertz
Ti	Titanium
TNT	2,4,6-Trinitrotoluene
U	Uranium
μg	Microgram
UK	United Kingdom
UN	United Nations
US/USA	United States of America
USGS	United States Geological Survey
UV	Ultraviolet
UV-Vis	Ultraviolet-Visible Spectroscopy
VPN	Virtual Private Network
XRD	X-Ray Diffraction
XRF	X-Ray Fluorescence
Υ	Yttrium
Zn	Zinc
Zr	Zirconium

## Summary

Improved methods for extracting intelligence linking one sample of energetic material to another or identifying the location and method of manufacture are important. By investigating several analytical techniques with chemometric analysis, this research aims to assist in developing methodologies which may provide indications of such linkages.

Samples were prepared utilising methods observed in clandestine manufacturing, to replicate real-world variability due to differing starting materials or manufacturing procedures. These samples were subjected to a wide range of analytical techniques to investigate characteristic signatures within improvised energetic materials. The techniques included isotope ratio mass spectrometry (IR-MS), inductively coupled plasma mass spectrometry (ICP-MS), Raman and infrared (IR) spectroscopy.

The spectrometric and spectroscopic data collected was analysed through chemometric means to accomplish two goals. Firstly, to establish the quality of data obtained through each analytical technique. Secondly, to enhance each dataset by combining them to increase the discriminatory power of the data analysis, thereby capturing the unique traits and chemical 'fingerprint' or profile of the material. Principal component analysis (PCA) was the primary method of analysis used, as it is an unsupervised analysis better suited for the real-world application of extracting intelligence from sample data where the identity is unknown.

Combining these goals through the exploratory multivariate data analysis, PCA, there is the potential to condense data and extract the maximum value from it. The relative contributions of analysis techniques were also assessed, leading to method optimisation. For example, every additional element selected for ICP-MS analysis adds a significant amount of time, cost, and resources in regard to sample analysis and method validation. Any additional element further complicates the multivariate analysis so the number of elements should be optimised for to save time or reduce cost.

Chemical profiles enable the comparison of newly and previously acquired sample data with high fidelity and a measure of confidence that samples, which may have been collected at different locations and times, have a common origin. This process can be applied to large databases where discrimination between samples is desired.

This research project investigated each of these aspects and the results confirm the ability for the chemometric analysis of spectrometric and spectroscopic datasets to yield discriminatory

information from both independent and combined datasets. The analysis also identifies where the discriminatory information comes from within each dataset. This allows a more targeted analysis and comparison of samples on a greatly reduced number of variables. Clear clustering of related samples was identified using an unsupervised multivariate analysis, rather than a supervised discriminatory analysis such as LDA, which would favour clustering. This is ideal in a real-world setting where the identities and relationships between samples are likely unknown prior to analysis.

## Declaration

## I certify that this thesis:

- 1. Does not incorporate without acknowledgement any material previously submitted for a degree or diploma in any university; and
- 2. To the best of my knowledge and belief, does not contain any material previously published or written by another person except where due reference is made in the text.

Roy Osamu Yutaka Lehmann

23/01/2020

## Acknowledgements

This research project was undertaken and funded by the partnership between the Defence Science and Technology Group (DST Group) and Flinders University. I would like to thank both parties for investing their time and funds in this project and as an extension, me. This partnership has enabled a great deal of learning and many experiences, from research to presenting results internationally.

I'd like to acknowledge all the people who have assisted me throughout the journey of conducting this PhD research. Firstly, my primary supervisors Associate Professor Stewart Walker and Dr David Armitt who have both provided me with as much of their time as I ask for and have assisted me whenever I encountered a serious hurdle. Secondly, all the people that were not required to assist as much as they did, including many individuals at DST Group (Phil, Mark, Ben H and Ben R) and Flinders University (Paul, Rachel and Alan).

Much of this research was undertaken at Flinders Analytical through the assistance and training provided by Dr Daniel Jardine and Jason Young. They have trained me well and though they left towards the end, they had taught me enough to carry on and now even provide technical assistance to the facility.

The understanding of the multivariate analysis utilised in this project was primarily self-taught however, Rachel Popelka-Filcoff and Pawel Skuza assisted my in answering any further questions I could not uncover the answers to myself.

The THz/Far-IR portion of this project was undertaken at the Australian Synchrotron THz/Far-IR beamline thanks to funding by Australian Nuclear Science and Technology Organisation (ANSTO) and in collaboration with the French-German Research Institute of St. Louis (represented by Bernd Fischer) and materials supplied by Victoria Police.

Finally, thank you to the members of the Walker research group and various others that I have met along the way who have imparted advice and knowledge. In particular; Jimmie Oxley, Arian van Asten and Sarah Benson who have all answered questions that helped guide my research over the course of the last 5 years with their wealth of knowledge.

## 1. Introduction

In today's digital age, information on almost any topic is accessible to the general population through the power of the Internet and the plethora of devices that can connect to it. This has allowed for the rapid progression of civilisation through the sharing of information at a previously unimaginable speed. Though this technological advancement has undoubtably been a net positive for humanity there are also negative aspects that are easy to identify but not so simple to mitigate or resolve.

An example of this is the transmission of potentially dangerous information on the topic of energetic materials which enables anyone with the desire for such knowledge to gather it without many, if any, barriers at all. The very real concern of such information falling into the wrong hands has been realised through the numerous terror attacks across the world as well as countless minor incidents involving hobbyists and other curious individuals. Much of this information is not only shared but also collaboratively developed through numerous users of web forums effectively developing and optimising methods for the production and use of energetic materials from commonly available materials. Though many are just curious and pose very little threat there is no stopping bad actors with nefarious intentions from participating in these open forums. This widely available information is complimented by online marketplaces such as eBay can be used as sources of starting materials, the equipment required to produce energetic materials and operational improvised explosive devices (IEDs).

One possible method of preventing the manufacture of explosive devices is through the restriction of access to such information and materials. Though in theory this would solve the issue, the implementation of such restrictions has been ineffective in most cases. Internet restrictions have been applied in certain countries around the world, the most notable case being China where the government has strong control over not only what the population has access to but can go so far as to suppress online discussions among citizens. Even in the case of China however, the use of IEDs has not been entirely eradicated. An example being on the 12 June 2016 where a man targeted Pudong International Airport, Shanghai, with homemade explosive devices.

In most democratic countries, however, Internet censorship is quite a contentious and divisive topic with many arguments surrounding protection but also censorship and restricting freedoms, particularly of speech. In 2012 a broad survey by The Internet Society of greater than 10,000 people from 20 countries were asked about their attitude towards the internet.<sup>3</sup> The results identified some

conflicting attitudes, with 71% of people agreeing that "censorship should exist in some form on the Internet" however 86% supported the stance that "freedom of expression should be guaranteed on the Internet". Even if stricter controls were to be implemented on users of the Internet, there are many ways to circumvent such efforts and neutralising the effectiveness of the controls.

One of the more popular methods to evade Internet censorship is the use of a virtual private network (VPN). According to GlobalWebIndex 30% of Internet users have used a VPN/proxy server in the last month.<sup>4</sup> A VPN provides a greater level of anonymity on the Internet by encrypting a user's data by "tunnelling" through a wide area network, in this case the Internet, effectively removing the physical location tag of the user.

With the limitations on Internet restrictions reducing the effectiveness of the strategy, another option is to restrict the materials required to produce HMEs and components for effective IEDs. This too has been implemented in the past, with many countries having lists of restricted and banned chemicals. However, this method is quite difficult to enforce as ill-intentioned groups and individuals find ways to smuggle the prohibited chemicals or find new methods to produce a different precursor or explosive with what is readily available. As an extreme example, in 2010 the Afghan government banned ammonium nitrate (AN) fertilisers due to its prevalent use in IEDs.<sup>5</sup> This ban was ineffective, however, due to the large stockpiles of AN already within the country and the lack of restrictions in neighbouring countries with shared land borders, making smuggling AN into the country a rudimentary and lucrative process.<sup>6,7</sup>

With neither the restriction on information or chemicals proving to be little more than a deterrent, this identifies the need for investigators to collect data from the scene of the crime and extract as much intelligence as possible from collected data.

## 1.1 Intelligence

Intelligence as defined by the United States Department of Defense<sup>8</sup> is: "the product resulting from the collection, processing, integration, evaluation, analysis, and interpretation of available information concerning foreign nations, hostile or potentially hostile forces or elements, or areas of actual or potential operations." The document also delves into the various methods of intelligence gathering and sources, including commonly utilised methods in police investigations and counter terrorism applications. Some of these include:

- Human intelligence (HUMINT): information collected and provided by human sources.
- Measurement and signature intelligence (MASINT): information from quantitative and qualitative analysis of physical phenomenon intrinsic to an object or event.
- Open source intelligence (OSINT): information derived from publicly available information.
- Scientific and technical intelligence (S&TI): product resulting from the collection, evaluation, analysis, and interpretation of foreign scientific and technical information that covers:
  - o Foreign developments in basic and applied research.
  - Scientific and technical characteristics, capabilities, and limitations of all foreign military systems, weapons, weapons systems, and material; the research and development related thereto; and the production methods employed for their manufacture.
- Technological intelligence (TECHINT): intelligence derived from the collection, processing, analysis and exploitation of data and information pertaining to foreign equipment and material.

In relation to the aims of this research project the primary types of intelligence being sought after are MASINT, S&TI and TECHINT: MASINT and S&TI through the forensic analysis of explosive materials via a range of analytical techniques including, infrared spectroscopy, Raman spectroscopy, isotope ratio mass spectrometry and inductively coupled plasma mass spectrometry; TECHINT through the chemometric analysis of collected data from the previously mentioned analytical techniques. This intelligence can then potentially be utilised to aid and assist criminal or terrorism investigations involving the use of explosives.

When an incident involving the use of homemade explosives (HMEs) is investigated it is primarily focused on two areas: associative evidence which tries to link an individual or group to the incident; and physical/chemical evidence which may be collected from the site of the incident. In the case of a one-off attack much of the physical/chemical evidence collected will be restricted to providing intelligence to link the IED to the suspect, for example, matching to evidence such as IED components (cabling, detonators, etc) or chemicals (same explosive material, precursor materials, etc) found at a suspect's property.

However, in the case of organised and coordinated attacks such as designated terrorist organisations or wartime conflicts there is a prolonged usage of IEDs. This opens the possibly that the materials used in one IED are potentially linked to another. Therefore, if an identifiable source of precursor chemicals can be linked to multiple IEDs there is a greater opportunity for data collection to yield potentially valuable intelligence. This may be in the form of impurities, common trace elements or stable isotope ratios of carbon/nitrogen/oxygen as previously explored in past research projects at Flinders University<sup>9,10</sup> and internationally<sup>11</sup>.

Though this is not a solution to preventing the use of such weapons or the manufacture of HMEs it would allow a greater understanding of the networks behind the attacks.

## 1.2 Chemometrics

Chemometrics has many definitions with slight variations. The Chemometrics Society defines<sup>12</sup> it as "The chemical discipline that uses mathematical and statistical methods to design or select optimal procedures and experiments, and to provide maximum chemical information by analysing chemical data." Chemometrics differs from traditional data analysis methods by interrogating the data as a collective multivariable dataset rather than analysing observations individually. This allows the development of a model to fit the data, contrasting the classical case where the data is investigated to test the validity of a theoretical model.

Advanced multivariate chemometric analysis could potentially be an integral component of forensic analysis as it is a powerful way of extracting the maximum amount of information from forensic chemical analysis techniques. This is an emerging field of study with research into multivariate analysis of individual analytical techniques and data fusion of data collected from spectroscopic and spectrometric analyses being undertaken. <sup>10,11,13</sup> For this application a technique specifically tailored to classification/clustering of samples is required and an added benefit would be the reduction of the dimensionality of the original dataset. Multivariate linear regression or multiple linear regression has this potential, however there are many different statistical approaches to enable such a result.

Three commonly discussed and utilised options are linear discriminant analysis (LDA), partial least squares discriminant analysis (PLS-DA) and principal component analysis (PCA). Whilst all very similar in outcome the process undertaken by each method is very different. The major difference is that LDA and PLS-DA are supervised methods, meaning sample identities are considered, whereas PCA is

an unsupervised method, meaning that no sample identification is considered. This alone makes PCA a strong choice as an unsupervised method of analysis that is well suited to an intelligence gathering application. PCA will investigate the variance in a multivariate dataset, enabling data exploration and dimensionality reduction through the transformation of the original data into linear orthogonal principal components to resolve variance, whereas LDA and PLS-DA investigate the variance between sample groups within a multivariate dataset. This unsupervised method allows an analysis to be entirely exploratory without any major restraints or restrictions, and in the case where sample identities can be entirely unknown this is the only option. A graphical representation of this distinction can be seen in Figure 1.1.

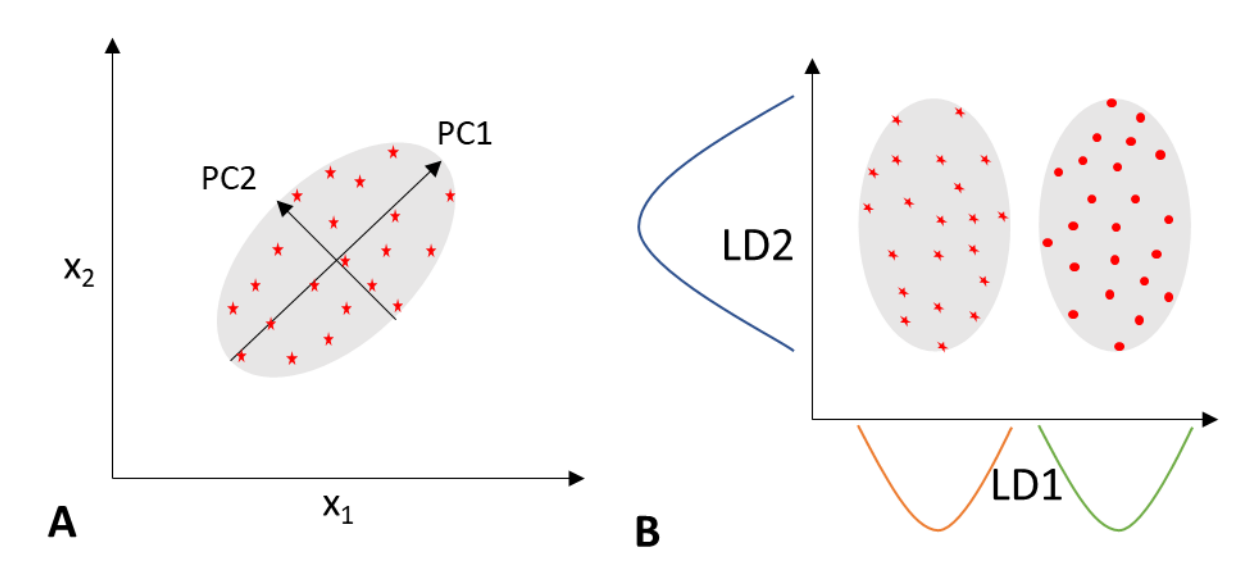


Figure 1.1: A) PCA data treatment. B) LDA data treatment.

As a result, the primary statistical method of analysis utilised in this research project will be principal component analysis (PCA). The data set is represented mathematically as an n x p matrix, where n is the number of samples and p is the number of variables. PCA is able to reduce this to a maximum n-1 or p principal components (PCs), depending on which is the lesser value. For example, if 10 samples were analysed by ICP-MS for 30 trace elements (10 x 30 matrix) this can be reduced to 9 PCs thus transforming the dataset into a  $10 \times 9$  matrix, effectively a third of the original data.

However, there are drawbacks to PCA. The most important of which is the effect data reduction has on the variance of the original data. As the data reduction is a key aspect of any PCA the end user must determine when an analysis has successfully compressed the data without losing vital, potentially discriminatory information. For example, if only 3 samples were analysed rather than the 10 in the previous example, the raw data consists of a 3 x 30 matrix and the PCA would reduce this

to 2 PCs, which in most cases cannot adequately represent the variance within the original dataset. This means that datasets with a small number of samples in comparison to the number of variables are not well suited for PCA analysis as the variance will not be well distributed.

Another important aspect of PCA are PC loadings as these identify the portion of the original dataset a PC represents. PCs themselves do not correspond directly to one variable but are a combination of multiple original variables and understanding this allows the analyst to determine where discriminatory data lies within a dataset. Continuing with the previous example of the 10 samples analysed for 30 trace elements, this analysis may conclude that for these 10 samples only 5 of the trace elements are required to discriminate the 10 samples from one another and that in analysing just those 5 elements 99.9% of the original variance is retained. In doing such an analysis the next time the analysis is done there would be no need for a full 30 elements to be measured but only 5. This greatly improves the efficiency of the chemical analysis, which is one of the core components of chemometrics.

As these multivariate analyses can be quite computationally demanding, a more basic overview of large datasets prior to analysis may be wise to determine if any discriminatory data is present. A well-suited technique to employ for this brief screening of a dataset is Hierarchical Cluster Analysis (HCA). This technique measures every data point to its closest neighbour and this is then displayed in the form of a dendrogram. This measurement can be done in multiple ways, however, for this project simple Euclidean distance is the selected metric. Euclidean distance is the length of a straight line in Euclidean space. A basic dendrogram is depicted in Figure 1.2 and shows two clear groupings (A and B) and also some closer relationships between individual samples within those groups such as A1/A2, A3/A4, B1/B2 and B3/B4. The vertical line length is the Euclidean distance between points and hence the shorter the length the more similar the sample. In the case of screening data this is an example of a dataset that would be well suited for PCA analysis to determine the variables leading to this separation. If on the other hand Euclidean distances between groupings is minimal this would be a distinct red flag of very little discriminatory data within the dataset.

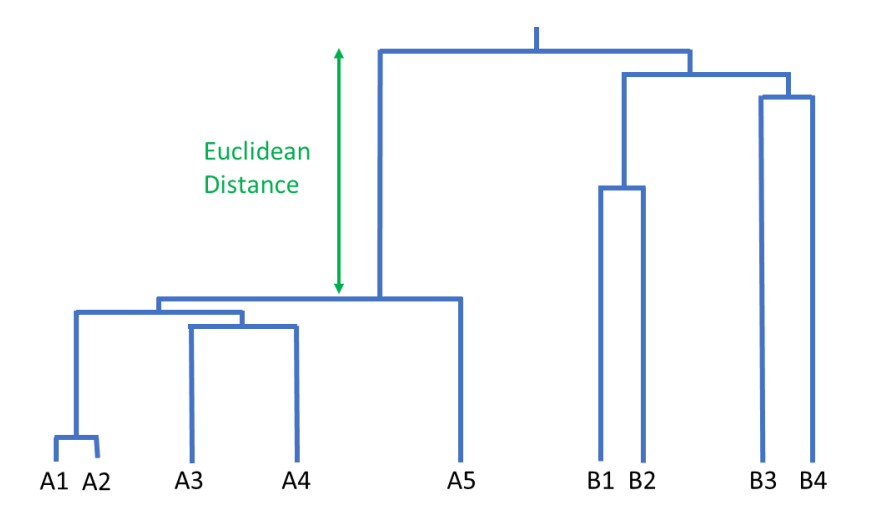


Figure 1.2: Dendrogram of 9 samples showing 2 distinct clusters and samples with close relationships.

The other benefit of undertaking an HCA is for the identification of significant outliers. Outliers can be identified in a dendrogram when the Euclidean distance between a datapoint or cluster of datapoints is far greater than the overall population. This will result in a compression of the dendrogram with only the outlier samples being distinguished as a grouping.

PCA too can identify outliers however, this is through a purely mathematical process rather than a simple graphical representation. This is done through the computation of either the Hotelling's T<sup>2</sup>-statistic or the Q-statistic. Both methods assume that the variance in the data follows a normal distribution. The difference between the two is that the T<sup>2</sup>-statistic measures the variation of each sample within the PCA model, whereas the Q-statistic measures the difference between a sample and its projection into the PCA model. Therefore, a sample with a larger T<sup>2</sup> indicates an outlier within the model and a larger Q indicates an outlier outside of the model.

## 1.3 Energetic Materials

Energetic materials (EMs) are compounds which store a large amount of chemical potential energy which may be released. EMs can then be categorised into a further three subcategories including explosives, pyrotechnics and propellants.

An explosive is a substance or mixture of substances that may be made to undergo a rapid chemical change without an external supply of oxygen with the liberation of large quantities of energy, generally accompanied by the evolution of hot gases or vapours.<sup>14</sup>

They may then be further categorised into primary and secondary explosives. Primary explosives are highly sensitive to heat, friction, impact and electrostatic discharge and will detonate or burn rapidly in very small quantities. These types of explosives are commonly used in the manufacture of detonators and are normally unimolecular explosives, which are compounds which require no additives to detonate. Examples of primary explosives are triacetone triperoxide (TATP) and lead azide ( $Pb(N_3)_2$ ).

Secondary explosives are much less sensitive and usually require the shockwave produced by a primary explosive in order to initiate a detonation. These types of explosives are used in military and commercial applications and some examples include 1,3,5-Trinitro-1,3,5-triazacyclohexane (RDX) and ammonium nitrate-fuel oil (ANFO). RDX is an example of a unimolecular explosive whereas ANFO is a fuel/oxidiser explosive involving the mixture of a fuel into the oxidiser in order to improve performance. These fuel/oxidiser explosives are commonly found in HMEs as they are easier to manufacture in large quantities.

The chemical energy previously mentioned within these compounds have two possible rapid energy release pathways, either deflagration or detonation. Deflagration is a relatively slow explosion, generating only subsonic pressure waves. This sort of explosion is usually produced by rapid chemical combustion reactions, for instance of gunpowder in a firearm, or fuel in an internal combustion engine.<sup>16</sup>

Detonation, however, is a much more instantaneous release of the chemical energy stored within the compound. In this case, rather than undergoing a combustion reaction the compound decomposes through a shock wave phenomenon. This shock wave causes the bulk of the explosive to decompose almost instantly releasing a large amount of heat and gas.<sup>17</sup> The fast rate of reaction and resulting rapid expansion of gases in conjunction with the shock wave itself produces the explosive effects.

The following review covers all energetic materials and ingredients that have been featured within this research project. Many are of interest as they are commonly featured in HMEs including: the fertiliser-based explosives urea nitrate and ammonium nitrate; erythritol tetranitrate and potassium chlorate. RDX and 1,3,5,7-Tetranitro-1,3,5,7-tetraazacyclooctane (HMX) are less commonly associated with HMEs as they are military grade high explosives. However, given their similar

molecular structure they were of interest in assessing the effectiveness of an emerging analytical method utilising THz/far-infrared spectroscopy.

## 1.3.1 Urea Nitrate/ Uronium Nitrate (UN)

#### 1.3.1.1 Background

Uronium nitrate (Figure 1.3), commonly referred to as urea nitrate (UN), is a fertiliser-based explosive. There have been several incidents where UN has been used in terrorist incidents across the world including those perpetrated by the Shining Path (South American terrorist cell). In the case of the Shining Path the use of urea nitrate became so prolific that the Peruvian government banned sales of urea. One high profile incident involving the use of UN was the 1993 World Trade Center bombing.

$$H_2N$$
  $O$   $OH$   $OH$   $OH$   $OH$   $OH$ 

Figure 1.3: Urea nitrate chemical structure.

#### 1.3.1.2 Production

Urea nitrate is a salt comprising of a nitrate anion and an uronium cation and takes the form of a white powder. The explosive is often found in improvised explosive devices (IEDs) and can be simply created by non-professionals with little to no specialised equipment via the simple combination of urea and nitric acid (Figure 1.4).<sup>20</sup>

$$H_2N$$
 $H_2N$ 
 $H_2N$ 

Figure 1.4: Reaction scheme for urea nitrate production from urea and nitric acid.

This synthesis may also involve the production of the nitric acid in situ from a nitrate salt (e.g., potassium nitrate) and a mineral acid (e.g., sulfuric acid).

#### 1.3.1.3 Forensic Analytical Techniques

Urea nitrate is an energetic material of high international interest as it has been used in illicit activities due to its simplicity when it comes to manufacturing and handling. Due to this many previous studies have been undertaken in order to be able to extract as much information out of the analytical techniques as possible for both pre and post-blast material. The techniques include isotope ratio mass spectrometry (IR-MS)<sup>10, 22</sup>, inductively coupled plasma mass spectrometry (ICP-MS)<sup>10</sup>, infrared spectroscopy (IR)<sup>10, 21</sup> Raman<sup>10,23</sup>, ultraviolet-visible spectroscopy (UV-Vis)<sup>23</sup>, thermal analysis<sup>17, 21</sup> and liquid chromatography mass spectroscopy (LC-MS)<sup>19</sup>.

Of these analytical techniques isotope ratio and inductively coupled plasma mass spectroscopy show potential discriminatory power between samples of like materials<sup>9,10</sup>. A major drawback of these analyses is that they do not chemically identify the material as they purely focus on isotope ratios and trace metal content. Therefore, techniques that provide material identification will be required and spectroscopic techniques are well suited for this application. Not only can they chemically identify materials but potentially identify additional impurities or additives contributing to the discrimination of samples of like material.

### 1.3.2 Ammonium Nitrate (AN)

#### 1.3.2.1 Background

Ammonium nitrate (Figure 1.5), much like urea nitrate, is common in cases involving the misuse of explosives such as terrorist attacks. Once again this is due to fertiliser-based explosives being quite easy to manufacture from readily available starting materials due to minimal security checks in some countries. An example of ammonium nitrate-based explosives being utilised as a key component of an HME is the 1995 Oklahoma City Bombing.<sup>24</sup> While ammonium nitrate can be an explosive in its pure form, it is more often mixed with fuels for greater sensitivity and reliability of detonation. An example of this is ammonium nitrate-fuel oil (ANFO) which in recent years has been found to be used in many malicious attacks.<sup>25</sup>

Figure 1.5: Ammonium nitrate chemical structure.

Though it is not feasible to completely restrict the usage of all AN purchased across the world, many countries have begun to monitor its purchase including Australia. The Council of Australian Governments (COAG) began this process in 2004 to restrict the widespread availability of AN that could potentially be used to create an explosive.<sup>26</sup> The class of AN to be restricted was termed security sensitive AN (SSAN) and encompasses any mixture containing greater than 45% AN.

#### 1.3.2.2 Production

AN is generally formed using the simple neutralisation of nitric acid with ammonia (Figure 1.6) resulting in an AN solution<sup>27</sup>.

Figure 1.6: Reaction Scheme for Ammonium nitrate production from ammonia and nitric acid.

An alternate source of AN is fertiliser-grade AN, generally purchased in solid form consisting of prills which may contain a wide range of additional minerals, metals and nutrients designed to feed plants or assist in slow release of fertiliser. This gives another avenue for forensic analysis through ICP-MS quantification of the trace metals and even the potential of spectroscopic techniques to obtain signals from the added nutrients.

Ammonium nitrate fuel oil (ANFO) is an explosive comprising of fertiliser-grade AN and a fuel. The AN can be in the form of a powder or prill and quite a number of fuels may be used, including sugars, starches, cellulose and diesel.<sup>28</sup> The prills can be used if small enough otherwise porous prills are manufactured in order to allow for the fuel to be well incorporated into the mixture which promotes the explosive capability of the mixture.<sup>29</sup>

Many other additives may also be used to improve the explosive properties of an AN explosive, each having a specific purpose and application. Aluminium powder is commonly added as it results in a much greater temperature of explosion, helping to increase the duration of vapour expansion and thereby its work capacity.<sup>30</sup> On the other hand other high explosives such as TNT or nitroglycerine may be added to sensitise the material rather than increase explosive performance.<sup>11</sup>

### 1.3.2.3 Forensic Analytical Techniques

The widespread misuse of AN has promoted the use of a wide range of analytical techniques for the forensic analysis of this material. AN, much like UN, can be effectively analysed via multiple techniques such as IR-MS<sup>10, 28, 31-35</sup>, ICP-MS<sup>10, 25</sup>, IR<sup>10</sup>, Raman<sup>10, 23, 30</sup>, UV-Vis<sup>23</sup> and laser induced breakdown spectroscopy (LIBS)<sup>36</sup>. The literature indicates that spectroscopic techniques can chemically identify the material analysed, however, they provide limited discrimination capabilities. Conversely, IR-MS and ICP-MS have powerful discriminating power however lack the ability to identify the material.

## 1.3.3 1,3,5-Trinitro-1,3,5-triazacyclohexane (RDX)

## 1.3.3.1 Background

1,3,5-Trinitro-1,3,5-triazacyclohexane (Figure 1.7) has been given various titles including cyclotrimethylenetrinitramine, hexogen and cyclonite; however, the acronym RDX is how it is most commonly known. The origin of this acronym is relatively unknown however two different possible explanations for this abbreviation is that it is an acronym of either Royal Demolition Explosive or Research Development Explosive where the second is more commonly quoted. It is mainly used in munitions as it is fairly stable and cheap to produce in comparison with other explosives with similar performance capabilities.

Figure 1.7: RDX chemical structure.

Though being made specifically for military application there have been cases of RDX or its formulations, including the plastic explosives Composition C-4 and Semtex, being stolen and/or misused, especially in terrorist activities. Some events include:

- The 2006 Mumbai train bombings<sup>37</sup>
- The 2008 Jaipur blasts<sup>38</sup>
- The 1999 Moscow blast<sup>39</sup>
- A plane attack in Russia in 2004<sup>40</sup>

#### 1.3.3.2 Production

There are three main methods of manufacturing RDX, with the Woolwich method being the most commonly used.<sup>41</sup> Firstly, however, the least commonly used method known as the Schiessler-Ross method will be discussed.

The Schiessler-Ross method reacts a 1:1 ratio of formaldehyde and ammonium nitrate in acetic anhydride as depicted below in Reaction Equation 1.1. Other methods are favoured over the Schiessler-Ross method in a commercial setting as it commonly utilises a catalyst which requires additional steps to be removed from the final product. For Clandestine synthesis however, this is a viable method as both formaldehyde and ammonium nitrate can be obtained.

$$3 CH_2O + 3 NH_4NO_3 \xrightarrow{Ac_2O} C_3H_6N_6O_6 + 6 H_2O$$

Equation 1.1: Reaction equation for the Schiessler-Ross method for manufacture of RDX.

The other methods of RDX production involve the nitration of hexamine and are known as the Woolwich and Bachmann methods.<sup>42</sup>

The most commonly chosen method for RDX specific manufacture is the Woolwich method as it produces less than 4% HMX impurity via Reaction Equation 1.2.

$$(CH_2)_6N_4 + 3 HNO_3 \xrightarrow{AcOH} C_3H_6N_6O_6 + 3 CH_2O + NH_3$$

Equation 1.2: Woolwich method for the production of RDX.

The final method known as the Bachmann process. It produces two moles of RDX for every mole of hexamine the final product has a larger HMX impurity percentage than that of the Woolwich method.

The Bachmann process was developed in the 1940s and builds on the Schiessler-Ross and Woolwich methods. In essence the Bachmann method forces the by-products of the Woolwich method to create an additional RDX molecule via the reaction with a surplus of nitric acid and ammonium nitrate. This second stage is, in actuality, the process undertaken in the Schiessler-Ross method, however, no catalyst is required as the activation energy of the second stage is overcome by the elevated temperature of the overall reaction.

$$(CH_2)_6N_4 + 4HNO_3 + 2NH_4NO_3 + 6Ac_2O \xrightarrow{AcOH, 75^0C} 2C_3H_6N_6O_6 + 12AcOH$$

Equation 1.3: Bachmann method for the production of RDX.

RDX is classified based on its HMX content, where RDX with less than 5% HMX is classed as Type I and is generally synthesised using the Woolwich method. Type II is synthesised using the Bachmann process and has a 4-17% HMX impurity and if desired can be recrystallised to reduce the amount of HMX to below 5% allowing it to be classed as Type I. This is undertaken to reduce the shock sensitivity of the RDX and to prevent deterioration through aging.<sup>43</sup>

#### 1.3.3.3 Forensic Analytical Techniques

Though clandestine RDX manufacture is not prevalent as it is not as easy to produce compared to a fertiliser-based explosive, there have been cases of material being stolen and misused as mentioned earlier. Therefore, there has been little interest in forensically analysing military explosives such as RDX other than to identify their presence in post-blast residues. Identification of RDX is possible through spectroscopic techniques such as IR<sup>44</sup>, UV-Vis<sup>44</sup>, Raman<sup>30,44,45</sup>. Techniques that have identified potential discriminatory power include gas chromatography coupled with IR-MS<sup>46,47</sup>, LIBS<sup>44</sup>, thermal analysis<sup>48</sup> and x-ray diffraction (XRD)<sup>49</sup>.

## 1.3.4 1,3,5,7-Tetranitro-1,3,5,7-tetraazacyclooctane (HMX)

## 1.3.4.1 Background

1,3,5,7-Tetranitro-1,3,5,7-tetraazacyclooctane (HMX, Figure 1.8)), much like RDX, has been referred to by a number of names including Her/His Majesty's Explosive, High Melting-point Explosive, and octogen. HMX has similar properties to RDX; even though its energetic performance is in fact greater than that of RDX it is much less commonly used as it is more sensitive and has a much greater cost of production.

Figure 1.8: Chemical structure of HMX.

### 1.3.4.2 Production

It is most commonly produced using the Bachmann method (refer to RDX section) with yields of up to 60%. <sup>41</sup> As HMX is typically a minor impurity a yield of greater than 50% is quite reasonable and is achievable through the manipulation of the reaction conditions, with the key being the temperature to be restricted to 45°C. This temperature requirement can be explained as a key intermediate is dinitropentamethylenetetramine (DPT), which decomposes at 50°C. Also, like RDX, HMX is graded into two categories, where Grade A HMX has less than 7% RDX impurity, while Grade B HMX requires less than 2% RDX.

### 1.3.4.3 Forensic Analytical Techniques

Though similar to RDX, HMX is mostly used for specific high-performance purposes. However, it is a co-product in the production of RDX and hence traces of HMX may be found in RDX samples to be forensically analysed. This ultimately means that literature relating to the forensic analysis of HMX alone is sparse, but it has been examined by Raman<sup>30</sup>, LIBS<sup>44</sup>, XRD<sup>49</sup> and ion chromatography (IC)<sup>50</sup>.

Though literature is lacking, the similar structure and properties to RDX should allow for the same methodologies employed to forensically analyse RDX to be applicable to HMX.

## 1.3.5 Erythritol Tetranitrate (ETN)

## 1.3.5.1 Background

ETN (Figure 1.9) is an explosive that was first created in 1849<sup>51</sup> and is closely related to pentaerythritol tetranitrate (PETN) and nitroglycerine which are commonly used in military and commercial applications. It is quite straightforward to prepare and performs comparatively to military explosives.<sup>52</sup> ETN is also quite sensitive and as a result there have been a number of incidents involving accidental initiation. ETN is a nitrate ester<sup>53,54</sup> and has a commercial application in the pharmaceutical industry where it is used as a vasodilator<sup>55,56</sup> for the treatment of high blood pressure.

Figure 1.9: Chemical structure of erythritol tetranitrate.

### 1.3.5.2 Production

The generally used synthesis of ETN involves the nitration of erythritol using an acid solution made up of nitric and sulfuric acid. The alternative involves the use of a nitrate salt (i.e. ammonium nitrate or potassium nitrate) and sulfuric acid and there is literature showing the success of both methods.<sup>57</sup> The general reaction for both cases is summarised in Figure 1.10.

HO OH 
$$KNO_3/$$
  $O_2NO$   $ONO_2$   $HNO_3$   $ONO_2$   $ONO_2$   $ONO_2$ 

Figure 1.10: Reaction Scheme for ETN production from erythritol with either potassium nitrate or nitric acid with sulfuric acid.

## 1.3.5.3 Forensic Analytical Techniques

As the mass production of erythritol has increased due to its use as a sugar supplement its use for the production of HMEs has emerged. The material is also of interest due to its properties surrounding melt casting as this is highly desirable as it enables many more uses of the material.<sup>58</sup> As a result, studies involving the characterisation of the material have been increasing. This includes the study of its general properties such as thermal behaviour<sup>57,58-61</sup>, eutectics<sup>62</sup>, decomposition<sup>60,61,63</sup>, explosive performance<sup>58,64</sup> and other basic physical properties<sup>57,58,65</sup> such as melting point, solubility, structure, etc.

Studies surrounding the forensic analysis and analytical characterisation of ETN have also been undertaken with its discovery in the HME setting. This includes studies utilising calorimetry<sup>66,67</sup>, Raman<sup>67,68</sup> and infrared<sup>67-70</sup> spectroscopy, gas chromatography mass spectrometry (GC-MS)<sup>57,71</sup>, LC-MS<sup>57</sup>, XRD<sup>66</sup>, nuclear magnetic resonance spectroscopy (NMR)<sup>67</sup> and various mass spectrometry methods<sup>67,72-74</sup>. Many of these studies identify the ability to detect and identify ETN however, they do not investigate the ability to provenance or discriminate between samples of like material.

## 1.3.6 Potassium Chlorate (KClO₃)

#### 1.3.6.1 Background

Potassium chlorate (KClO<sub>3</sub>, Figure 1.11) is a strong oxidising agent and once mixed with a fuel, can form an effective explosive composition. The high level of oxygen in the molecule has made it interesting to propellant designers and has been combined on a molecular level with RDX to design a new propellant.<sup>75</sup>

Figure 1.11: Chemical structure of potassium chlorate.

Previously discussed in this review have been fertiliser-based explosives such as ammonium nitrate which have been consistently used in terrorist activities. However, in some areas of the world potassium chlorate is more readily available and therefore features in HMEs. This gives a reason for KClO<sub>3</sub> to be added to the list of energetic materials of interest to counter terrorism experts. Some of the major events involving the use of KClO<sub>3</sub> include the 2004 car bombing of the Australian Embassy in Jakarta and the 2002 Bali car bombing.<sup>76</sup>

#### 1.3.6.2 Production

Industry manufacture of KClO<sub>3</sub> utilises the Liebig process which is commonly used in the preparation of the majority of chlorates.<sup>77</sup> In the case of KClO<sub>3</sub> the Liebig process involves adding chlorine into a calcium hydroxide solution then the final addition of potassium chloride as depicted in Reaction Equation 1.4 below.

$$6Ca(OH)_2(aq) + 6Cl_2(g) + 2KCl(aq) \rightarrow 2KClO_3(s) + 6CaCl_2(aq) + 6H_2O(l)$$

Equation 1.4: Reaction equation of overall Liebig process for the production of KCIO<sub>3</sub>.

Though this process is quite straightforward, the chemicals are not highly accessible so other clandestine methods have been developed and spread through the Internet.<sup>78</sup> The majority of clandestine KClO<sub>3</sub> is made using chlorine bleach and the salt substitute potassium chloride. This method involves boiling the bleach (sodium hypochlorite, NaClO) until crystals form, effectively forming sodium chloride and sodium chlorate. The next stage is to simply add a saturated solution of potassium chloride which will cause a metathesis reaction and the produced KClO<sub>3</sub> precipitates out. This process can also be adjusted to utilise pool chlorine rather than household bleach so long as the pool chlorine contains calcium hypochlorite (Ca(ClO)<sub>2</sub>). The overall reaction schemes for these methods are summarised in the reaction equations below.

$$3NaClO(aq) \rightarrow 2NaCl(aq) + NaClO_3(aq)$$

Equation 1.5: Reaction equation for the disproportionation stage of KClO<sub>3</sub> synthesis from household bleach.

$$NaClO_3(aq) + KCl(aq) \rightarrow NaCl(aq) + KClO_3(s)$$

Equation 1.6: Reaction equation for the metathesis stage of KCIO<sub>3</sub> synthesis from household bleach.

$$3Ca(ClO)_2(aq) \rightarrow 2CaCl_2(aq) + Ca(ClO_3)_2(aq)$$

Equation 1.7: Reaction equation for the disproportionation stage of KClO<sub>3</sub> synthesis from pool chlorine.

$$Ca(ClO_3)_2(aq) + 2KCl(aq) \rightarrow CaCl_2(aq) + 2KClO_3(s)$$

Equation 1.8: Reaction equation for the metathesis stage of KClO<sub>3</sub> synthesis from pool chlorine.

A second method that is discussed online which is a little less common due to the requirement for more equipment is the synthesis of potassium chlorate by the electrolysis of sodium chloride and/or potassium chloride solution. This involves the use of an electrochemical cell, electrodes, power supply unit, sodium chloride, potassium chloride and water. The general reaction mechanism is described in the following reaction equations.

$$NaCl(aq) + 3H_2O(l) + 6e^- \rightarrow NaClO_3(aq) + 3H_2(g)$$

Equation 1.9: Reaction equation for the electrolysis stage of KClO<sub>3</sub> synthesis from sodium chloride.

$$NaClO_3(aq) + KCl(aq) \rightarrow NaCl(aq) + KClO_3(s)$$

Equation 1.10: Reaction equation for the metathesis stage of KClO<sub>3</sub> synthesis from sodium chloride.

$$KCl(aq) + 3H_2O(l) + 6e^- \rightarrow KClO_3(aq) + 3H_2(g)$$

Equation 1.11: Reaction Equation for the Electrolytic synthesis of KClO₃ directly from potassium chloride.

#### 1.3.6.3 Forensic Analytical Techniques

Potassium chlorate and the related potassium perchlorate (KClO<sub>4</sub>) have not been extensively studied apart from thermal decomposition analysis<sup>79-85</sup>. There have been general studies including IR and Raman spectroscopy<sup>57,86</sup>, XRD<sup>84</sup> and IC<sup>87</sup>. The use of KClO<sub>3</sub> in HMEs tends to be seen in Asian countries for two reasons. Firstly, the regulations are less strict and secondly fireworks are abundant and so KClO<sub>3</sub> is much easier to obtain.

## 1.4 Analytical Techniques

This project aimed to analyse explosives using a variety of analytical techniques to determine any potential for discrimination between samples of like material. Additionally, data from the techniques that led to any form of discrimination were combined and a second exploratory multivariate data analysis was undertaken to determine if the discriminatory information is retained in a combined dataset. The following analytical techniques have been selected based on the results of prior studies undertaken.<sup>9,10</sup>

## 1.4.1 Isotope Ratio Mass Spectrometry (IR-MS)

#### 1.4.1.1 Background

Isotope ratio mass spectrometry enables the comparison of two or more chemically identical compounds (e.g. two AN samples) by comparing the ratio of the stable (i.e. non-radioactive) isotopes. Most commonly carbon ( $^{13}$ C/ $^{12}$ C) and nitrogen ( $^{15}$ N/ $^{14}$ N) isotopes are utilised, however, hydrogen ( $^{2}$ H/ $^{1}$ H), oxygen ( $^{18}$ O/ $^{17}$ O/ $^{16}$ O) and sulphur ( $^{36}$ S/ $^{34}$ S/ $^{33}$ S/ $^{32}$ S) isotopes may also be investigated. Isotopes are atoms of an element which vary in the number of neutrons held within the nuclei of the atom. Each element tends to have one major isotope ( $^{1}$ H,  $^{12}$ C,  $^{14}$ N,  $^{16}$ O and  $^{32}$ S) and one or more minor isotopes ( $^{2}$ H,  $^{13}$ C,  $^{18}$ O,  $^{17}$ O,  $^{36}$ S,  $^{34}$ S and  $^{33}$ S). For the elements that may be used in IR-MS the relative abundances of the naturally occurring isotopes are summarised in Table 1.1.

Table 1.1: Relative abundances of isotopes which may be analysed using IR-MS.88

Element (Chemical Symbol)	Isotope	Relative Abundance (%)
Liverage (LI)	<sup>1</sup> H	99.984
Hydrogen (H)	<sup>2</sup> H	0.0156
Corbon (C)	<sup>12</sup> C	98.892
Carbon (C)	<sup>13</sup> C	1.108
Nitrogon (NI)	<sup>14</sup> N	99.635
Nitrogen (N)	<sup>15</sup> N	0.365
	<sup>16</sup> O	99.759
Oxygen (O)	<sup>17</sup> O	0.037
	<sup>18</sup> O	0.204
	<sup>32</sup> S	95.02
Sulphur (C)	<sup>33</sup> S	0.76
Sulphur (S)	<sup>34</sup> S	4.22
	<sup>35</sup> S	0.014

The ratio of these stable isotopes has been shown to vary between samples due to differing precursors and geographic location.<sup>28</sup> Investigating a number of elements, such as nitrogen and carbon, allows discrimination between samples<sup>89</sup> as the measured isotopic ratios can provide an indication of the similarity between the samples.

This variation is a result of isotopic fractionation during chemical or physical processes. The fractionation occurs as the slight difference in intra- or intermolecular bond energies, as a consequence of the variance of atomic weight in the different isotopes, causes a difference in rates during bond forming and breaking processes. Natural isotopic fractionation involves the removal of either the heavier or lighter isotope due to a process, as an example the evaporation of water. The lighter water molecules (such as  $^1H^1H^{16}O$ ) require less energy to vaporise and so the bulk body of water will become enriched in the heavier isotopes (such as  $^2H^2H^{18}O$ ,  $^1H^2H^{18}O$ ) as the lighter water molecules more readily evaporate. This also applies to materials in solution as evaporation may lead to artificial fractionation hence samples are to be thoroughly dried and kept dry immediately after synthesis. Therefore, the isotopic ratios associated with a sample are a record of the chemical and environmental history of that sample and can be exploited to provide discriminatory power.

In terms of this project, the explosives and ingredients synthesised using differing starting materials could contribute to different isotope ratios in the end products. The method of synthesis may also result in a variation in isotopic composition as they are carried out under different environmental conditions as well as potentially using different reagents.

The isotopic ratios are measured by introducing a very small amount (50  $\mu$ g of carbon or 65  $\mu$ g of nitrogen) of sample into a combustion furnace. The sample undergoes rapid combustion, and/or pyrolysis reactions to quantitatively transform the sample from the solid state to its gaseous form. For the commonly investigated elements of carbon and nitrogen the sample is converted to carbon dioxide (CO<sub>2</sub>) and nitrogen gas (N<sub>2</sub>) respectively through the process of combustion and reduction of resultant gases.

These gas molecules are then ionised prior to travelling through a magnetic field where the ion trajectory will be altered depending on the mass of the ion which varies based on the carbon and nitrogen isotope ratios of the gaseous ion.<sup>91</sup> This allows the separation and hence detection/collection of the different mass-to-charge ratio (m/z) ions via a Faraday cup detector. This is depicted in the schematic Figure 1.12 below.

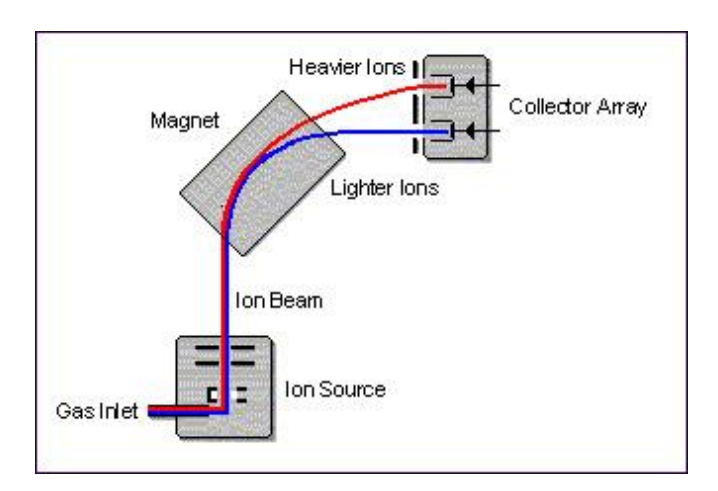


Figure 1.12: Schematic diagram of the separation and collection of ions within a magnetic field. 92

As the amount of sample is typically on the microgram scale care must be taken during sample preparation as the slightest contaminant would throw results significantly. Therefore, the sample is placed in tin capsules and crushed into a ball using steel tweezers to avoid contact with fingers or rubber/latex gloves.

#### 1.4.1.2 Resultant Data

There are three mass-to-charge ratios for the carbon isotope analysis (CO<sub>2</sub>) 44, 45 and 46. These are made up as follows:  $^{12}C^{16}O_2$ = 44 m/z;  $^{13}C^{16}O_2$  and  $^{12}C^{16}O^{17}O$ = 45 m/z;  $^{12}C^{17}O_2$ ,  $^{12}C^{16}O^{18}O$  and  $^{13}C^{16}O^{17}O$ = 46 m/z.

For the analysis of nitrogen isotope analysis ( $N_2$ ) three mass-to-charge ratios are recorded, 28, 29 and 30. These are made up as follows:  $^{14}N^{14}N = 28 \text{ m/z}$ ,  $^{14}N^{15}N = 29 \text{ m/z}$  and  $^{15}N^{15}N = 30 \text{ m/z}$ .

This data is then used to calculate delta ( $\delta$ ) values using Equation 1.13, where the isotope ratio of the sample is compared to that of a known standard.<sup>5</sup> The units of the delta value are per mil.<sup>16</sup> It is significant to note that the natural abundance of isotopes summarised in Table 1.1 previously are an average and that these values vary depending on the location in the world.<sup>93</sup>

$$R(ratio) = \frac{abundance \ of \ heavy \ isotope}{abundance \ of \ light \ isotope}$$

Equation 1.12: Equation for the calculation of isotope ratio values.

$$\delta = \frac{1000(R_{Sample} - R_{Standard})}{R_{Standard}}$$

Equation 1.13: Equation for the calculation of delta values.

These delta values provide a comparison of the isotopic ratio of the respective element in the sample to the standard. These standards are internationally recognised zero-point samples, including:

- Vienna Peedee Belemnite (VPDB) for carbon (<sup>13</sup>C/<sup>12</sup>C),
- Atmospheric nitrogen (Air-N<sub>2</sub>) for nitrogen (<sup>15</sup>N/<sup>14</sup>N),
- Vienna Standard Mean Ocean Water (VSMOW) for hydrogen (<sup>2</sup>H/<sup>1</sup>H) and oxygen (<sup>18</sup>O/<sup>16</sup>O).

All samples are relative to these zero-point values and therefore, measured values may be positive or negative. Positive delta values indicate that the sample has more of the heavier isotope than the zero-point standard and negative values means there is a greater abundance of the lighter isotope in the sample.

As most of the energetic materials previously discussed are organic molecules containing both carbon and nitrogen (excluding AN and KClO<sub>3</sub>), this can provide useful data when it comes to discriminating between samples of like material. One important drawback to keep in mind, however, is that the

resultant data cannot identify the chemical being analysed. It purely focusses on the isotope ratio of the specified element under investigation and not the chemical structure of the molecule.

Analysis of the collected data is quite simple as a material may only result in up to five delta values (C, N, O, H and S). This is further simplified in the scenario of explosives, as typically only one to three elements are investigated of carbon, nitrogen and oxygen, depending on the explosive and its elemental or mixture composition. Chemometric analysis on such a dataset requires no additional analysis as a simple one to three-dimensional plot can display the entire dataset without losing any information. This data, however, when added to a larger database as additional variables then undergo chemometric analysis to determine how much it may contribute to the building of a profile for a sample of explosive.

## 1.4.3 Inductively Coupled Plasma Mass Spectrometry (ICP-MS)

## 1.4.3.1 Background

Inductively coupled plasma mass spectrometry (ICP-MS) allows ultra-trace detection for a range of elements. With time instruments are becoming more compact and yet the low detection limit is still being improved.<sup>94</sup> A typical ICP-MS setup includes an introduction device (depicted in Figure 1.13) which vaporises the sample prior to being sent to the mass spectrometer.<sup>95</sup>

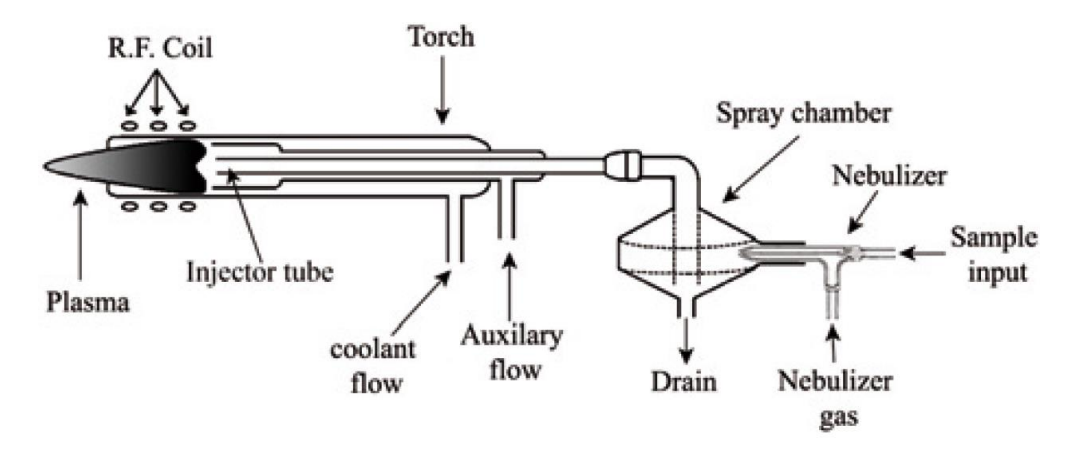


Figure 1.13: Schematic of a general sample introduction device.

Liquid samples are pumped into the nebuliser at a controlled rate with a peristaltic pump where they are transformed into an aerosol. This aerosol is then exposed to an argon plasma with a gas temperature of up to 10,000 K. The plasma maintained through the constant introduction of argon gas to a magnetic field provided by the radio frequency (RF) coil and depicted around the plasma in Figure 1.13. This plasma vaporises and ionises the sample resulting in the atomisation of the majority

of the molecules. The minority that are not atomised may be reduced by a flow of helium passed through the atom stream post-plasma which either breaks them apart or dislodges them from the ion beam. Gas samples are introduced to the plasma at a controlled flow rate and solid samples may be dissolved in a solution then introduced in the same manner as liquid samples. Solid samples may also be directly transformed into an aerosol via the use of laser ablation (LA-ICP-MS).

In general, explosive samples are analysed for a wide range of elements as the exact composition of trace elements in each sample is unknown and the greater the number of elements the greater the resolution of a sample's elemental profile. This however raises a number of potential issues that must be addressed. The limitations of the analysis must be understood starting with the plasma utilised. In the case of this project the plasma is argon based and therefore some elements are not very well ionised. The first ionisation energy of argon is 15.8 eV and therefore, elements with ionisation energies near this energy, such as selenium (9.8 eV), sulphur (10.4 eV) and chlorine (13.0 eV), are not well ionised in the plasma resulting in poor sensitivity. 95

As the ICP-MS analysis undertaken in this project quantifies trace elements to low ppt levels potential interferences must be understood and minimised. There are three key interferences which must be considered.

The first is isobaric interference. This occurs when two different elements have isotopes which have very similar masses and therefore, share the same mass-to-charge ratio if within the resolution of the mass spectrometer. This can easily be avoided by selecting isotopes for which this overlap is minimal or non-existent, keeping in mind the natural abundance of the isotopes. An example of this is <sup>74</sup>Ge (35.94% relative abundance) which clashes with <sup>74</sup>Se (0.89% relative abundance); however, if Ge is a target element selecting <sup>72</sup>Ge (27.66% relative abundance) may be a better choice as there is no overlap in mass with any other element's isotope. <sup>96</sup>

Doubly charged interference is when a species obtains a double charge rather than ionising to a single charged species. This means the mass-to-charge ratio is effectively halved and so is recorded at that level far from what is expected. This can be avoided by altering the ionisation conditions in the plasma, however, some elements are more prone to this than others.  $^{97}$  An example of a commonly doubly charged species includes  $^{140}$ Ce $^{2+}$  which results in a mass-to-charge ratio of 70 which will cause issues for the measurement of  $^{70}$ Ge $^{+}$  and  $^{70}$ Zn $^{+}$  species.  $^{97}$ 

The final and most significant form of interference is polyatomic interference, and this is when multiple atomic ions combine to form a molecule of high mass-to-charge ratio. This can be broken into two key groups, plasma-based and sample-based. Plasma-based interferences have a direct correlation with the type of plasma used and its interaction with the aqueous solution such as (in the case of argon plasma)  $^{40}$ Ar $^{38}$ Ar or  $^{40}$ Ar $^{16}$ O. These two examples create large interferences at a mass of 78 and 56 respectively. Though 78 is not an issue as it does not interfere with any other elemental mass, the atomic mass of 56 directly corresponds to  $^{56}$ Fe which is an issue if this is a measured element.

Sample-based interferences are directly linked to sample matrix components, examples of this being <sup>35</sup>Cl<sup>16</sup>O or <sup>34</sup>S<sup>32</sup>S. Though polyatomic interferences are by far the greatest interference issue involved in ICP-MS analysis, techniques have been developed to eliminate or mitigate their effects. The helium collision mode developed by Agilent Technologies utilises an inert collision gas (He) to remove all polyatomic species. This same mode is called the KED or Kinetic Energy Discrimination mode in Perkin-Elmer ICP-MS systems. As the polyatomic species have a greater cross-sectional area this means that they have a much greater collision rate with the He gas, significantly lowering their kinetic energy and preventing them from leaving this region of the He gas cell.

Ultra-trace detection requires that the sample preparation for the ICP-MS analysis must be strictly controlled in order to avoid any possible minor impurities as detection limits extend to the ppt level. Samples are to be prepared with trace grade digestion acids and ultrapure water in closed vessels to avoid any interaction with the surrounding environment. Samples are digested to ensure that the target trace elements are free from the sample and stable in solution for analysis.

Though methodology exists on some of the proposed energetic materials and ingredients such as AN and UN, (which involves a nitric acid digest)<sup>9,10</sup>, other materials require methodologies to be developed or altered, such as a change in digestion acid, conditions (temperature) and dilution factors. The methodology will have to be modified based on the success of digestion and concentration of elements within the samples themselves. For example, calcium content in potassium chlorates made from calcium hypochlorite may have greatly elevated levels of calcium and therefore, may require further dilutions to reduce this to within the working range of the instrument.

This will not only lead to a clear method of digestion but also an outline of target elements which allow discrimination for the samples.

#### 1.4.3.2 Resultant Data

Data from ICP-MS analysis are collected in the form of concentrations for the target elements of each sample which is then processed using the dilution factor of the acid digestion to calculate the total concentration of the element in the original sample. This data may then be statistically interrogated using principal component analysis which effectively reduces the large multivariate dataset into a condensed and more easily manageable and interpretable data set. This simplification of the raw data allows for the elements with highest discriminatory power to be clearly identified and hence distinguish between samples based on the elemental variation of the key trace elements. An additional benefit of such an analysis is that not only will the useful elements be identified but so too will the elements that do not contribute to the overall "fingerprint" of the sample. This may allow future analysis on the same explosive to become more efficient and streamlined by only routinely analysing for the elements regularly found in that explosive saving time and reducing the costs associated with analysis.

## 1.4.4 Raman Spectroscopy (Raman)

#### 1.4.4.1 Background

Raman spectroscopy is an ideal analytical technique for forensic applications as it is non-destructive, allowing the same sample to be analysed by more than one technique. It is a non-destructive, rapid analysis and samples to be analysed generally require little to no sample preparation prior to analysis. The technique also requires no alterations to analyse a variety of sample types and can easily be utilised to measure gases, liquids and solids.<sup>105</sup>

Over the years the instrumentation required to perform the technique has evolved rapidly and the technique now has high portability with a small sacrifice in performance. Compared to many other typically used analytical techniques the equipment required to perform a basic analysis for Raman is quite small and can be scaled all the way down to a handheld device such as the Thermo Scientific FirstDefender RM (depicted below in Figure 1.14). This portability makes Raman spectroscopy an ideal technique to transport to any location requiring the analysis with minimal effort rather than relocating the sample to a laboratory. The portable systems also allow a "Point-and-Shoot" analysis which enables the device to analyse a sample through some sealed containers avoiding any direct contact to a potentially harmful/unstable substance, i.e., an energetic material. 106



Figure 1.14: Thermo Scientific FirstDefender Portable Handheld Raman Spectrometer. 106

The sample is analysed by firing a monochromatic light source, usually a laser, at the sample and measuring the wavelength and intensity of the inelastic scattering (Raman scattering) of the incident light from the sample. <sup>107,108</sup> The spectrum obtained from the Raman scattering can then be investigated to determine the composition of the sample. This Raman scattering is produced by the changes in the induced dipole moment of a molecule or polarisation, which depends on how tightly the electrons are bound to the nuclei. As long as the molecule has a change in polarisation due to the energy of the incident light, then the molecule is Raman active. As varying functional groups will cause different scattering of the light, this information allows the determination of functional groups within the sample.

Raman spectroscopy has been used to forensically analyse a vast array of substances including narcotics, <sup>109-111</sup> paints, <sup>112</sup> alcoholic beverages <sup>113</sup> and explosives <sup>109</sup> displaying the applicability of the technique for sample discrimination. Though it is quite simple and fast for even a weaker portable Raman spectrometer to identify different materials it is much more difficult to distinguish between samples of like material. The key difficulty in discriminating between samples of like material is that this relies on impurities to be present in a concentration great enough to have a statistically significant effect on the resultant spectrum. This will vary depending on the material and components within the sample as Raman analysis can suffer from fluorescence which will effectively mask any Raman signals. However, altering the instrumentation in terms of laser wavelength can reduce this fluorescence as longer wavelengths may reduce fluorescence to reveal vital Raman signals. This also reduces the intensity of the Raman signals and therefore an optimal middle ground must be maintained.

#### 1.4.4.2 Resultant Data

The data collected as a result of Raman analysis will be in the form of spectra identifying Raman shifts (cm<sup>-1</sup>). The Raman shifts and peak intensity ratios may be statistically analysed via PCA. Ideally the statistical analysis will be able to reduce the dimensionality of the data set from being "number of samples" × "range of wavenumbers" to just a handful of principal components in the form of certain Raman shifts. The dataset for the application of statistical methods may also include signal intensities at selected key frequencies.

## 1.4.5 Infrared (IR) Spectroscopy

## 1.4.5.1 Background

Like Raman spectroscopy, infrared spectroscopy is an optical analysis technique. However, they are commonly referred to as complementary techniques as they measure the effects due to differing physical processes. IR spectroscopy requires the dipole moment of a molecule to change in order to detect vibrational motion. For example, some molecules are not IR active as there is no dipole moment; however, they may be Raman active as the stretching of the bonds changes the molecular polarizability. Another difference is that IR spectroscopy measures the absorption of light of certain energies which correspond to vibrational excitations within the molecule rather than light scattering. 99 As they are complementary techniques, using both to analyse a single sample will ensure the maximum amount of information may be gathered for any given sample. This is particularly important in forensic analysis as one technique may be able to highlight an impurity that is unresponsive in the other technique. Maximal discriminatory data allows for greater statistical significance, which is the basis of forensic analysis.

IR spectroscopy is highly versatile as it can be used to analyse gases, liquids and solids, although sample preparation for IR analysis can sometimes require additional processes. For example, a solid may be ground into a fine powder and pressed into a KBr disk rather than analysed directly.

IR spectroscopy has been used for forensic examination of a variety of sample types similar to the Raman spectroscopy, including, but not limited to, narcotics, <sup>100</sup> paints <sup>101,102</sup> and explosives <sup>103,104</sup>. Though IR has been shown to identify material quite rapidly and with little preparation the ability to discriminate between like material samples is more difficult. In order for this higher level of discrimination the impurities within the sample would have to affect the resultant spectra on a

magnitude that is statistically significant, which may not be possible for every sample depending on the resolution power of the instrument utilised.

#### 1.4.5.2 Resultant Data

Much the same as Raman, IR analysis results in a spectrum of the sample identifying the frequencies, generally expressed in wavenumbers (cm<sup>-1</sup>), at which the molecule interacts with the incident light. Once again this may be investigated statistically using PCA. Ideally this analysis will be able to reduce the dimensionality of the data set from being "number of scans" × "range of wavenumbers" to just a handful of principal components in the form of certain wavenumber ranges. The dataset for the application of statistical methods may also include signal intensities at selected key frequencies.

## 1.4.6 Terahertz/Far-Infrared Spectroscopy (THz/Far-IR)

The terahertz radiation band is located between microwave and infrared radiation. This region is typically regarded as the frequencies between 100 GHz and 30 THz or 3-1000 cm<sup>-1</sup> and recent technological advancements have made research into the field more prominent<sup>114</sup>. Extending into this frequency range beyond the standard fingerprint region of a typical infrared analysis may yield additional signature peaks. A key development, terahertz domain spectroscopy (TDS), has allowed the analysis of molecules in the condensed phase.<sup>115</sup> This has shown potential, especially in explosives screening applications as various materials such as paper, leather, cotton and synthetic fabrics are transparent in the THz region.<sup>115-122</sup> Recently, this technology has been harnessed to develop a portable laser device able to perform standoff GHz to mid-infrared analysis making it an ideal technique for the screening of explosives.<sup>115</sup> This may lead to future far-infrared spectroscopy capabilities being added to the toolbox of onsite investigators to identify unknown materials even within some wrappings or containers. Other benefits of THz spectroscopy include the non-destructive nature of the analysis ensuring the same sample material can be interrogated using other analytical techniques. It is also rapid with an instant result that can identify the material being analysed so long as the material's spectrum has been recorded into a library.

This project explored this fast-developing novel technology to provide additional information including extending the region of the infrared spectra currently acquirable with modern technology. As the THz radiation harnessed is from a Synchrotron (Australian Synchrotron, ANSTO), the spectra acquired are of very high resolution and can be the beginning of an explosives database for THz

spectra. With this high level of resolution, a determination on whether or not the technology can also provide discriminatory signals between samples of like material may be possible based on the detection of impurities within samples.

# 2. Method Development

In this chapter the development of synthesis and analysis methods is discussed.

This includes the synthesis of potassium chlorate via three methods. These methods included the use of household bleach, pool chlorine and the electrolysis of saltwater. Erythritol tetranitrate was synthesised by explosives chemists at DST Group and supplied for analysis.

The analytical methods employed include; isotope ratio mass spectrometry, inductively coupled plasma mass spectrometry, infrared spectroscopy, Raman spectroscopy and terahertz/far-infrared spectroscopy. All aspects of sample preparation, data collection and data handling/analysis are covered.

## 2.1 Synthesis

In today's world of information technology any individual with access to the Internet may search for information on how to synthesise almost any chemical in the world and purchase the precursors required. Confronting this issue is a formidable task as forums are too difficult to police due to their number, and some precursors cannot be regulated due to their abundance of legitimate uses.

An alternate approach is to identify signatures which may allow the connection of starting materials and synthesis methods to their final products. This would result in being able to collect data that may provide vital intelligence in an investigation and, while the information may not be rigorous enough to be presented as incontrovertible evidence in a court of law, it may lead to finding more concrete evidence through a more targeted investigation.

To this end, two materials have been selected for examination, KClO<sub>3</sub> and ETN. These two materials are of particular interest due to the prevalence of their usage in illicit activities including the production of homemade IEDs. Both substances may be easily produced using basic household items and precursors sourced from either Internet marketplaces or even local supermarkets and hardware stores. Information on how to perform the synthesis for both materials can be openly sourced through the Internet.

## 2.1.1 Potassium Chlorate (KClO₃)

Potassium chlorate is an inorganic oxidiser which can form an explosive when mixed with a fuel and is commonly discussed online amongst hobbyists due to its ease of synthesis and availability of

precursors. Common methods openly discussed typically involve synthesis from household bleach, swimming pool chlorine or through the electrolysis of saltwater. In each case minimal equipment is required, with the first two methods only requiring the ability to heat a volume of solution by any means, and the electrolysis typically utilising a standard desktop computer power supply. There is also no chemistry knowledge required as forums will allow individuals with no knowledge to use other people's experiences and discussions to understand enough to successfully perform a synthesis.

The final procedures utilised in this project have undergone significant alteration and amendment, starting with basic instructions from online forums and YouTube videos then developing them further to yield the desired product on a consistent basis. Details of the optimised procedures will not be given in this publicly available thesis due to security concerns but will be published in a classified report. Starting materials were sourced from supermarkets, hardware shops and online marketplaces and the exact identities have been redacted and replaced with codes (refer to sample matrix in Table2.1). Therefore, the final products therefore should mimic real world samples and their variability.

Care was taken not to inadvertently introduce potential fuels into the potassium chlorate samples manufactured to minimise the risk of formation of sensitive explosive mixtures. Potassium chlorate is a strong oxidiser with known incompatibilities with combustible materials, ammonium salts and acids. Solid potassium chlorate and solutions should be kept at neutral pH and should be stored and handled with this in mind. All procedures were undertaken at the minimum scale for practicality and consistency.

#### 2.1.1.1 Potassium Chlorate from Household Bleach

The synthesis of potassium chlorate from household bleach is easily found in message boards and forums online. In theory it is a simple process requiring household bleach containing sodium hypochlorite (NaOCI) and potassium chloride (KCI) salt. The reagents can be easily sourced from supermarkets, health food shops, hardware stores and online. Equipment requirements are also minimal with only the need for a receptacle capable of being heated, a heat source and a basic filter such as filter paper. In practice, however, the process is not very efficient or consistent as there are many types of bleach products and they can behave very differently due to other ingredients in their formulations.

The general method utilised was as described below:

- 1. Household bleach was placed in a beaker.
- 2. This was boiled on a hotplate with magnetic stirring until visible crystals formed and precipitated out of solution.
- 3. Potassium chloride was added to the solution, stirred and chilled in an ice bath. At this point a visible potassium chlorate precipitate was formed.
- 4. The solution was then filtered and washed with chilled water.
- 5. This solid was then recrystalised with boiling water to remove sodium/potassium chloride.
- 6. This final product was then dried in a desiccator for 24 hours and stored in plastic containers. Safety points relating to this procedure are:
  - Care must be taken to ensure that the hot and corrosive bleach solution does not bubble over or overflow. This bubbling over is due to the presence of detergent in the solution and the amount varies depending on the brand of bleach.
  - The vapour released from the heating is also quite corrosive and toxic so the entire procedure from start to finish was completed within a fume hood.
  - The entire process was undertaken behind a blast shield for added safety.

One precursor that did not successfully produce the desired product was a health food supplement salt labelled as LITE in the sample matrix (Table 2.1). This was a low sodium alternative to table salt and is a mixture of sodium and potassium chloride. Samples KClO<sub>3</sub> 40-45 have been included, however, the yields were very poor and as recrystallisation was not possible the end products were essentially a mixture of potassium and sodium chloride with trace amounts of potassium chlorate as shown below in Figure 2.1.

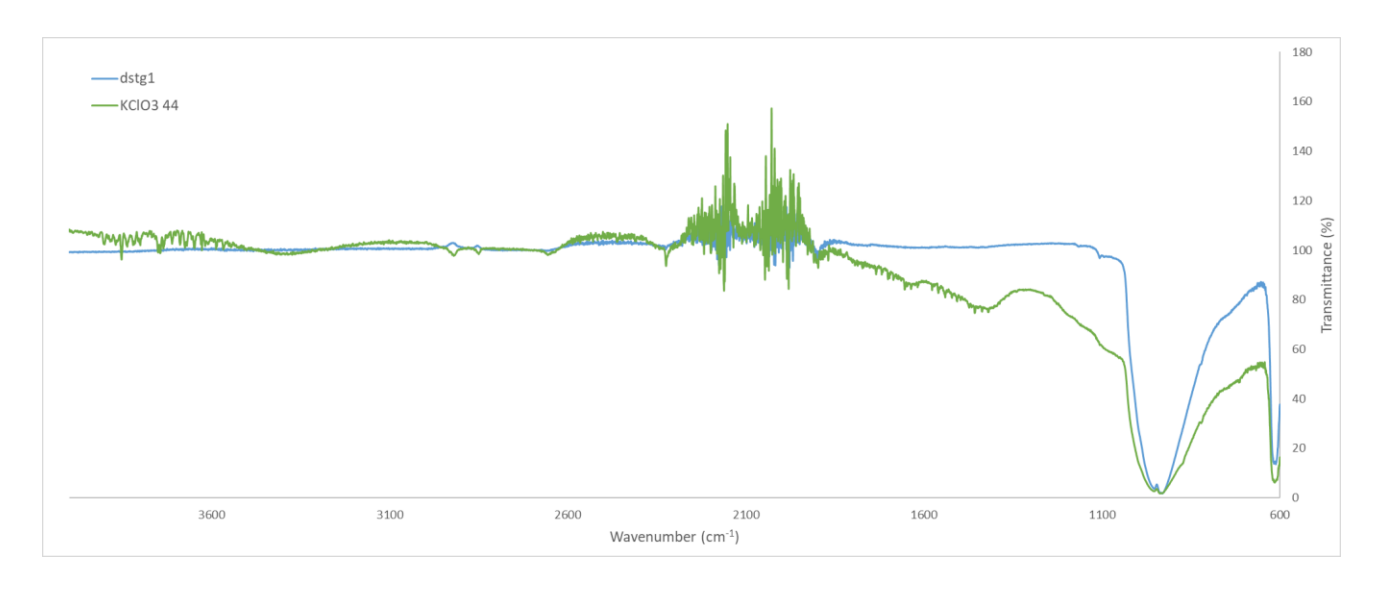


Figure 2.1: Spectra comparison between commercial KClO<sub>3</sub> (blue) to LITE salt precursor KClO<sub>3</sub> (green).

#### 2.1.1.2 Potassium Chlorate from Pool Chlorine

The synthesis of potassium chlorate from pool chlorine is equally as easy to find in message boards and forums online as the bleach method previously described; typically, it is mentioned as an alternative to the bleach method. The procedure is very similar to the bleach method, with substitution of the bleach solution for pool chlorine liquid or granules containing calcium hypochlorite (Ca(OCl)<sub>2</sub>). The reagents can be easily sourced from supermarkets, health food shops, hardware stores and online. Equipment requirements are also minimal with only the need for a receptacle capable of being heated, a heat source and a basic filter such as filter paper.

The general method utilised was as described below:

- 1. Pool chlorine granules or liquid chlorine (containing calcium hypochlorite) was dissolved in water.
- 2. The solution is then heated to boiling temperature on a hotplate with stirring until there is a substantial volume reduction (approximately 90%).
- 3. This solution was then filtered to remove calcium solids, retaining the filtrate.
- 4. The filtrate was the reheated to boiling point briefly and potassium chloride was added, and the solution stirred.
- 5. The solution was then removed from heat and cooled to room temperature then chilled in an ice bath. At this point crystals of potassium chlorate will become visible and precipitate out of solution.
- 6. This solution is then filtered and washed with chilled water.

- 7. The crude product was then recrystalised with boiling water to remove calcium/potassium chloride.
- 8. The final product was then allowed to dry in a desiccator for 24 hours and stored in a plastic container.

Throughout the procedure the vapours released from the heating are toxic, so the entire process was completed within a fume hood. A small blast shield was used for added safety.

The synthesis of one sample, KClO<sub>3</sub> 20, was only partially successful. As with samples KClO<sub>3</sub> 40-45, the yield was very poor and as recrystallisation was not possible the end product was essentially potassium chloride with trace amounts of potassium chlorate as shown below in Figure 2.2.

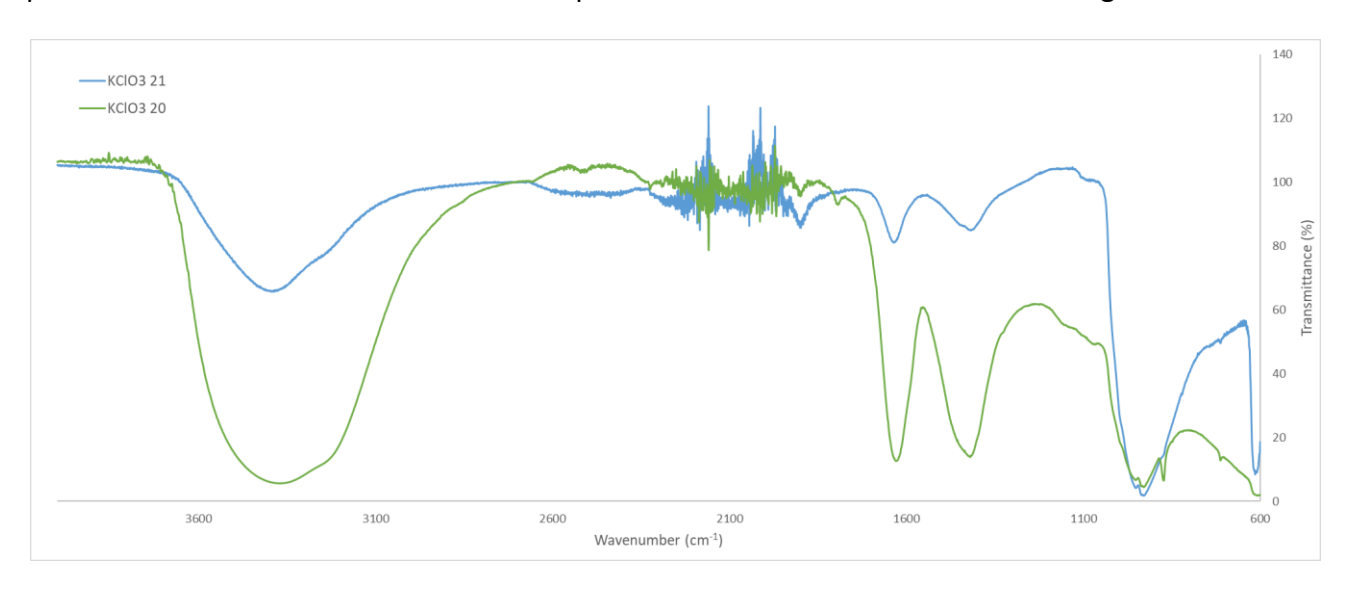


Figure 2.2: Spectra comparison between successful pool chlorine KClO<sub>3</sub> (blue) to a partially successful KClO<sub>3</sub> (green).

#### 2.1.1.3 Potassium Chlorate from the Electrolysis of Sodium Chloride Solution

This synthesis is commonly described on the Internet by hobbyists; however, many variations are found due to differing equipment used. To mimic these improvised methodologies a homemade electrochemical cell was produced and connected to a DC power generator that can reach and maintain the required voltage and current. This did not directly mimic the method of using computer power supplies from desktop computers but provided a greater level of control and safety.

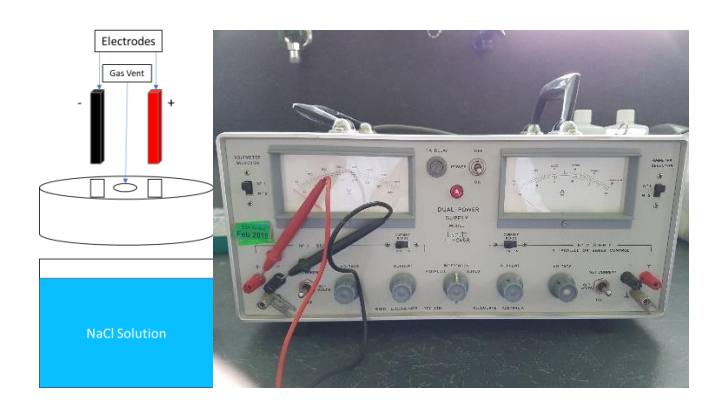


Figure 2.3: Schematic of the basic electrochemical cell constructed for the synthesis of potassium chlorate from sodium chloride solution (left) and DC power supply used (right).

The only reagents required for this process are sodium chloride and potassium chloride making the method highly consistent and the chemicals required trivial to obtain. The difficulty of this manufacturing method is the experimental set up of the electrolytic cell and cell conditions including electrodes, salt concentration, temperature, concentration, voltage and current. The specific optimised cell conditions and the process of optimising this synthesis have been redacted from this document due to its sensitive nature.

The general method utilised was as described below:

- 1. A sodium chloride solution was added into the electrochemical cell.
- 2. Electrodes were introduced and the current passed through the solution, topping up the cell with water occasionally depending on the rate of evaporation.
- 3. The power supply was then turned off after the optimal length of time and the electrodes disconnected and removed.
- 4. The solution is then filtered to remove and metal particulates from the degradation of the electrodes. Resulting in a yellow/brown clear solution as depicted in Figure 2.4.



Figure 2.4: Filtered solution post electrolysis.

5. The filtrate was then heated, and potassium chloride was added until saturation.

- 6. The solution is brought up to a boil to remove any remaining chlorine gas then allowed to cool and chilled in an ice bath. Crystals of crude product will become visible and precipitate. At this point crystals of potassium chlorate will become visible and precipitate out of solution.
- 7. The crude product was then filtered and washed with chilled water.
- 8. This was then recrystalised with boiling water to remove any sodium/potassium chloride resulting in the final product as depicted in Figure 2.5.
- 9. The final product was then allowed to dry for 24 hours in a desiccator and stored in a plastic container.



Figure 2.5: Final filtered product potassium chlorate.

Though this method seems simple theoretically, in practice discovering the correct set up and conditions of the electrochemical cell was quite arduous.

Aside from the complexities of the electrochemical cell this synthesis also has many other hazards:

- The procedure involves the application of electricity to saltwater which is highly conductive and so general electrocution is a very real hazard.
- The synthesis produces a significant amount of gas which includes highly toxic chlorine gas
  and so a suitably rated fume hood was used throughout the entirety of the synthesis. The
  gases are also highly corrosive and so any exposed metal surrounding the reaction vessel was
  corroded.
- This reaction was also conducted behind a blast shield to provide protection against unexpected pressure build up.

## 2.1.1.4 Potassium Chlorate Samples

The following Tables 2.1-2.3, display details on the precursors for all  $KCIO_3$  samples.

Table 2.1: Sample matrix for KClO<sub>3</sub> samples made using the bleach method.

Dlooch	Potassium chloride				
Bleach	KCl1	E508	LITE		
	KClO3 1				
	KClO3 2				
	KClO3 3	KClO3 28	KClO3 43		
SACB	KClO3 3_2	KClO3 29	KClO3 44		
	KClO3 4	KClO3 30	KClO3 45		
	KClO3 5				
	KClO3 6				
	KClO3 7				
HBL	KClO3 8				
	KClO3 9				
	KClO3 10	KClO3 37			
WKR	KClO3 11	KClO3 38			
	KClO3 12	KClO3 39			
	KClO3 13	KClO3 35			
WKL	KClO3 14	KClO3 36			
	KClO3 15	KClO3 36_2			
	KClO3 16	KClO3 31	KClO3 40		
FCB	KClO3 17	KClO3 32	KClO3 41		
	KClO3 18	KClO3 33	KClO3 42		

Table 2.2: Sample matrix for KClO₃ samples made using the pool chlorine method.

Pool chlorine	Potassium o	Potassium chloride				
Pool Chlorine	KCI1	E508				
	KClO3 19					
	KClO3 20 (partially successful					
	synthesis)	KClO3 25				
HCSS	KClO3 21	KClO3 25_2				
	KClO3 22	KCIO3 26				
	KClO3 23	KCIO3 27				
	KClO3 24					
	PT1					
Sigald Ca(OCI)2	SIGALD					

Table 2.3: Sample matrix for KClO<sub>3</sub> samples made using the electrolysis method.

Sample Code	Anode	
Cu	Copper	
E1	Titanium	
E2	Titanium	
ICPMS1	Titanium	
SS	Titanium	

All used the same sodium chloride (Univar), potassium chloride (KCl2) and a titanium Cathode.

As well as these synthesised samples of potassium chlorate DST Group supplied 3 commercial samples labelled DSTG1, DSTG2 and DSTG3.

## 2.1.2 Erythritol Tetranitrate (ETN)

The synthesis of ETN in a clandestine HME setting is relatively new and on the rise since the large-scale synthetic production and increasing use of erythritol as an artificial sweetener.<sup>57</sup> These advancements have made erythritol a household staple for many looking at reducing their calorific intake. As a result, erythritol can now be purchased at low cost and in large quantities from any supermarket or health food store in most countries around the world.

The most commonly discussed method of ETN production online is through a mixed acid synthesis. However, rather than imitating these crude methodologies, adaptations of literature methodologies were used to prepare samples by three different methods.<sup>57,138</sup> The three methods utilised mixed acid, acetyl nitrate and nitrate salt nitration mixtures.

All samples analysed in this investigation were prepared by experienced staff at the Defence Science and Technology Group, Edinburgh, South Australia, in laboratories designed for the synthesis of explosives. Samples were prepared using both commercial and laboratory grade erythritols. The nitric acids were also made in-house from the same nitrate salts used in the nitrate salt method samples in addition to one commercially obtained fuming nitric acid. The specific identities of the precursors are once again redacted and are rather denoted by codes, for example, potassium nitrates PN1 and PN2 are sourced from two different manufacturers.

#### 2.1.1.1 ETN Samples

The following Tables 2.4-2.7, display details on the precursors for all ETN samples. Some nitric acids used were also produced by DST Group and the details for these are described in Table 2.4.

**Table 2.4: Nitric acid precursors** 

DST NA1	Manufactured from PN1 + H <sub>2</sub> SO <sub>4</sub> . Two batches produced.			
DST NA2	ST NA2 Manufactured from PN2 + H <sub>2</sub> SO <sub>4</sub> .			
DST NA3	Manufactured from AN1 + H <sub>2</sub> SO <sub>4</sub> . Redistilled during ETN syntheses.			
DST NA4	Manufactured from AN2 + H <sub>2</sub> SO <sub>4</sub> . Two batches produced.			
DST NA5	Manufactured from CN + H <sub>2</sub> SO <sub>4</sub> .			

Table 2.5: Sample matrix for ETN samples produced via the acetyl nitrate nitration method.

Nitric acid		Erythritol		
Nitric acid	Sigma-Aldrich	Unison International (Ausweet)	Natvia	
DST NA1 (Batch 2)	d-15-4 e-16-4		f-17-4	
DST NA2	g-8-5	h-8-5	i-13-5	
DST NA3	<b>3</b> j-13-5 K-14-5		L-14-5	
DST NA4 (Batch 2)	DA-95A	DA-96A	DA-97A	
DST NA5	P-23-5	Q-22-5	R-27-5	

All syntheses used a common acetic anhydride (Ajax).

Table 2.6: Sample matrix for ETN samples produced via the mixed acid nitration method.

Nitric acid		Erythritol			
Mitric acid	Sigma-Aldrich	Unison International (Ausweet)	Natvia		
Sigma-Aldrich 100%	a-12-6	b-13-6	c-15-6		
DST NA1 (Batch 1)	d-18-6	e-19-6	f-20-6		
DST NA2	g-25-6	h-26-6	i-27-6		
DST NA3	j-25-7	K-27-7	L-7-8		
DST NA4 (Batch 1)	M-5-12	N-6-12	0-7-12		
DST NA4 (Batch 2)	DA-98A	DA-99A	DA-100A		
DST NA5	P-25-3	Q-27-3	R-1-4		

All syntheses used a common 98% sulfuric acid (APS Specialty Chemicals).

Table 2.7: Sample matrix for ETN samples produced via the nitrate salt nitration method.

Niturata calt	Erythritol				
Nitrate salt	Sigma-Aldrich	Unison International (Ausweet)	Natvia		
Potassium Nitrate 1 (PN1)	DA-84A	BCH-1-27	BCH-1-32		
Potassium Nitrate 2 (PN2)	DA-85A	BCH-1-37	BCH-1-33		
Ammonium Nitrate 1 (AN1)	DA-86A	BCH-1-29	BCH-1-34		
Ammonium Nitrate 2 (AN2)	BCH-1-25	BCH-1-30	BCH-1-35		
Calcium Nitrate (CN)	BCH-1-26	BCH-1-31	BCH-1-36		

All syntheses used a common 98% sulfuric acid (APS Specialty Chemicals).

## 2.2 Analytical Techniques

Many techniques have been used in the forensic analysis of explosives as well as other materials as previously discussed. However, methods of extracting the maximal amount of forensic intelligence from gathered data can be improved. In this chapter the methodologies for both the collection and analysis of data for each analytical technique employed within the project are outlined.

## 2.2.1 Isotope Ratio Mass Spectroscopy (IR-MS)

#### 2.2.1.1 Sample Analysis

The IR-MS system was located in Flinders Analytical and consists of an IsoPrime (GV Instruments) stable isotope ratio mass spectrometer including an Elementar Vario Isotope elemental analyser coupled with an Isoprime diluter. The system utilised Isoprime's Stable Isotope Ratio Mass Spectrometry software, IonVantage for isoprime<sup>123</sup>, Build 1.6.1.0 and Elementar's varioISOTOPE cube software<sup>124</sup>. The analysis method was continuous flow, elemental analysis, nitrogen and diluted carbon isotope ratio utilising helium as the carrier gas.

Samples were prepared in tin boats (4 x 4 x 11 mm) manufactured by Elementar Analysensysteme GmbH (batch S22137418). Standards were supplied by Flinders Analytical and included the NIST reference materials:

- 8573 L-Glutamic Acid USGS40: Light carbon (-26.39 ± 0.09‰) and nitrogen (-4.52 ± 0.12‰) isotopes in L-glutamic acid.
- 8574 L-Glutamic Acid USGS41: Heavy carbon (+37.63 ± 0.10%) and nitrogen (+47.57 ± 0.22%) isotopes in L-glutamic acid.

These reference materials are internationally recognised, and their values are determined through comparison to the zero-point standards previously discussed. These have been used instead due to their cost, availability and in order to allow a two-point linear calibration between distant delta values.

Samples were weighed using a Satorius Cubis microbalance with a readability of 0.001 mg, into tin boats and these are then carefully sealed and crushed into round balls using tweezers to avoid contamination. The final balled sample is then reweighed to confirm no loss of sample during the preparation and the mass recorded. 1.2-1.6 mg (1.4  $\pm$  0.2 mg) of both standards and samples were weighed out in triplicate. Samples are then loaded into their assigned positions within a 96 welled

sample holder and stored within a desiccator until ready for analysis at which point the samples are loaded into the autosampler.

#### 2.2.1.2 Data Analysis

This is a very small dataset in comparison to all the other analytical methods within this project with only 2 variables, carbon and nitrogen delta values, and so, was treated quite differently. The raw data was examined by plotting the isotope ratios for both carbon and nitrogen individually and as a two-dimensional combination. This can highlight similarities and differences within samples based on these ratios and can also identify linkages to precursor materials. The second stage of analysis for this data was to incorporate it into the ICP-MS dataset.

## 2.2.2 Inductively Coupled Plasma Mass Spectrometry (ICP-MS)

### 2.2.2.1 Sample Analysis

The ICP-MS instrument used was located at Flinders Analytical and is a Perkin-Elmer NexION 350D utilising the Syngistix Version 1.1 (Build 1.1.4624.0) software<sup>125</sup>. The system is equipped with a PC<sup>3</sup> Peltier Cooler Organics Sample Introduction Kit allowing for the chilling of the nebuliser to reduce polyatomic interferences, such as oxides, and nickel cones were used for all analysis. The ion path is unique with a schematic shown below in Figure 2.5 below<sup>126</sup>. The unique features of this system are the triple cone interface to focus the ion beam for extra stability and a quadrupole ion deflector to redirect positively charged ions 90° rather than the use of lenses as in other systems.

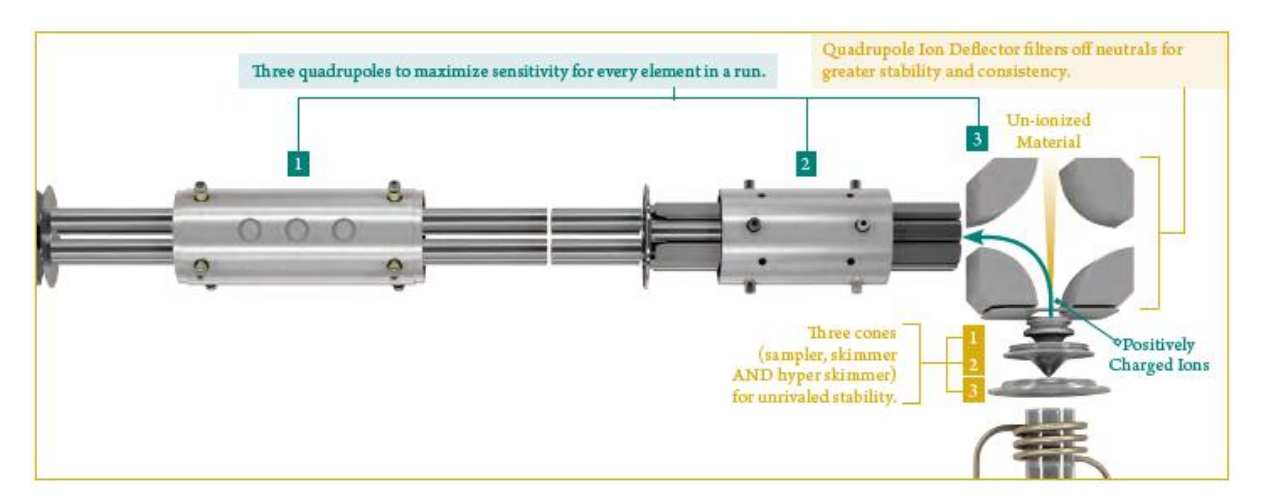


Figure 2.6: Schematic of the Perkin Elmer NexION 350D.

All analysis was done in a collision mode using the instrument's kinetic energy discrimination (KED) mode which fills the cell with helium gas to collide with interfering ions with larger cross sections and hence remove them prior to detection.

Before every use the ICP-MS was tuned with a daily tuning solution containing 1 ppb of Be, Ce, Fe, In, Mg, Pb and U and a Kinetic Energy Discrimination (KED) mode tuning solution containing 1 ppb Ce and 10 ppb Co to within the specifications displayed in Table 2.8. The system was also tested for stability by measuring the ion counts for the internal standard solution for an extended period of time (6 minutes) prior to analysis. In the case of this project a 100 ppb indium solution was utilised as the internal standard and across this period of time the acceptable relative standard deviation (%RSD) was below 3%.

Table 2.8: Nexion ICP-MS tuning specifications.

Daily tune criteria	KED tune criteria
Be 9 > 2000 cps	Co-high 58.93 > 15000 cps
In 115 > 50000 cps	Ar <sup>2</sup> -high 77.92 ≤ 30 cps
U 238 > 40000 cps	CIO-high 50.96/Co-high 58.93 ≤ 0.005
Background 220 ≤ 1 cps	CeO-high 155.9/Ce-high 139.91 ≤ 0.01
CeO/Ce ≤ 0.015	CIO-low 50.97/Co-low 58.94 ≤ 0.02
Ce <sup>2+</sup> 70/Ce 140 ≤ 0.03	

Many of the instrument operating conditions were based on these daily tunings including the torch position, nebuliser flow rate and standard/KED mode quadrupole ion deflector voltages. Further static operating conditions are displayed in Table 2.9.

Table 2.9: Operating conditions for the ICP-MS instrument.

RF Power	1600 W
Nebuliser	Meinhard Glass TR-50-C0.5, 0.5 mm I.D.
Spray chamber	Quartz glass cyclonic with Peltier Cooler (PC <sup>3</sup> )
Injector	2 mm I.D. Quartz Injector
Torch	Demountable quartz
Triple cone interface	Nickel/Aluminium
Plasma gas flow	18 L/min
Nebuliser gas flow	0.87 L/min*
Sweeps per reading/replicates per sample	10 sweeps/3 replicates
Helium gas flow	4.7 mL/min
Detector mode	Dual (pulse/analog)
*may vary as optimised by tunings	

The sample solution was introduced via a peristaltic pump under the parameters recorded in Table 2.10. The internal standard moves through a 0.19 mm internal diameter tube while the sample travels through a 0.76 mm internal diameter tube to the mixing junction. At the pump rotation of sample introduction during measurements (9 rpm), 0.45 mL of sample and 0.03 mL of internal standard are introduced per minute.

Table 2.10: Sample introduction parameters for the peristaltic pump.

	Time (s)	Speed (rpm)
Sample flush	35	24
Read delay	45	9
Wash	45	24

ICP-MS sample preparation was identical for both the KCIO<sub>3</sub> and ETN samples. 50 mg of sample (weights recorded) were weighed out into 50 mL plastic digestion vessels from Environmental Express (Cole-Palmer). Each batch of these vessels are tested for volume graduation lines and trace metal contents of 68 elements for quality assurance purposes and the resultant report is delivered with each order. This is vital when considering ultra-trace detection research. For example, a randomly selected vial not specifically manufactured for trace elemental analysis was tested for the same range of elements during the ETN analysis and produced the following results (Table 2.11). 1 mL of nitric acid was placed in the vial and left overnight then made up to 50 mL and analysed.

Table 2.11: Results of preparing a blank in a randomly selected 15 mL vial showing its lack of suitability for ultra-trace elemental analysis.

	Al ppb	Ca ppb	K ppb	Co ppb				Sr ppb		_	
Vial	15.5	80.8	0	0	0	0	0	0	8.7	3.2	1.0

The results show that a vial such as this would not be acceptable as the levels in a blank would have ppb levels of Al, Ca, Fe, Mg and Zn whilst the measured range in this project is as low as 100 ppt or 0.1 ppb for these elements.

To prepare samples for analysis 100  $\mu$ L of ultrapure water (Milli-Q) followed by 1000  $\mu$ L of trace grade 69% nitric acid was added to the digestion vessels. The water was added prior to the introduction of the acid purely for the minimisation of any reaction between the nitric acid and the samples which may result in the loss of elements. For example, the ETN and KClO<sub>3</sub> from pool chlorine starting materials tended to react with neat acid and resulted in some bubbling and degassing which could potentially affect the retention of trace metals within the solution and so the addition of 100  $\mu$ L of

water was utilised. The vessels were then lightly capped and left in a fume hood overnight to ensure a complete digestion and any potential gas production was safely contained and removed. The vials were then inspected to confirm the digestion by examining the solutions for any particulates and or colour to indicate an incomplete digestion. This is a gentle digestion method requiring no heat or the use of a microwave digestion system, however, if desired the process may be accelerated using a heating block or water bath at 60°C in which case digestion may be complete typically within an hour. Digested samples are then made up to 50 mL with ultrapure water making up the sample solution to 2% nitric acid, which is the selected matrix for the internal standard as well as all calibration solutions. This is an important factor as matrix matching ensures that all the solutions have the same aerosol characteristics when being introduced into the plasma by the nebuliser.

The calibration solutions for KClO<sub>3</sub> and ETN differ in their trace elemental contents as differing elements were targeted in each material depending on predicted elements that may be contained within real world samples. For example, as KClO<sub>3</sub> may be created using an electrochemical cell, metals that may be used as electrodes (copper, titanium, etc.) were investigated, whereas for ETN elements that were reported to be more commonly found in artificial sugars were selected.<sup>127</sup>A summary of the target elements for each material is described in Table 2.12. The elemental standards were sourced from either Choice Analytical or Australian Chemical Reagents and were all in 2% nitric acid.

Table 2.12: Range of elements selected for ICP-MS analysis for both KClO<sub>3</sub> and ETN samples.

KClO₃ Target Elements		ETN Target Elements	
Choice Analytical	Australian Chemical Reagents	Choice Analytical	Australian Chemical Reagents
Al, Ca, Cu, Mg, Ru, U, Zn	Ba, Cr, Fe, Mn, Ni, Pt, Sr, Ti	Al, Ca, K, Mg, Ru, U, Zn	Co, Fe, Ni, Sr

These were used to make 5-point calibration curves between 100 ppt and 100 ppb (100 ppt, 500 ppt, 1000 ppt, 10 ppb and 100 ppb) for all elements apart from the rarer elements Ru, Pt and U where a range of 10 ppt to 10 ppb (10 ppt, 50 ppt, 100 ppt, 1 ppb and 10 ppb) were used.

Quality control in trace metal quantification is paramount in producing reliable results. All ICP-MS analyses should incorporate a minimum level of quality control procedures including an internal standard together with regular blank and check solutions.

The internal standard ensures that the system is not unknowingly drifting over time by either increasing or decreasing counts. If not measured throughout an analysis the samples measured

towards the beginning may not be comparable to samples measured towards the end of the batch. This is the reason for the internal standard stability test prior to commencing analysis. If a trendline is identified it may be used to correct across the batch analysis by accounting for drift, however, it is preferable for the system be confirmed to be stable prior to starting an analysis. The secondary purpose for the internal standard is to measure any matrix effects present within digested sample solutions. This is important as samples must have similar matrix behaviours to the calibration standards they are being measured against, otherwise the comparison is unreliable. Differences in the matrices of the sample solutions and the internal standard and calibration solutions result in dissimilar aerosol characteristics in the nebuliser and spray chamber. This difference in aerosol droplet size then leads to a differing ionisation once exposed to the plasma, greatly affecting the recovery of internal standard. Examples of a poor matrix matching, and acceptable matrix matching are displayed in Figure 2.7. This acceptable matrix range is between 80%-120% internal standard recovery.

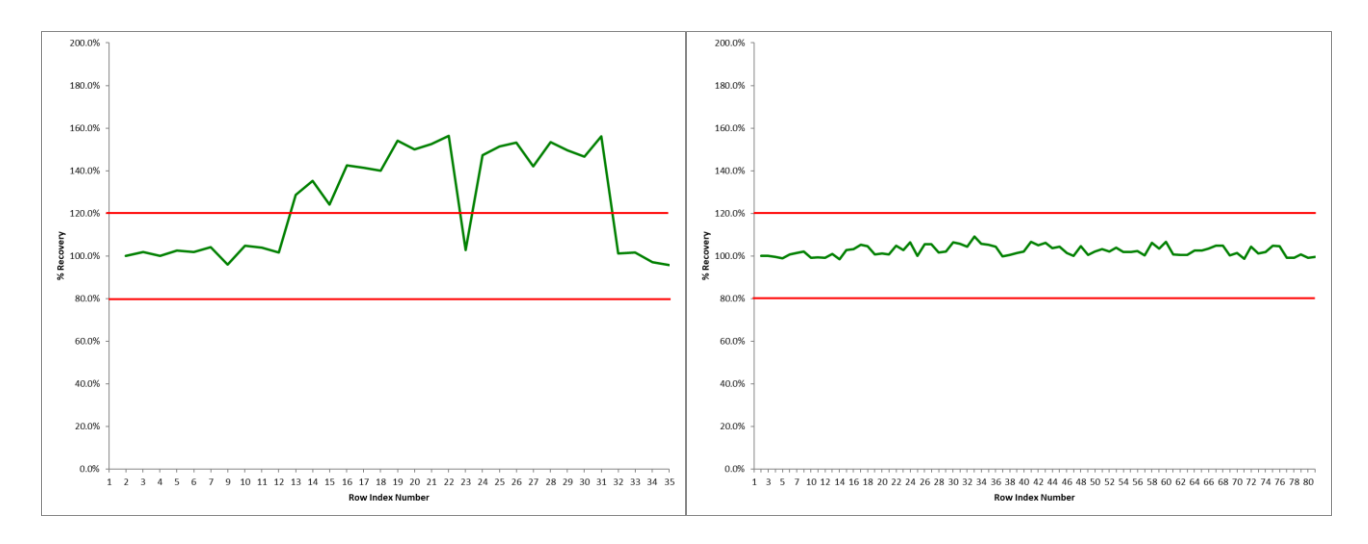


Figure 2.7: An example of significant matrix effects within a batch (left) and of acceptable matrix effects (right).

The blank solutions ensure that there is no carry over or contamination effects due to samples with high concentrations of measured elements. This should be run every 10 samples at a minimum to confirm that trace elements are being properly washed out by the rinse solution. The readings for blanks should be below the limit of quantification.

In an ideal situation check solutions should consist of certified reference materials. These are samples with known concentrations for the elements being analysed which are chemically and physically similar to the samples being analysed. For example, when plant samples are being analysed a certified

reference plant material may be used which has known amounts of all the elements being measured. The analyses performed in this project did not involve the use of a certified reference material and so additional quality control methods were employed. Firstly, a pre-digestion blank was prepared in order to guarantee that the handling and digestion of samples did not introduce trace elements to the samples. This also ensures that the plasticware and trace grade acids did not contribute to the concentration of elements within samples. Secondly, a dilution check is regularly measured immediately after the regular blank which is simply a dilution of the stock solution of the standard to track any drift in calibration during a run. Thirdly, random duplicates were run alongside samples to ensure that the digestion and sample preparation methods result in consistent measurements. This is not necessary if all samples are measured in duplicate or triplicate, however, in the analysis of trace or residual explosives where only very small amounts of sample may be analysed this may not be possible. There may only be the possibility of a single sample solution and so the digestion method should be well validated prior to the analysis of these samples.

If ICP-MS analysis is to be used in the future to create profiles for explosive samples, an in-house reference material should be developed for each type of material to ensure reliability and validity of the analysis of such materials. Ideal reference materials should be highly stable but have similar chemical and physical properties to the samples being analysed. As both KClO<sub>3</sub> and ETN are not as stable it would be better to select their more stable and less sensitive counterparts. For potassium chlorate a reference material of potassium perchlorate and for erythritol tetranitrate PETN could be selected.

#### 2.2.2.2 Data Analysis

Raw data was first examined to identify variables that provide no information i.e. elements below the limit of quantification for all samples. These may be removed prior to commencing the multivariate exploratory analysis as each variable included in the analysis requires additional computational power and time to perform. Therefore, any reduction of ineffectual data possible prior to the pre-processing and multivariate analysis should be undertaken.

The raw data was then investigated using a combination of HCA for the initial overview of potential clustering followed by PCA to explore the level of discrimination possible from the raw dataset. As this is a raw data analysis there will always be a high probability of outliers resulting in poor

discrimination due to the nature of PCA as previously discussed in the introduction. Therefore, a further elimination of these outliers was undertaken, and the analysis repeated.

A second PCA was then undertaken in a similar fashion to the analysis of spectral data, where prior to analysis a pre-processing method was utilised. In the case of elemental data, however, the pre-processing procedure was quite different. This dataset required pre-processing not to correct for physical phenomena effecting the true value of a measurement but rather to somewhat standardise the data due to the various elemental mass fractions having varying orders of magnitude across the dataset. This can be accomplished by a variety of methods, however, the method selected for this analysis is done through the use of a logarithmic transformation for elemental data which has been used for elemental data in other studies and seems well suited to this role. This method transforms an asymmetrically skewed dataset, such as in the case of trace element analysis, where some commonly abundant elements (e.g., K, Na, etc.) may be in far greater levels than other rarer elements (such as Ti, Pt, etc.). Taking the logarithm of heavily skewed data shrinks the distribution tail centralising the data and making it more symmetrically distributed as is ideal for PCA. 128,129

Prior to a log transformation the values require an initial translation by the scalar addition of a constant (in this case 1) as elements below the limit of quantification are reported as 0 ppb and the log of zero is undefined. Once the entire dataset is translated by 1 the log transformation can be undertaken and results in the null data reverting to zero as  $\log_{10} 1 = 0$ . This scalar addition is allowed as adding a constant value to a variable does not change the variance as the mean increases by the same amount<sup>130</sup>.

# 2.2.3 Infrared Spectroscopy (IR)

### 2.2.3.1 Sample Analysis

The IR spectrometer utilised was located at Flinders University and manufactured by Perkin-Elmer in the Frontier FTIR range. The system utilises a rotary Michelson interferometer resulting in a wavelength accuracy of  $\pm$  0.1 cm<sup>-1</sup> at 1600 cm<sup>-1</sup>, spectral resolution of 0.4-64 cm<sup>-1</sup> and a spectral range of 8300-350 cm<sup>-1</sup>. The attenuated total reflectance (ATR) sampling accessory was used however it must be noted that this may not be the correct procedure for all energetic materials due to the pressure and friction involved. The Spectrum Software Package<sup>131</sup> was used to export the raw data as well as some basic processing including the baseline correction and normalisation of the data.

The collection of the data involves cleaning the ATR crystal with an ethanol wipe, allowing to dry and collecting a background scan. A small amount of sample was then placed on the crystal (just enough to cover it, approximately 1 mg) and pressure carefully applied to an appropriate level. Data was then collected, the parameters selected were 32 scans between 600-4000 cm<sup>-1</sup> with a resolution of 1 cm<sup>-1</sup> in percent transmittance (%T) output mode. The number of scans was varied between 8, 16, 32, 64, 128 and 256 scans, however the resulting spectra for 32 scans were indistinguishable from any higher number of scans and takes approximately 15 minutes to complete rather than 30 mins or greater for no added information, consistency or higher resolution. Post data collection the sample may be retrieved from the crystal platform as this is a non-destructive analytical technique and therefore may be saved for further analysis.

### 2.2.3.2 Data Analysis

Raw data was initially examined in the standard manner, by visual inspection of the spectra, to confirm the identity of the material by comparing it to the spectra of known material. This examination also gives an overview of the variance in the dataset and identifies potential discriminatory signals within the material. Following this a hierarchical cluster analysis (HCA) is undertaken to identify the level of discriminatory variance within the dataset.

The dataset was then altered using a pre-processing stage prior to further exploratory data analysis of the dataset. There are many forms of pre-processing employed for the transformation of spectral datasets, with researchers selecting various procedures based on their specific dataset and the issues encompassed within it. Potential issues include; distinct outliers which will render PCA unusable as it will overshadow the rest of the variance within the dataset and uneven magnitudes of variance across variables which will reduce the equal comparison of all variables within a dataset reducing the effectiveness of the PCA. Many of the methods only slightly differ, all striving to accomplish the same goal and are rarely contrasted and compared to one another. A review article discussing this lack of comparison published in 2009 aimed to discuss and evaluate many of the most common preprocessing methodologies in the case of near-infrared spectral datasets<sup>132</sup>.

The goal of the pre-processing is to improve the quality and consistency of the data by minimising or removing physical phenomena within the data to enhance further multivariate statistical or exploratory analysis. This is not a substitute for collecting the highest quality of data possible, however, it can to some extent increase the quality of non-optimal data collection especially when

considering the quality of the instrument employed. In the case of spectral datasets, it must be noted that no level of pre-processing can correct for specular reflectance (direct scattering) and any spectra significantly affected by this phenomenon must be removed as outliers prior to multivariate analysis.

In the case of this project's infrared spectra, the pre-processing involves two key steps. Firstly, a polynomial baseline correction was performed for all spectra. Secondly, a normalisation of each spectrum to the largest common signature peak across all spectra in the dataset. This is a very minor pre-processing procedure as one the goals of this project was to investigate the application of a standard process to a variety of spectral datasets and a major disadvantage of increasing the pre-processing model complexity will begin to reduce the robustness of the model for predictions of additional datasets. There is also the possibility of valuable variability to be lost the more the data is transformed or manipulated prior to multivariate analysis. The initial baseline correction will adjust the baseline of each spectrum to mitigate systemic variability due to the device used to collect the data. Normalisation is a scatter correction method designed to reduce the physical variability between samples due to scatter and adjusts for baseline shifts between samples. This will allow for a greater level of consistency between spectra and enable much more suitability for direct comparison which is vital when a mathematical approach such as PCA is utilised.

PCA is performed to interrogate and reduce the dimensionality of the dataset to identify discriminatory areas of the spectra and determine any level of clustering within the samples.

### 2.2.4 Raman Spectroscopy (Raman)

#### 2.2.4.1 Sample Analysis

The bench-top Raman used was located at Flinders University manufactured by DeltaNu in their Advantage series. The system utilises a 633 nm 3 mW HeNe laser with a spectral resolution of 5-7 cm<sup>-1</sup> and spectral range of 200-3400 cm<sup>-1</sup>. Baseline removal was employed through the NuSpec<sup>133</sup> program then exported in printable file format (.prn) for Microsoft Excel compatibility.

Minimal sample preparation is required as the explosives are placed in a 5 mm diameter vial and inserted into the Raman spectrometer. Depending on the sample, a delay timer may be set allowing the user to create some distance between themselves and the analysis if there are concerns for safety surrounding potential laser induced initiation.

Prior to the data collection of each sample the signal is tuned to maximise the signal to noise ratio by setting a survey scan, the sample vial is rotated and its distance from the laser source manipulated. Once this optimised position is located the data is collected with a 10 s integration time over the range 200-3400 cm<sup>-1</sup>.

Due to failure of the DeltaNu spectrometer data collection for ETN samples required the use of a different instrument. The Raman spectra were recorded between -199 and 4000 cm<sup>-1</sup> on a XploraRA Horiba Scientific Confocal Raman microscope using a 50× objective (numerical aperture 0.6) at an excitation wavelength of 786 nm and using a grating of 600 gratings min<sup>-1</sup>. The acquisition was 6 accumulations of 20 s integration times. The instrument was calibrated to the 520.7 cm<sup>-1</sup> line of silicon and an additional spectrum was collected at a laser wavelength of 532 nm to confirm the spectrum recorded at 786 nm.

Sample preparation involved placing a very small amount of sample (barely visible) onto a glass microscope slide and placing it under the lens of the microscope. The sample platform is then moved to place a small indicator light from the microscope on to the sample then further fine translations are done using the microscope camera to ensure a good positioning. The focus was then adjusted by moving the sample closer or further away from the lens for maximum signal to noise ratio. Once the signal was optimised the acquisition was conducted and the sample removed. Though the power level of the laser is much greater than in the case of the DeltaNu spectrometer this is still a non-destructive technique and so the sample may be reclaimed. This may not be the case for all energetics, especially mixtures where laser sensitivity may be heightened and therefore caution must be used prior to using full power on any sample and slowly increased for greater levels of signal.

#### 2.2.4.2 Data Analysis

The analysis of this dataset was be identical to the IR spectroscopy method as the spectral datasets are highly similar.

## 2.2.5 Terahertz/Far-Infrared Spectroscopy (THz/Far-IR)

All measurements were taken at the THz/Far-IR Beamline at the Australian Synchrotron with samples of explosives provided by Forensic Science Service, Victoria Police. This synchrotron project was also in collaboration with the French-German Research Institute of Saint-Louis and conducted in three stages.

The initial experiments involved developing a method to consistently prepare non-energetic samples through the pelletisation of materials into thin film 3 mm diameter pellets of polyethylene (PE) and/or wax. These findings were used to prepare explosives and ingredients for analysis and to collect high resolution spectra of both explosives and potential packaging materials (various plastics and paper). Following this, an investigation utilising the recent additional capability of the THz/Far-IR beamline to be able to collect Far-IR spectra using an out-of-vacuum ATR accessory was undertaken.

The materials investigated throughout included the following:

- Explosives and ingredients
  - o RDX
  - HMX
  - o PETN
  - $\circ$  AN
  - o KClO₃
  - Hexamethylene triperoxide diamine (HMTD)
  - o UN
  - Nitrourea (NU)
- Precursors
  - Hexamine
  - Erythritol
  - Urea

All these materials were sourced in a powdered form and as the samples for the initial experiments prior to the availability of the ATR accessory required mounting onto a sample holder and placed under vacuum these powders had to be pelletised. Initially PE pelletising methodology was developed by altering the ratio of sample to PE and it was found that the optimal amount of sample was 15-25% by weight. Typically, 1.5 mg of the sample/PE mixture is pelletised using a PIKE Technologies hand pelletiser (further details below). Similar methodology was used with paraffin wax as the matrix material and the same ratio was selected to provide a strong signal without saturation. This was performed with samples of precursor materials only as the first set of experiments did not involve the direct use of explosives.

The developed method was then applied to the pelletising of explosives. However, the previously optimised methodology was not robust and applicable to all the explosive materials as there were significant absorption differences between materials. For example, RDX and HMX absorb 60% of the THz radiation at a 1:1 sample:PE ratio. However, the same ratio of PETN:PE will only absorb 10% of the THz radiation producing a far weaker peak intensity in the resultant spectrum. Therefore, the

methodology was modified increasing the percentage of sample in PE to between 25-50% depending on the material. PE was chosen over paraffin wax due to the difficulties involved with handling wax as it tended to have adhesive properties.

The pellets were pressed with a PIKE Technologies Hand Press using a 3 mm die set. These pellets were then mounted into a three-position sample mount and placed onto a Cryostat (Janis Research) and mounted to the sample compartment of the Bruker IFS 125HR FTIR spectrometer. Though mounted on the cryostat, the heating and cooling functions were not utilised for any of this research; it was just used as a sample holder. The compartment was then evacuated to approximately 10<sup>-3</sup> mbar and the beamline from the synchrotron was opened. The system utilises a Michelson interferometer with an optical path length of 942 cm and resolves linewidths of <0.0009 cm<sup>-1</sup> over a broad spectral range of 5 cm<sup>-1</sup> (Far-IR) to >50,000 cm<sup>-1</sup> (UV). The detector used was a liquid nitrogen and helium cooled Si Bolometer with a 6 μm Multilayer Mylar beam splitter and data was processed through the Bruker software package OPUS<sup>134</sup>. The data processing for pelletised samples involved the averaging of 10 spectra, subtracting the background and converting these averaged spectra to absorbance spectra. The spectra are then cropped to between 30-650 cm<sup>-1</sup> as this is the optimum window utilising the chosen detector and PE as the pelletising material. This data was exported into a data point table (.dpt) format for compatibility in Microsoft Excel.

The third set of experiments with the beamline involved collecting the spectra of the same materials with the new GladiATR<sup>TM</sup> Single Reflection ATR Accessory mounted onto the sample compartment of the Bruker IFS 125HR FTIR spectrometer. For this analysis a very small amount of sample is placed to cover the top of the crystal (<1 mg), the anvil is positioned on top and lightly screwed down to ensure good contact between the diamond and the sample. After data collection, an extended ATR correction was applied through OPUS to account for the difference in refractive indices between sample and diamond. Though refractive index is referred to as an optical constant it does vary depending on the wavelength of light due to optical dispersion and this has been studied for explosives.<sup>135</sup> The mean refractive index was used for each material to apply the ATR correction. This then allowed the development of a spectrum from the THz/Far-IR region all the way through to the near-IR region by combining the THz/Far-IR spectrum with the mid- to near-IR spectrum collected using a standard FTIR instrument. To do this the spectra were normalised to a common peak recorded in both spectra in the 600-650 cm<sup>-1</sup> region.

# 3. Initial Development of Data Analysis and Fusion Methodology

In this chapter the data from a past project<sup>9</sup> was re-examined to develop a suitable data pre-processing method to combine IR-MS and ICP-MS data. The resultant data was analysed using the exploratory multivariate data analysis technique, PCA, to assess the suitability and success of the pre-processing employed. The PCA results were then used to identify any information that may be valuable for intelligence gathering purposes. This includes any information that may indicate a link between sample and precursor.

# 3.1 Background

Data collected as part of a past research conducted by Dr Paul McCurry at Flinders University and the Centre of Expertise in Energetic Materials in 2015 was re-examined to test and develop the initial chemometric analysis utilising principal component analysis. The thesis titled "The use of Advanced Analytical Techniques to Enable Batch and Source Matching of Homemade Explosives" aimed to highlight the use of IR-MS and ICP-MS for the provision of chemical intelligence in the analysis of HME. The materials analysed were ammonium nitrate and calcium ammonium nitrate (CAN) based HME samples and ingredients (i.e. without a fuel component). The research successfully identified the potential of IR-MS and ICP-MS to contribute chemical intelligence in an investigation showing there was discriminatory information within the collected data which may be able to link batches of HME to sources. Though successful, one major limitation was identified and that was the way the collected data was analysed, specifically surrounding ICP-MS data analysis and the combination of IR-MS and ICP-MS datasets.

# 3.2 IR-MS Data of AN and CAN Samples

The IR-MS data collected included both carbon and nitrogen isotope ratios, however, not all ammonium nitrate samples contained significant amounts of carbon and therefore the isotopic ratio could not be obtained for all samples. The samples that contained sufficient carbon were typically CAN, which have enough carbon from the calcium carbonate content, or prilled AN that were coated with carbon containing substances in order to mitigate against the high hygroscopicity of AN and improve storage life.

The data was then displayed by plotting the carbon delta values against the nitrogen delta values (Figure 3.1).

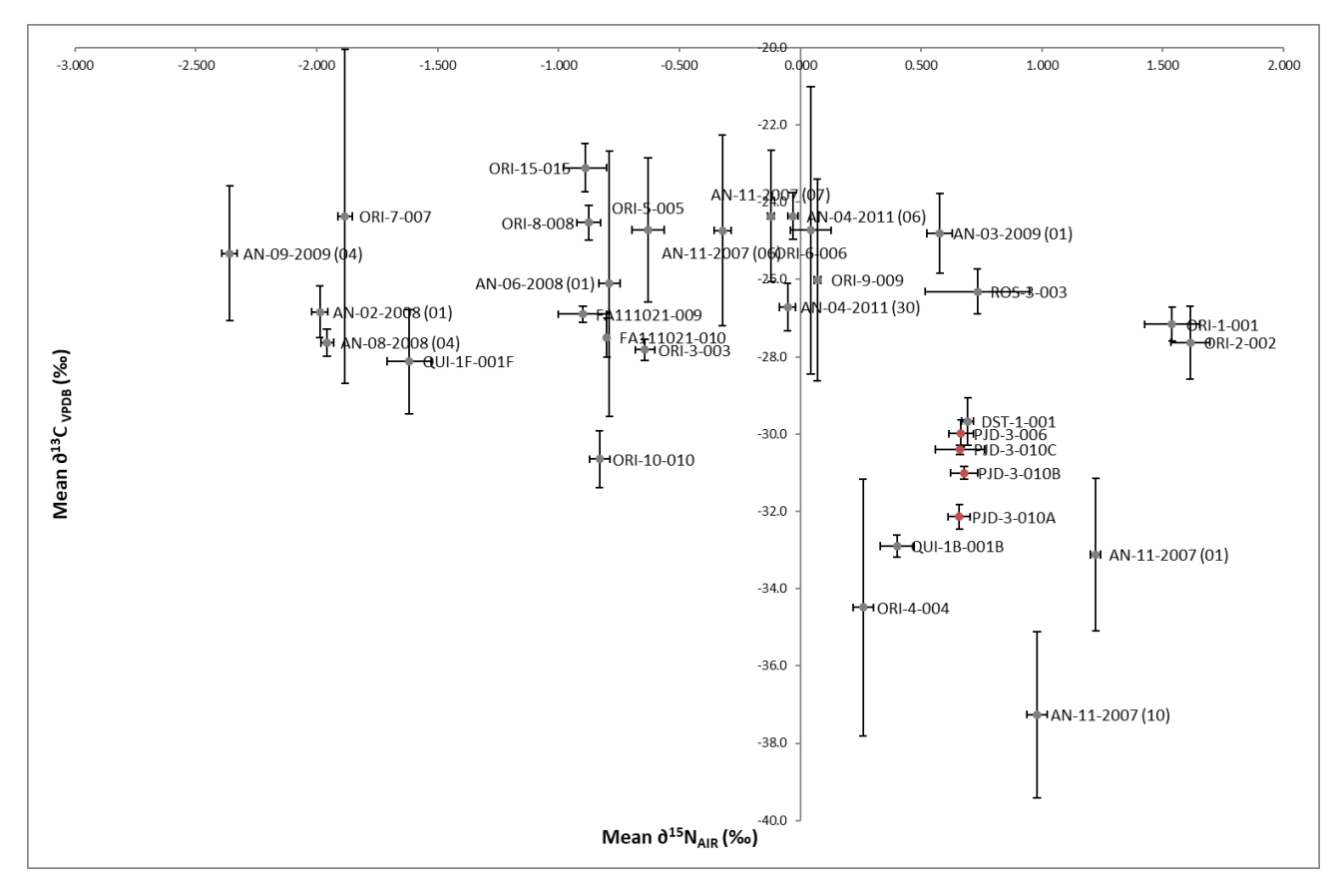


Figure 3.1: IR-MS data plotted as carbon delta values vs nitrogen delta values.

These results could identify some minimal groupings and clustering but there is a clear lack of reliable discrimination between samples of differing origin. The two-dimensional nature of the data means this is the optimal presentation of such data and a chemometric approach could not provide an improvement from this dataset alone. There was, however, an opportunity to incorporate this into the larger ICP-MS dataset also collected from the same samples, effectively combining the discriminatory power of both datasets.

# 3.3 ICP-MS Data of AN and CAN Samples

The original dataset collected is from the quantitative trace metal analysis of 66 ammonium nitrates sampled from numerous countries for 32 elements, as well as, calcium ammonium nitrate, aluminium powders and mock HME samples from DST Group. These results were then displayed in the form of radar plots in order to graphically display a multivariate dataset to allow direct visual comparisons between samples. Though radar plots do allow a visual comparison to some extent, it is clear upon

examining such a method of display that it is hard to interpret the level of discrimination between any two given samples. For example, below in Figure 3.2 four of the resultant radar plots are displayed side by side and though it can be confidently concluded that each sample is different the level of difference or similarity is hard to determine and impossible to quantify. This issue is compounded when hundreds of samples are compared to one another as would be the case in a real-world database.

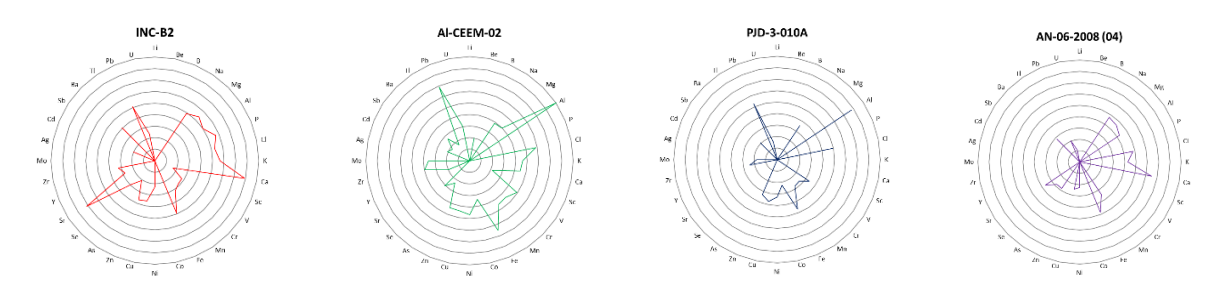


Figure 3.2: Example of ICP-MS data depicted in the form of radar plots for discriminating between samples.

This limitation highlights the need for more post collection data analysis and this analysis must be able to handle large datasets of a multivariate nature. Therefore, a chemometric method was required. Principal component analysis was selected over linear discriminant analysis and partial least squares regression due to the exploratory and unsupervised nature of the analysis being fit for purpose. As the real-world application of this research is intelligence gathering, when a new sample is being investigated and there is no viable way to assign it to a grouping prior to statistical analysis an exploratory and unsupervised analysis is ideal. This is particularly the case when identifying information about the sample has been redacted for security reasons due to the lack of security clearance possessed by the analyst.

# 3.4 Chemometric Analysis of AN/CAN Datasets

# 3.1 Exploratory Multivariate Data Analysis of Raw Data

The first step of any chemometric analysis is determining if any pre-processing of the original data is required. This requires a sound understanding of both what the data means and how the selected statistical analysis handles data. In this case the data consists of the quantifiable trace elements present within each sample as well as carbon and nitrogen isotope ratios. Keeping these raw datasets in mind, issues can immediately be identified with the application of PCA:

- 1. The trace element analysis included a large number of target elements that were below the limit of quantification and as PCA will not handle data with non-numerical values this must be altered.
  - This can be mitigated by simply replacing these "not a number" or NaN fields to zero
    as this effectively indicates that there was not a significant amount of the element
    present.
- 2. After the replacement of NaN fields with zero values, various elements can be identified as undetected in all samples.
  - As they contributed nothing to the variance of the dataset they may be removed.

    This included the elements: Li, Be, Cr, Mn, Co, Ni, Cu, Se, Y, Mo, Cd, Sb, Tl and U.
    - i. Though this was the case for all the samples in this dataset, subsequent analysis of authentic samples of CAN and CAN-based HMEs revealed that many of these elements were present. Therefore, these elements can still be valuable forensic markers just not across these specific samples.
- 3. The ratios of the stable isotopes of an element are represented as delta values from universally accepted reference standards and therefore may be negative or positive values, meaning any value is considered a measurement. Therefore, unlike in the ICP-MS case unmeasurable samples cannot simply be reduced to zero as that would indicate a measurement.
  - The pre-processing resolution for this is to omit any samples with unrecorded data, however, as this was the majority of samples the carbon isotope ratios will be omitted from the PCA analysis to retain sample size over the addition of one potentially discriminatory variable.

After these pre-treatments the dataset had no clearly identifiable issues and therefore a PCA may be undertaken.

This initial analysis concluded that out of the original 34 elements and nitrogen delta values, 8 trace element measurements were responsible for 99.96% of the original dataset's variance.

This is understood through the latent values of the PCA, by calculating the ratio of the cumulative sum and sum of latent values for each PC. This ratio reveals the amount of original variance retained in the transformed data. The latent variable table (Table 3.1) shows that the original data was

transformed into 19 principal components, however, many are irrelevant as the original dataset's variance has been accounted for prior to that point. This may be plotted in the form of a scree plot (Figure 3.3).

Table 3.1: Latent variable table.

Principal	Latent	Percentage				
Component						
PC1	4223281.96	72.37				
PC2	927654.87	88.27				
PC3	337222.11	94.05				
PC4	283803.67	98.91				
PC5	42996.85	99.65				
PC6	10914.96	99.83				
PC7	7296.62	99.96				
PC8	1719.18	99.99				
PC9	348.37	99.99				
PC10	239.52	100				
PC11	97.39	100				
PC12	35.46	100				
PC13	3.26	100				
PC14	1.68	100				
PC15	0.80	100				
PC16	0.68	100				
PC17	0.23	100				
PC18	0.11	100				
PC19	0.01	100				

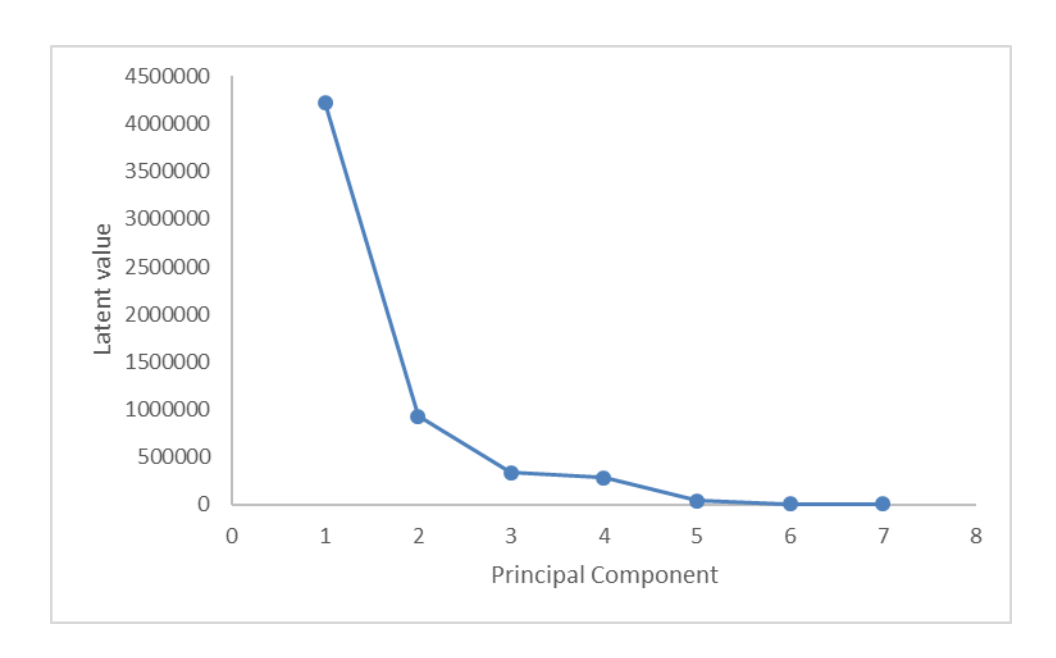


Figure 3.3: Scree plot for the raw data PCA.

An additional consideration to determine the significant number of PCs other than the shape of a scree plot, is to limit the PCs to the point where measurement variance is incorporated into the model. In this case, the ICP-MS measurements have an RSD of up to 3% and therefore, PCs could be taken into account until the cumulative variance retained reaches 97%. The IR-MS data also has an RSD of up to 5% however, in this current analysis the IR-MS data does not contribute to the early PCs.

The next stage of the analysis is to determine what is accounting for these first 7 principal components, which may be done through interrogating the coefficient values (Table 3.2). These coefficient values are commonly referred to loading factors or loadings and identify the variables contributing to each principal component as well as the magnitude of their respective contributions. This format is quite difficult to interpret so transforming it to highlight the important elements is helpful (Table 3.3).

Table 3.2: Raw coefficient values to 1 decimal place.

Element	PC1	PC2	PC3	PC4	PC5	PC6	PC7
N IR-MS	0.0	0.0	0.0	0.0	0.0	0.0	0.0
В	0.0	0.0	0.0	0.0	0.0	0.0	0.0
Na	0.0	-0.1	1.0	0.0	0.0	0.0	0.0
Mg	<b>1g</b> 0.0 1.0 0.1		0.1	-0.1	0.0	0.0	0.0
Al	0.0	0.0	0.0	0.0	0.1	-0.1	0.0
Р	P 0.0 0.1 0.0		0.0	1.0	-0.2	-0.1	-0.1

CI	0.0	0.0	0.0	0.0	0.1	0.0	0.0
K	0.0	0.0	0.0	0.0	0.0	-0.1	0.0
Ca	0.0	0.0	0.0	0.0	0.0	0.0	0.0
Sc	0.0	0.0	0.0	0.1	0.0	0.0	0.0
V	0.0	0.0	0.0	0.0	0.0	0.0	0.0
Fe	0.0	0.0	0.0	0.0	0.3	-0.3	0.2
Zn	0.0	0.0	0.0	0.0	0.0	0.0	0.0
As	0.0	0.0	0.0	0.1	0.0	0.3	1.0
Sr	1.0	0.0	0.0	0.0	-0.1	0.0	0.0
Zr	0.1	0.0	0.0	0.2	0.7	0.7	-0.2
Ag	0.0	0.0	0.0	0.0	0.0	0.0	0.0
Ва	0.0	0.0	0.0	0.0	0.0	0.0	0.0
Pb	0.0	0.0	0.0	0.0	0.6	-0.6	0.1

Table 3.3: Coefficient table colour coded to highlight major contributors.

Element	PC1	PC2	PC3	PC4	PC5	PC6	PC7
N IR-MS							
В							
Na			1.0				
Mg		1.0					
Al							
Р				1.0			
Cl							
K							
Са							
Sc							
V							
Fe						-0.3	
Zn							
As						0.3	1.0
Sr	1.0						
Zr					0.7	0.7	
Ag							
Ва							
Pb					0.6	-0.6	

This colour coded table makes it much easier to understand which elements are contributing to each PC. To the 7<sup>th</sup> PC only Na, Mg, P, Fe, As, Sr, Zr and Pb are contributing significantly to the variance of the PCA. This information can be used to return to the original dataset to identify why these elements are causing discrimination between samples. To this end, a bar chart of the raw data for these elements has been plotted in Figure 3.4. This identifies that the reason for the overwhelming contributions is the large magnitudes of variation due to only a few outlier samples. The sole dependence of PC1 on Sr content is understandable as two samples, INC-B1 and INC-B2, have high relative concentrations of Sr in comparison to other samples which have little to none. The same reasoning applies to all of these elements with many samples having very little to no concentration of the element and one or more samples containing a very large amount. Outliers like this have a detrimental impact on the success of a PCA which has a purely mathematical approach and identifies these magnitude of order differences as the variables containing the most variance. This minimises any possible discrimination based on minor differences which could highlight trends rather than distinct outliers.

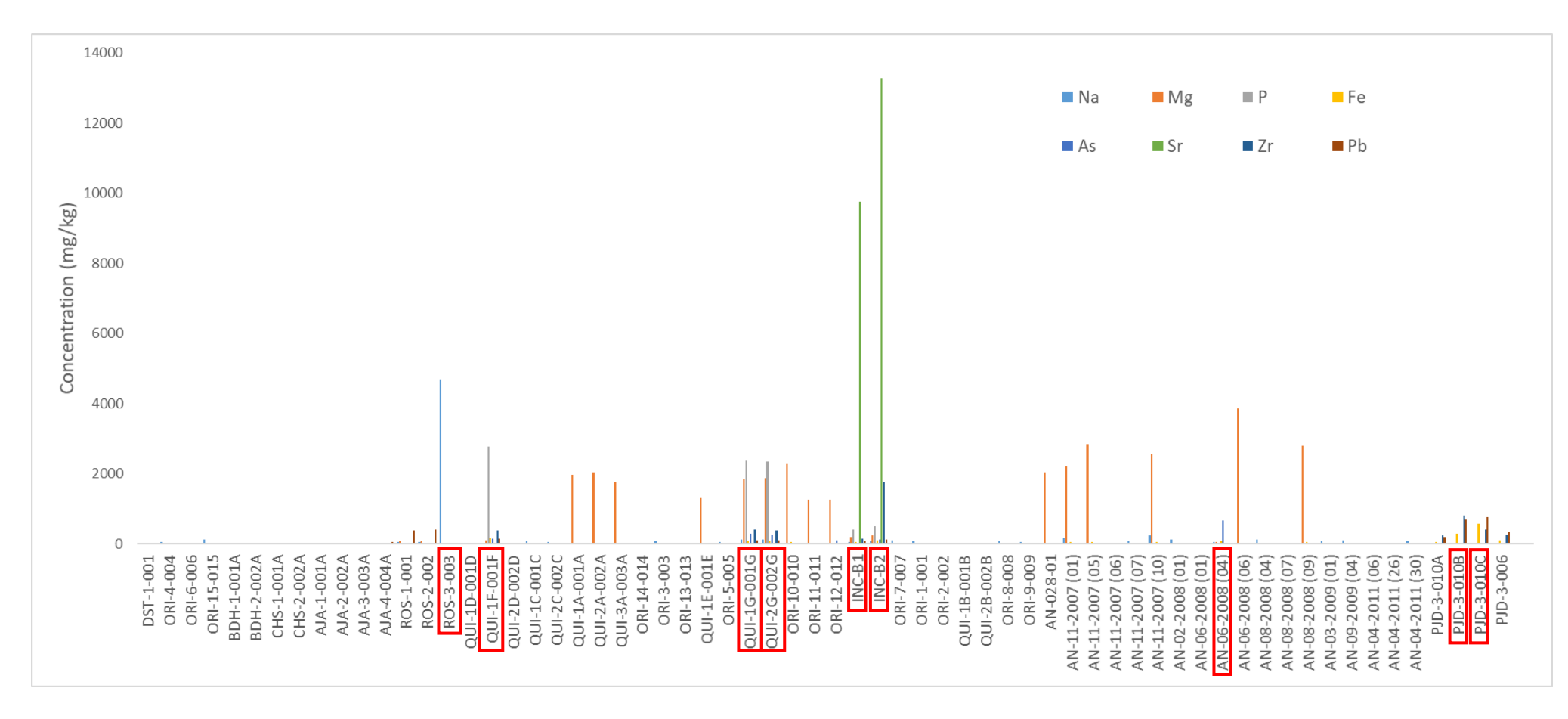


Figure 3.4: Bar chart of raw data for elements contributing to PC1-7. Red boxes highlighting outlier samples

This may be validated by calculating correlation coefficient values, to check if the lack of variance in the other elements is due to lack of data or a correlation in elements. It is quite evident that displaying the information in the form of Table 3.4 is not easily interpreted and so it may be transformed in a similar manner to Tables 3.2 and 3.3, as shown in Table 3.5. This involves bracketing the correlation coefficient values and colour coding from white to black: 0.0-0.25 (white), 0.26-0.50, 0.51-0.75, 0.76-0.95 and 0.96-1 (black). Only the magnitude of the value is considered in this transformation, as the sign indicates a positive or negative correlation. These brackets do not necessarily indicate anything other than forming a greyscale guide to highlight variables with strong relationships.

There are two strong relationships identified in this case with K, Ca and Sr correlating positively and Ag and Sc also positively correlating. The relationships between K, Ca and Sr are not uncommon as K-40 undergoes a beta decay to form Ca-40. When potassium levels are high, calcium tends to follow. The correlation between Ca and Sr is an unfortunate shortcoming of the original ICP-MS analysis undertaken, as Ca-44 was measured alongside Sr-88. Therefore, as Sr counts increased, so did Ca as doubly charged ions interfere with the selected Ca-44. This can be avoided by selecting a different isotope of calcium as doubly charged species cannot be entirely eliminated. This pair of correlations has then had a follow up effect of linking K to Sr, which again could have been avoided through the analysis of a different Ca isotope.

The relationship between Ag and Sc is more puzzling but indicates that within these samples, the concentration of the two elements follow each other. Knowing more about the samples could identify how it is that Ag and Sc have come to positively correlate. However, there is very little of either of these elements in the samples and so do not affect the PCA. Where this analysis could indicate a problem is where elements that do not typically correlate due to their similar properties have a strong relationship. This can arise for many reasons such as contaminations during sampling, handling and/or analysis. Another reason specific to trace element analysis is the digestion method not being suitable for certain elements. For example, gold requires the use of aqua regia as it requires HCl to remain stable in the digested solution. Whereas for other elements, such as silver, the presence of chlorine ions can lead to silver chloride precipitating out of solution.

Table 3.4: Correlation coefficient raw table.

	δΝ	В	Na	Mg	Al	Р	Cl	K	Ca	Sc	V	Fe	Zn	As	Sr	Zr	Ag	Ва	Pb
δΝ	1.00																		
В	-0.14	1.00																	
Na	0.01	0.00	1.00																
Mg	-0.04	0.16	-0.06	1.00															
Al	0.02	-0.07	-0.05	-0.14	1.00														
Р	0.01	-0.07	-0.01	0.15	-0.06	1.00													
Cl	-0.10	0.02	-0.20	0.11	0.39	0.17	1.00												
K	0.04	-0.04	-0.01	-0.03	-0.05	0.16	0.69	1.00											
Ca	0.05	-0.06	-0.01	-0.03	-0.05	0.18	0.68	1.00	1.00										
Sc	0.07	-0.07	-0.01	0.21	-0.06	0.94	0.26	0.23	0.26	1.00									
V	0.04	-0.09	-0.04	-0.05	0.88	0.25	0.42	0.02	0.03	0.26	1.00								
Fe	0.02	-0.04	-0.05	0.02	0.75	0.22	0.40	0.11	0.10	0.18	0.60	1.00							
Zn	0.14	-0.14	-0.05	0.07	0.50	0.52	0.60	0.45	0.47	0.65	0.58	0.68	1.00						
As	0.19	-0.07	-0.02	0.07	-0.06	0.47	0.20	0.11	0.12	0.51	0.10	0.14	0.28	1.00					
Sr	0.03	-0.05	-0.01	-0.05	-0.04	0.11	0.69	0.98	0.98	0.19	0.01	0.10	0.42	0.08	1.00				
Zr	0.04	-0.09	-0.03	-0.03	0.38	0.37	0.72	0.63	0.61	0.43	0.44	0.49	0.64	0.23	0.69	1.00			
Ag	0.12	-0.05	0.00	0.26	-0.05	0.75	0.13	0.01	0.06	0.91	0.25	0.10	0.59	0.47	-0.03	0.22	1.00		
Ва	0.10	0.17	0.01	0.27	-0.07	0.18	0.55	0.64	0.62	0.26	0.01	0.12	0.33	0.15	0.65	0.55	0.13	1.00	
Pb	0.18	-0.11	-0.04	-0.14	0.82	0.10	0.35	0.06	0.05	0.08	0.69	0.81	0.61	0.00	0.05	0.45	0.05	0.00	1.00

Table 3.5: Correlation coefficient colour coded table.

	δΝ	В	Na	Mg	Al	Р	Cl	К	Ca	Sc	V	Fe	Zn	As	Sr	Zr	Ag	Ва	Pb
δΝ			· L		· L	l	I	I.	I	I.	l		l		· L	LEGEND			L
В				_												0.00	0.25		
Na					_											0.26-	0.50		
Mg						_										0.51-	0.75		
Al							•									0.76-	0.95		
Р																0.96-	1.00		
Cl																			
K																			
Ca											•								
Sc												-							
V													_						
Fe														-					
Zn															_				
As																			
Sr																			
Zr																		•	
Ag																			
Ва																			
Pb																			

Now that this necessary analysis is completed, the resultant score values may be utilised to produce plots to examine groupings of elements (Figures 3.5 to 3.10) and judge if the data transformation by PCA is acceptable. Though many of the PCs may be examined as they cover various elements, this report will show plots between PC1 through PC3, as these contain almost 95% of the original variance contained within the dataset.

Plotting the data exposes that the resultant PCA was ineffective highlighting the major drawback of PCA, as outliers have caused poor separation of the remainder of the samples as shown in Figures 3.5 to 3.7. These outliers have been removed by omitting the data points from the samples in Figures 3.8 to 3.10. However, they have already negatively impacted on the PCA. The removal of the outliers' post analysis does not remove the variance that these samples accounted for, and hence the variance between the other samples has been overshadowed due to the order of magnitude of separation between the outliers and other samples. This can be fixed by removing those outlier samples prior to a PCA to perform a more effective PCA.

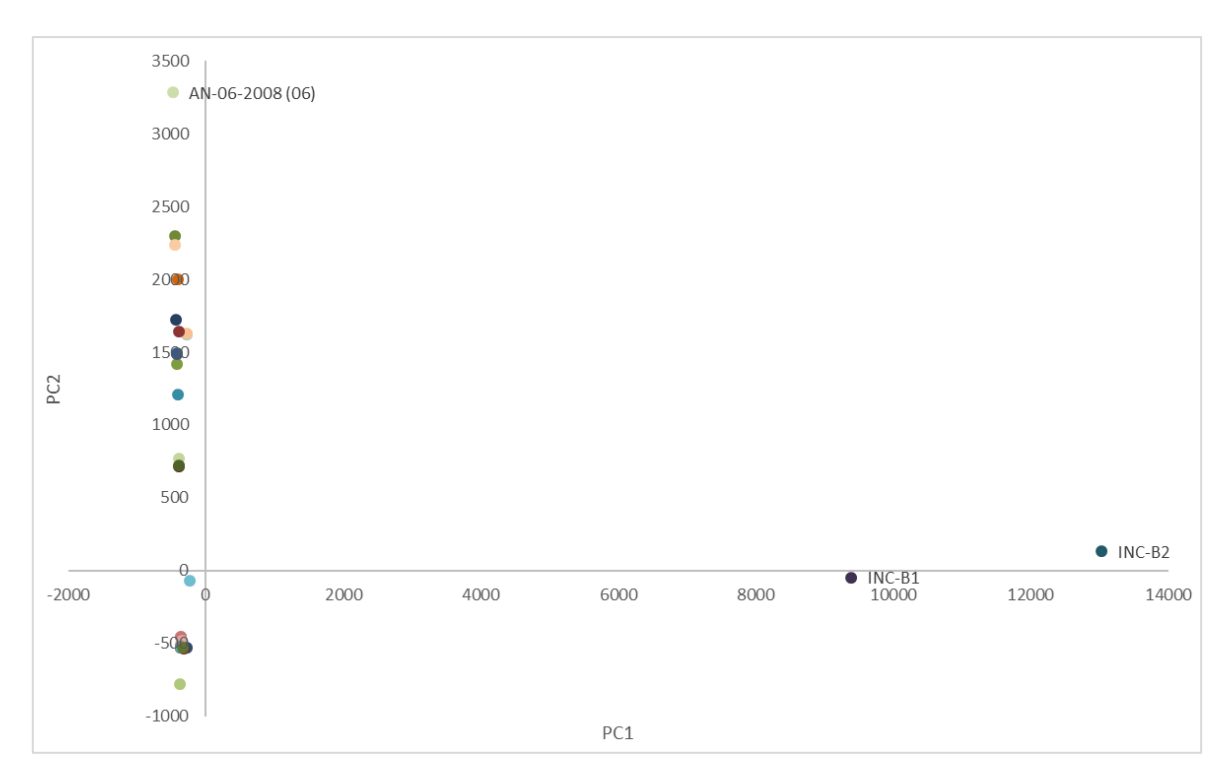


Figure 3.5: PC1/PC2 score plot for all samples.

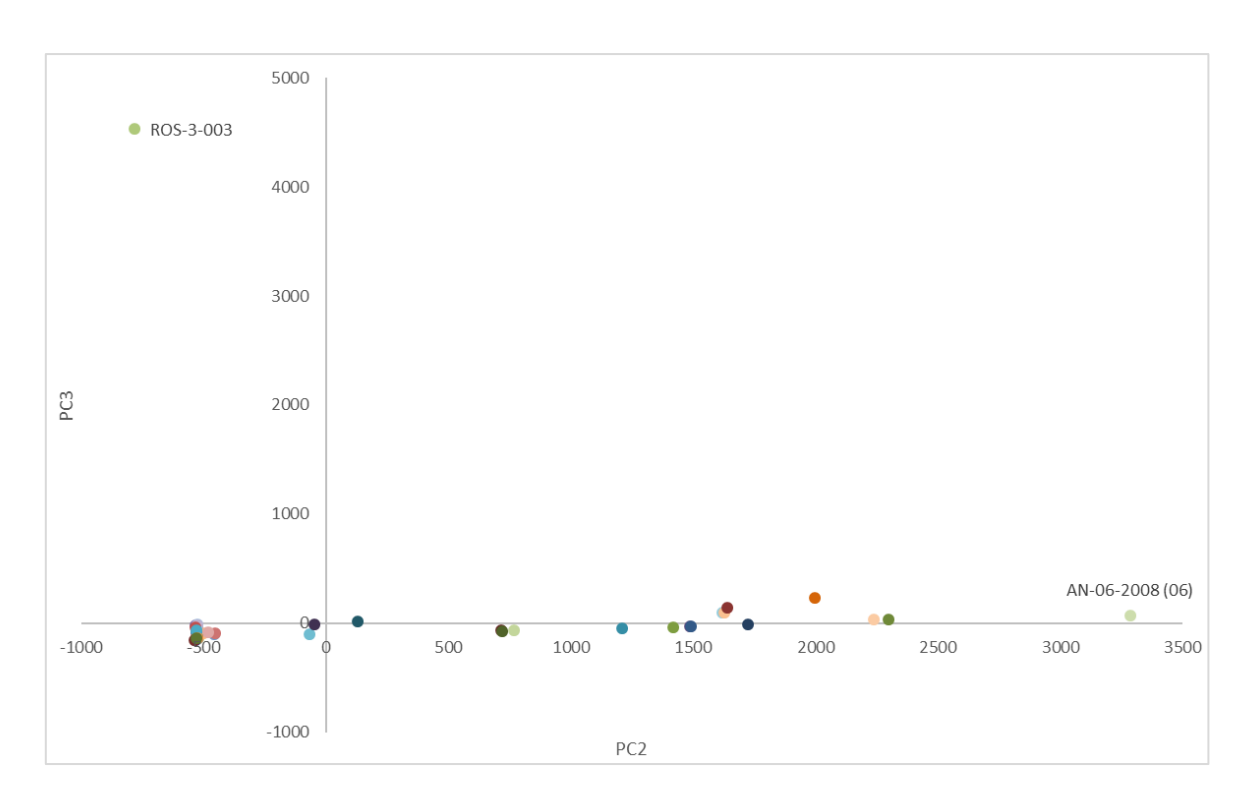


Figure 3.6: PC2/PC3 score plot for all samples.

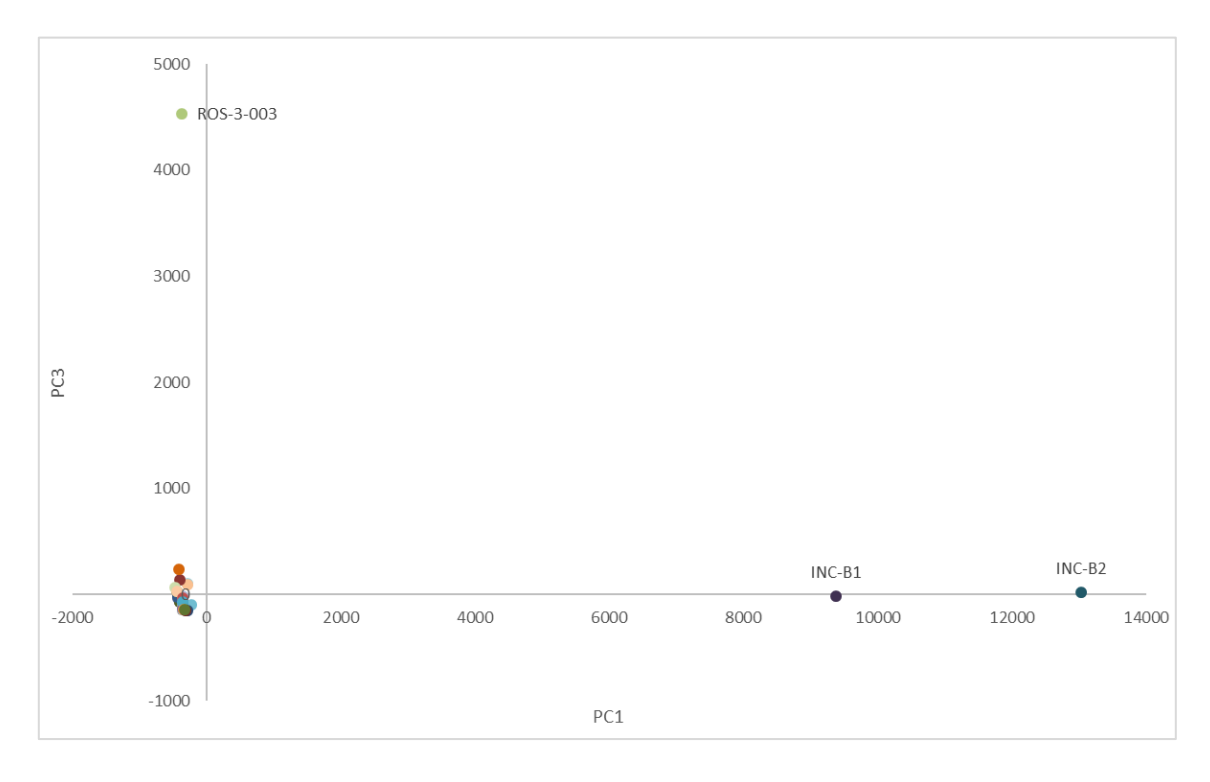


Figure 3.7: PC1/PC3 score plot for all samples.

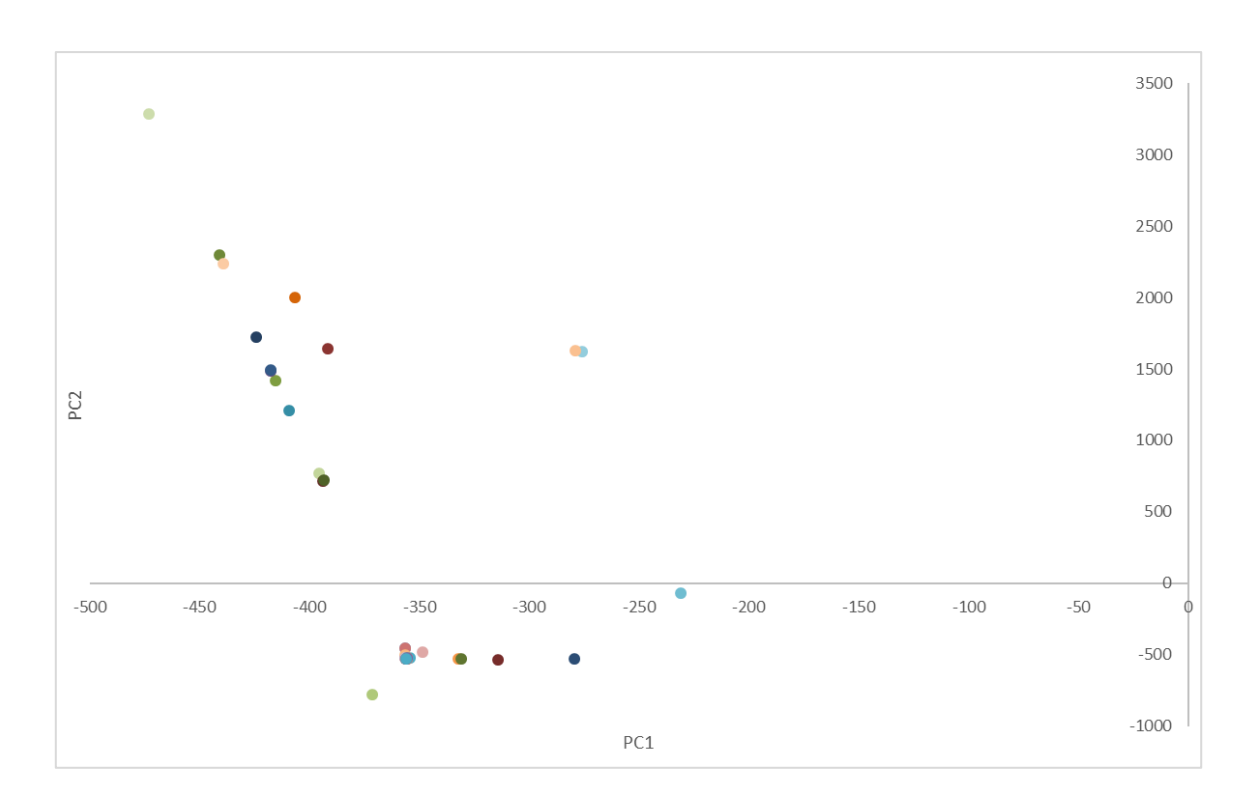


Figure 3.8: PC1/PC2 score plot after outlier omission.

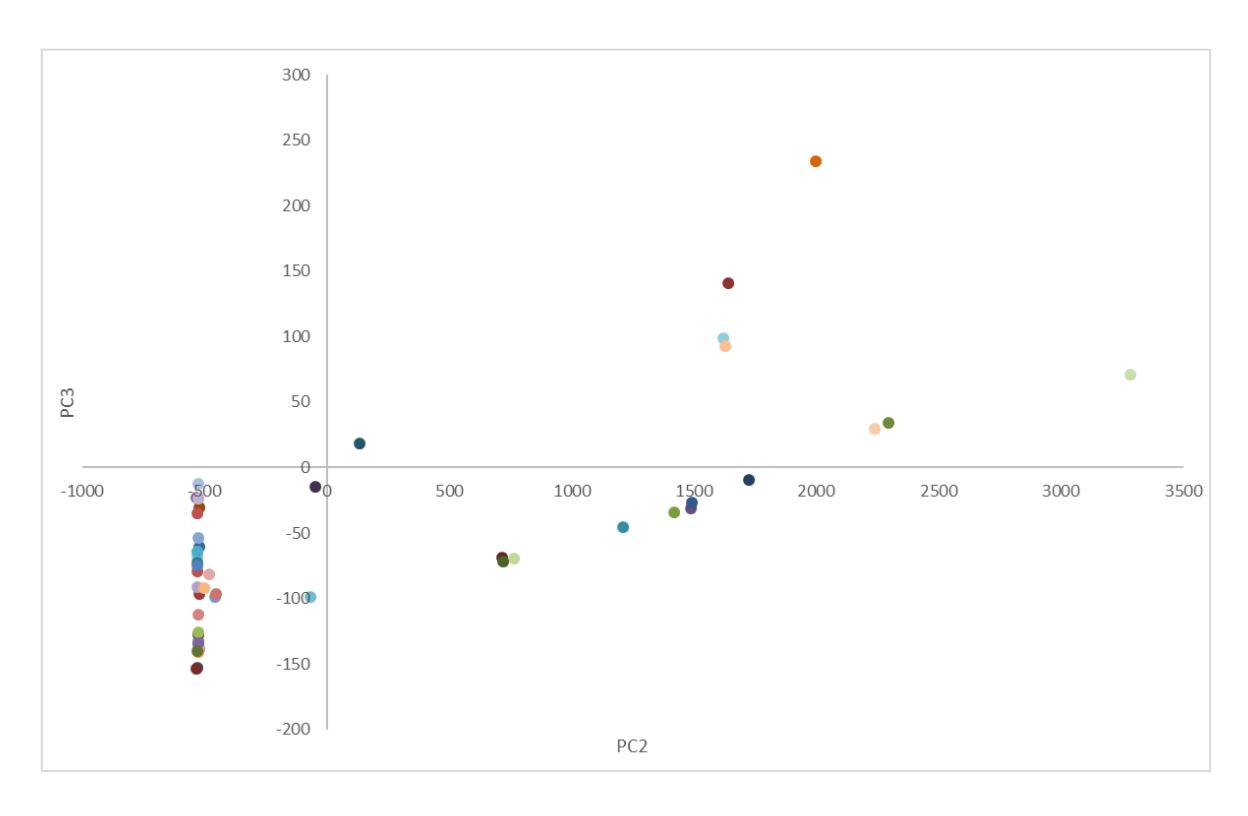


Figure 3.9: PC2/PC3 score plot after outlier omission.

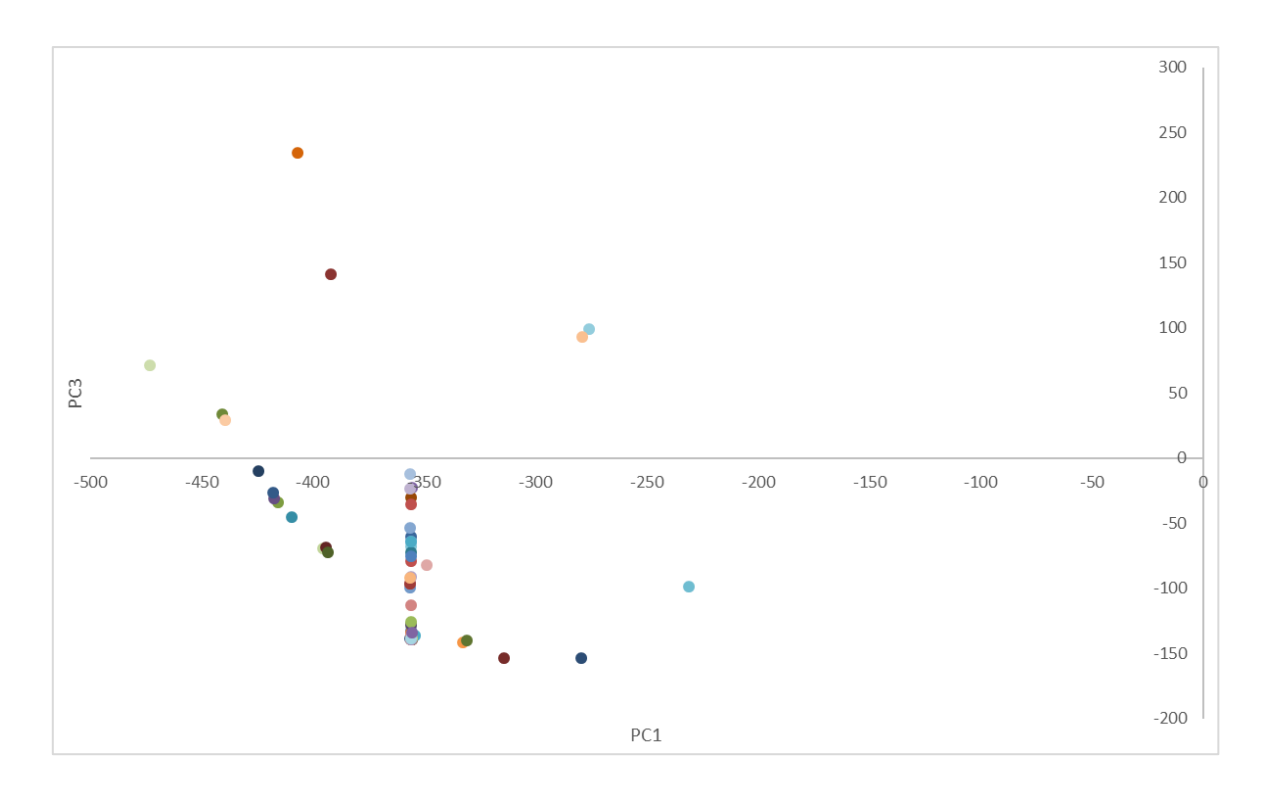


Figure 3.10: PC1/PC3 score plot after outlier omission.

## 3.2 Data Analysis Following Removal of Outliers in Raw Data

The same analysis was repeated after the removal of the previously identified outlier samples: ROS-3-003, QUI-1F-001F, QUI-1G-001G, QUI-2G-002G, INC-B1, INC-B2, AN-06-2008 (04), PJD-3-010B and PJD-3-010C. These were marked on the bar chat in Figure 3.4 and have been removed for various reasons. ROS-3-003 had orders of magnitude more sodium than any other sample; QUI-1F-001F, QUI-1G-001G, QUI-2G-002G, INC-B1 and INC-B2 all had high levels of phosphorus whereas all other samples did not record any; AN-06-2008 (04) contained a large amount of arsenic only rivalled by the previous group of outlier samples, whereas all other samples did not contain any arsenic. Lastly both PJD-3-010B and PJD-3-010C had elevated levels of iron, an order of magnitude greater than other samples. Some elements as a result no longer have any measured values and so have also been removed including the elements P, Sc and Ag.

Although these samples have now been removed from the dataset as outliers, this is a valuable piece of information, as they have been identified as being greatly different from the remaining samples. This effectively discriminates them and as mentioned, relationships between these samples exist clustering them and identifying why they cluster. The issue is that the level of discrimination is so great it minimises the smaller differences between the other samples.

Prior to discussing the final score plots, it is vital to gain an overview of the process. Examining the Latent variable table, 99.4% of the original variance is contained within the first 3 principal components in contrast to the 94.1% of the first analysis. This shows that the few outliers that existed within the first analysis did greatly affect the results of the PCA.

Table 3.6: Latent variable table.

	Latent	Percentage
PC1	771476	97.28
PC2	8908	98.40
PC3	8059	99.41
PC4	2487	99.73
PC5	1826	99.96
PC6	193	99.98
PC7	93	99.99
PC8	20	100.00

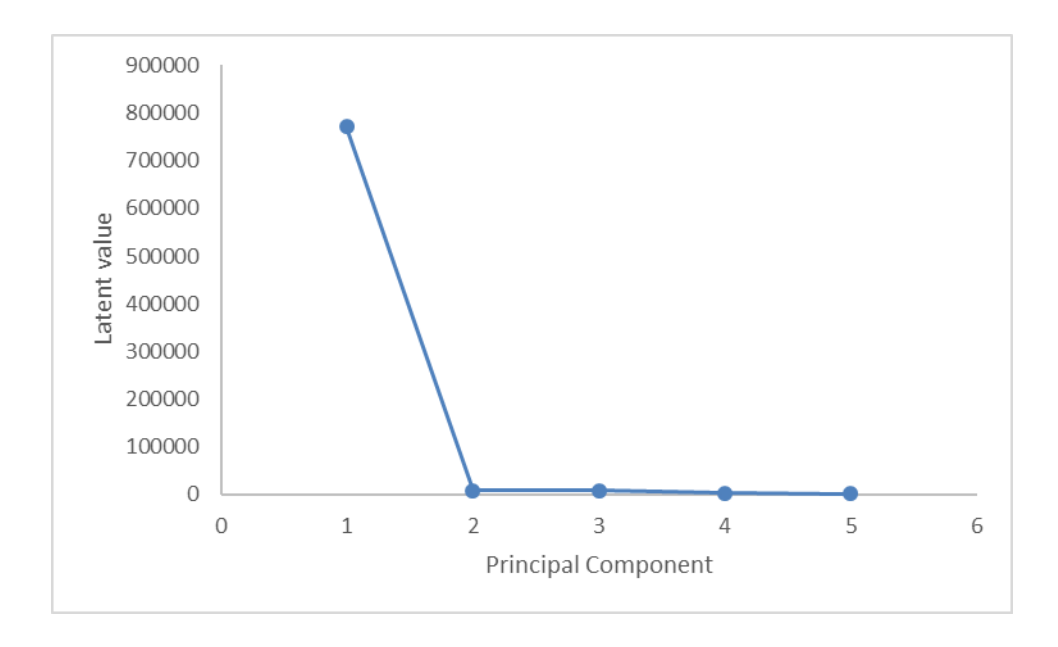


Figure 3.11: Scree plot for the PCA after outlier removal.

The coefficient or loadings Table 3.7 reveals that only 5 elements contribute to the first 3 PCs and it must be noted that magnesium is the sole contributor to PC1. Such a result indicates that magnesium has a very large variance within this reduced dataset. Although this is a positive as it indicates that it does have discriminatory power, it is also a red flag that it is an outlier element.

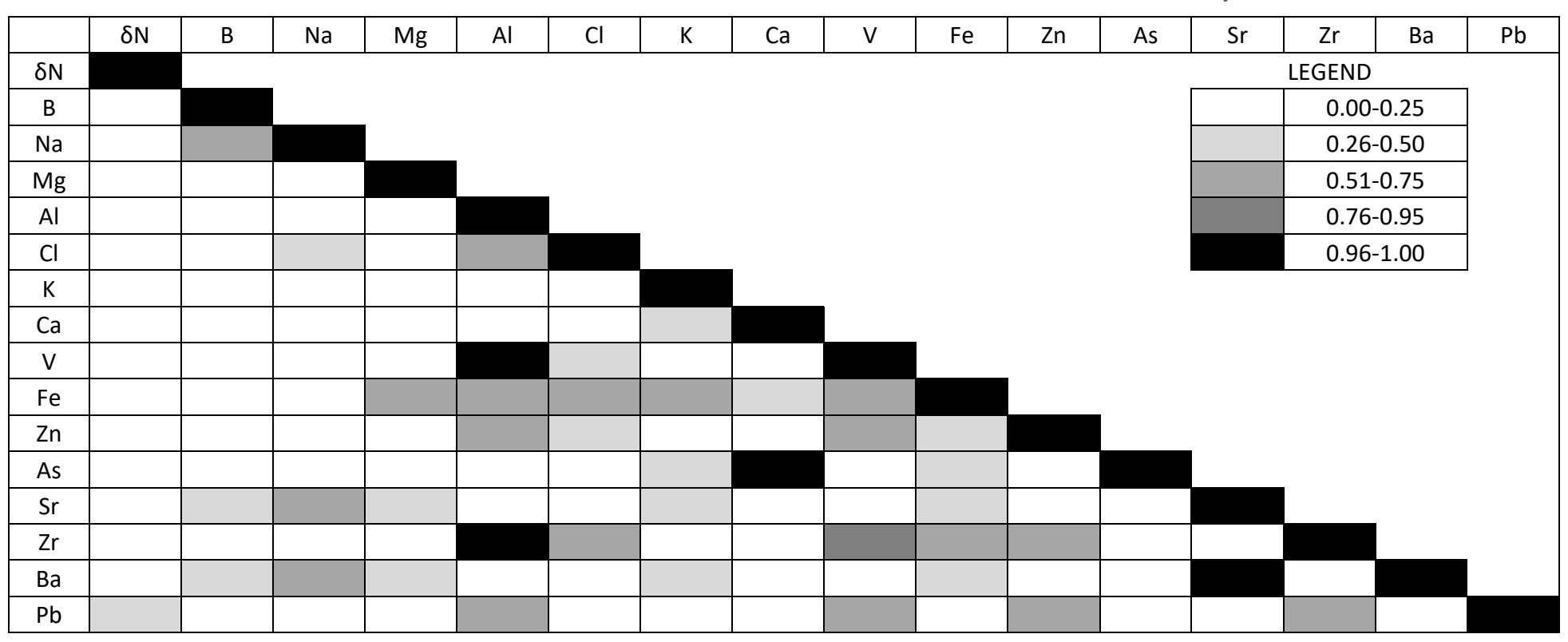
This can be confirmed by interrogating the score plots containing PC1 (such as Figures 3.12 and 3.13) and in doing so, it is apparent that there is a small group of samples that have strongly diverged from the bulk of the samples, predominantly samples categorised as "ORI" and "QUI" as well as a single "AN" sample. Although this can lead to the conclusion that these samples are effectively discriminated using PC1, all the remaining samples are then compressed into an indistinguishable cluster and 97% of the total variance of the dataset is assigned to just magnesium.

This highlights a clear issue with utilising PCA on raw data as elements are present in unequal magnitudes, and so more should be done to transform the original data to not strongly favour one element over the rest, to gain the most out of the data. This is referred to as skewed data in a multivariate dataset, where variables are not naturally distributed.

Table 3.7: Coefficient table colour coded (figures included for magnitude).

PC1	PC2	PC3	PC4	PC5
			0.98	0.12
1.00				
				0.26
				0.24
		0.13		0.23
	-0.58	0.80		
	0.27	0.20	-0.11	0.82
	0.76	0.53		-0.36
		-0.58 0.27	1.00  0.13  -0.58  0.80  0.27  0.20	0.98 1.00  0.13  -0.58 0.80  0.27 0.20 -0.11

Table 3.8: Correlation coefficient colour coded table for outlier removed data analysis.



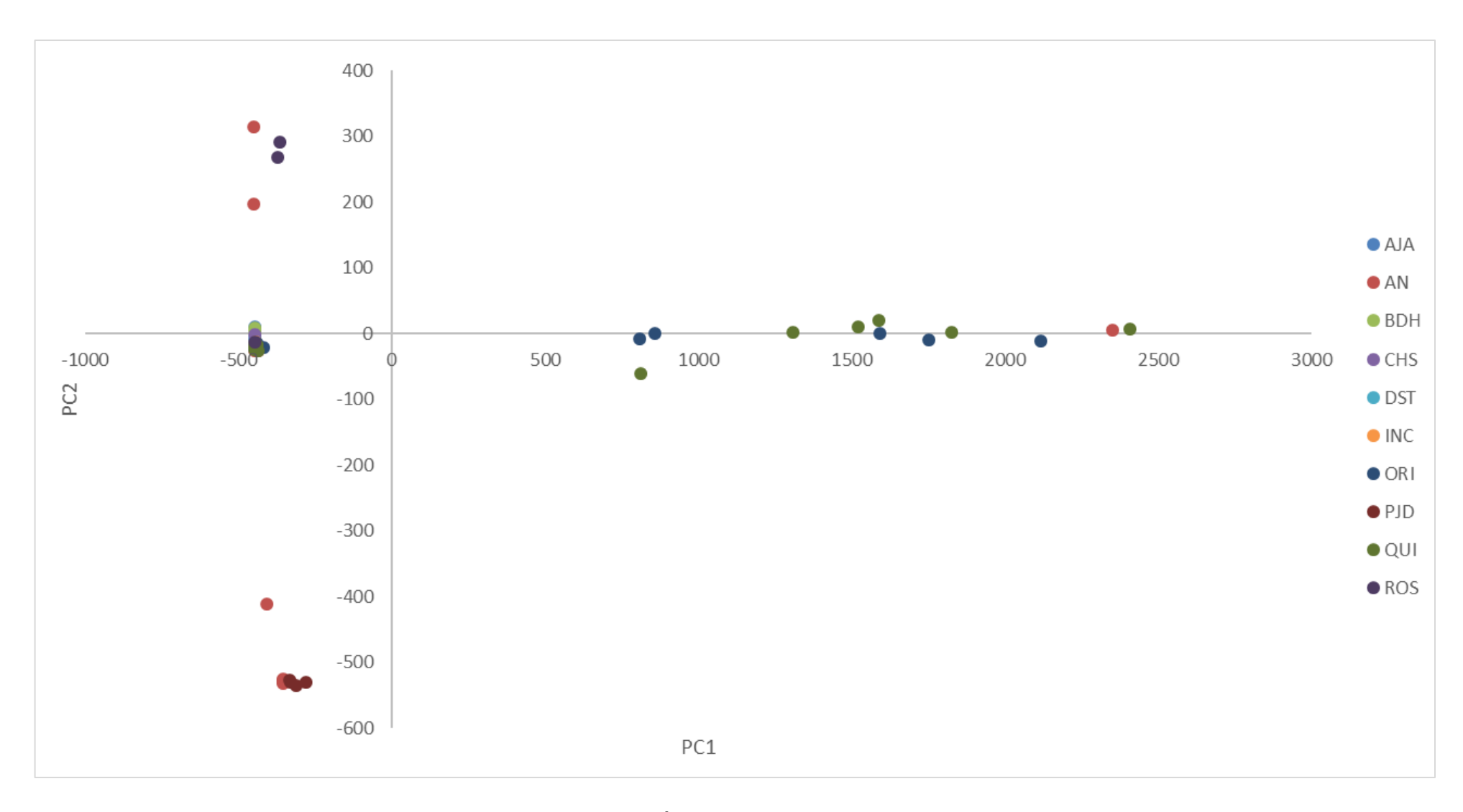


Figure 3.12: PC1/PC2 score plot for all samples.

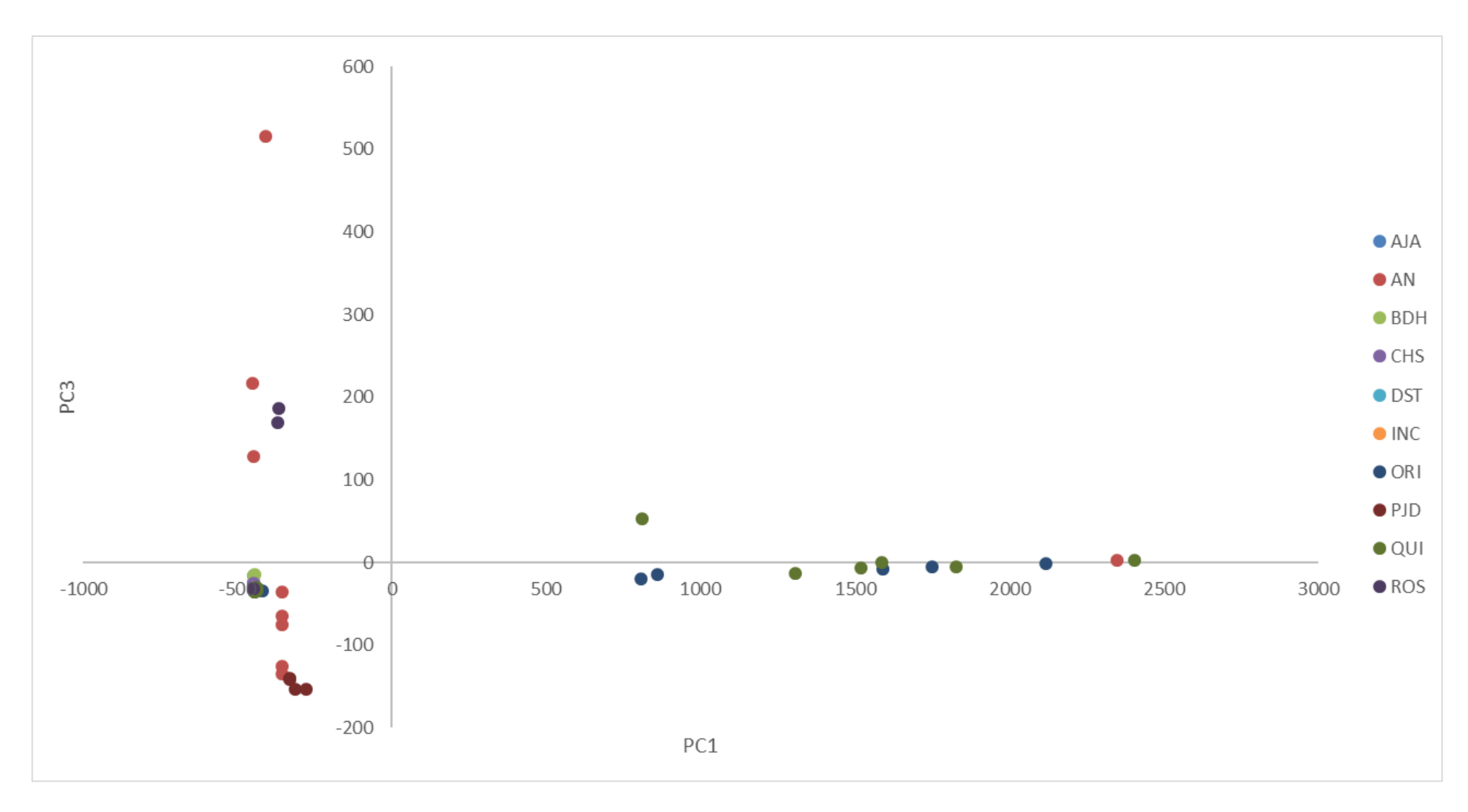


Figure 3.13: PC1/PC3 score plot for all samples.

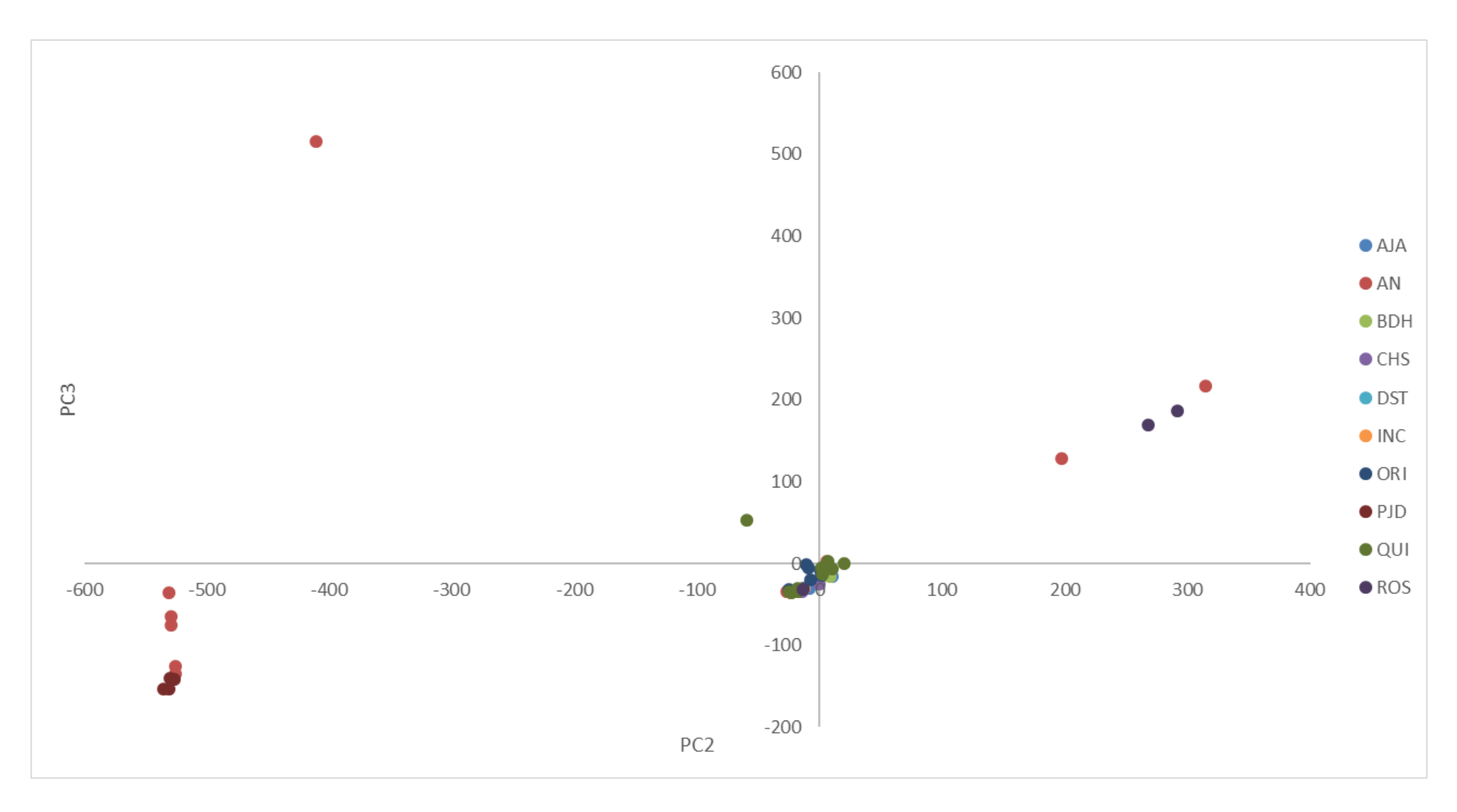


Figure 3.14: PC2/PC3 score plot for all samples.

One method of tackling this issue is to simply remove all magnesium data for the samples. However, this is removing significantly useful information which can contribute to the overall aim of intelligence gathering. An additional drawback to this method is that there is nothing preventing the next element with a large magnitude of difference having the same effect as magnesium in this case.

Another option is to further transform the data to somewhat standardise the raw data to minimise such an effect. This would retain the data rather than remove it and would shift the weighting of the variables to more equally distribute the magnitude of variance across the dataset. Therefore, further transformation of the data is preferable.

## 3.3 Analysis of Logarithmically Transformed Data

The first method of transforming the data was to perform a logarithmic transformation to the entire dataset. This is a commonly used method when variables are not normally distributed, and as a result do not fit the assumptions of standard parametric statistical analyses.

Prior to any transformation the suitability of the transformation must be considered. In this case, IR-MS results range from negative values to positive values, which is an issue as the logarithm of a negative value cannot be performed. To manage this, the data will need to be translated by the addition of a constant to all measurements, to bring the all values above zero. Adding a constant value to each measurement of a variable does not influence the variance of a variable as the mean increases by the same amount. A similar translation is required for the ICP-MS values, as measurements below the limit of quantification are recorded as zero and the logarithm of zero is undefined. This can be solved by a simple addition of 1, which will be returned to zero after the logarithmic transformation.

These translations and transformations were performed on the raw dataset prior to the removal of identified outliers and the PCA was undertaken.

The results of the PCA immediately show signs of skew correction. Firstly, the percentage of variance becomes far less concentrated in the first three principal components, and 90% of the variance is accounted for by the fifth principal component, compared to 99.7% in the initial raw data analysis. The scree plot in Figure 3.15 also shows a more gradual and smoother curve, meaning a greater number of PCs are required to accurately represent the overall dataset.

Table 3.9: Latent variable table.

	Latent	Percentage
PC1	4.475085	43.4
PC2	2.550273	68.2
PC3	1.029427	78.2
PC4	0.757628	85.5
PC5	0.452464	89.9
PC6	0.265109	92.5
PC7	0.221787	94.7
PC8	0.196417	96.6
PC9	0.162675	98.1
PC10	0.075919	98.9

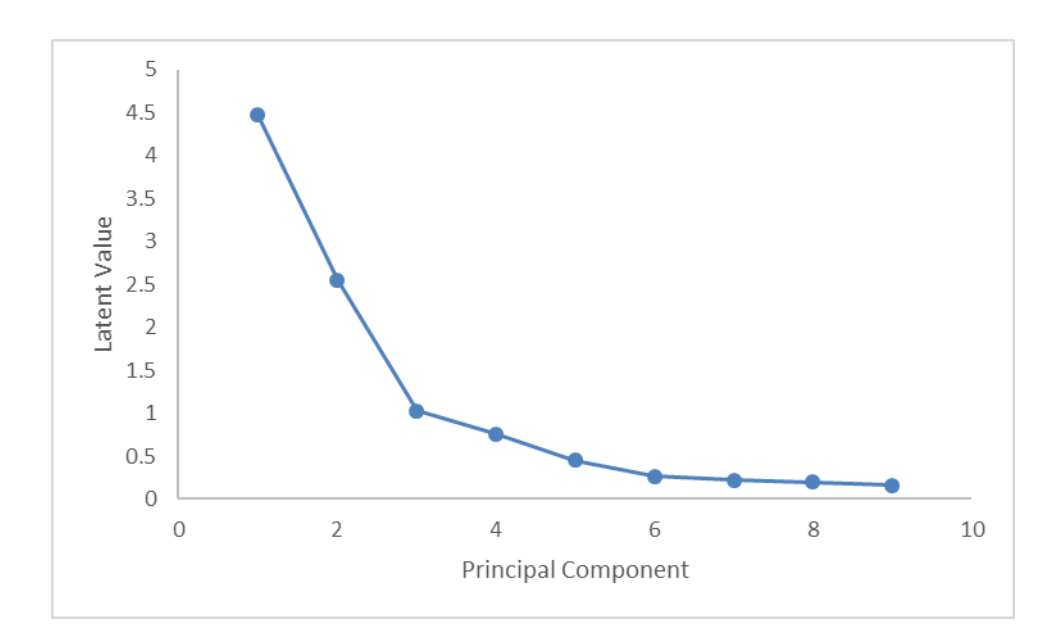


Figure 3.15: Scree plot for PCA of log transformed data.

The coefficients table (Table 3.10) highlights a dramatic change in the make-up of these principal components. Rather than the first few PCs being made up of just one or two variables it is now a combination of many. The scree plot confirms that the skewed nature of the dataset has been tamed and now more of the data is being incorporated into the development of a "fingerprint" for samples. There are still variables that do not contribute to any of the first 7 PCs, however these were elements with very little variation and therefore did not contribute to discrimination.

Now that there are more elements contributing, colour coding the coefficient table overly simplifies the information resulting in the loss of important information. To identify contributing elements, the

magnitudes of contribution now becomes vital. This information is not easily obtained examining Table 3.10, and so a bar chart may be created to depict this data more effectively (Figure 3.16). The first 7 PCs have been considered and the loadings charted in Figure 3.16. The correlation coefficients were also examined (Table 3.11) and here the effects of the logarithmic transformation continue to be evident, as once again the level of correlation has diminished as outlier elements are no longer distorting the PCA.

Table 3.10: Coefficient table for the first 7 PCs.

	PC1	PC2	PC3	PC4	PC5	PC6	PC7
N				0.1	0.1	0.2	-0.1
В				-0.1			-0.1
Na	0.1	-0.1	0.6	-0.4	0.6	-0.2	-0.1
Mg	0.5	-0.4	-0.6	-0.1	0.3	-0.1	0.1
Al	0.2	0.8	-0.2	-0.4	-0.1	-0.2	-0.1
P	0.3	0.1	0.3	0.3	-0.1	-0.1	0.8
Cl	0.1			-0.3	-0.2	0.1	0.3
K	0.2		0.2	0.1		0.4	-0.1
Ca	0.6	-0.2	0.1		-0.4	-0.4	-0.3
Sc							
V		0.1			0.1	-0.1	0.1
Fe	0.3	0.2	-0.1	-0.1	0.2	0.6	0.1
Zn	0.1	0.1		0.1			
As							
Sr	0.3		0.3	0.1	-0.2	0.4	-0.2
Zr							
Ag							
Ва	0.1		0.1			0.1	-0.1
Pb	0.1	0.3	-0.1	0.7	0.4	-0.2	-0.2

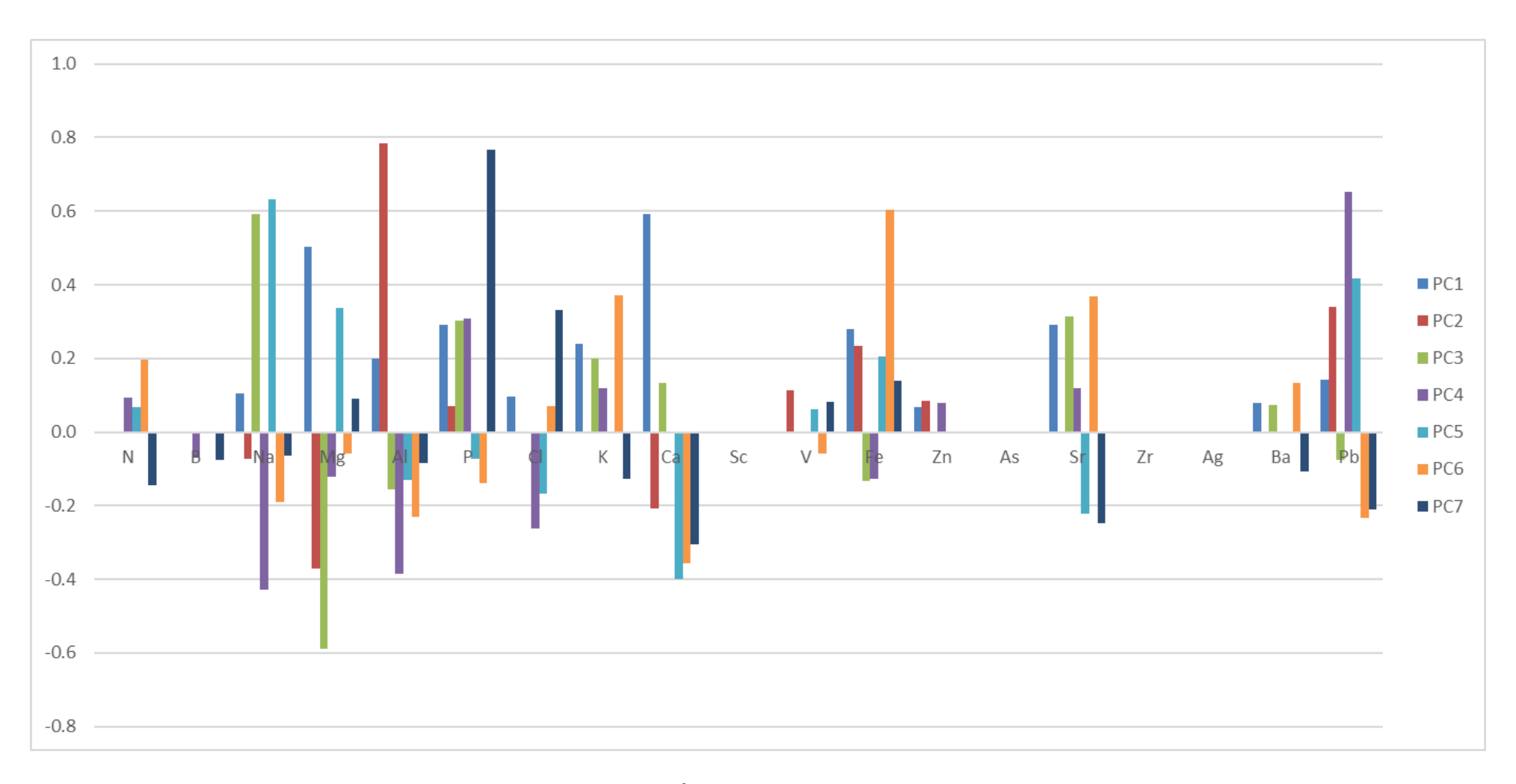


Figure 3.16: Coefficient/loading breakdown for the first 7 PCs.

Table 3.11: Correlation coefficient colour coded table for log transformed raw data analysis.

	N	В	Na	Mg	Al	Р	Cl	K	Ca	Sc	V	Fe	Zn	As	Sr	Zr	Ag	Ва	Pb
N							l.				<u> </u>				LEGEND				<u> </u>
В																0.00	0.25		
Na					_											0.26	0.50		
Mg						_										0.51	0.75		
Al							-									0.76	0.95		
Р								_								0.96	1.00		
Cl																			
K																			
Ca											•								
Sc												_							
V													_						
Fe																			
Zn															-				
As																•			
Sr																			
Zr																			
Ag																			_
Ва																			
Pb																			

Finally, the results of the analysis (Figures 3.17 to 3.19) have been plotted and examined. There have been dramatic improvements to the analysis in comparison to the attempted initial analysis of the raw data. The original outliers are present once again, however to a lesser degree and are very well clustered. This is an interesting result as this highlights the power of transforming the data in such a way to reduce the skew of the data, without dramatically removing the variance, which can be used to "fingerprint" or profile these samples.

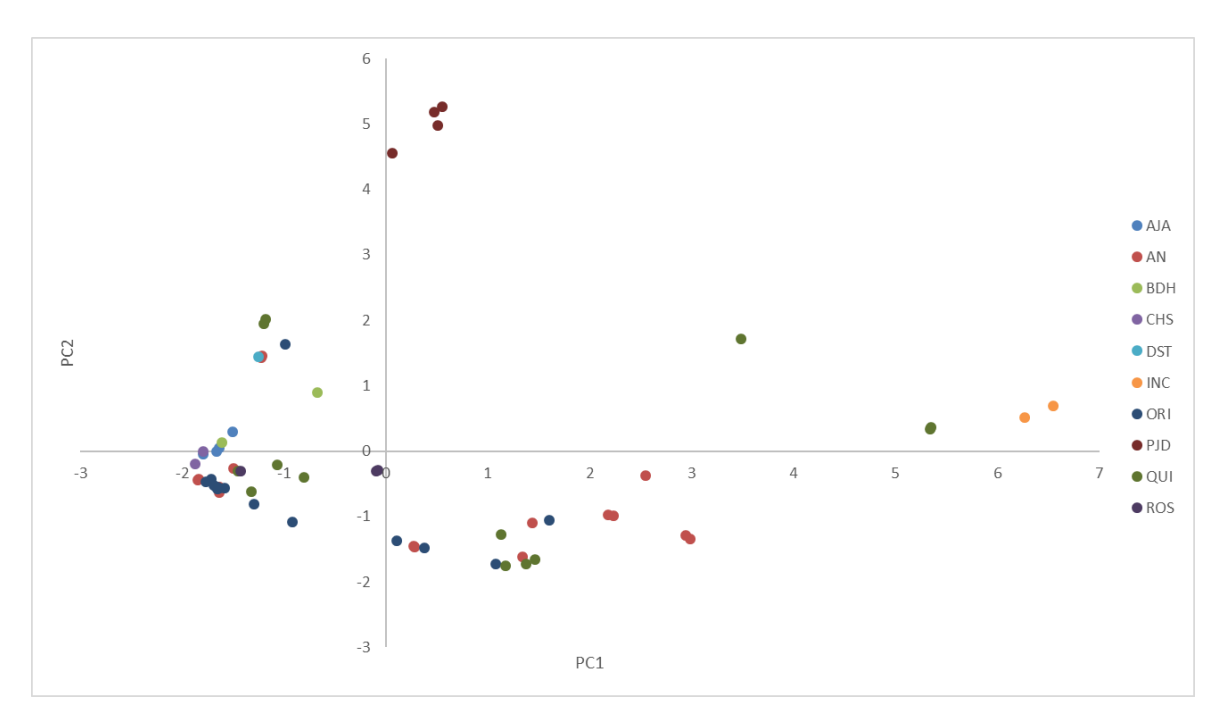


Figure 3.17: PC2/PC1 score plot for all samples after logarithmic transformation.

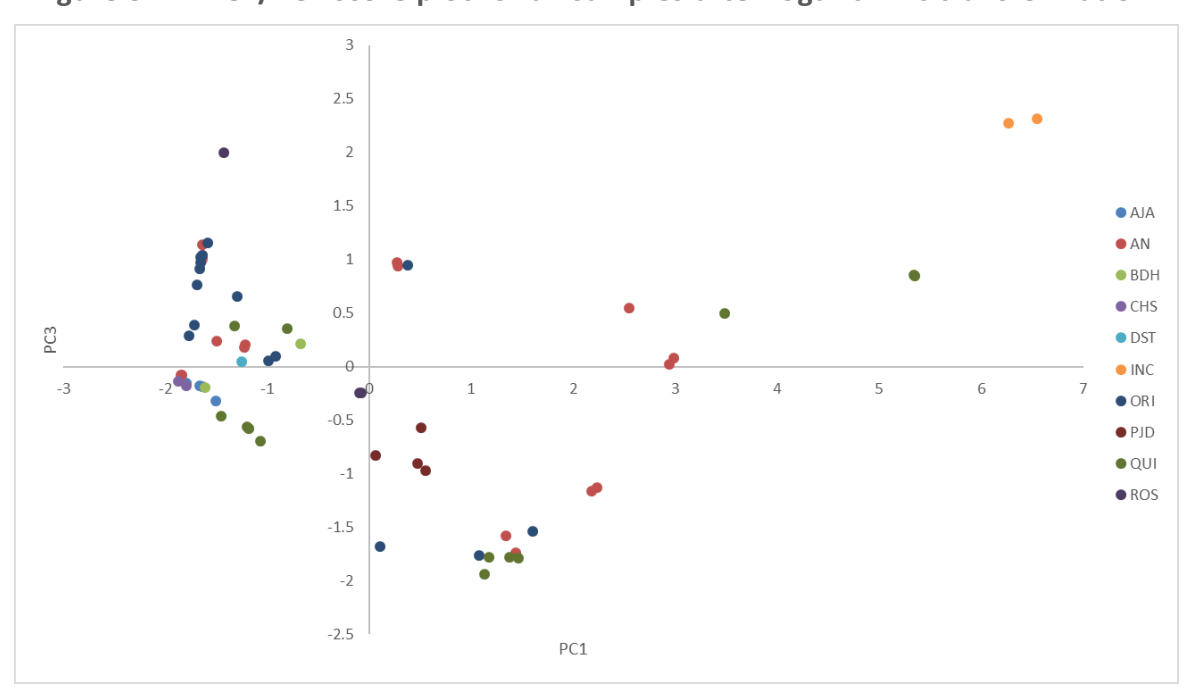


Figure 3.18: PC3/PC1 score plot for all samples after logarithmic transformation.

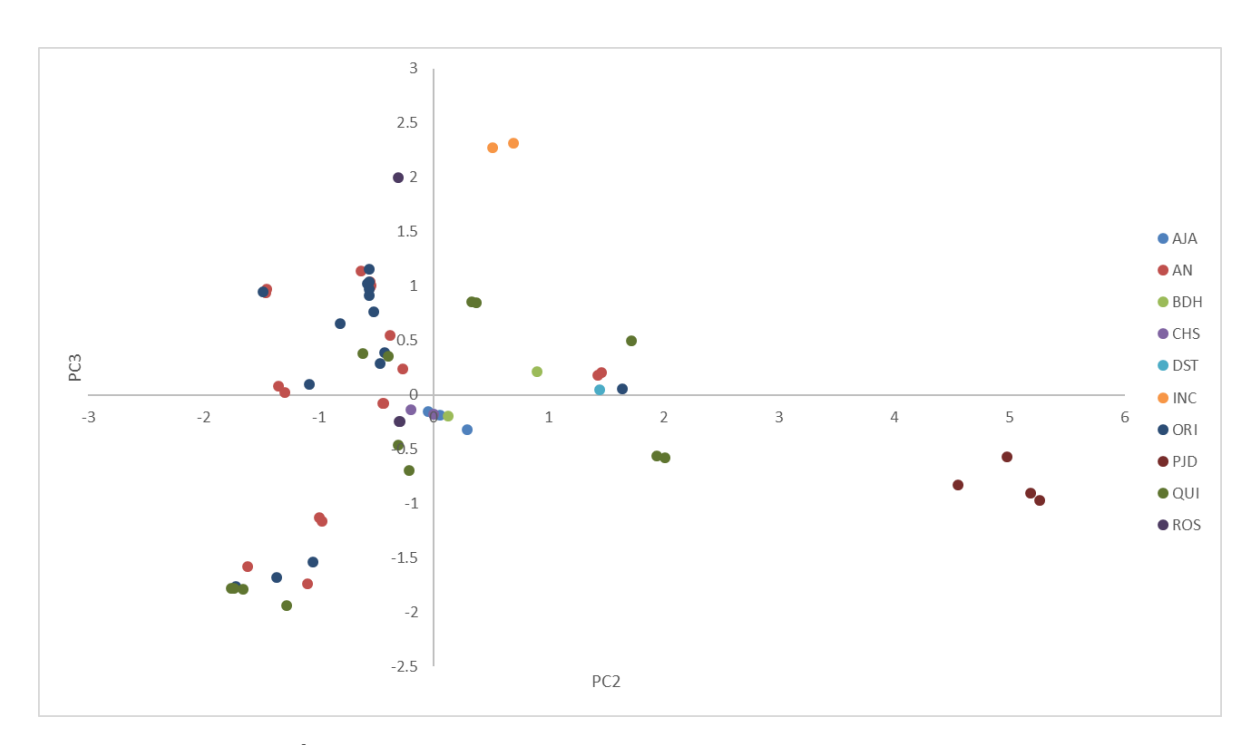


Figure 3.19: PC3/PC2 score plot for all samples after logarithmic transformation.

Although a promising result, a final test with the removal of the same outlier samples from the previous analysis (Chapter 3.2) ROS-3-003, QUI-1F-001F, QUI-1G-001G, QUI-2G-002G, INC-B1, INC-B2, AN-06-2008, PJD-3-010B and PJD-3-010C may help with separating the other samples, just as it did in the previous case without the logarithmic transformation.

## 3.4 Analysis after Logarithmic Transformation and Outlier Removal

This final iteration of the analysis followed the same process as the previous, however, with the removal of the outlier samples.

Beginning with the variance retention, it can be seen in Table 3.12 that there is only a minor change and the variance is now further spread over the first four PCs. This is understandable as the outliers would have represented a large amount of variance in the previous analysis and would concentrate more variance in PC1 and PC2. This is displayed in the scree plot (Figure 3.20) as now the inflection point has shifted to PC4 rather than PC3 in the previous iteration.

Table 3.12: Latent variable table for the log transformed data set PCA.

	Latent	Percentage
PC1	2.740177	41.12
PC2	1.591525	65.01
PC3	0.951969	79.29
PC4	0.435329	85.83
PC5	0.323615	90.68
PC6	0.245889	94.37
PC7	0.170006	96.93

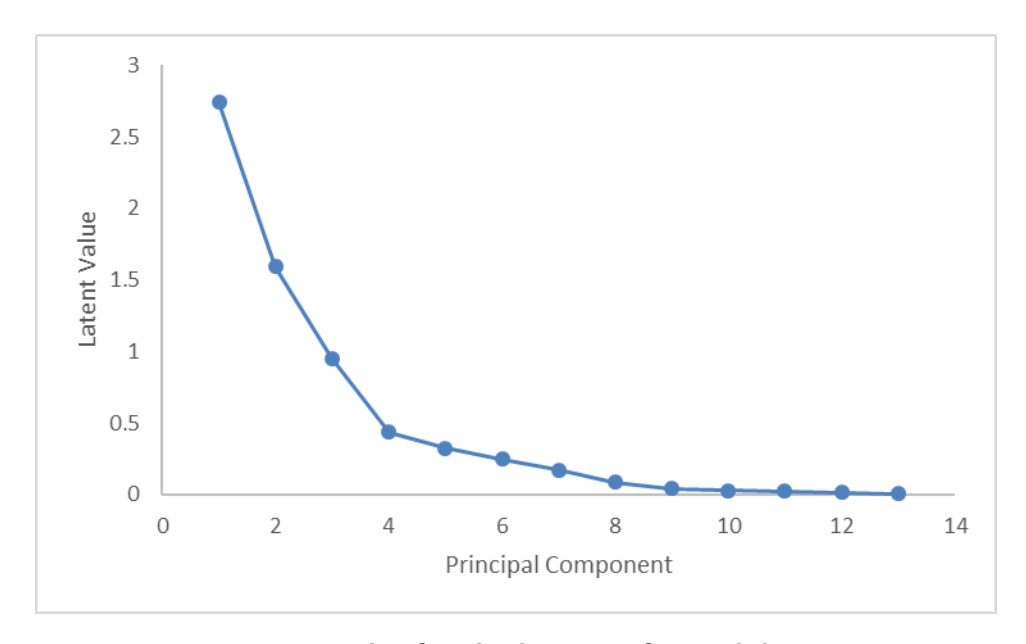


Figure 3.20: Scree plot for the log transformed data set PCA.

The coefficients table (Table 3.13) has shown little difference with only minor changes in the magnitude of contribution of elements to each PC. In PC1 Mg and Ca still dominate the discrimination, however, Mg has increased in its importance. PC2 is still mainly determined by Al. The major difference can be found in PC3, where Pb was not a major contributor in the past however, is a key factor in this analysis. This amounts to Mg, Ca, Al, Na and Pb accounting for nearly 80% of the discriminatory variance within the dataset. A final check on the correlation coefficients was performed to identify whether there is any correlation affecting a number of factors within the PCA. Examining Table 3.14, there is less covariance between any elements with no 1:1 covariance. Two moderate covariances are seen in Zr/V and Ba/Sr however, neither pair can be explained through an interference of one with another. This partial correlation may be a result of the elements being measurable in only a small number of samples, yielding a false correlation.

Table 3.13: Coefficients for the log transformed data set PCA.

	PC1	PC2	PC3	PC4	PC5	PC6	PC7
N			-0.1	0.1		0.1	-0.1
В			0.1		0.1		-0.1
Na	0.1	-0.1	0.7	0.6		-0.2	-0.2
Mg	0.8		-0.3	0.1	-0.4	-0.3	-0.3
Al	-0.1	0.9	0.2	-0.2		-0.2	-0.2
CI	0.1	0.1	0.2	-0.1	-0.2	-0.4	0.8
K	0.1	0.1	0.1	0.4		0.3	0.2
Ca	0.5		0.1	-0.3	0.8	0.1	0.1
V		0.1		0.1			0.0
Fe	0.2	0.3		0.1	-0.3	0.7	0.2
Zn				0.1			0.1
As							
Sr	0.1		0.1	0.1		0.2	
Zr							
Ва	0.1		0.1	0.1		0.1	
Pb	-0.1	0.2	-0.6	0.6	0.4	-0.2	0.1

Table 3.14: Correlation coefficient colour coded.

	δΝ	В	Na	Mg	Al	Cl	K	Ca	V	Fe	Zn	As	Sr	Zr	Ва	Pb
δΝ													LEGENE	)		
В													0.00-0.	25		
Na													0.26-0.	50		
Mg													0.51-0.	75		
Al													0.76-0.	95		
Cl													0.96-1.	00		
K																
Ca																
V																
Fe																
Zn																
As																
Sr																
Zr																
Ва																
Pb																

The final results are examined in the form of two-dimensional score plots, as displayed in Figures 3.21-23. With the removal of the obvious outliers, the score plots are slightly improved. This has less to do with the analysis and more to do with the variance within the dataset. Either there is minimal variance or further outliers are affecting the PCA.

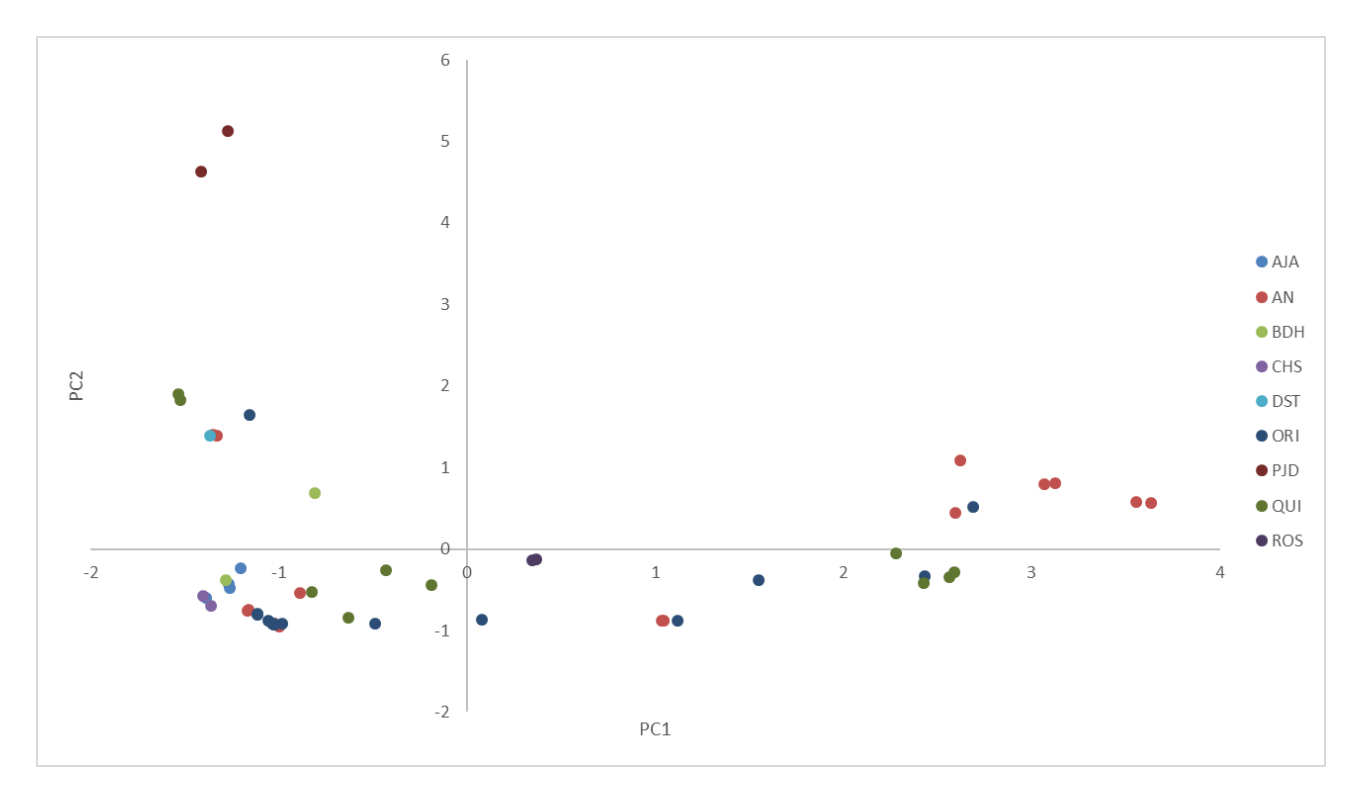


Figure 3.21: Score plot of PC2 vs PC1 for log transformed ICP-MS data.

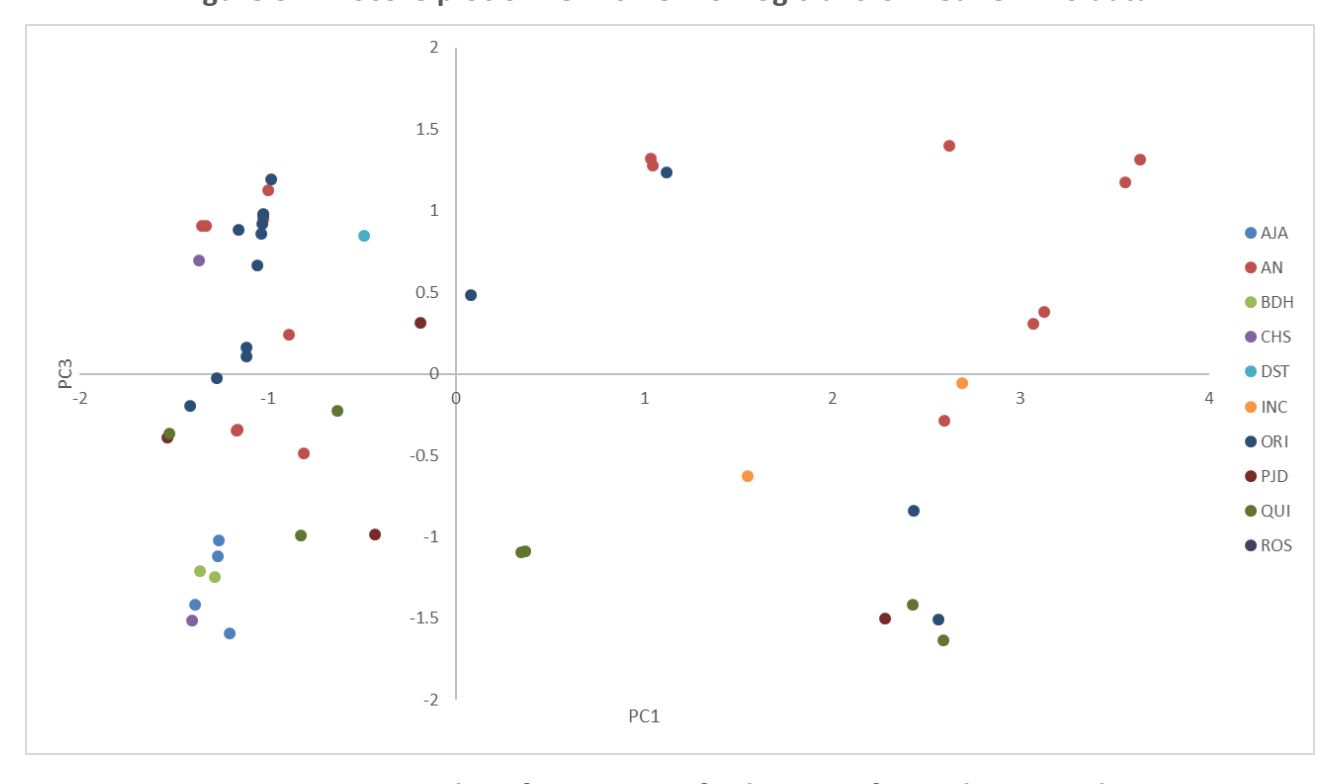


Figure 3.22: Score plot of PC3 vs PC1 for log transformed ICP-MS data.

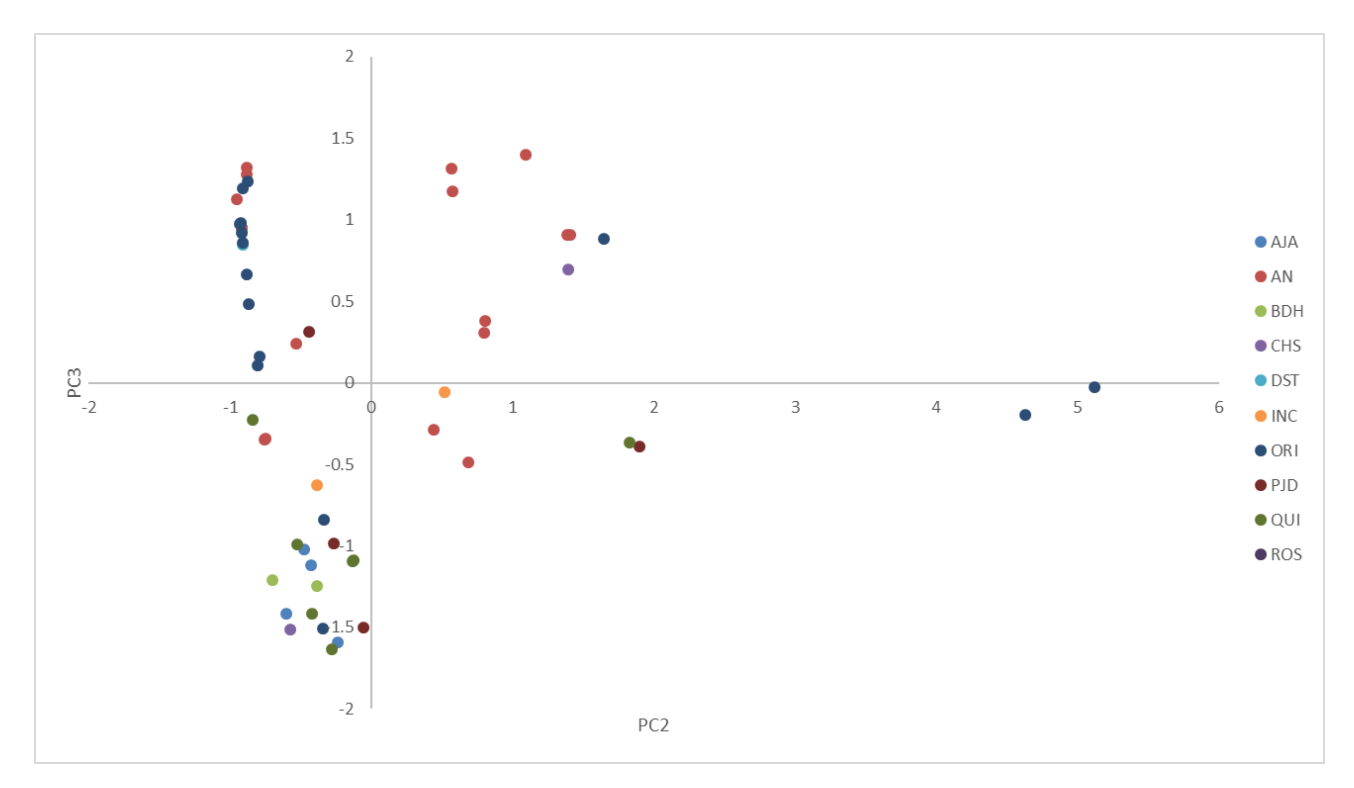


Figure 3.23: Score plot of PC3 vs PC2 for log transformed ICP-MS data.

To test whether the lack of distinct and clear groupings between samples is due to little variance or large differences between samples, the primary factors for the early PCs may be examined. As previously discussed, Mg, Ca, Al, Na and Pb were the key factors contributing to the first three PCs. These elements may therefore be investigated further and a bar chart (Figure 3.24) displays the log transformed data for these elements.

Examining this bar chart, it can be seen that the level of distinct differences is minimal. These elements are the few that provide the most discrimination in this dataset. This highlights that there is not clearly defined distinct segregation between samples other than the few that have been removed as outliers previously.

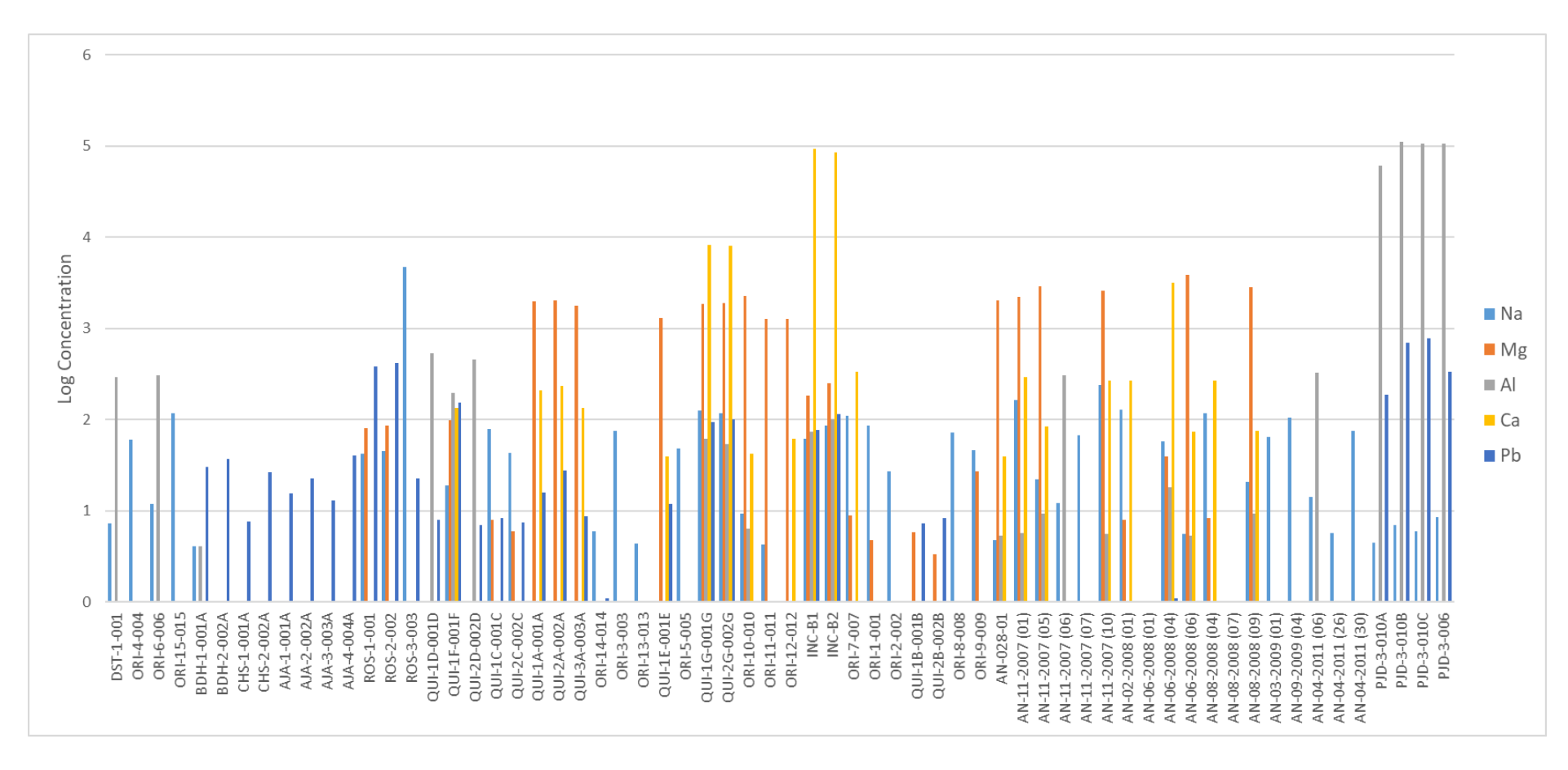


Figure 3.24: Bar chart for Na, Mg, Al, Ca and Pb ICP-MS analysis of AN.

#### 3.5 Conclusions

The pre-processing and combination of the IR-MS and ICP-MS datasets was successful. The analysis has been able to identify some clear outlying groups, which were then removed from the dataset to allow further groupings to be identified. However, even after this removal of outlier samples, further groups were not distinctly separated with a large amount of crossover between sample groups. This indicates that the discriminatory value of the data was not as strong as originally expected. Delving deeper into the details of the sample codes assigned to each sample, the attempted groupings are over ambitious. Although the code identifies the supplier, the samples were still sourced from diverse locations and so further sub groupings should be employed.

This is still an improvement on the previous method of data analysis and result presentation in the form of radar plots, as samples may be easily compared to each other in a mathematical manner. Radar plots did not yield a mathematical value to describe the difference in samples, rather it was up to the examiner to determine if the shape of one radar plot was similar to another. This makes it incredibly difficult to assess the level of similarity or difference between two radar plots. An additional complexity is to do this comparison with hundreds or thousands of samples (and their individual radar plots), whereas PCA can graphically represent a large number of samples and variables in much simpler plots, allowing a better comparison between samples.

Another benefit of the PCA was the identification of where discriminatory data was located within the dataset. This helps to identify the typical elements worth measuring in an ICP-MS analysis, which for future analysis may allow the removal of elements not contributing to the discrimination between samples. There is an important drawback to this however, as this may miss vital forensic markers in the form of the presence of less commonly found elements in a sample, which would clearly discriminate between samples. Therefore, it may still be necessary to analyse for as many elements as feasible and allow the multivariate analysis to highlight which elements are or are not discriminatory.

The pre-processing method involving the logarithmic transformation of the original data was much better at highlighting any minor amount of discriminatory information contained within the dataset. It was also far more robust in terms of the handling of outlier samples, effectively lessening their negative impact upon the PCA analysis. Therefore, this pre-processing method will be used for further datasets involving the use of ICP-MS and IR-MS data.

# 4. Analysis of Potassium Chlorate Samples

In this chapter a number of potassium chlorate samples and their precursors were analysed using ICP-MS, ATR-FTIR and Raman spectroscopy. Each dataset was interrogated individually to identify discriminatory information. The datasets providing to discriminatory information were merged into a singular database and re-examined to determine the most successful pre-processing method of data integration. The PCA of the combined dataset was undertaken to attempt to retain or enhance the original discrimination provided by the individual analytical techniques.

Minor additional studies were also undertaken, including how electrodes and electrolytes affect trace elemental profiles in electrochemically prepared samples, and the consequences of long-term aging of digested samples.

### 4.1 ICP-MS of Potassium Chlorate

The ICP-MS of potassium chlorate samples and precursors involved the analysis of the trace metals listed previously in Chapter 1.4.1. All samples, standards and controls for this analysis used 2% nitric acid as a matrix and prepared gravimetrically for precision. As the aim of the analysis performed was quantitation, the following limits of quantification (LOQ) were obtained for each of the elements. This LOQ was calculated through the analysis of at least 5 blanks and taking ten times their standard deviation (Table 4.1).

Table 4.1: Typical quantification limits for elements analysed in the ICP-MS of potassium chlorate.

Element	Fe	Fe	Mg	Zn	Cu	Al	Ca	Ti
LOQ (mg/kg)	0.41	0.22	0.27	0.54	0.27	1.10	0.41	0.12
Element	Cr	Mn	Ni	Ru	Pt	U	Ва	Sr
LOQ (mg/kg)	0.03	0.05	0.05	0.01	0.01	0.02	0.01	0.02

The calibration of each element requires fitting a line of best fit to the calibration data depending on the model of fit selected. This line of best fit was linear, y = mx + c such that y is the intensity (counts per second) and x is the concentration of standards (ppb). The model to fit the data varied between the elements analysed in KClO<sub>3</sub> samples. In Table 4.2, an example of the calibration for this analysis is displayed. A simple linear model uses a line of best fit across the entire range of calibration

solutions. This calculates the least squared sum of errors using the absolute error of the standards  $(x^2)$ . A weighted linear model on the other hand calculates the linear fit from the least squared sum of 1/error of the standards  $(1/x^2)$ . This results in the higher concentration standards now having less impact on the linear regression, effectively weighting the fit to the lower concentration standards. This is advantageous in cases where samples are measured towards the low end of the calibration curve, as this improves low end accuracy. It should be noted, however, that this can have a negative impact on the high end of the calibration curve and therefore a simple linear model is better suited for elements commonly measured at high concentrations. To be certain of the correct model, the results of each standard calibration curve must be examined and contrasted for each element, and so the calibration data must be reprocessed with both models.

Alongside this linear model fitting, a working range must be kept in mind. Although the linear model may predict instrument response down to 1 ppt, this in an unreliable measurement if the lowest standard in the calibration range was only 100 ppt. Therefore, results outside of an element's working range should be treated with caution.

Table 4.2: Example of calibration data for elements selected in the ICP-MS analysis of potassium chlorate.

Element	Mass	Linear Model	Coefficient of Correlation (R <sup>2</sup> )	Working Range (ppb)
Mg	24	Weighted Linear	0.996273	0.1-100
Al	27	Simple Linear	0.999869	10-100
Ca	44	Simple Linear	0.999970	1-100
Ti	48	Weighted Linear	0.999690	0.1-100
Cr	52	Weighted Linear	0.999906	0.1-100
Mn	55	Weighted Linear	0.999448	0.1-100
Fe	56	Weighted Linear	0.988981	0.1-100
Fe	57	Weighted Linear	0.989050	0.1-100
Ni	60	Weighted Linear	0.999850	0.1-100
Cu	63	Weighted Linear	0.998068	0.1-100
Zn	66	Weighted Linear	0.993199	0.1-100
Sr	88	Weighted Linear	0.999903	0.1-100
Ru	102	Weighted Linear	0.999878	0.1-100
Ва	138	Weighted Linear	0.999948	0.1-100
Pt	195	Weighted Linear	0.999980	0.1-100
U	238	Weighted Linear	0.999301	0.1-100

A few samples where larger quantities of material were available were tested in triplicate to assess the consistency of the sample preparation and validity of the resultant data, to accurately represent the bulk sample, represented as "SAMPLE (replicate number)". From this triplicate analysis, the percent coefficient of variation (%CV) was calculated by taking the standard deviation, dividing it by the mean and multiplying by 100. These results are displayed in Table 4.3 and highlight a few important aspects and drawbacks of the analysis. The %CV has been coloured green (0-10%), yellow (10.01-20%), orange (20.01-40%) and red (>40.01%). These brackets have been designed to indicate the level of reliability in the measurements with green being ideal, yellow acceptable, orange questionable and red being unacceptable.

Using these brackets, the results show that the majority of elements within the replicates are within acceptable levels of variance. However, some are not, which must be interrogated further. Although there are many unacceptable results, upon further inspection, many are due to the measurements being close to the LOQ. Replicates below LOQ were recorded as 0 mg/kg, and this has a major influence on the calculation of %CV values, as in reality the concentration may have only just been under the LOQ. This makes the %CV highly sensitive at these ultra-trace levels making the context of the %CV an important aspect to consider and not just the value alone. For example, the titanium %CV for replicates Cu1-Cu3 was 141.42%, as the replicates measured 0.00, 0.00 and 0.13 mg/kg. The LOQ for titanium however, was 0.12 mg/kg and therefore the two 0.00 mg/kg measurements could have been 0.11 mg/kg, which would have resulted in a %CV of 6.38%, which is within the acceptable limit of 10%.

Table 4.3: Percent coefficient of variation analysis of random triplicates.

Sample	Fe	Fe	Mg	Zn	Cu	Al	Ca	Ti	Cr	Mn	Ni	Ru	Pt	U	Ва	Sr
Sample	mg/kg	mg/kg	mg/kg	mg/kg	mg/kg	mg/kg	mg/kg	mg/kg	mg/kg	mg/kg	mg/kg	mg/kg	mg/kg	mg/kg	mg/kg	mg/kg
	30.77	30.62	27.45	1.10	0.00	7.27	5.02	0.49	1.77	0.65	0.75	0.00	0.00	0.00	0.43	0.04
DSTG3	30.88	30.69	34.14	1.23	0.39	10.92	5.64	1.04	1.91	0.77	0.82	0.00	0.00	0.00	0.45	0.05
	31.15	31.59	29.00	3.93	3.55	10.19	5.32	0.58	1.79	1.15	0.86	0.00	0.00	0.00	0.31	0.04
%CV	0.51	1.42	9.47	62.57	121.18	16.65	4.70	33.98	3.49	25.02	5.78	0.00	0.00	0.00	16.03	9.57
DCTC4	48.63	48.96	29.19	1.80	0.00	3.67	8.13	0.26	1.17	0.75	0.10	0.00	0.00	0.00	1.15	0.44
DSTG1	40.55	41.20	28.64	2.10	0.00	3.26	8.23	0.18	1.11	0.62	0.09	0.00	0.00	0.00	0.93	0.46
	43.30	44.70	32.49	1.86	0.00	4.90	12.64	0.44	1.26	0.75	0.11	0.00	0.00	0.00	1.28	0.51
%CV	7.60	7.06	5.65	6.64	0.00	17.64	21.77	37.28	5.34	8.35	7.75	0.00	0.00	0.00	12.60	5.99
KCIO 3	2.22	1.75	29.50	2.59	2.38	5.81	4.22	1.05	0.08	0.11	0.13	0.00	0.00	0.00	0.22	0.07
KClO <sub>3</sub> 2	3.97	3.96	31.96	2.76	2.70	5.37	5.47	1.17	0.08	0.13	0.33	0.00	0.00	0.00	0.25	0.09
	2.17	2.14	28.60	2.46	2.33	4.80	4.18	1.01	0.07	0.11	0.20	0.00	0.00	0.00	0.21	0.08
%CV	30.04	36.75	4.73	4.75	6.66	7.78	12.99	6.48	5.59	6.61	38.94	0.00	0.00	0.00	6.01	10.81
	0.72	0.69	0.64	1.45	0.00	0.00	0.61	0.00	0.00	0.00	0.00	0.00	0.00	0.00	0.02	0.00
E1	1.30	1.24	0.54	8.29	0.32	0.00	1.25	0.00	0.00	0.00	0.00	0.00	0.00	0.00	0.02	0.00
	0.81	0.66	0.58	1.06	0.00	0.00	0.00	0.00	0.00	0.06	0.00	0.00	0.00	0.00	0.01	0.00
%CV	26.99	31.08	6.79	92.25	141.42	0.00	82.30	0.00	0.00	141.42	0.00	0.00	0.00	0.00	10.73	0.00
	5.04	4.99	0.00	0.90	45.31	1.37	0.75	0.00	0.05	0.07	0.22	0.00	0.00	0.00	0.00	0.00
SS	7.85	7.94	0.00	2.32	89.14	3.85	0.88	0.00	0.06	0.09	0.28	0.00	0.00	0.00	0.00	0.00
	5.78	5.36	0.00	1.57	95.54	1.72	1.00	0.00	0.06	0.09	0.24	0.00	0.00	0.00	0.00	0.00
%CV	19.09	21.56	0.00	36.29	29.12	47.43	11.96	0.00	11.03	12.83	9.75	0.00	0.00	0.00	0.00	0.00
	3.46	3.64	0.00	1.77	157.32	0.00	1.28	0.00	0.07	0.05	0.36	0.00	0.00	0.00	0.00	0.02
CU	3.08	2.92	0.00	2.00	146.25	2.19	1.00	0.00	0.00	0.00	0.00	0.00	0.00	0.00	0.00	0.02
	4.22	4.20	0.00	1.72	168.28	0.00	1.27	0.13	0.00	0.05	0.00	0.00	0.00	0.00	0.00	0.03
%CV	13.22	14.52	0.00	6.73	5.72	141.42	10.85	141.42	141.42	70.72	141.42	0.00	0.00	0.00	0.00	13.88

#### 4.1.1 Exploratory Multivariate Analysis of ICP-MS Data

The raw results of the analysis were transformed in the same manner as previously described in Chapter 3.3. This includes the values below the LOQ being transformed to zero values and the entire dataset undergoing a logarithmic transformation. The data then underwent the exploratory data analysis, including HCA and PCA of the dataset. Firstly, the HCA was performed to allow an assessment of the potential of a further PCA analysis. The resultant dendrogram and sample identity correlation table are displayed in Figure 4.1 and Table 4.4. This initial overview of the data shows great clustering potential, without any further data transformations.

The dendrogram indicates that there are three to four densely packed branches. The other indication of importance from the HCA are the two samples 78 and 79 that are closely related but separated from the rest of the samples. This could have been detrimental to PCA, which is greatly affected by the presence of any outliers. However, these two samples are the two calcium hypochlorite precursors, rather than potassium chlorate samples and the PCA should identify why these are being segregated. These samples would also be identified as outliers by other means, such as FTIR analysis or even by physical examination.

For this first analysis, they were included within the dataset to assess their similarity to the end products. Even prior to PCA, the samples closest to these outlying precursors were examined more closely and seen to contain the potassium chlorate made from these two precursors (#34-42 and 61, i.e. KClO<sub>3</sub> 19-27 and PT1). There are, however, additional samples between the pool chlorine manufactured samples and their precursors (#55-60, i.e. KClO<sub>3</sub> 40-45) and these were all the partially successful syntheses, attempting to use "Lite salt", a low-sodium alternative to table salt, to synthesise potassium chlorate. Additional samples of potassium chloride (KCl, KCl2) and sodium chloride (NaCl2) were added to this analysis to investigate any differences between these, and the precursors used in material synthesis.

The link between the trace metals from the pool chlorine to the final product suggests that the elemental profile can carry over to the product from the precursor materials, supporting the aim of the project to link precursor to product. This could potentially be used to link source materials to the end product, however, the dendrogram does not delve into the details of why these trends are apparent. To this end, PCA was run after these positive indications, on both precursors and end products.

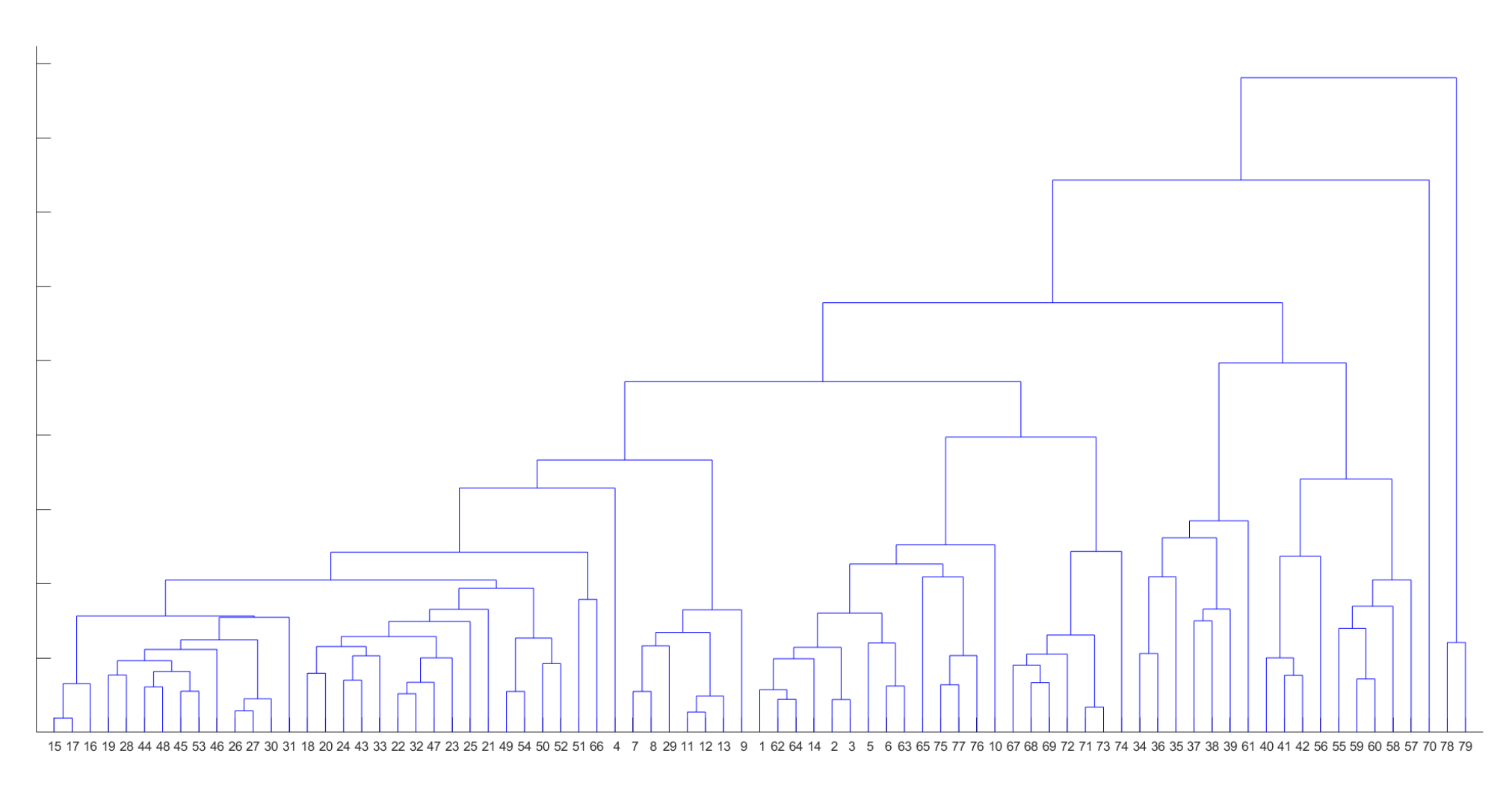


Figure 4.1: Resultant dendrogram from the hierarchical cluster analysis of potassium chlorate ICP-MS data.

Table 4.4: Sample correlation to number identifiers in HCA dendrogram in Figure 4.1.

Number	Sample	Number	Sample	Number	Sample	Number	Sample	Number	Sample	Number	Sample	Number	Sample
1	KCI	13	DSTG1 (3)	25	KClO <sub>3</sub> 10	37	KClO <sub>3</sub> 22	49	KClO₃ 35	61	PT1	73	Cu (3)
2	KCl1	14	KClO <sub>3</sub> 1	26	KClO <sub>3</sub> 11	38	KClO <sub>3</sub> 23	50	KClO <sub>3</sub> 36_1	62	E1 (1)	74	FCB
3	KCI2	15	KCIO <sub>3</sub> 2 (1)	27	KClO <sub>3</sub> 12	39	KClO <sub>3</sub> 24	51	KClO <sub>3</sub> 36_2	63	E1 (2)	75	SACB
4	E508	16	KCIO <sub>3</sub> 2 (2)	28	KClO <sub>3</sub> 13	40	KClO <sub>3</sub> 25	52	KClO <sub>3</sub> 37	64	E1 (3)	76	WKR
5	NaCl1	17	KClO <sub>3</sub> 2 (3)	29	KClO <sub>3</sub> 14	41	KClO <sub>3</sub> 26	53	KClO <sub>3</sub> 38	65	E2	77	WKL
6	NaCl2	18	KClO <sub>3</sub> 3	30	KClO₃ 15	42	KClO <sub>3</sub> 27	54	KClO₃ 39	66	ICP1	78	Sigald Ca(OCI)2
7	DSTG3 (1)	19	KClO <sub>3</sub> 4	31	KClO <sub>3</sub> 16	43	KClO <sub>3</sub> 28	55	KClO <sub>3</sub> 40	67	SS (1)	79	HCSS
8	DSTG3 (2)	20	KClO₃ 5	32	KClO₃ 17	44	KClO <sub>3</sub> 29	56	KClO <sub>3</sub> 41	68	SS (2)		
9	DSTG3 (3)	21	KClO <sub>3</sub> 6	33	KClO <sub>3</sub> 18	45	KClO <sub>3</sub> 30	57	KClO <sub>3</sub> 42	69	SS (3)		
10	DSTG2	22	KClO₃ 7	34	KClO <sub>3</sub> 19	46	KClO <sub>3</sub> 31	58	KClO <sub>3</sub> 43	70	SIGALD		
11	DSTG1 (1)	23	KClO <sub>3</sub> 8	35	KClO <sub>3</sub> 20	47	KClO <sub>3</sub> 32	59	KClO <sub>3</sub> 44	71	Cu (1)		
12	DSTG1 (2)	24	KClO <sub>3</sub> 9	36	KClO <sub>3</sub> 21	48	KClO <sub>3</sub> 33	60	KClO <sub>3</sub> 45	72	Cu (2)		

DSTG3, DSTG1, KClO<sub>3</sub> 2, E1, SS and Cu were analysed in triplicate. Replicate number represented in brackets.

PCA analysis was undertaken and the quality of the analysis must be scrutinised. This began with the variance breakdown through the percentage of variance retained by each principal component (Table 4.5), which may also be graphically displayed in a scree plot (Figure 4.2).

Table 4.5: Variance retention table for the PCA of KClO<sub>3</sub> ICP-MS data.

Component	Principal Component Eigenvalues	Cumulative Percentage of Variance Explained
PC1	1.394769	44%
PC2	0.699795	65%
PC3	0.634484	85%
PC4	0.211191	92%
PC5	0.123422	96%
PC6	0.05054	97%
PC7	0.042824	98%
PC8	0.017902	99%

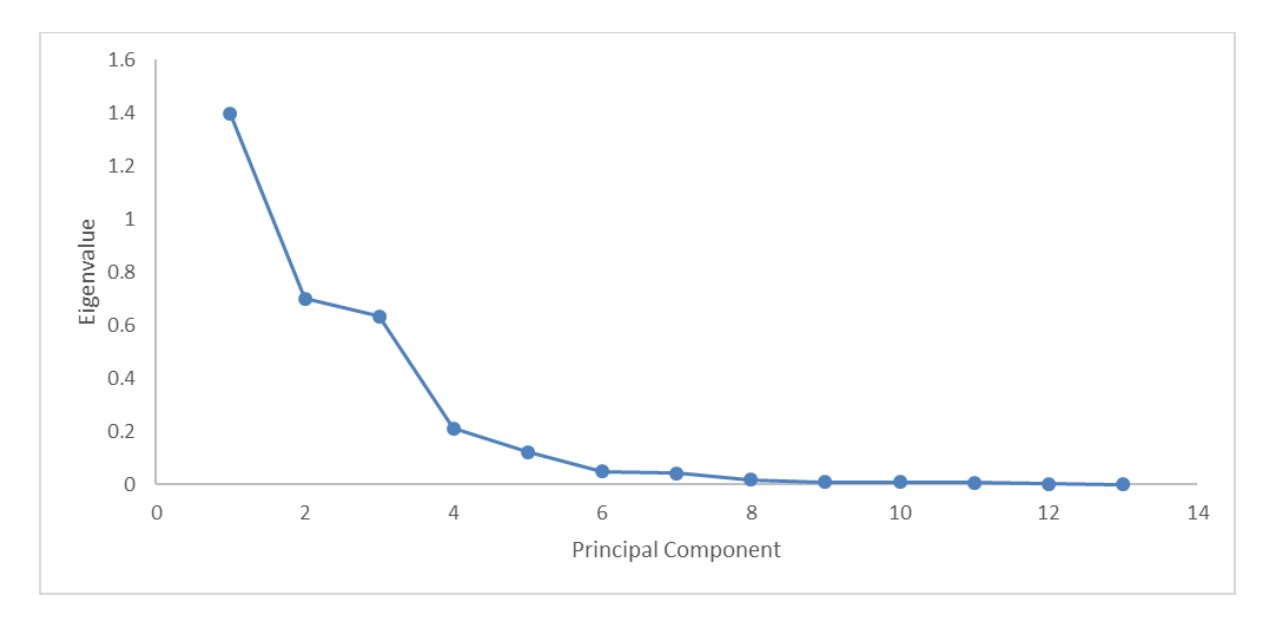


Figure 4.2: Scree plot for the PCA of KCIO<sub>3</sub> ICP-MS dataset.

This variance distribution is a little unusual as PCs 2 and 3 have similar levels of variance. However, the percentage of variance indicates a moderately successful PCA, with 85% of the original variance being represented in the first 3 principal components. The scree plot also shows the desired rapid decrease in eigenvalue after PC4, indicating a successful PCA.

The coefficient table (Table 4.6) reveals the key contributors of each of the principal components. There are many elements that do not influence the major PCs, most of which are because of rarity.

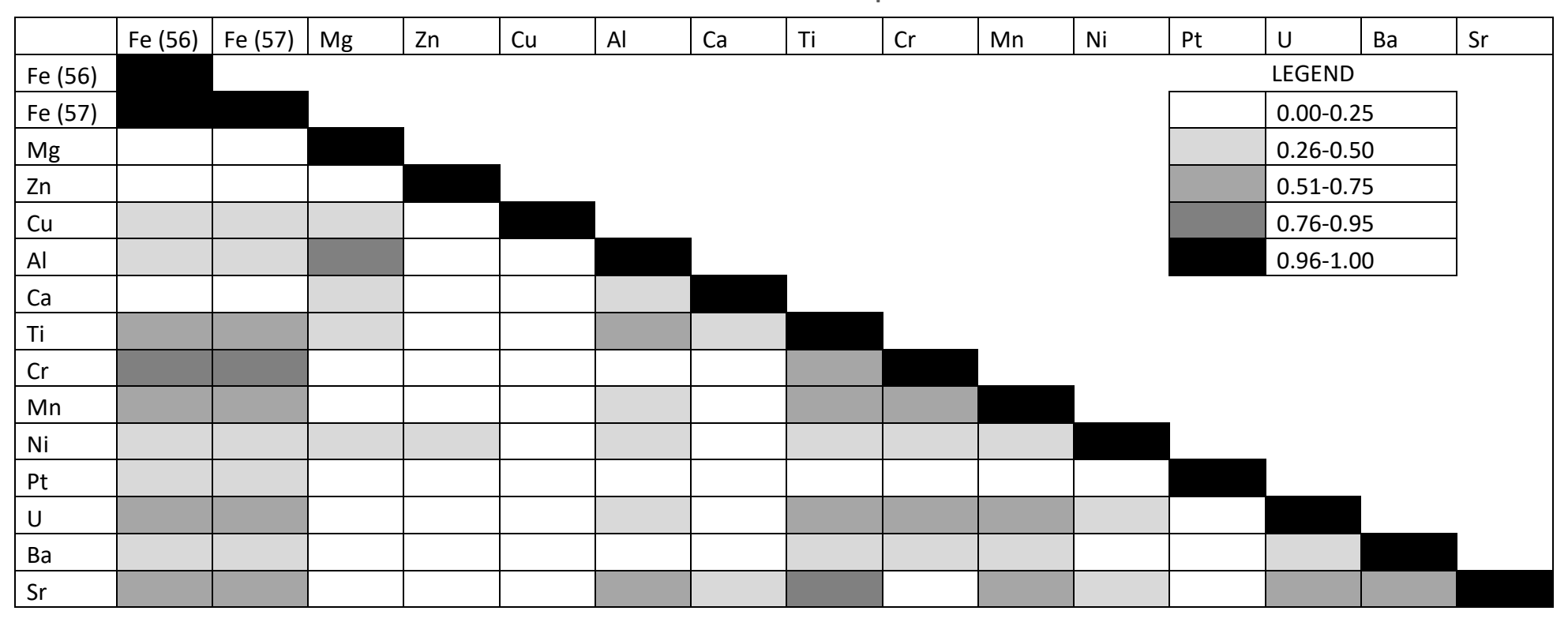
However, one element in particular stands out and that is zinc. This is an element that is present in significant amounts in the raw data, across every sample, and yet the variance is not significant enough to provide great insight into the discrimination of samples. This is a good sign that other elements are providing significant discrimination, so that even elements present in all samples do not have a significant effect on the early PCs.

Table 4.6: Coefficient table for the first eight PCs of potassium chlorate ICP-MS data.

	PC1	PC2	PC3	PC4	PC5	PC6	PC7	PC8
Fe (56)		-0.4		-0.3	-0.3			
Fe (57)		-0.4		-0.3	-0.3			
Mg	0.5		-0.5		-0.3	0.4	-0.3	
Zn						0.6	0.8	
Cu			0.5	0.7				
Al	0.5	-0.3		0.4	0.3	-0.5	0.3	-0.2
Ca	0.6	0.6	0.5					
Ti					0.5	0.4	-0.3	-0.5
Cr								
Mn								-0.2
Ni								
Pt								
U								
Ва								0.7
Sr					0.6			0.5

With so few elements providing variance across the sample set, a real concern is the potential for covariance relationships between elements to be the cause of this effect. As the samples had been synthesised with a single set of labware, this could lead to a consistent glassware contamination of the KClO<sub>3</sub> produced, which would result in a significant covariance relationship forming between elements present within the glassware. In order to clarify the level of covariance within the dataset, the correlation coefficients (Table 4.7) were examined. This shows very little correlation between elements excluding the two isotopes of iron, which was expected unless there is an interference at the mass of one of the isotopes. Hence, correlation between elements was not a reason for the small number of elements contributing to the PCs, but rather the elements of significance really are few in number.

Table 4.7: Correlation coefficients for the PCA of potassium chlorate ICP-MS data.



The results of the PCA could now be examined and as the first three PCs account for 85% of the original variance within the dataset, these are a good representation of the original data. Firstly, they may be examined individually as in Figures 4.3-4.5. The sample numbers are consistent from the HCA analysis expect KClO<sub>3</sub> is denoted as KClO3 as subscripts could not be used.

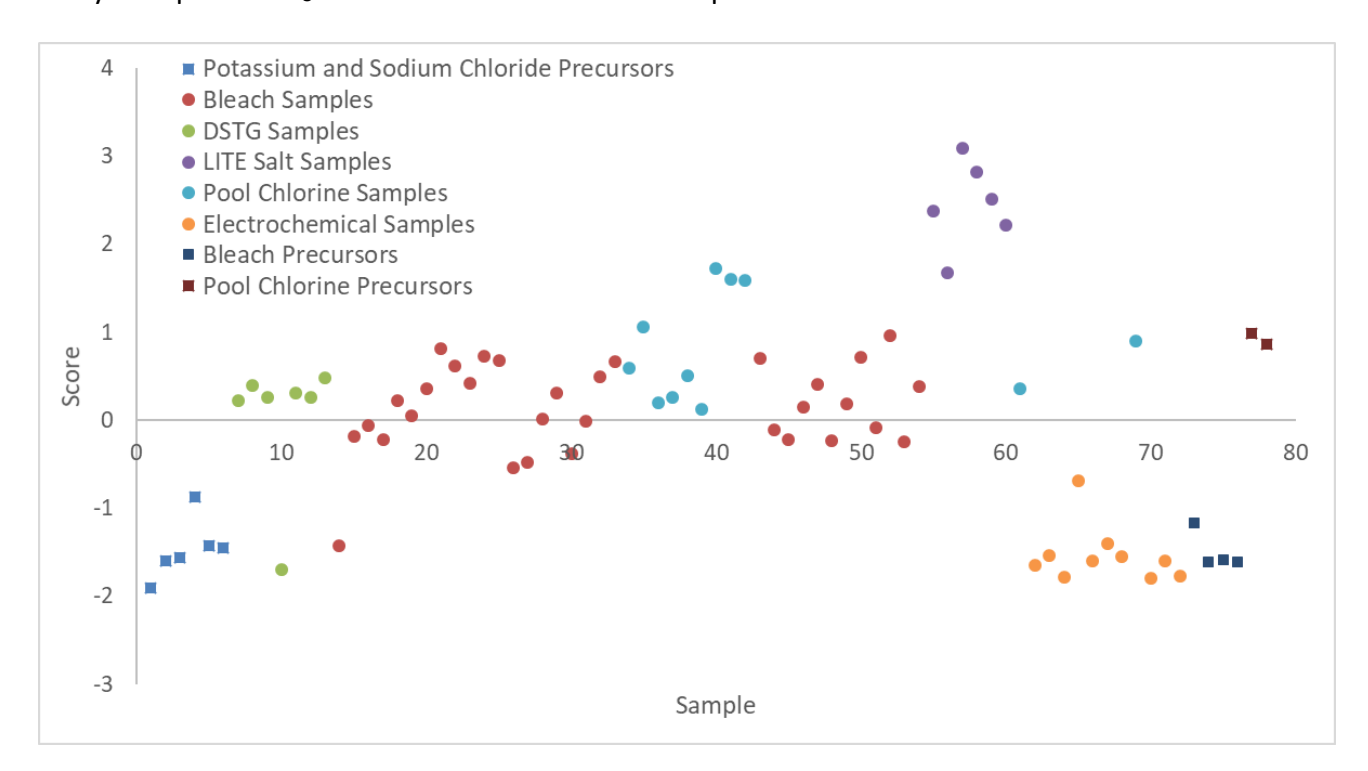


Figure 4.3: Score plot of PC1 from the PCA of ICP-MS data for KClO<sub>3</sub> samples and precursors.

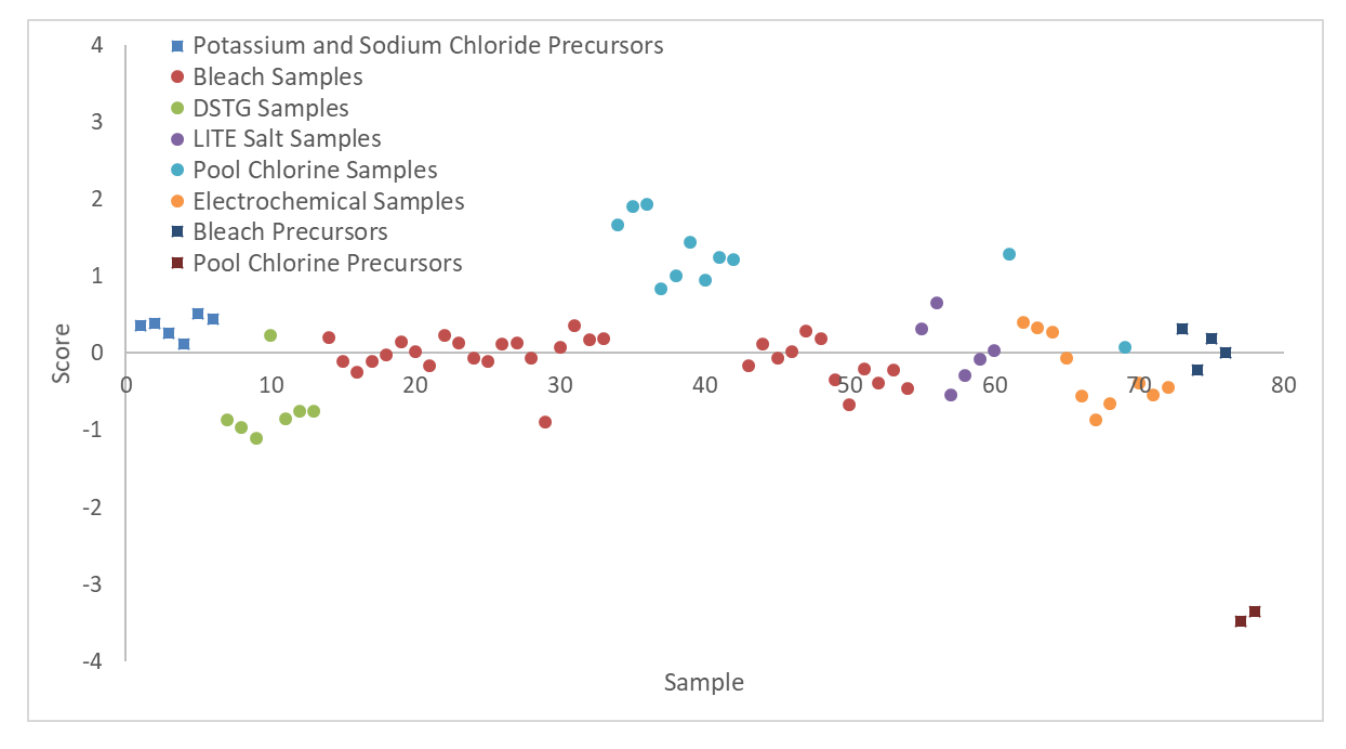


Figure 4.4: Score plot of PC2 from the PCA of ICP-MS data for KClO₃ samples and precursors.

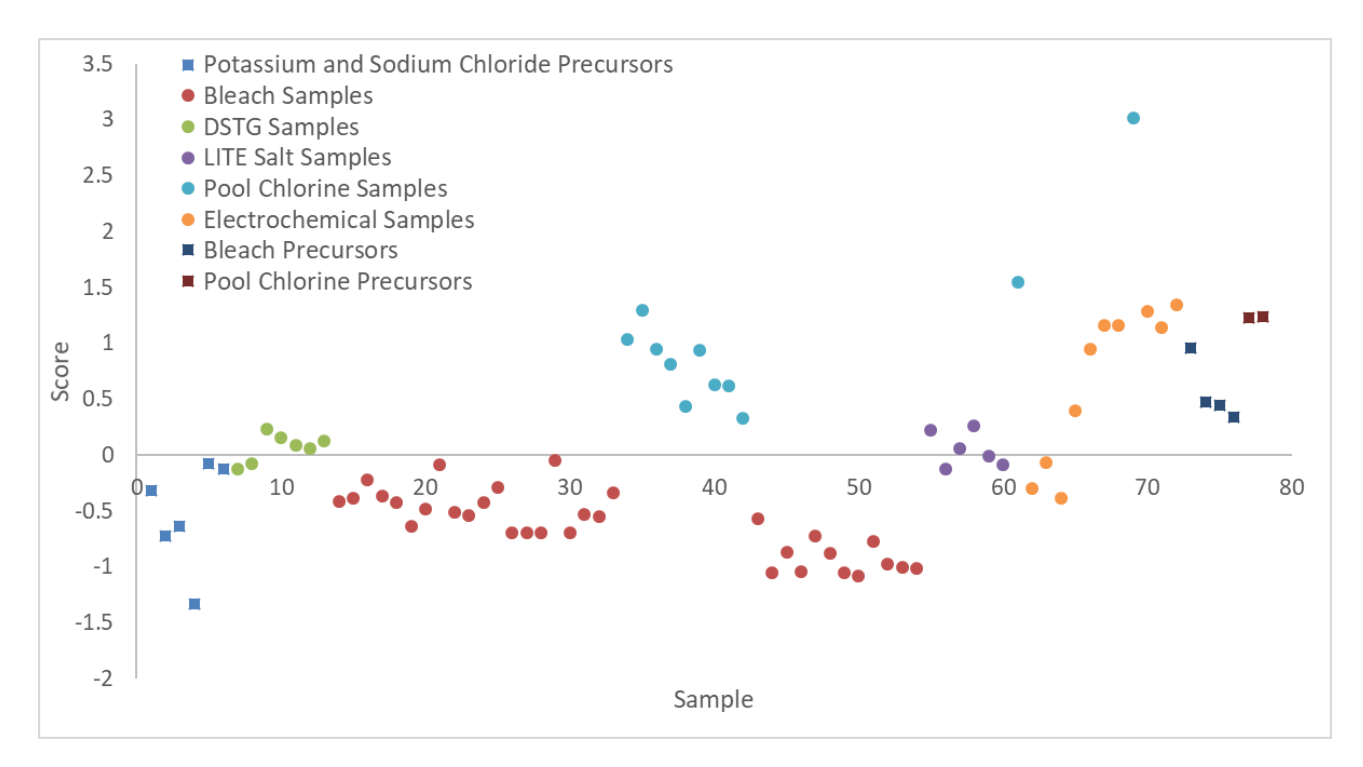


Figure 4.5: Score plot of PC3 from the PCA of ICP-MS data for KClO₃ samples and precursors.

Examining these score plots, it could be seen immediately that there were clearly datapoints breaking away from the main body of the dataset in PC1 and PC2. However, by PC3 the clustering is diminished and from PC4 onwards, there is no longer any consistent discrimination between sample types.

In the results for PC1 (Figure 4.3), nearly all the starting materials break away, including the potassium chlorides, sodium chlorides and household bleaches. This only leaves the calcium hypochlorite (pool chlorine) starting materials not being separated from the main grouping of KClO<sub>3</sub> samples.

Samples produced by the electrochemical synthesis method also not only separated from the majority of samples but remain tightly clustered apart from sample E2. E2 is an electrochemically produced sample that involved a large spiking of the full range of analysed elements in the electrolyte, to test the effect of trace metal incorporation from the electrolyte solution (further examined in subchapter 4.1.2).

There are a number of samples that have separated above the main cluster including KClO<sub>3</sub> 25-27 and 40-45. Samples KClO<sub>3</sub> 25-27 are just three of the samples using pool chlorine as a starting material, so not all of the pool chlorine samples were discriminated in this case. Samples KClO<sub>3</sub> 40-45 are all the samples created using a low sodium salt supplement. This supplement is a mix of sodium and potassium chloride sold at supermarkets. Synthesis involving this starting material was

only partially successful, with very poor yields and a high concentration of the salt remaining, not allowing recrystallisation without the loss of the final product. There were also two other outlier samples, including one provided by DST Group, and the first KClO<sub>3</sub> sample produced from bleach. The DST Group sample (DSTG2) was obtained commercially and therefore the precursors and synthesis pathway are unknown. There are distinct differences in the elemental profiles of samples within the dataset, which have been identified by the PCA. KClO<sub>3</sub> 1 was prepared with the same precursors as many of the other samples using bleach, however, this was the first successful synthesis which was not yet optimised, and further adjustments were made to the procedure. This may have had a significant impact on the elemental profile of further samples.

The electrochemical samples and starting materials as well as the two outlier samples, DSTG2 and KClO<sub>3</sub> 1, are separated below the main cluster and KClO<sub>3</sub> 25-27 and 40-45 are above. Referring to the coefficients in Table 6 this would suggest that the primary trace elements leading to this discrimination were Mg, Al and Ca. This could be investigated further by plotting bar charts for each sample of the elements with this valuable discriminatory information (Figure 4.6).

The charts in Figure 4.6 show that data points below the main group have low or no quantifiable concentration in at least two or three of the elements. The samples above the main bulk of data points, however, are more difficult to identify, but the calcium chart does show that they have higher than average concentration. The correlation between these bar charts and the level of discrimination in the score plot, especially for the samples with a high score value, is not entirely clear. If calcium content was the driver for the higher score samples, then samples like sigald and KClO<sub>3</sub> 19-24 should also have been separated but were not. This shows the power of PCA and highlights that the PC1 score also includes minor contributions from other elements. In this study only a relatively small number of samples have been analysed, as opposed to a real-world database, which could potentially have thousands of samples. Without the PCA highlighting these elements for further inspection, an analyst is confronted with the task of examining all elements analysed, which may be dozens, and using those to discriminate between potentially thousands of samples.

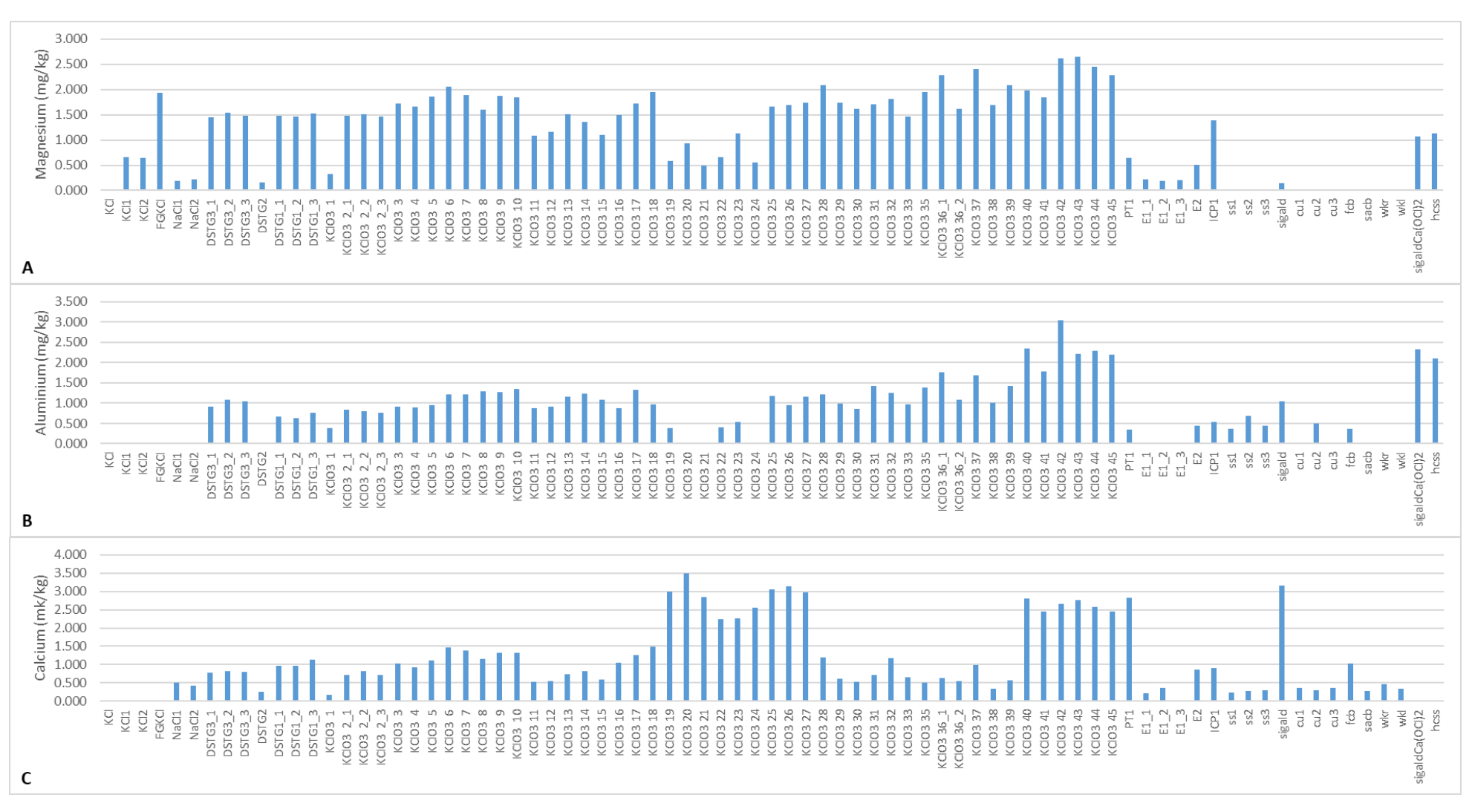


Figure 4.6: Bar charts for the ICP-MS analysis of A) magnesium, B) aluminium and C) calcium content for KClO₃ samples and precursors.

The score plot for PC2 is interesting as it highlights separation between different samples to PC1. The samples discriminated in this case were all of the KClO<sub>3</sub> samples produced using the pool chlorine synthesis method, and the calcium hypochlorite which is the active ingredient of pool chlorine. One sample (sigald) was a pool chlorine sample, however, this was not created using the same precursor as the others, and instead used a Sigma-Aldrich laboratory grade calcium hypochlorite. This result suggests the removal of the pool chlorine impurities greatly affects the elemental profile of the end product.

The pool chlorine samples have higher scores, however, the precursor HCSS has a very low score value. Referring to the coefficients in Table 4.6 once again, the only difference between PC1 and PC2, other than the magnitudes of contribution, was the removal of magnesium and the addition of iron to the list of elements of influence. This immediately suggests that these samples were discriminated based on their iron concentrations. Interrogating the data further with a bar chart for iron content of samples (Figure 4.7), this is shown to not entirely be the case. The chart does show that the calcium hypochlorite precursors have a very large amount of iron in comparison to the other samples, however, this high iron content was not conferred into the resulting potassium chlorate products. In fact, two samples provided by DST Group (DSTG1 and DSTG3) have much higher than average iron concentrations, however, are not strong outliers in the score plot for PC2. This displays the ability for multivariate analysis to not only take all the elements into account, but also the amount of discriminatory information each possesses within a large and complicated database.

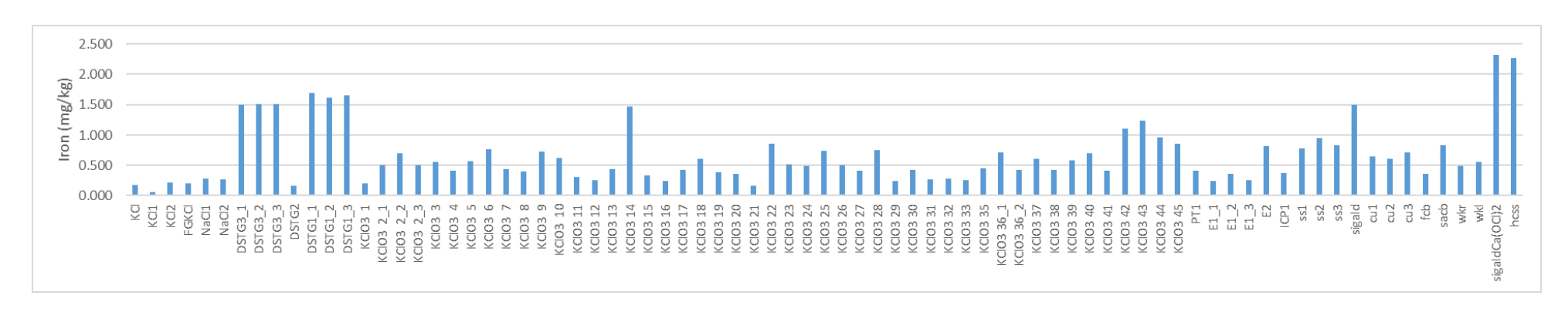


Figure 4.7: Bar chart for the ICP-MS analysis of iron content for KClO<sub>3</sub> samples and precursors.

The score plot for PC3 (Figure 4.5) begins to show signs of weakened discrimination however, there are some interesting takeaways. Firstly, the pool chlorine samples (light blue) and bleach samples (red) are quite well separated. There is one pool chlorine sample that has become somewhat of an outlier; however, this is the same sample (SIGALD) previously discussed to be different to the others. The other key point of interest in this PC is the slight separation of one of the electrochemical sample triplets (E1). Sample E1 used only titanium electrodes and is the only electrochemical cell to have two inert electrodes and no additional trace metals within the electrolyte. This highlights the effect electrodes and electrolytes can have, as the degradation of metal electrodes or presence of trace metals in the electrolyte affects the elemental profile of the final product. The effect on the elemental profile is also significant enough to be identified through a multivariate analysis such as PCA.

With each individual PC up to PC3 showing signs of discrimination, two-dimensional plots can be examined. First PC1 and PC2 were plotted (Figure 4.8). This highlights the discrimination between samples by combining the discrimination in the individual PCs.

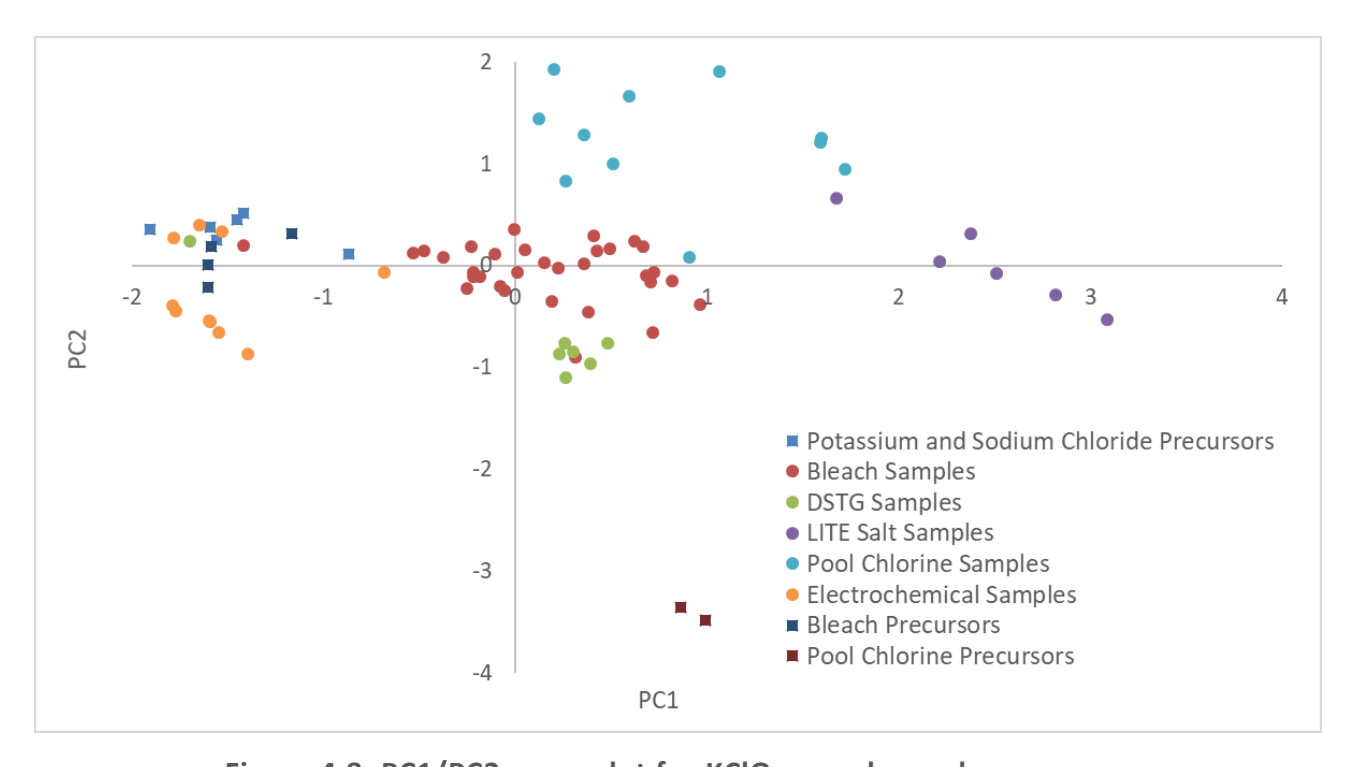


Figure 4.8: PC1/PC2 score plot for KClO<sub>3</sub> samples and precursors.

This plot has many interesting features, with the bleach samples clustering in a central location with very little overlap with other types of sample apart from 2 triplicate analyses of commercial samples (DSTG2). The pool chlorine samples are located above the bleach samples with just the one previously discussed outlier sample (SIGALD). The partially successful syntheses resulting from using the health

supplement KCI "LITE" have all been separated to the right of the bleach cluster. The final group of samples from the electrochemical synthesis method are located to the left of the central cluster quite distinctly apart from the previously discussed spiked electrolyte sample (E2). Mixed in with this cluster are many of the precursor materials as expected from the analysis of individual PCs due to the low concentration of trace elements in comparison to bleach and pool chlorine samples. The pool chlorine precursors are separated once again due to PC2 as expected.

PC3 will give another perspective to these results and so a plot of PC1/PC3 can be created (Figure 4.9).

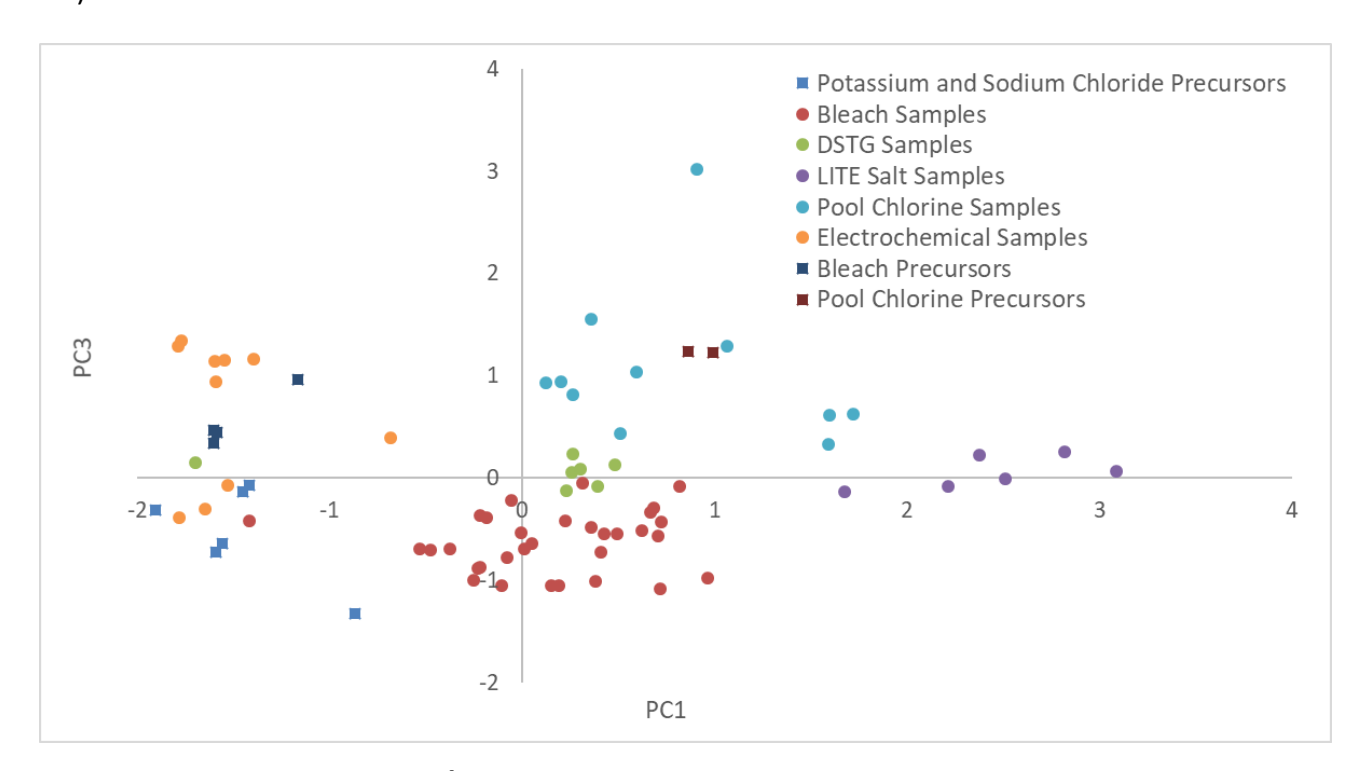


Figure 4.9: PC1/PC3 score plot for KClO<sub>3</sub> samples and precursors.

This has not greatly improved the level of separation between clusters, as PC3 is where the discrimination between groupings began to greatly diminish. However, as previously noted, the electrochemical sample E1 (PC3 score of <0) has separated from the other electrochemical samples' SS and Cu (PC3 score ≈1).

Through the application of class groupings as the sample precursors are known, clear groupings relating to the various synthetic routes can be identified. One of the major drawbacks of undertaking PCA without labelling sample types, as would be common in a real-world database, is the determination of what constitutes separation or clustering. Without the potential to group samples

based on knowledge of precursors and/or synthesis pathways in a real world scenario, more research into mathematically quantifying separation and clustering is required.

#### 4.1.2 Trace Element Profile Retention Using Electrochemical Synthesis

The elemental profiles for potassium chlorates made via the electrolysis method were shown to contain very little of the trace elements, contributing to the score plot of PC1 (Figure 4.3) compared to other samples. This allowed the identification of these samples as a clustering group, however, a closer examination was undertaken to assess the effect of modifying electrodes and spiking the saltwater solution on the final product. To test the effect of elemental profile retention, an adulterated sample was prepared and compared to the samples prepared by electrolysis.

The data is shown in Table 4.8, with E2 being the adulterated sample. For this sample, the synthesis was identical to that of E1, which involved the same NaCl, volume and dual titanium electrodes. The difference between them was the addition of all the elemental stock solutions to the cell electrolyte, to give a concentration of 50 ppb prior to applying the current. For further comparison, samples SS and Cu had stainless steel and copper anodes, respectively, and titanium cathodes, and are also included within the table.

Table 4.8: ICP-MS data for potassium chlorate samples produced via the electrolysis method.

Sample	Fe 56 (mg/kg)	Fe 57 (mg/kg)	Mg (mg/kg)	Zn (mg/kg)	Cu (mg/kg)	Al (mg/kg)	Ca (mg/kg)	Ti (mg/kg)
<b>E2</b>	5.54	5.58	2.27	3.58	1.88	1.75	6.26	0.32
E1	0.95	0.86	0.59	3.60	0.11	0.00	0.62	0.00
SS	6.22	6.10	0.00	1.60	76.66	2.31	0.87	0.00
Cu	3.58	3.59	0.00	1.83	157.28	0.73	1.19	0.04
Sample	Cr	Mn	Ni	Ru	Pt	U	Ва	Sr
	(mg/kg)	(mg/kg)	(mg/kg)	(mg/kg)	(mg/kg)	(mg/kg)	(mg/kg)	(mg/kg)
E2	0.10	0.17	0.29	0.00	0.06	0.00	0.19	0.75
E1	0.00	0.02	0.00	0.00	0.00	0.00	0.01	0.00
SS	0.05	0.08	0.24	0.00	0.00	0.00	0.00	0.00
Cu	0.02	0.03	0.12	0.00	0.00	0.00	0.00	0.02

Comparing the spiked E2 sample to E1, many of elements had elevated concentrations, however, this is not consistent across the board. This indicates that the presence of trace metals within the water used for synthesis can be incorporated into the final material produced. These final products were

also heavily washed and recrystallised with ultrapure water. The indications are that trace impurities have not been removed from the KClO<sub>3</sub> crystals by these common purification processes.

Examining the SS and Cu samples the level of trace metal released through the degradation of the electrodes, even while under anodic protection, is significant. This is particularly evident with copper, whose content in the resulting KClO₃ is high when a stainless-steel anode was used, and even greater when a copper electrode was used. This means that samples produced in an electrochemical cell could potentially be identified by the electrodes selected for their synthesis. The previous PCA analysis in sub-chapter 4.1.1 confirms that the electrode degradation trace element contribution separated the electrochemical samples from the bleach and pool chlorine samples. The SS and Cu samples were not separated from each other by examining Table 4.8 above. It is clear that the samples are quite different to each other, especially when comparing copper and iron levels. This highlights a drawback of PCA when examining individual data as differences may be found between the Cu and SS samples. In the PCA however, this difference is not significant enough in comparison to the wider differences within the overall dataset. Further iterations of PCA could be undertaken to further discriminate within clusters, however this is limited. PCA requires a larger number of samples in comparison to variables as previously discussed in the introduction. A PCA to examine just 2 samples will result in a singular principal component, as the maximum number of PCs is determined by the number of samples minus one. This issue may be avoided if there was a larger population of samples within a cluster and therefore, further iterations may be conducted.

#### 4.1.3 Sample Digest Solution Aging Study

Samples synthesised for ICP-MS studies within this research were produced in very small quantities. This resulted in sample digestions consuming close to the entire sample, which cannot be recovered. In a real-world scenario, this could be a significant issue as this destructive analysis would be the last possible analysis undertaken on a trace amount of explosive. This raises the question of the reliability of retaining the digestion solution for future testing, for example, against additional elements, as this is the last of the sample and could be stored.

To investigate this, a selection of 20 digested potassium chlorate samples previously tested were retained for 9 months and retested. The samples were tightly sealed in plastic trace grade 50 mL digestion vials, stored in a cupboard out of direct sunlight in 2% nitric acid, and kept at a laboratory room temperature of 22-25°C. There was no visible change in the solutions after the storage with a

stable volume, and no change in colour or precipitate formation. Prior to analysis, samples were vortex mixed for 30 seconds, subsampled into 15 mL vials and loaded onto the autosampler. The results were then used to calculate the change for each element and these results are recorded in Table 4.9 which highlights some key trends.

It must be noted that in the case of trace analysis, many of the elements were not present at high levels and so a minor change in concentration can lead to large relative differences. Also, as some samples originally not containing quantifiable concentrations of an element have gained concentration, the calculation will result in an undefined value due to the division of zero, and these will be recorded as "UND". The final consideration is the %CV of the ICP-MS method for each element as previously examined in Table 4.3, as this will determine whether a change is within experimental error

The resultant shift across all elements is not consistent, with some elements being affected by the passing of time far more than others. The most dramatic of which was the copper measurements, as this has increased by up to 10,876%. Some samples that originally did not contain copper measured at 13-25 mg/kg upon the second analysis, which is just above the quantification limit. The previous measurement may have been just below the limit of quantification and hence recorded as 0 mg/kg. However, a minor increase in concentration cannot explain the 10,000% differences in other samples, as these involved much larger increases of up to 294 mg/kg. Therefore, the stability of copper ions within a 2% nitric acid solution at these levels is highly unreliable on long-term storage under the conditions described. Although copper shows a distinct increase in concentration, there are elements that were affected in the opposite direction, reducing their concentrations to below quantifiable levels. This includes magnesium and barium; magnesium consistently lost 99-100% of the original concentration, however, barium only lost concentration in samples with very low-level concentrations to begin with and samples that contained higher levels remained more stable. Iron and zinc were quite unstable as well, with significant consistent increases in concentration, however, there were elements that showed some promise for storage under these conditions. These more stable elements could still be reliable, even after a nine-month storage period even at very low levels; there are small fluctuations with many measurements resulting in less than a 20% change. Comparing this to the %CVs of the method from Table 4.3, this is a significant variation as prior to aging, many random triplicates were shown to vary by a similar amount.

Table 4.9: Change (in percentage) of ICP-MS results for KClO₃ digestion solutions stored for 9 months.

	Fe (56)	Fe (57)	Mg	Zn	Cu	Al	Са	Ti	Cr	Mn	Ni	Ru	Pt	U	Ва	Sr
Average Mass mg/kg	13.45	13.61	58.99	2.77	1.47	62.10	250.85	1.21	0.50	0.33	0.32	0.00	0.00	0.00	0.71	0.85
KClO <sub>3</sub> 2 (1)	109	184	-99	146	10671	-10	1	7	7	26	4	0	0	0	-100	-6
KClO₃2 (2)	189	180	-99	139	10876	4	-3	8	14	23	7	0	0	0	-100	-26
KClO₃2 (3)	203	212	-99	136	10763	2	0	7	8	7	4	0	0	0	-100	-15
KClO₃6	66	38	-99	111	10533	-7	-2	-10	0	6	3	0	0	0	-100	0
KClO₃10	56	44	-99	160	10666	-3	6	20	0	8	2	0	0	0	-100	15
KClO₃20	30	30	-100	120	10542	UND	1	-4	3	UND	4	0	0	0	-100	-1
KClO₃26	32	38	-99	141	10821	-6	-2	0	3	14	1	0	0	0	-100	-5
KClO₃37	38	38	-99	151	10732	-14	7	2	0	51	32	0	0	0	-100	-11
KClO₃42	18	29	-99	111	9569	-28	-12	-3	-10	-11	-8	0	0	0	10	-5
E1 (1)	58	45	-100	125	UND	UND	-32	0	0	0	0	0	0	0	-100	0
E1 (2)	47	35	-100	168	10704	UND	-27	0	0	0	0	0	0	0	-100	0
E1 (3)	54	67	-100	99	UND	UND	0	0	0	16	0	0	0	0	-100	0
E2	38	32	-100	157	10806	101	2	-16	28	10	8	0	28	0	-100	1
dstg1 (1)	35	34	-99	128	UND	48	18	-20	3	12	3	0	0	0	11	0
dstg1 (2)	13	9	-99	142	UND	41	9	-5	1	11	9	0	0	0	3	-3
dstg1 (3)	47	43	-99	106	UND	19	3	-38	3	10	-3	0	0	0	18	-2
dstg2	70	136	-100	189	10852	UND	-22	0	23	0	6	0	0	0	36	-6
dstg3 (1)	34	36	-99	72	UND	15	0	-9	7	4	4	0	0	0	-40	-17
dstg3 (2)	53	51	-99	72	10625	-5	11	-38	5	7	2	0	0	0	-35	-16
dstg3 (3)	25	22	-99	151	10421	-1	-4	6	1	20	3	0	0	0	-66	-21

<sup>\*</sup>UND=undefined

Examining these results, storage under these conditions would not be recommended as there is far too much variance for a forensic investigation. Further research could be done in this area by varying these storage conditions to attempt to increase the reliability using methods such as freezing samples or increasing acidity prior to storage to promote stability.

## 4.2 IR Spectroscopy of Potassium Chlorate

In this chapter potassium chlorate samples were analysed by ATR FTIR, to determine the potential for the analytical technique to provide discriminatory information on the samples. Initially this was done through the visual comparison of raw spectra, to identify any possible trends separating groupings of samples, followed by further exploratory data analysis in the form of PCA. This was utilised to better examine the entire dataset for less obvious differences between groups of samples, and to reduce the dimensionality of the dataset to identify the exact areas of the spectra that lead to discrimination.

Authentic commercial samples of potassium chlorate were sourced through the Defence Science and Technology Group (DST Group) and below in Figure 4.10 is an example of an infrared spectrum of potassium chlorate from the analysis of sample DSTG1.

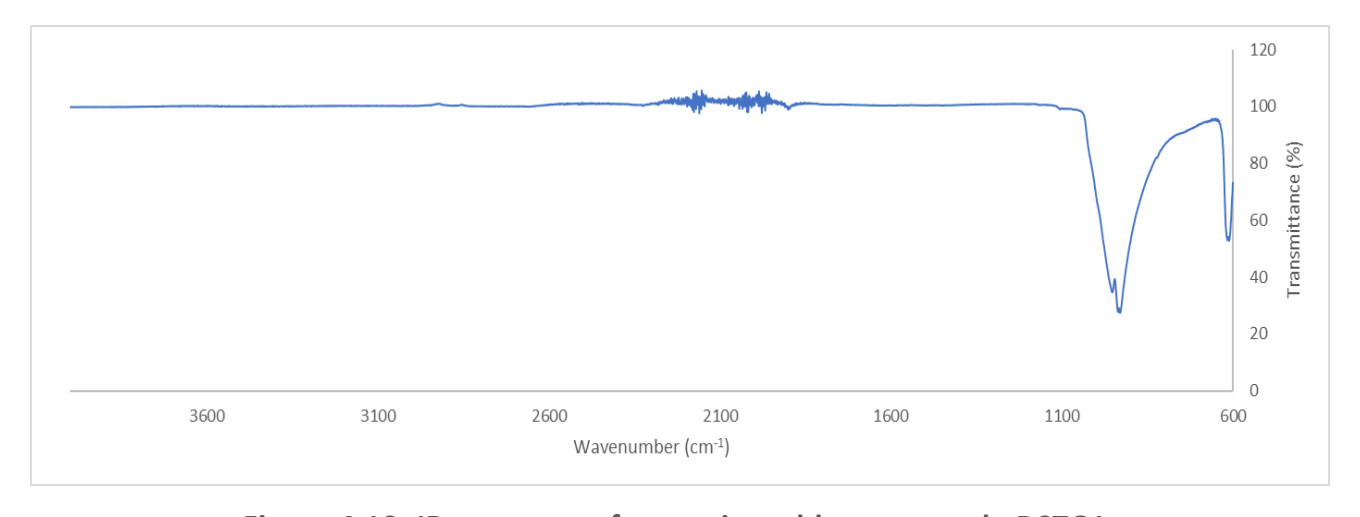


Figure 4.10: IR spectrum of potassium chlorate sample DSTG1.

Peaks in the infrared spectrum of potassium chlorate include signals at approximately 615 cm<sup>-1</sup> (sharp), 930 cm<sup>-1</sup> (sharp, major) and 955 cm<sup>-1</sup> (shoulder). The area between 1950 and 2300 cm<sup>-1</sup> is noisy due to the diamond ATR crystal having multiphonon intrinsic absorption in this range, causing vibrations within the diamond lattice resulting in reduced transmission.<sup>136</sup>

Figure 4.11 presents the spectra of all KClO<sub>3</sub> samples plotted collectively showing that the samples are quite similar and contain the expected peaks; however, some clear differences are apparent. Many of the samples display common additional peaks at 610 cm<sup>-1</sup> (sharp), 930 cm<sup>-1</sup> (sharp), 1087 cm<sup>-1</sup> (broad), 1198 cm<sup>-1</sup> (shoulder), 1425 cm<sup>-1</sup> (broad), 1628 cm<sup>-1</sup> (sharp) and 3383 cm<sup>-1</sup> (broad). These indicate the presence of impurities which can be used to discriminate between samples. Figure 4.12 shows the collective spectra of all samples after a normalisation of transmission percentage to the major peak at 930 cm<sup>-1</sup> to enable a more suitable comparison between the samples.

As a result, the samples could be separated into two groups; spectra with and without these additional peaks. This pattern directly correlates between spectra of potassium chlorate samples made from bleach and electrochemistry, which do not contain the additional peaks, and the pool chlorine samples, which do contain the additional peaks.

This key identifier was suspected to be due to remnants of the various stabilisers present in pool chlorines, primarily the UV stabiliser cyanuric acid. Although this is the main common additive, others exist including pH regulators such as sodium bisulphate. However, this is to a much lower concentration; much of the time it is not listed in the active ingredients and not as likely to produce noticeable additional peaks in the final IR spectrum.

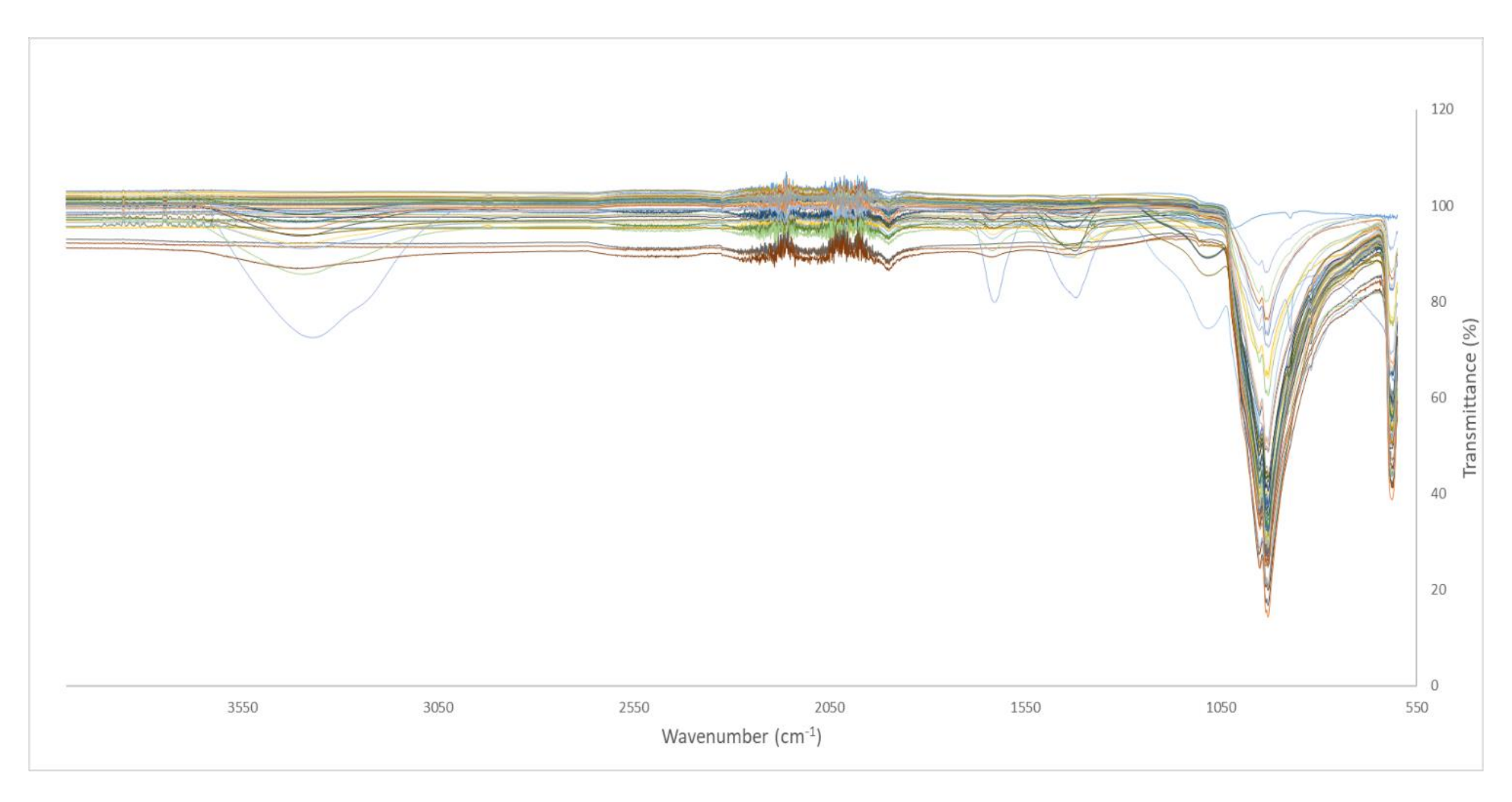


Figure 4.11: Raw IR spectra of all potassium chlorate samples.

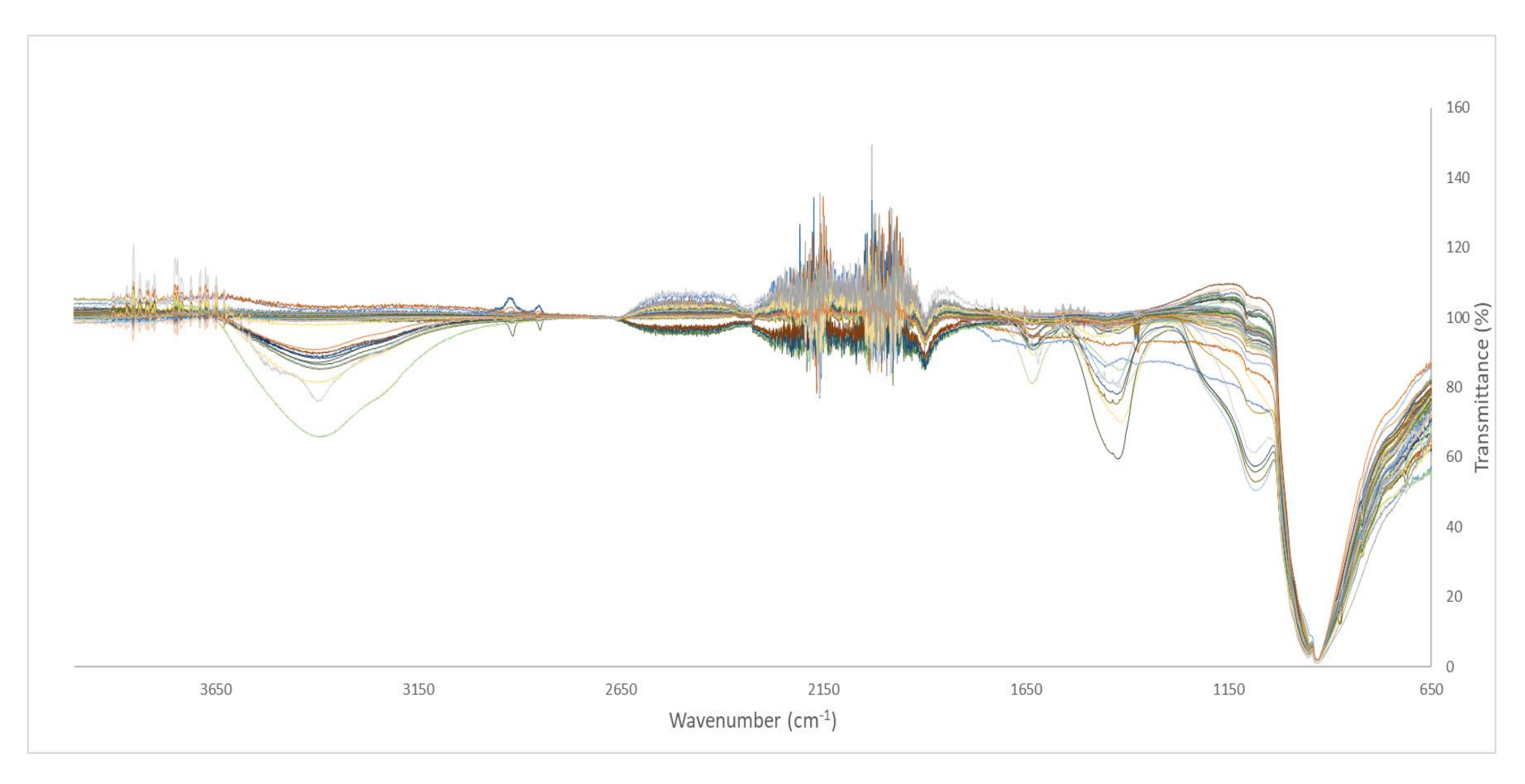


Figure 4.12: IR spectra of all potassium chlorate samples normalised to the major peak at 930 cm<sup>-1</sup>.

To test this hypothesis, a sample of cyanuric acid was obtained from a pool supplies store, sold as pool chlorine UV stabiliser and its IR spectrum collected as shown in Figure 4.13.

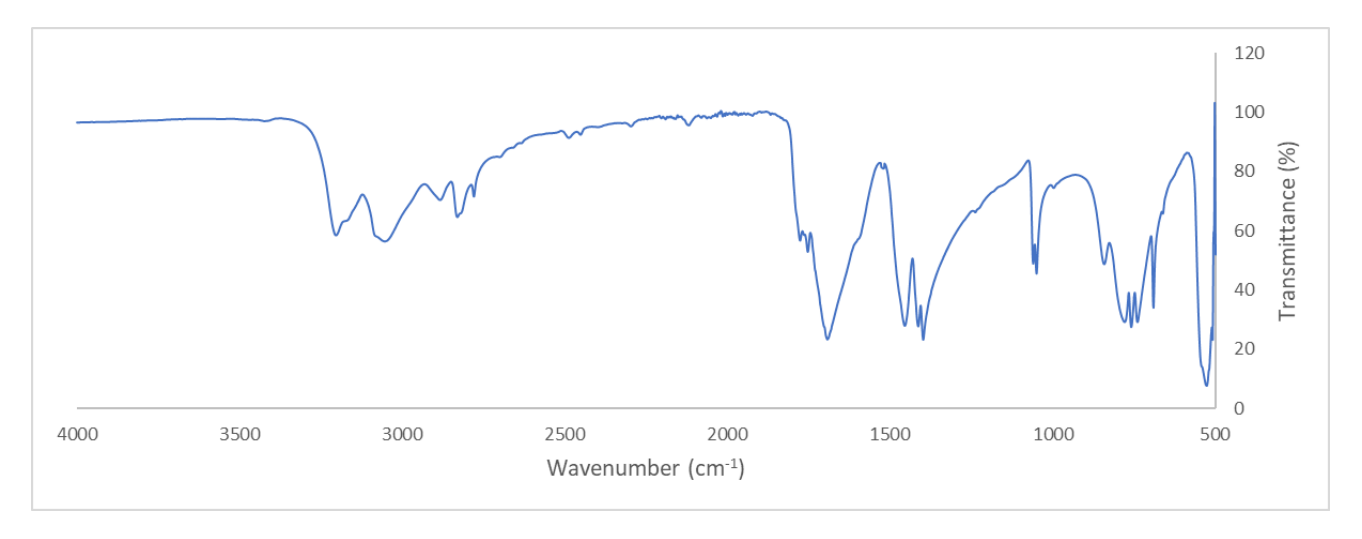


Figure 4.13: IR spectrum of cyanuric acid.

Though this does have a few signals that are in the correct regions, it is evident that many additional peaks are present, that are not found in the spectra of the potassium chlorate samples. Therefore, the conclusion was made that this was not the explanation for the additional signals in the pool chlorine derived samples.

Predicting the other minor additives in the pool chlorine granules, that are not listed in the active ingredients would be incredibly difficult and therefore a sample of pure calcium hypochlorite was obtained from Sigma-Aldrich to repeat the synthesis with just the chemical required to produce potassium chlorate. This was unexpectedly difficult, as following the same method described in the synthesis of potassium chlorate from pool chlorine did not yield any potassium chlorate. To resolve this lack of production the pH of the calcium hypochlorite solution was manipulated via the addition of hydrochloric acid to reach a pH of between 4 and 6. At this pH, synthesis was successful, however, only minor amounts were produced and further modifications did not result in greater yields. This indicates that the additional chemicals within a pool chlorine product stabilise the hypochlorite ions to enable them to react further to form the desired chlorate ion required to produce potassium chlorate. Lowering the pH with hydrochloric acid also favours this reaction to occur, however, it does not stabilise the hypochlorite ions to the same extent.

A benefit of IR spectroscopy is that even with almost trace amounts of material an analysis may be performed and so an IR spectrum for a low yield sample could be obtained as in Figure 4.14.

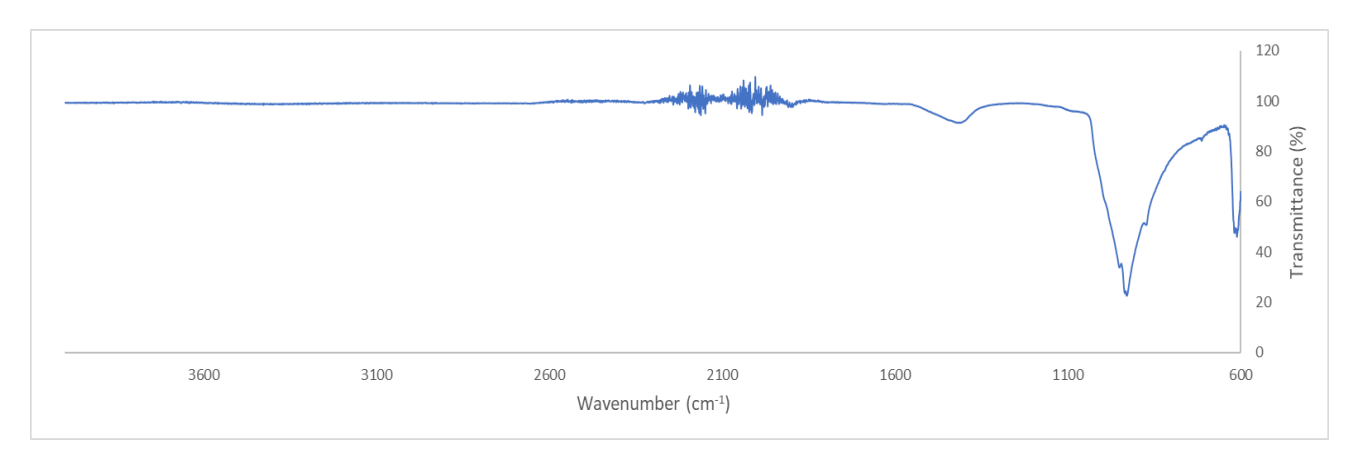
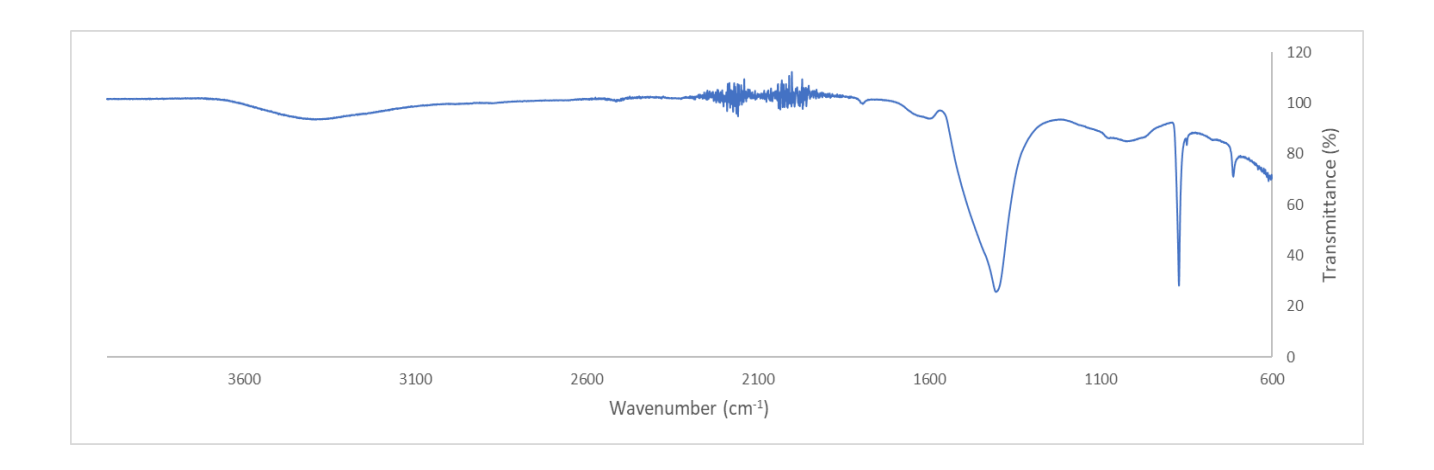


Figure 4.14: IR spectrum of potassium chlorate made using Sigma-Aldrich calcium hypochlorite and hydrochloric acid.

This spectrum does show that some of the additional peaks found in samples produced from pool chlorine are no longer present, however, there are features that still separate this from bleach derived samples, including the broad peak at 1415 cm<sup>-1</sup> and small shoulders at 715 cm<sup>-1</sup> and 890 cm<sup>-1</sup>. As these features were present in the pure calcium hypochlorite derived sample this leaves just the origin of the large peaks at 1100 cm<sup>-1</sup>, 1700 cm<sup>-1</sup> and 3400 cm<sup>-1</sup> unassigned. Additionally, the relative amplitude of the 1415 cm<sup>-1</sup> peak is lower than that of the pool chlorine samples.

One noticeable difference between the pool chlorine and bleach methods is the production of an insoluble calcium deposit on all glassware, requiring acid cleaning to remove. This could potentially be present in the final product and so was isolated by dissolving a large amount of laboratory grade Sigma-Aldrich calcium hypochlorite in water, filtering the insoluble solids and performing an IR analysis (Figure 4.15).



This unknown solid has many of the unassigned peaks including 715 cm<sup>-1</sup>, 870 cm<sup>-1</sup>, 1400 cm<sup>-1</sup> and the broad stretch at 3400 cm<sup>-1</sup>. Based on its low solubility, the unknown product was predicted to be calcium hydroxide. To confirm this, a sample of calcium hydroxide was prepared for comparison by

Figure 4.15: IR spectrum of isolated insoluble material from calcium hypochlorite solution.

combining aqueous sodium hydroxide and calcium chloride. The calcium hydroxide was washed with a large volume of hot water to remove any possible impurities; hot water was used as calcium hydroxide has inverse solubility where it is more soluble in cold rather than hot water. This was then

dried in a desiccator for 2 days prior to IR analysis.

The prediction is somewhat confirmed, however, the broad peak at 3400 cm<sup>-1</sup> has been replaced with a sharp peak at 3640 cm<sup>-1</sup> (Figure 4.16). A possible explanation for this lack of broad stretch could be the formation of a hydrate, rather than in the case of the pool chlorine samples, where free water may be trapped within the sample.

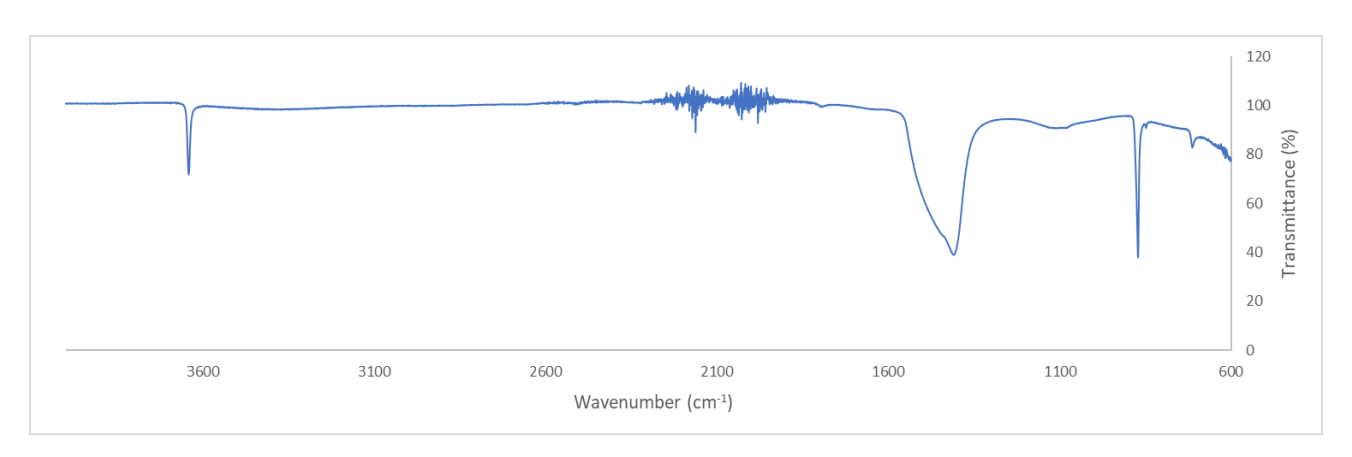


Figure 4.16: IR spectrum of prepared calcium hydroxide.

Although both the calcium hydroxide and cyanuric acid can account for many of the peaks present in the pool chlorine samples, it is not a direct match. This could be due to the presence of an additional unidentified impurity in the pool chlorine starting material or the product of an unknown reaction between the chemicals throughout the synthesis process.

The differing spectral features between potassium chlorate samples is useful, as it allows for some insight to be gained as to the synthetic pathways and starting materials used in its production. However, there may be more discriminatory information that is not so obvious and so a chemometric approach was undertaken.

# 4.2.1 Exploratory Multivariate Analysis of FT-IR Data

The first step in any chemometric approach is a well-defined pre-processing methodology. As PCA is a purely mathematical approach, some level of normalisation must be employed to allow the spectra to be compared to one another. Normalisation was undertaken using the major common signal of the spectra at 930 cm<sup>-1</sup> and setting the transmittance to at this point to 1% (Figure 4.12). The transformed spectra are now comparable to each other. Another aspect of PCA is that all datapoints will now be treated equally, and so abnormalities must be carefully considered; for example, the noisy ATR region in the FTIR spectra (1750-2675 cm<sup>-1</sup>). This will have to be removed as it is a large source of variation between samples, which cannot be attributed to the differences between samples but rather a limitation of the analytical equipment.

Some samples also had weaker absorbances, which could be a result of sodium/potassium chloride impurities within the samples, which are transparent in the frequency range being analysed. This effectively dilutes the potassium chlorate signals and once normalised, will negatively impact the signal to noise ratio of these spectra. This alone can be valuable information as it indicates a less efficient method of manufacture, however, outliers such as these will hinder the discriminatory power of the PCA. When such spectra were examined, the signal to noise ratio is unfavourable, and if excessive noise exists in regions with characteristic signals, this will cause issues as it introduces artificial variance in the dataset. Unfortunately, little can be done to negate this other than excluding the spectra. Excluded samples include KClO<sub>3</sub> 20, KClO<sub>3</sub> 40-45, which were all partially successful syntheses.

This highlights a major drawback of a purely mathematical approach such as PCA used in isolation increases the importance of high-quality spectra. This high quality and consistency of data may not be possible in real world scenarios, where different instrumentation is used, producing a variety of resolutions and quality. This is further compounded if there are additives in an analysed HME such

as fuels, stabilisers, etc. These real-world complications may make comparisons of samples to a database more difficult, much like the case for other database matching applications, e.g., poor quality fingerprints found at crime scenes or low-quality photos for facial recognition.

The final step of the pre-processing is a visual screening of data as there may be clear visual signs of outlier spectra when examined. After this pre-processing, the spectra were transformed to a more suitable state as pictured in Figure 4.17 and the exploratory data analysis was undertaken.

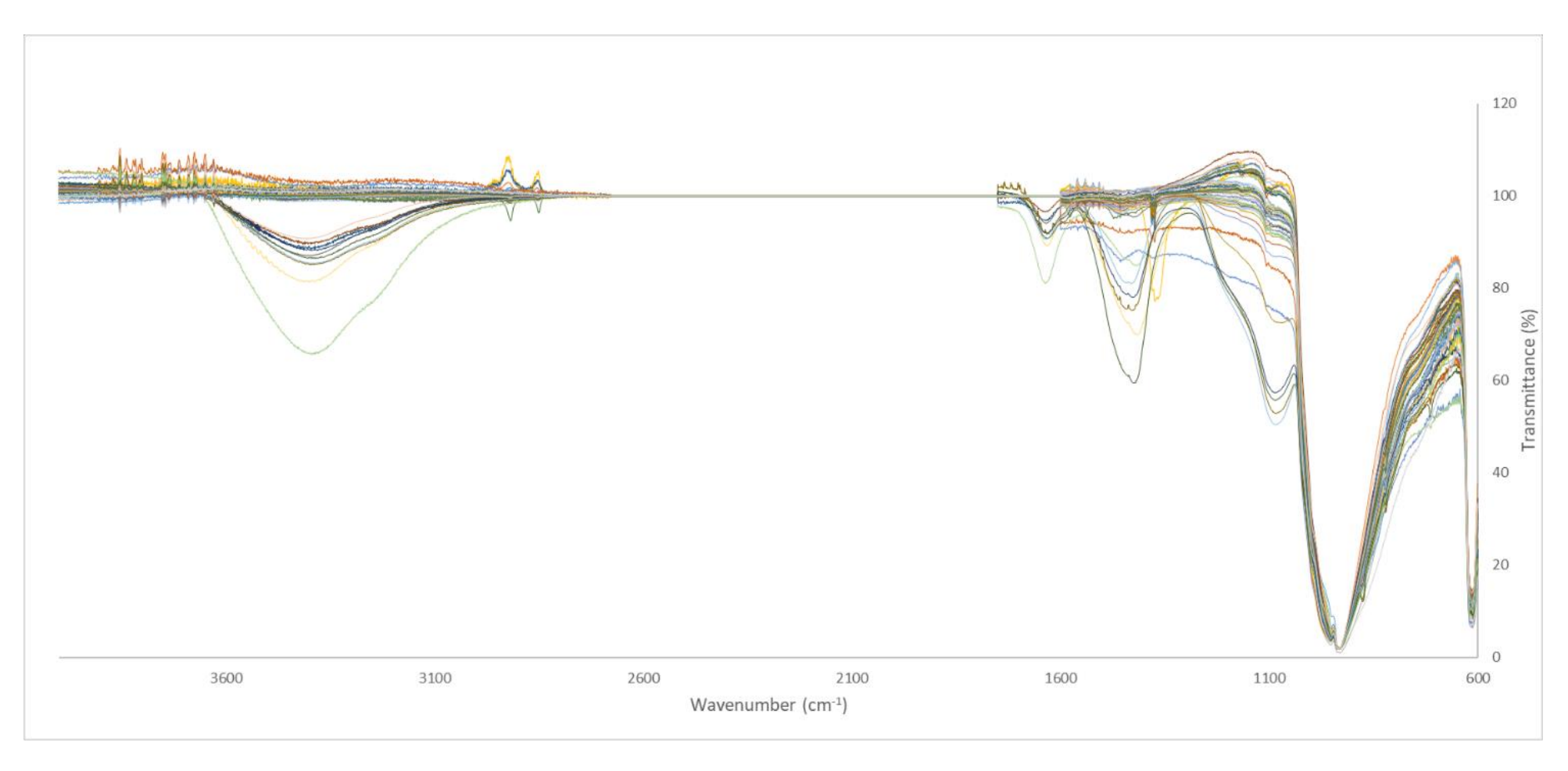


Figure 4.17: IR spectra of KClO<sub>3</sub> samples after initial pre-processing of data.

Firstly, a hierarchical cluster analysis (HCA) was performed on the normalised data to identify any clear groupings within the spectra. The results are displayed in Figure 4.18 in the form of a dendrogram, and the accompanying Table 4.10 displays the corresponding sample identities. This analysis shows that there are not many clear groupings as the majority of the samples are very similar to each other. There are, however, several samples that stand out including samples 28, 29, 33, 34, 36 and 35, which correspond to KClO<sub>3</sub> 19, KClO<sub>3</sub> 21, KClO<sub>3</sub> 25, KClO<sub>3</sub> 25\_2, KClO<sub>3</sub> 27 and KClO<sub>3</sub> 26. These are all samples produced through the pool chlorine synthesis method and therefore this is not an unexpected result. As previously mentioned, their IR spectra looked visibly different with some clear additional signals within the spectra. This highlights that potential discrimination may exist within the dataset, however, this is a very basic non-transformative analysis and for more information PCA needs to be performed as HCA does not identify why some spectra are different to others in any level of useful detail. While in this exploratory study the HCA is just as useful as the visual inspection, in a real-world database where thousands of samples may be analysed, a visual inspection would be difficult and time consuming.

Table 4.10: Sample correlation to number identifiers in HCA dendrogram.

Number	Sample	Number	Sample	Number	Sample
1	cu	19	KClO <sub>3</sub> 10	37	KClO <sub>3</sub> 28
2	dstg1	20	KClO <sub>3</sub> 11	38	KClO <sub>3</sub> 29
3	dstg2	21	KClO <sub>3</sub> 12	39	KClO <sub>3</sub> 30
4	dstg3	22	KClO <sub>3</sub> 13	40	KClO <sub>3</sub> 31
5	e1	23	KClO <sub>3</sub> 14	41	KClO <sub>3</sub> 32
6	e2	24	KClO <sub>3</sub> 15	42	KClO <sub>3</sub> 33
7	icpms1	25	KClO <sub>3</sub> 16	43	KClO <sub>3</sub> 35
8	KClO <sub>3</sub> 1	26	KClO <sub>3</sub> 17	44	KClO <sub>3</sub> 36
9	KClO <sub>3</sub> 2	27	KClO <sub>3</sub> 18	45	KCIO <sub>3</sub> 36_2
10	KClO <sub>3</sub> 3	28	KClO <sub>3</sub> 19	46	KClO <sub>3</sub> 37
11	KClO <sub>3</sub> 3_2	29	KClO <sub>3</sub> 21	47	KClO <sub>3</sub> 38
12	KClO <sub>3</sub> 4	30	KClO <sub>3</sub> 22	48	KClO <sub>3</sub> 39
13	KClO <sub>3</sub> 5	31	KClO <sub>3</sub> 23	49	pt1
14	KClO <sub>3</sub> 5_2	32	KClO <sub>3</sub> 24	50	Ss
15	KClO <sub>3</sub> 6	33	KClO <sub>3</sub> 25		
16	KClO <sub>3</sub> 7	34	KClO <sub>3</sub> 25_2		
17	KClO <sub>3</sub> 8	35	KClO <sub>3</sub> 26		
18	KClO <sub>3</sub> 9	36	KClO <sub>3</sub> 27		

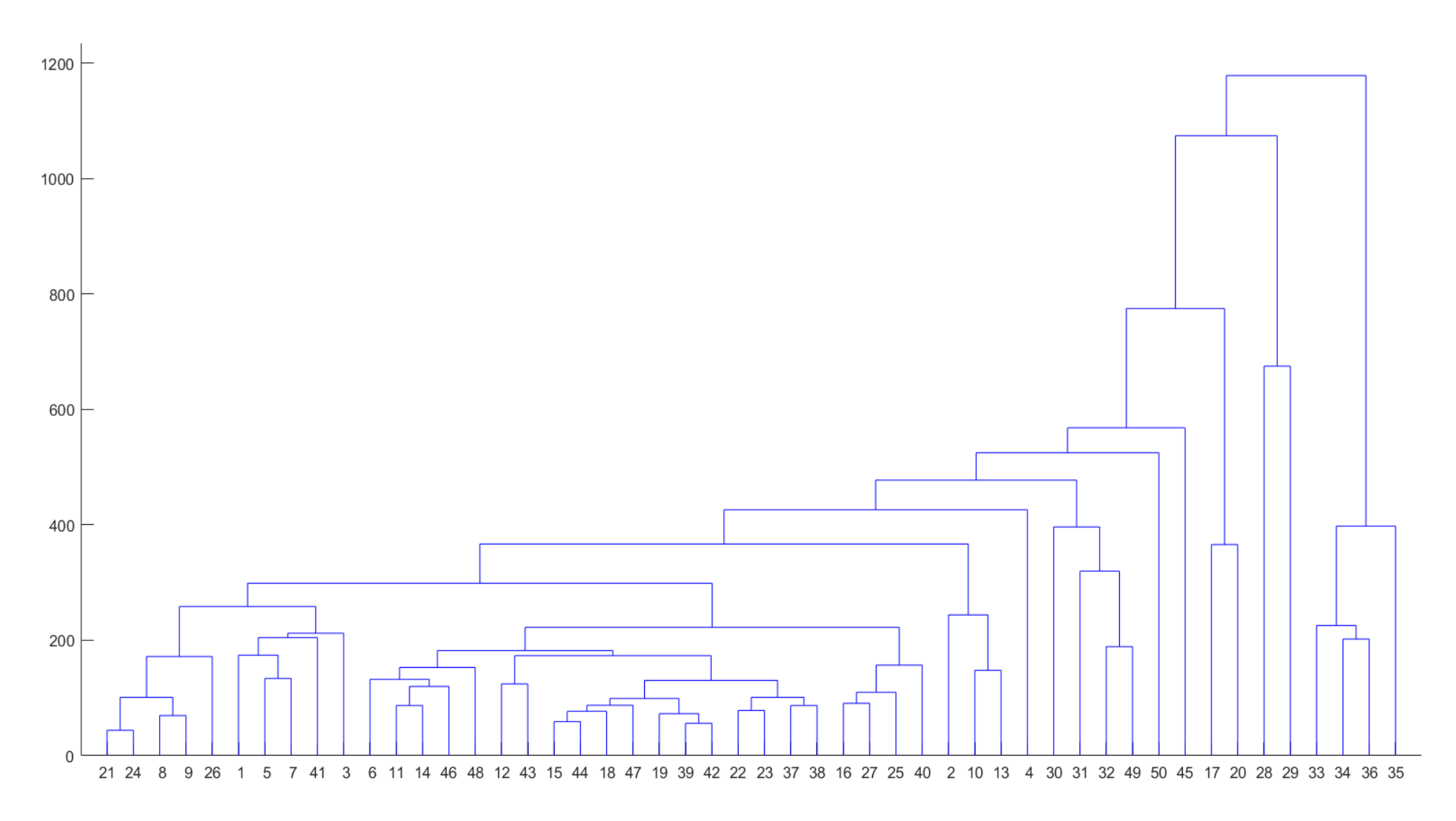


Figure 4.18: Resultant dendrogram from the hierarchical cluster analysis of potassium chlorate IR spectra.

Prior to inspecting the results of the PCA analysis it is important that the quality of the analysis is reviewed. Firstly, as the data has been completely transformed, it is crucial to determine how much of the original dataset's variance has been retained. This can easily be calculated using the cumulative sum of the principal component eigenvalues divided by the total variance. Tabulated in Table 4.11 below are the results of the variance retention calculations, and the accompanying scree plot in Figure 4.19.

Table 4.11: Variance retention table.

	Principal Component	Cumulative
Component	Eigenvalues	Percentage of Variance Explained
·		-
PC1	124843.5549	57%
PC2	48651.70041	80%
PC3	28343.92219	93%
PC4	7310.307275	96%
PC5	3299.430407	98%
PC6	1378.324004	98%
PC7	1237.631349	99%

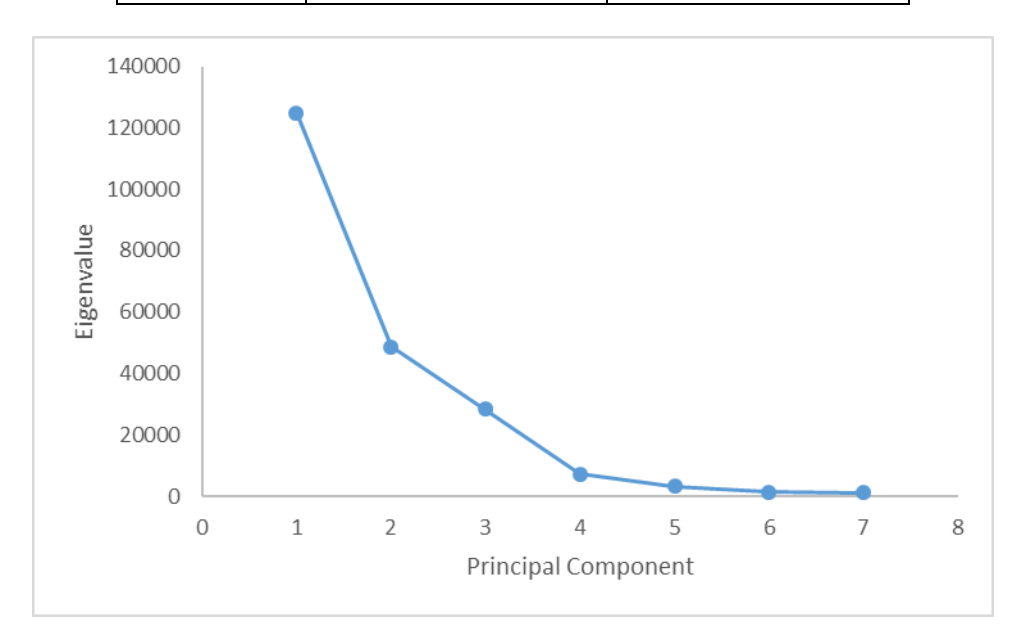


Figure 4.19: Scree plot for the PCA of pre-processed KClO<sub>3</sub> IR data.

This variance breakdown illustrates that 96% of the variance is retained within the first 4 principal components and 99% by the seventh component. A clear elbow in the scree plot curve at component 4 indicates that further components have a dramatic reduction of variance within the data.

PCA performs a dimensionality reduction and as such, each principal component is made up of many variables of the original dataset. In the case of IR spectra, these variables consist of the wavenumbers of the spectra and it is important to understand the make-up of the factors/loadings in each principal component. These loadings are summarised numerically in Table 4.12 and graphically in Figure 4.20. The data has been presented differently to the previous ICP-MS analysis due to the large number of datapoints as each 0.25 cm<sup>-1</sup> is counted as a variable. As a result, listing individual loadings rather than ranges would result thousands of data points, rather than a few elements as was the case in ICP-MS analysis.

Table 4.12: Loading factors for principal components 1-4.

Principal Component	Key Loading Regions (cm <sup>-1</sup> )				
PC1	628-726, 1019-1247, 1382-1507, 3308-3474				
PC2	1011-1238, 1622-1648, 3165-3585				
PC3	600-610, 619-893, 985-1026, 1049-1143				
PC4	601-604, 765-863, 1027-1030, 1039-1128, 1245-1537, 3629-3630				

The loadings plots identify the regions of the IR spectra that contribute to each of the principal components and should somewhat resemble a spectrum in that they are smooth curves that correspond to signals in the original spectrum. Once a loadings plot begins to stop resembling a spectrum, this is an indication that the component is no longer representing a significant amount of variance within the original dataset. This can start to be seen in PC4, where the curves form sharper points, which is understandable as 93% of the dataset's variance is accounted for prior to PC4, which then only accounts for an additional 3%.

The representation in Figure 4.20 is quite informative as it shows the location and magnitude of influence various regions of the spectrum have on each PC. A shortcoming, however, is that without the direct comparison to the original spectrum, the greater picture of exactly where the contribution relates to can be lost. Therefore, a loadings breakdown (Figure 4.21) can be created to supplement these plots to clearly highlight this aspect.

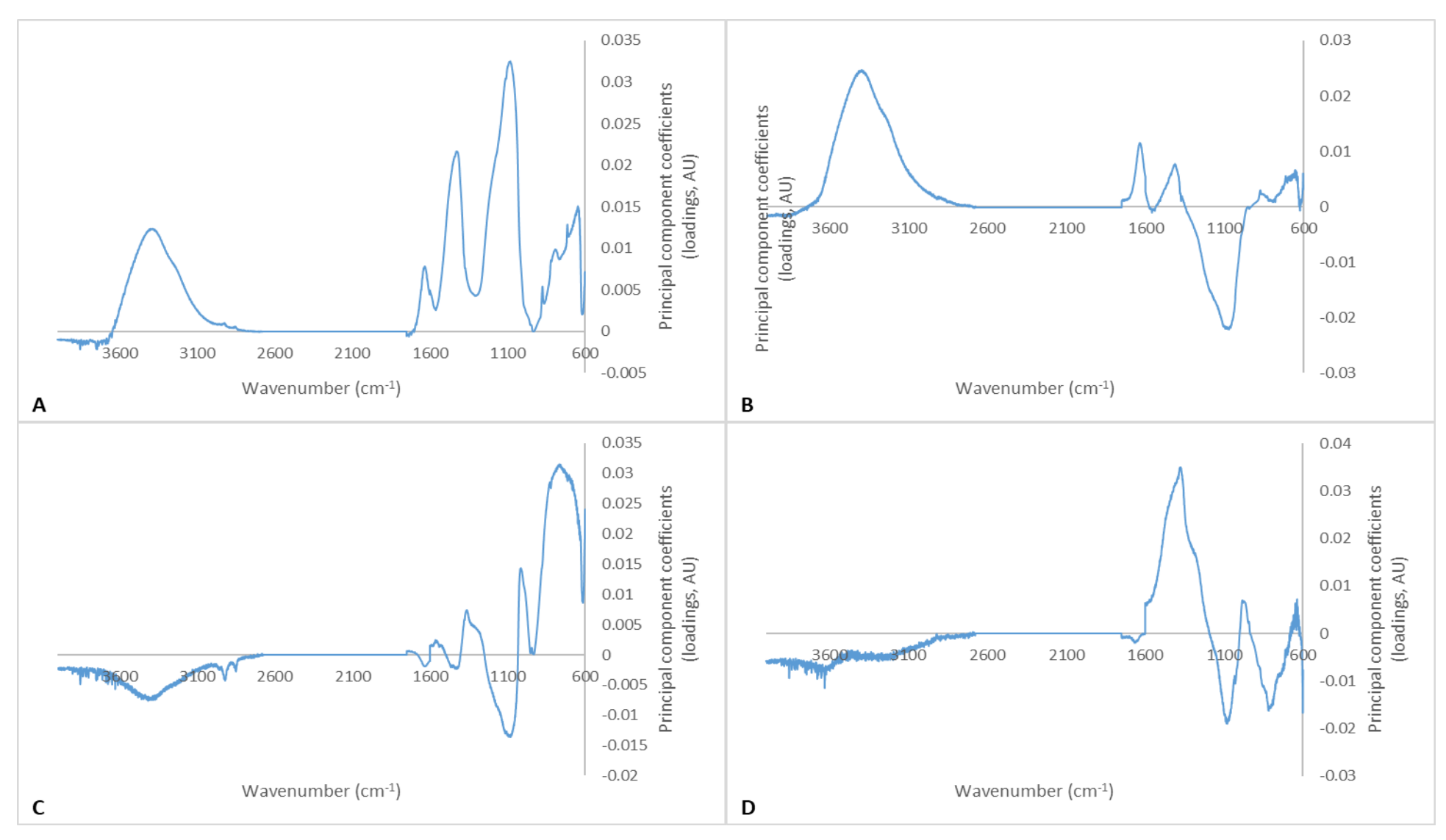


Figure 4.20: Spectrum loadings for A) PC1, B) PC2, C) PC3 and D) PC4 of the KClO3 FT-IR dataset.

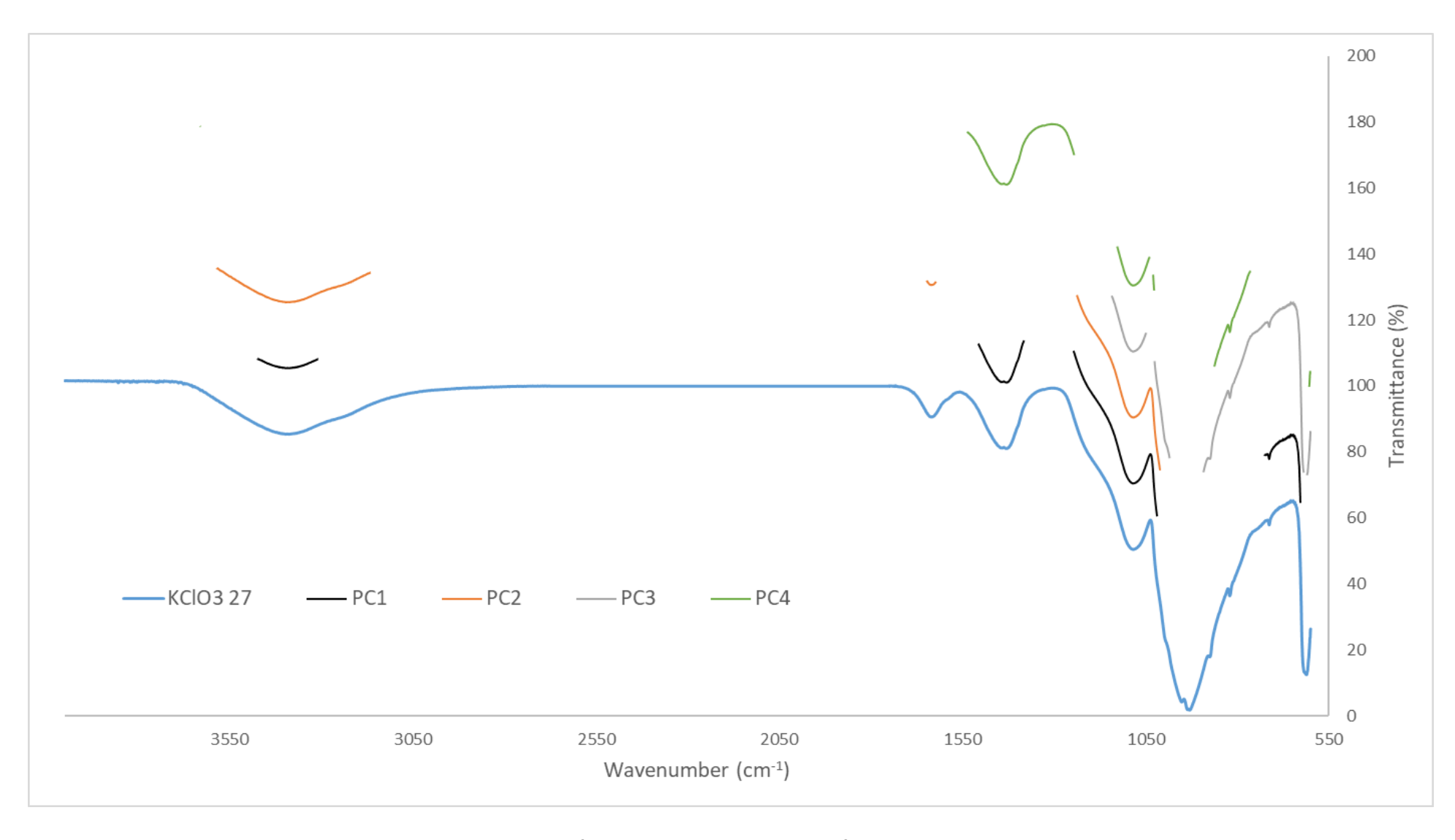


Figure 4.21: Loadings breakdown for first 4 PCs (20% offset between each) highlighting the focus regions of each PC against a representative IR spectrum of KClO<sub>3</sub>.

The initial analysis of the variance retention and loadings of the PCA is incredibly important in understanding and being able to extract useful information from the results. These results come in the final form of scores, which can then be used to identify clustering through the use of various plotting strategies.

The individual components may be plotted to examine the discriminatory power of each principal component as in Figure 4.22. Examining these plots, PC1 shows that there is no large separation between any of the groups of samples. There are a few low score samples, most of which are pool chlorine samples however, there this clear crossover with bleach samples and even four pool chlorine samples, mixed in with the bulk of the other samples. This indicates that the previously identified visual differences between the pool chlorine samples and non-pool chlorine samples were not identified as significantly discriminatory in this analysis.

This suggests that the pre-processing has affected the PCA in a negative manner. When re-examining the plot of pre-processed spectra in Figure 4.17, it is evident that the baselines of the spectra are variable, including over the regions with impurity peaks. This minimises the discriminatory variability across the samples and so a baseline correction will be a required addition to the pre-processing method.

This information is from just one principal component and more can be examined to see further discrimination; however, as PC1 accounts for 57% of the dataset's original variance, the amount of variance explained by further components does diminish. This is apparent when reviewing PC3 (Figure 4.22C) where there is no clear separation between sample types, as the main cluster of samples has spread into a disparate cloud of data points. This provides no beneficial information to help discriminate samples from one another.

The benefit of PCA is that each component is a multitude of dimensions in the original dataset and hence combining multiple components in a single plot allows the analyst to encompass up to 93% of the original variance (in this dataset) by performing up to a three-dimensional plot. Figures 4.23 and 4.24 show two-dimensional plots between principal components 1, 2 and 3.

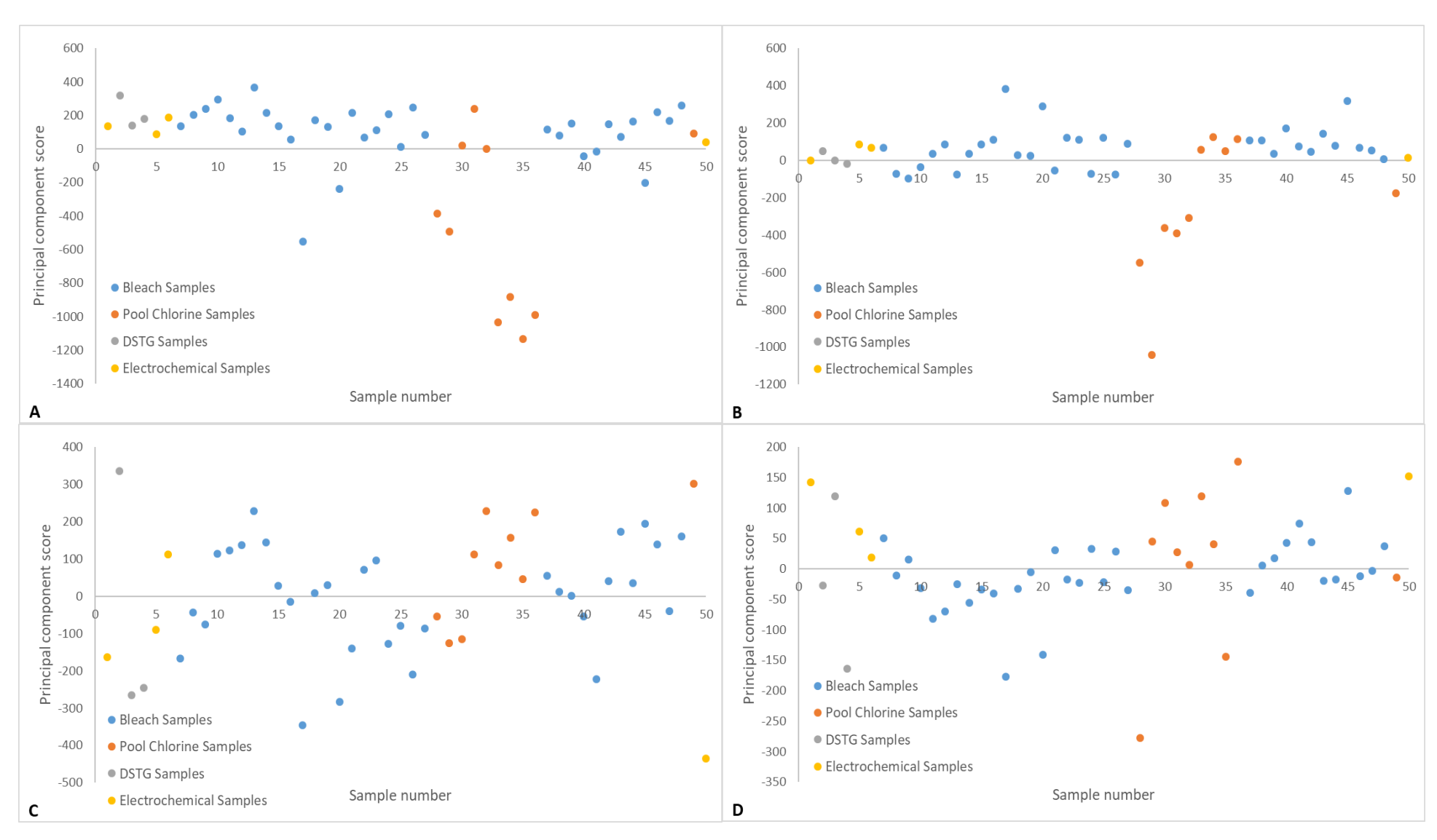


Figure 4.22: One dimensional score plots for A) PC1, B) PC2, C) PC3 and D) PC4 of the normalised KClO₃ FT-IR dataset

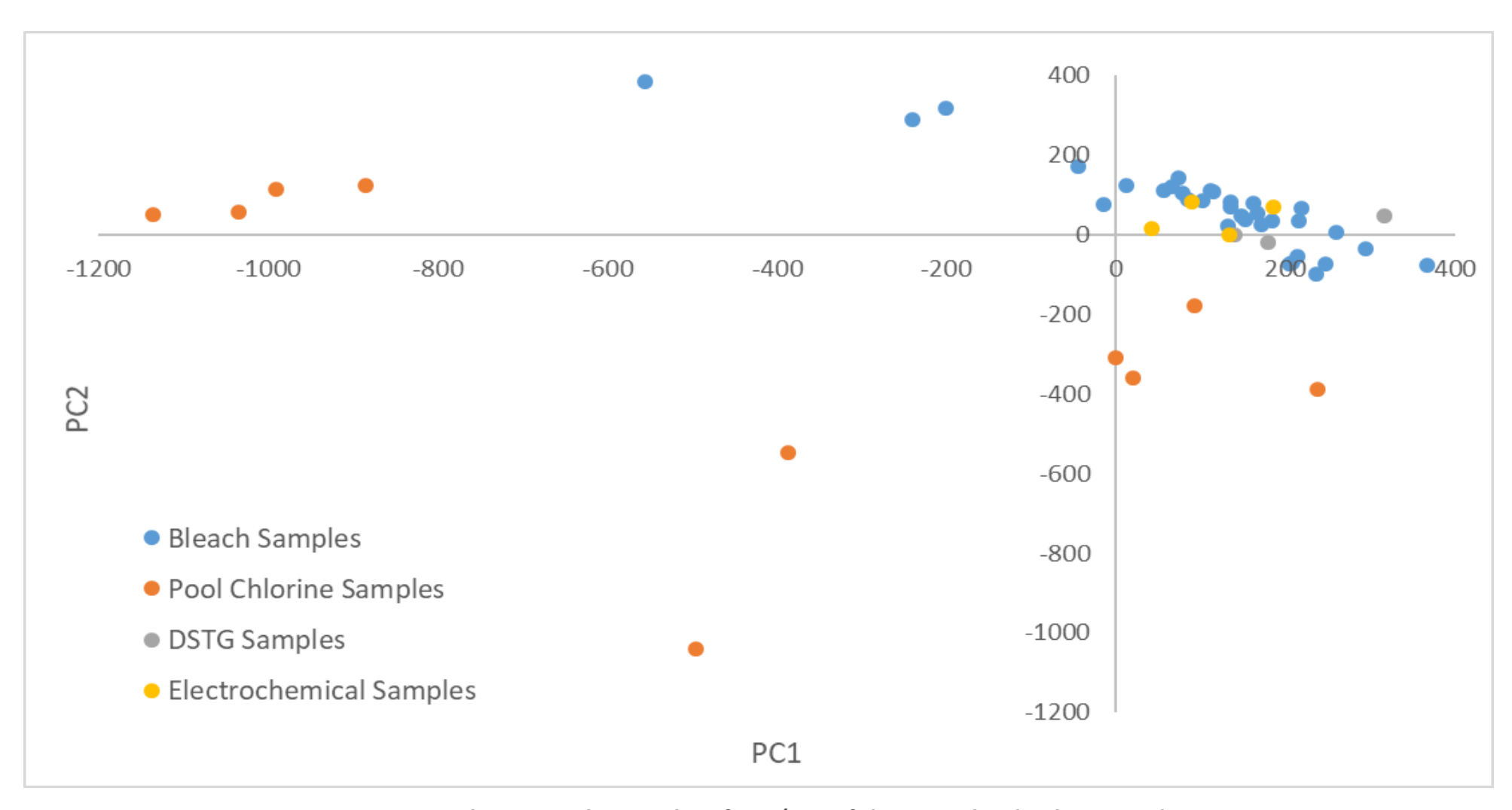


Figure 4.23: Two-dimensional score plot of PC1/PC2 of the normalised KClO<sub>3</sub> FT-IR dataset.

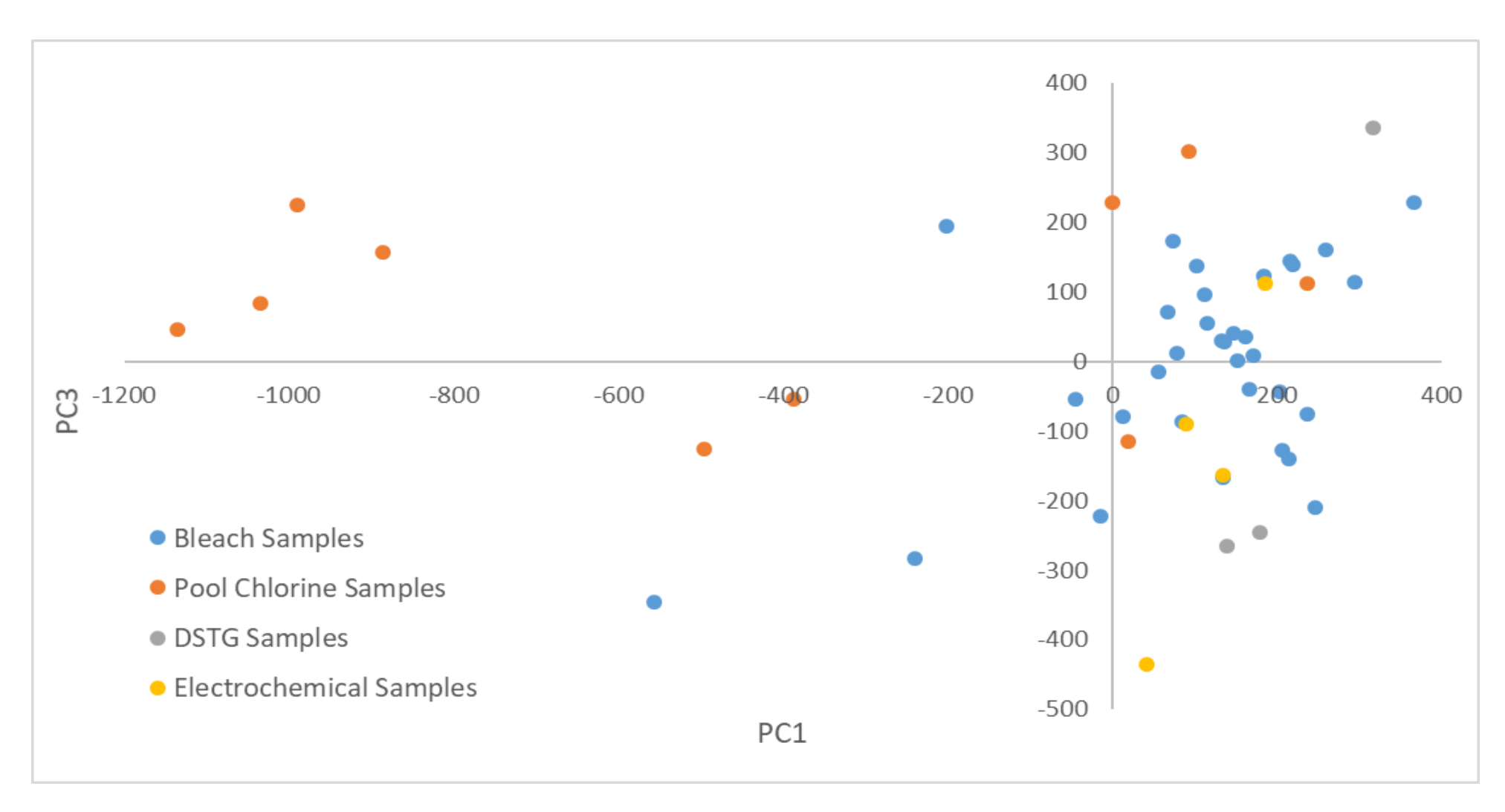


Figure 4.24: Two-dimensional score plot of PC1/PC3 of the normalised KClO<sub>3</sub> FT-IR dataset.

The plot of PC1/PC2 highlights the slight separation of all the pool chlorine method samples from the rest. This separation, however, is not very distinct and if sample types were not colour coded only the distinctly separated samples could be confidently identified as a separate grouping.

The plot of PC1/PC3 shows the lack of discriminatory information contained within PC3, as there is very minimal separation between sample types other than the cluster of four distinctly separated samples purely from the PC1 scores.

The ideal representation of PC data is in the form of a three-dimensional plot, as it can display all the variance within 3 PCs. Unfortunately, this does not present well in a static form as shown in Figure 4.25 but is incredibly informative in an interactive state such as MATLAB, where the plot may be rotated to examine the clustering from various perspectives. In this way, two-dimensional planes of separation may be identified to separate groups of samples.

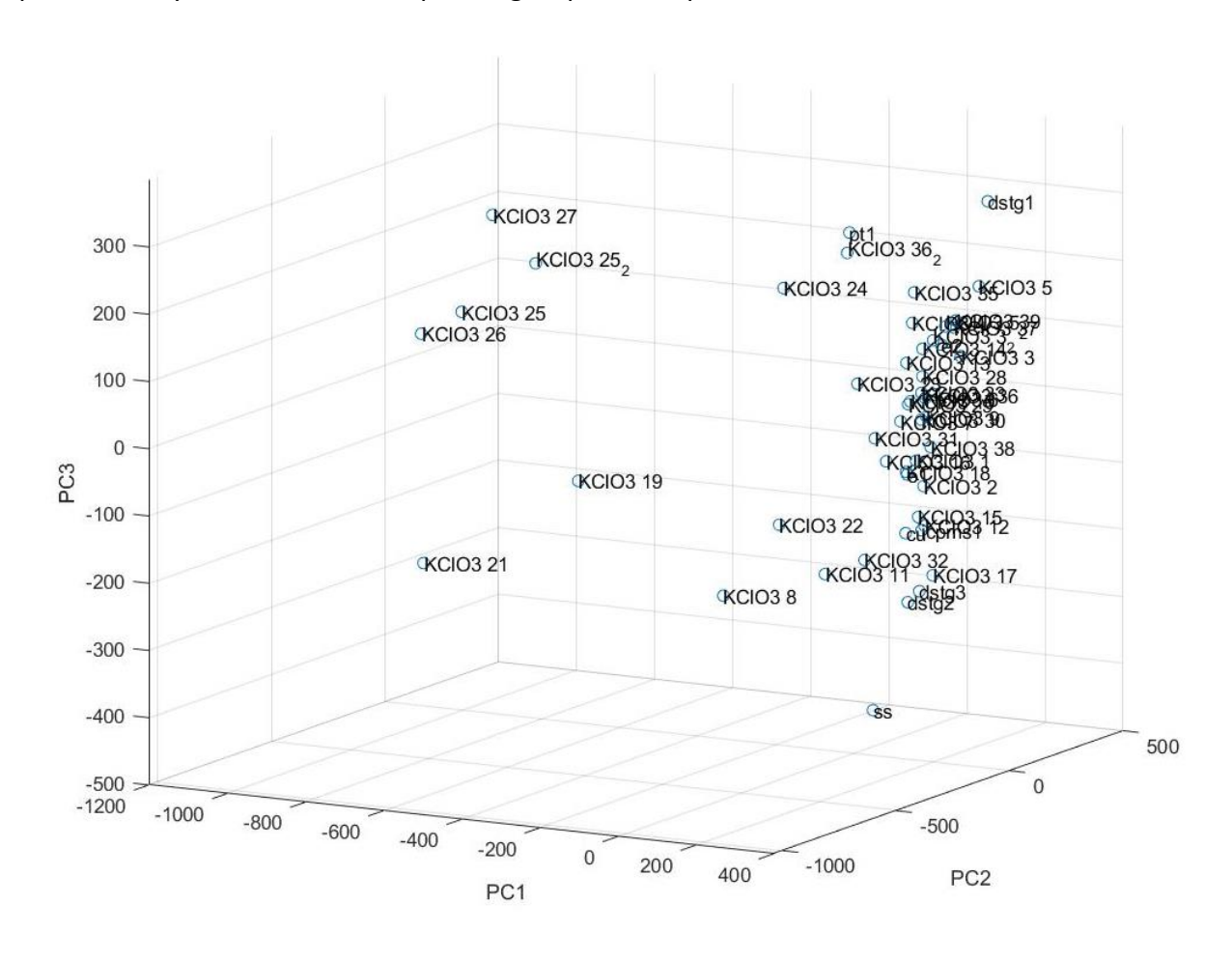


Figure 4.25: Three-dimensional plot of PC1, PC2 and PC3 of the normalised KClO₃ FT-IR dataset.

This analysis can identify that there is some minimal level of discriminatory identification within the infrared spectroscopy dataset through the use of PCA on normalised data. As previously mentioned, more pre-processing could be undertaken to try and improve the analysis, for example, a baseline correction. There are complications to such a pre-processing technique, as it must be applied consistently across all samples and in this case the Spectrum<sup>131</sup> software package was used to apply a polynomial correction across all the samples together.

Applying a manual baseline correction to the original dataset using the 6 base points in Table 4.13, and depicted in Figure 4.26, results in the dataset transforming to Figure 4.27. These points were selected based on the collected spectra, which indicated that these points were a return to baseline. The software can also select and apply these positions automatically, however, to record and retain these positions a manual method was selected, rather than an unknown computer correction.

Table 4.13: Manual baseline correction base points selection.

Base Point	Position (cm <sup>-1</sup> )
1	647
2	1308
3	1558
4	1730
5	2995
6	3678

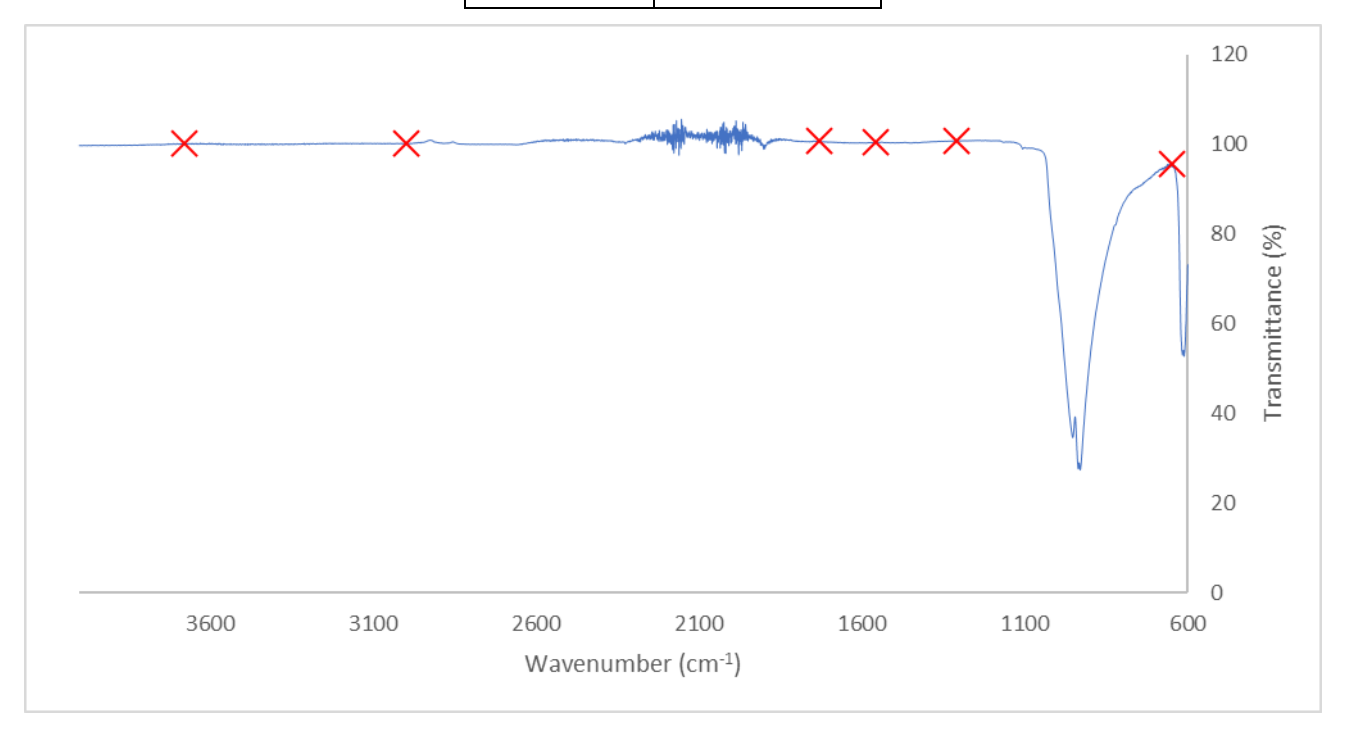


Figure 4.26: Manual baseline correction base points marked on KClO3 1 spectrum.

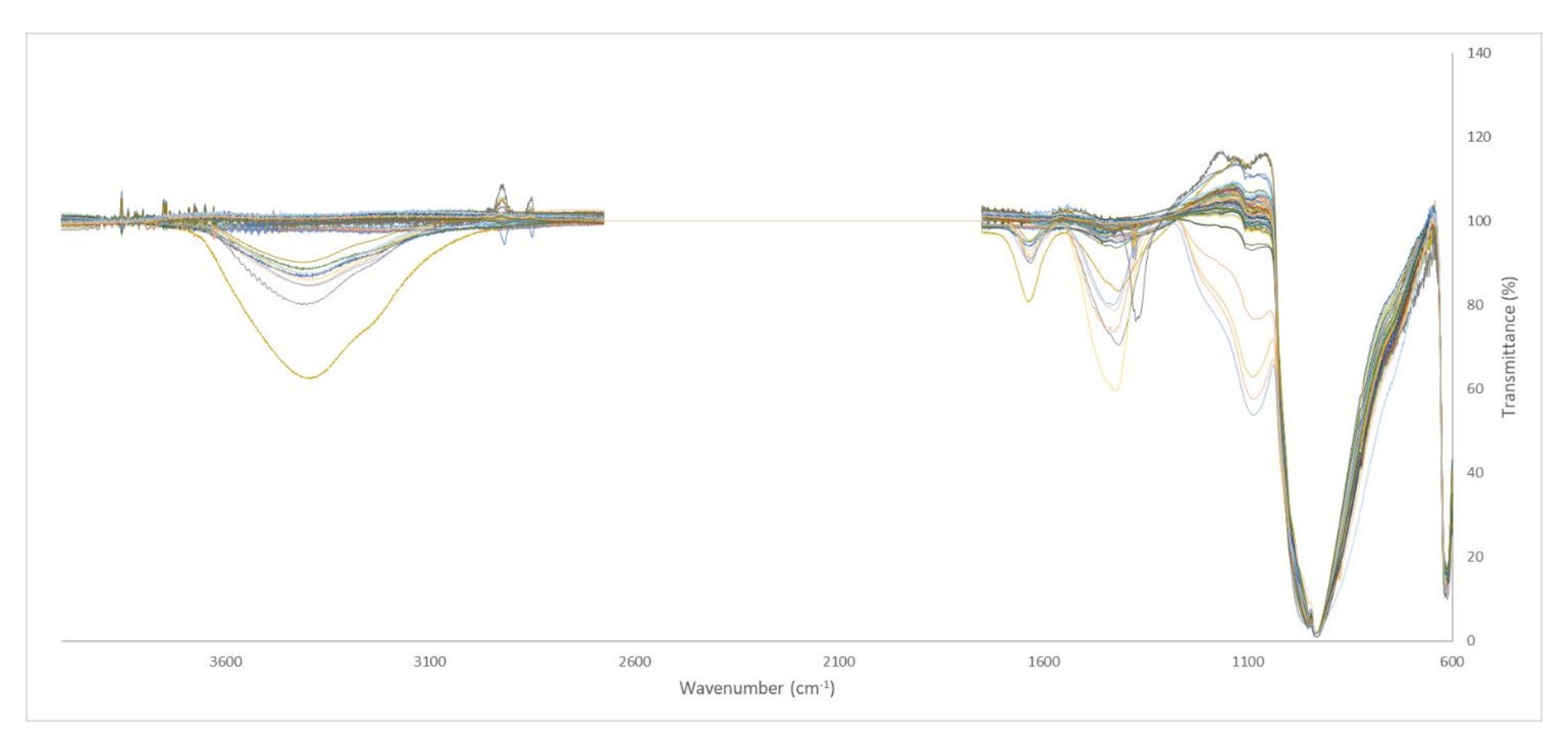


Figure 4.27: Spectra of KClO<sub>3</sub> samples after 6 base point baseline correction followed by normalisation to the major peak at 930 cm<sup>-1</sup> (ATR region removed).

The HCA of this dataset as shown in Figure 4.28 very closely resembles that of the original dataset, with the 6 samples clearly separated from the main body of samples being those of the pool chlorine synthesis method. The distance between the clusters of samples within the dataset are now greater and indicate a more discriminatory dataset.

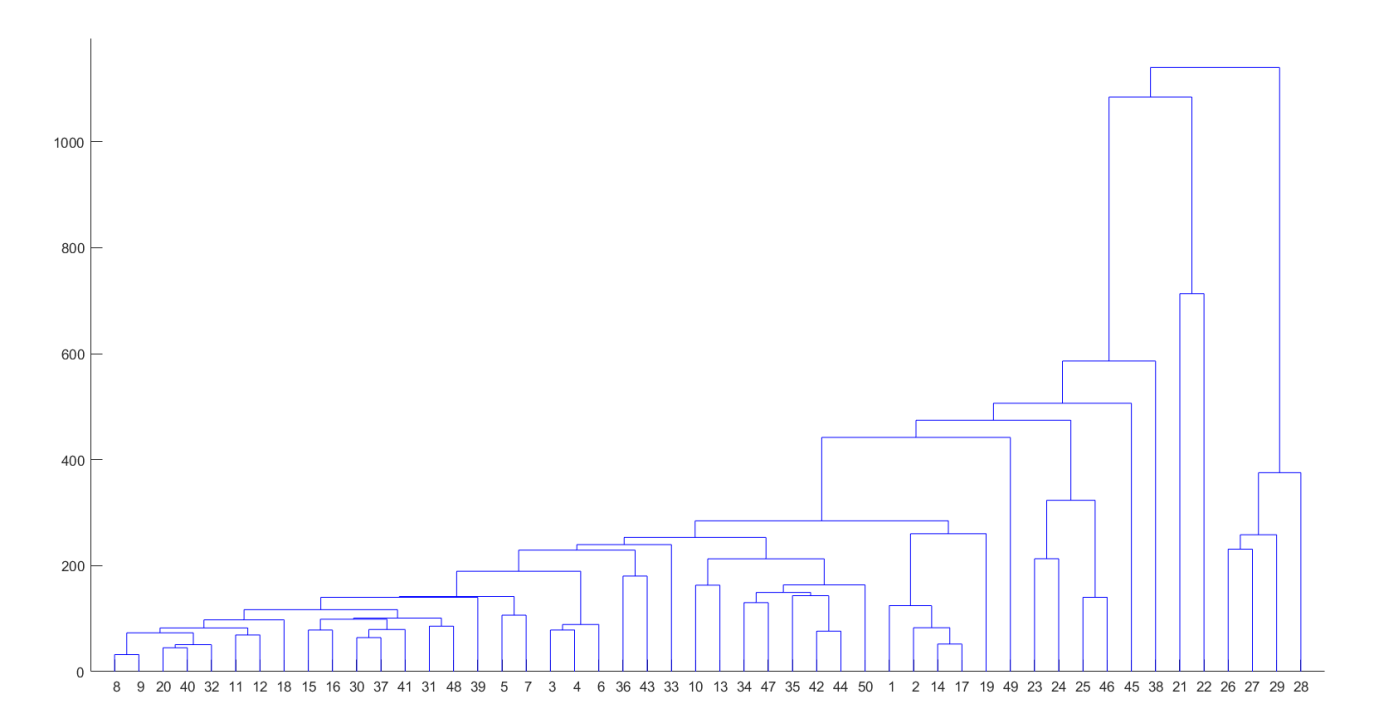


Figure 4.28: Hierarchical cluster analysis of potassium chlorate IR spectra after 6-point baseline correction and normalisation.

Table 4.14: Sample correlation to number identifiers in HCA dendrogram.

Number	Sample	Number	Sample	Number	Sample	Number	Sample	Number	Sample
1	KClO₃ 1	12	KClO <sub>3</sub> 10	23	KClO <sub>3</sub> 22	34	KClO <sub>3</sub> 32	45	DSTG3
2	KClO₃ 2	13	KClO₃ 11	24	KClO₃ 23	35	KClO₃ 33	46	PT1
3	KClO₃ 3	14	KClO₃ 12	25	KClO <sub>3</sub> 24	36	KClO₃ 35	47	E1
4	KClO <sub>3</sub> 3_2	15	KClO <sub>3</sub> 13	26	KClO <sub>3</sub> 25	37	KClO <sub>3</sub> 36	48	E2
5	KClO₃ 4	16	KClO₃ 14	27	KClO₃ 25_2	38	KClO₃ 36_2	49	SS
6	KClO₃ 5	17	KClO₃ 15	28	KClO₃ 26	39	KClO <sub>3</sub> 37	50	Cu
7	KClO <sub>3</sub> 5_2	18	KClO₃ 16	29	KClO <sub>3</sub> 27	40	KClO <sub>3</sub> 38		
8	KClO₃ 6	19	KClO <sub>3</sub> 17	30	KClO <sub>3</sub> 28	41	KClO₃ 39		
9	KClO <sub>3</sub> 7	20	KClO <sub>3</sub> 18	31	KClO₃ 29	42	ICPMS1		
10	KClO <sub>3</sub> 8	21	KClO₃ 19	32	KClO <sub>3</sub> 30	43	DSTG1		
11	KClO₃ 9	22	KClO <sub>3</sub> 21	33	KClO <sub>3</sub> 31	44	DSTG2		

Following this preliminary analysis, PCA was undertaken to further understand and possibly enhance the discriminatory data within this dataset. As in the previous analysis, the variance and loadings were investigated to understand how the exploratory data analysis has performed. The variance has the same breakdown with 96% of the variance being retained within the first 4 principal components and 99% by the seventh component. The scree plot is slightly different with the initial slope remaining almost linear to the third component and has a clear point of inflection in the curve at PC3.

Table 4.15: Variance retention table.

Component	Principal Component Eigenvalues	Cumulative Percentage of Variance Explained
PC1	102339	55%
PC2	56529	85%
PC3	15337	93%
PC4	5928	96%
PC5	2430	97%
PC6	1758	98%
PC7	906	99%

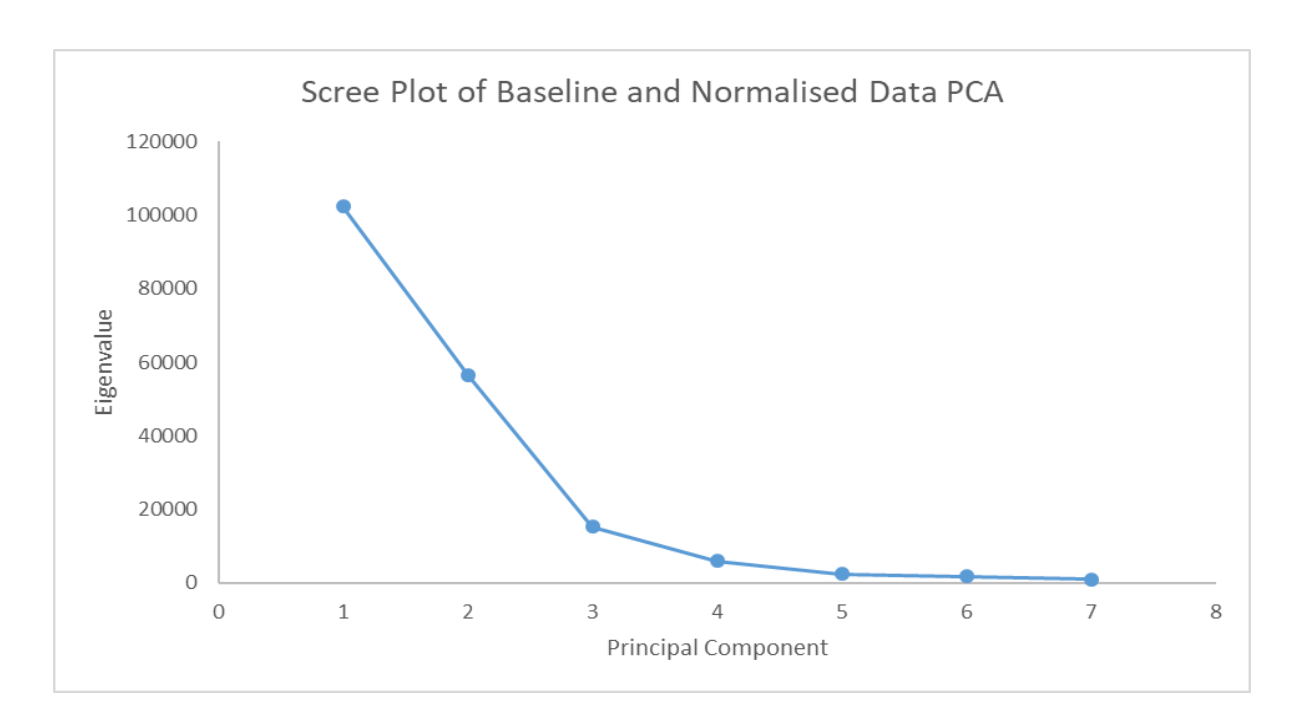


Figure 4.29: Scree plot for the PCA of KClO<sub>3</sub> IR baseline corrected and normalised data. The loading plots are displayed in Figure 4.30 and are very similar to the original data loading plots in Figure 4.20 apart from two details. First, in PC1 the value of the loading in the 600-1000 cm<sup>-1</sup> region

has been greatly reduced to insignificant levels. Second, the PC2 loadings have reversed in terms of the direction of the loading factors, with the region between approximately 900 and 1400 cm<sup>-1</sup> now being a positive weighting rather than negative, and the region between approximately 2700 and 3800 cm<sup>-1</sup> switching from a positive loading to a negative loading.

With this understanding of the analysis the results may now be examined. First, the one-dimensional form was examined for groupings within the first four principal components (Figure 4.31).

PC1 (Figure 4.31A) shows that there is a separation of the pool chlorine samples (orange) from the rest of the samples, however, that is the extent of the discrimination within this PC. This is a very similar result to the data prior to baseline correction, with the one difference being that there is less crossover between the pool chlorine samples and the rest. In this case, KClO<sub>3</sub> 36\_2 is the only bleach sample located with the pool chlorine samples, rather than the previous analysis where multiple bleach samples were. This clearer separation of the pool chlorine samples indicates that the new preprocessing method is an improvement upon the last method, highlighting the importance of a baseline correction.

PC2 (Figure 4.31B) shows a similar result with only five pool chlorine samples with higher scores separating significantly from the bulk of samples. One interesting point, however, is that the samples separated by the greatest difference were some of the poorly discriminated samples within the previous PC1 score plot. A combination of these two principal components may therefore yield a much greater distinct separation of these samples from the bleach and electrolytic cell samples. PC3 and onwards show very poor discriminatory ability, and so scores beyond PC2 provide very little useful information.

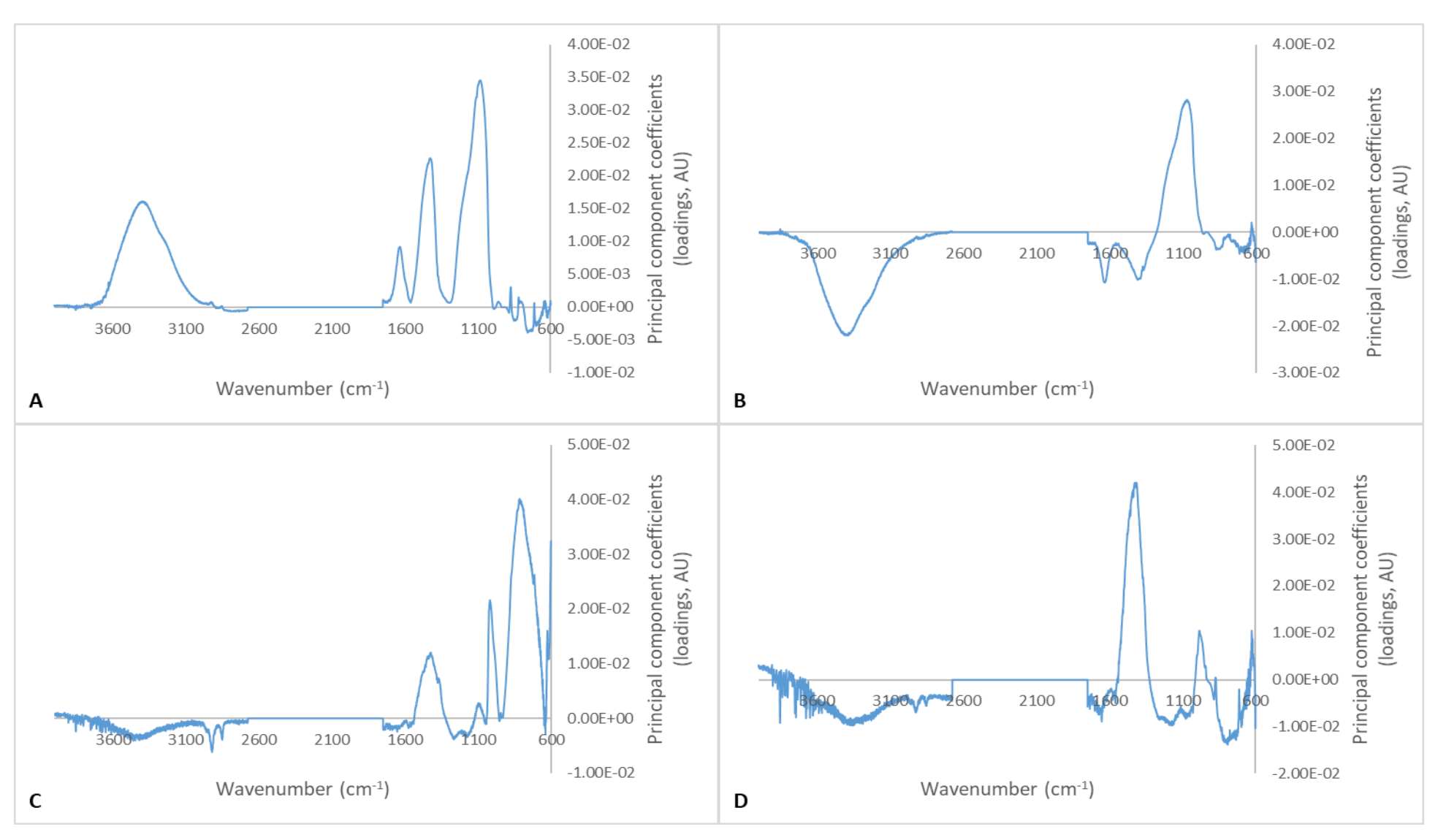


Figure 4.30: Spectrum loadings for A) PC1, B) PC2, C) PC3 and D) PC4 of the KClO<sub>3</sub> FT-IR dataset after baseline correction and normalisation.

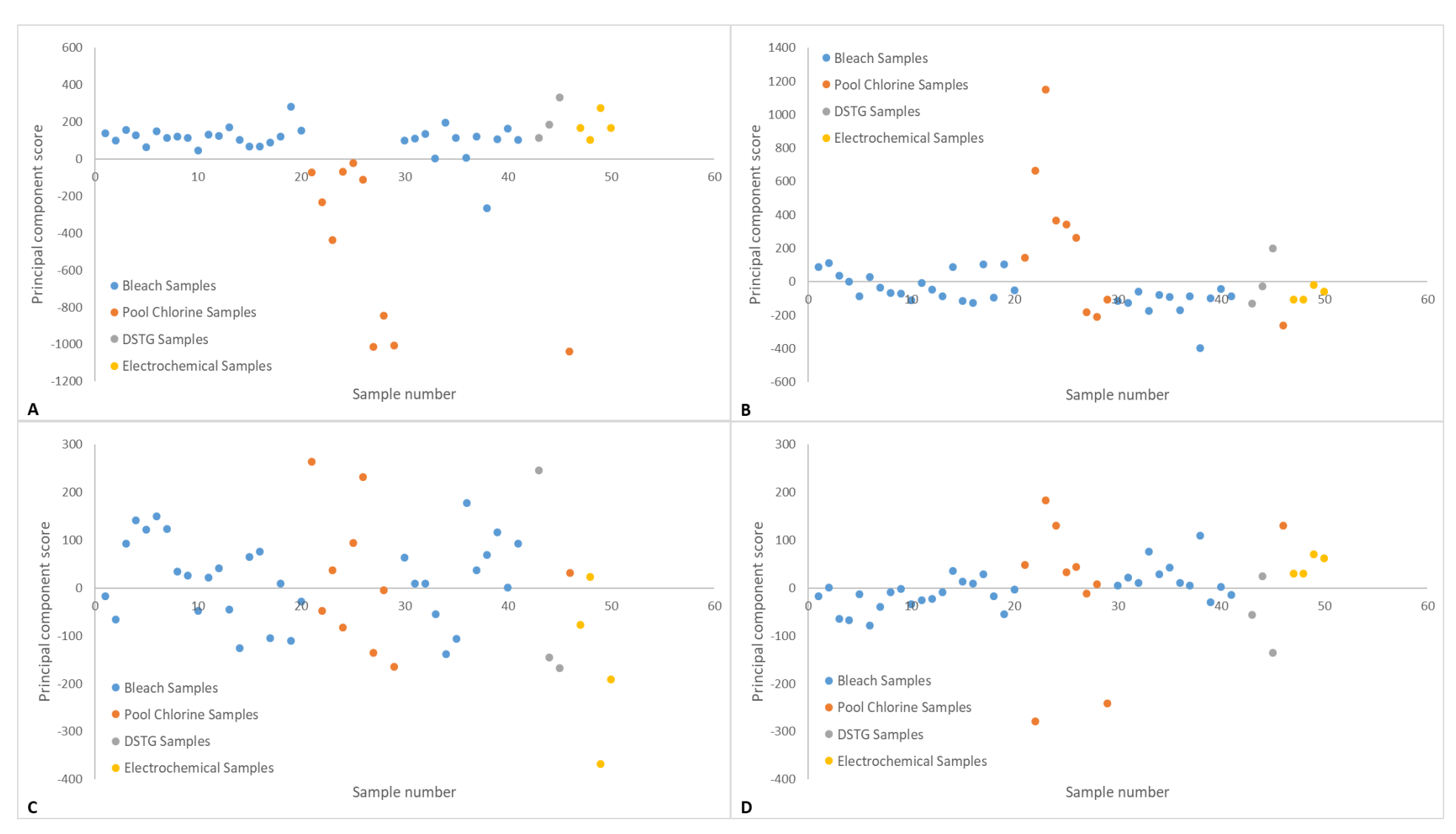


Figure 4.31: One dimensional score plots for A) PC1, B) PC2, C) PC3 and D) PC4 of the baseline corrected and normalised KClO<sub>3</sub> FT-IR dataset.

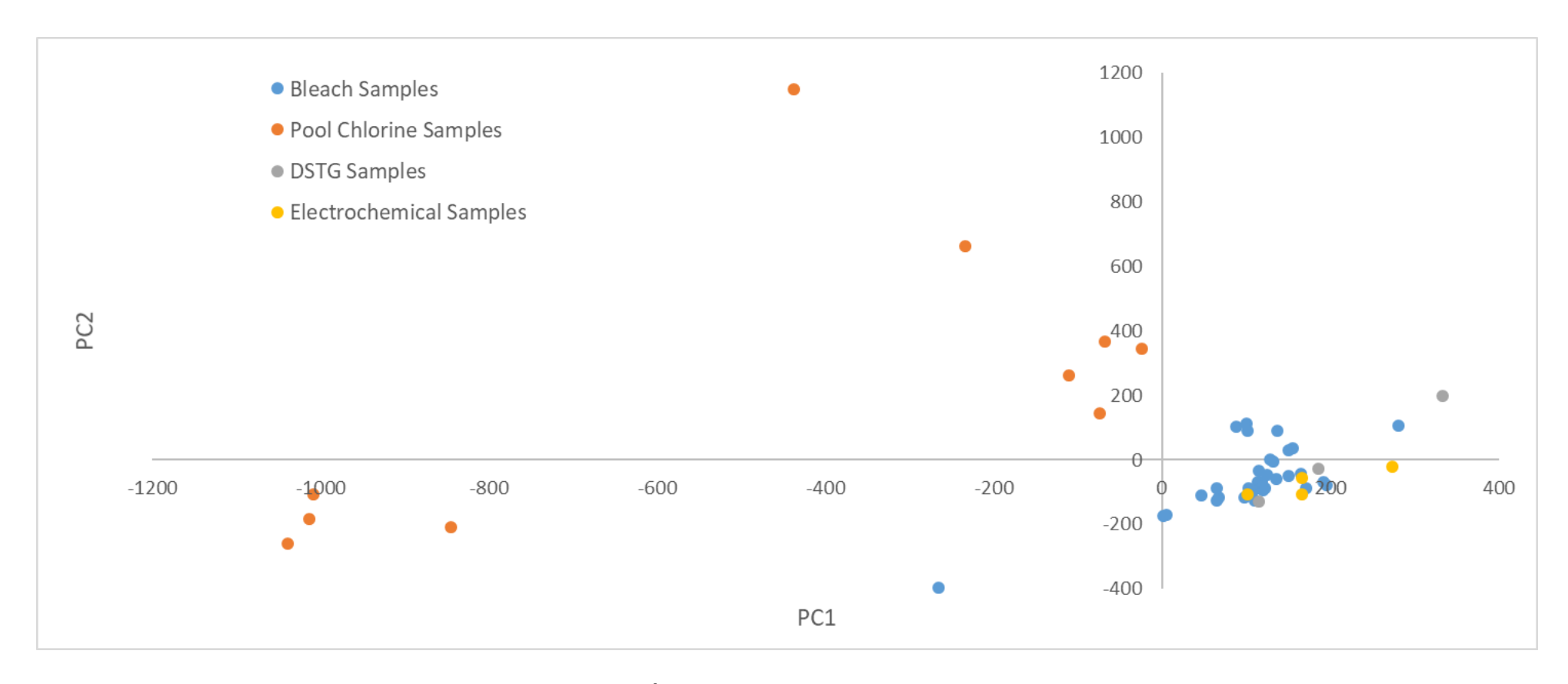


Figure 4.32: Two dimensional plot of PC1/PC2 of the baseline corrected and normalised KClO<sub>3</sub> FT-IR dataset.

With these results, a two-dimensional plot of PC1 and PC2 yields a good level of discrimination between the samples as shown in Figure 4.32. The same pool chlorine precursor samples are discriminated as the previous analysis, however, the separation between them and the others is stronger. Referring back to the coefficients plot for PC1 and PC2 (Figure 4.30 A/B), we can see that this separation is due to the additional impurity peaks carried over from the pool chlorine precursor, as previously discussed. This aligns much better with the initial visual inspection of the spectra undertaken prior to any chemometric analysis.

This analysis of infrared spectra has resulted in some discrimination of samples through the presence of impurities due to differing starting materials. The samples produced through the pool chlorine method are all successfully separated from the remainder of the samples.

There are, however, a large number of samples where no discrimination was possible as the synthesis methods did not result in any impurities at significant enough levels to perturb the IR spectra from pure KClO<sub>3</sub>. As the chemometric methodology used was able to separate samples based on trace amounts of impurities as a result of the starting material utilised, application of this same procedure to a database of real-world KClO<sub>3</sub>-based HME samples could potentially discriminate samples based not only on the impurities present in the KClO<sub>3</sub> component but also fuels and their fuel:KClO<sub>3</sub> ratio. These would all affect the signals in the spectra and also their peak ratios. The extent of discrimination based on fuel type and fuel ratio is a future study that would need to be undertaken.

The analysis of baseline corrected and normalised data provided a greater level of discrimination than just normalisation. The normalised data did show some level of discrimination based on the additional peaks identified by basic visual examination but did not fully separate all spectra with these peaks due to baseline differences. The baseline corrected data, however, had a much greater match with groupings identified by the preliminary visual inspection of the dataset greatly reducing the effect of discrimination due to baseline differences.

# 4.3 Raman Spectroscopy of Potassium Chlorate

Figure 4.33 shows an example of a Raman spectrum of a commercially sourced potassium chlorate sample DSTG1.

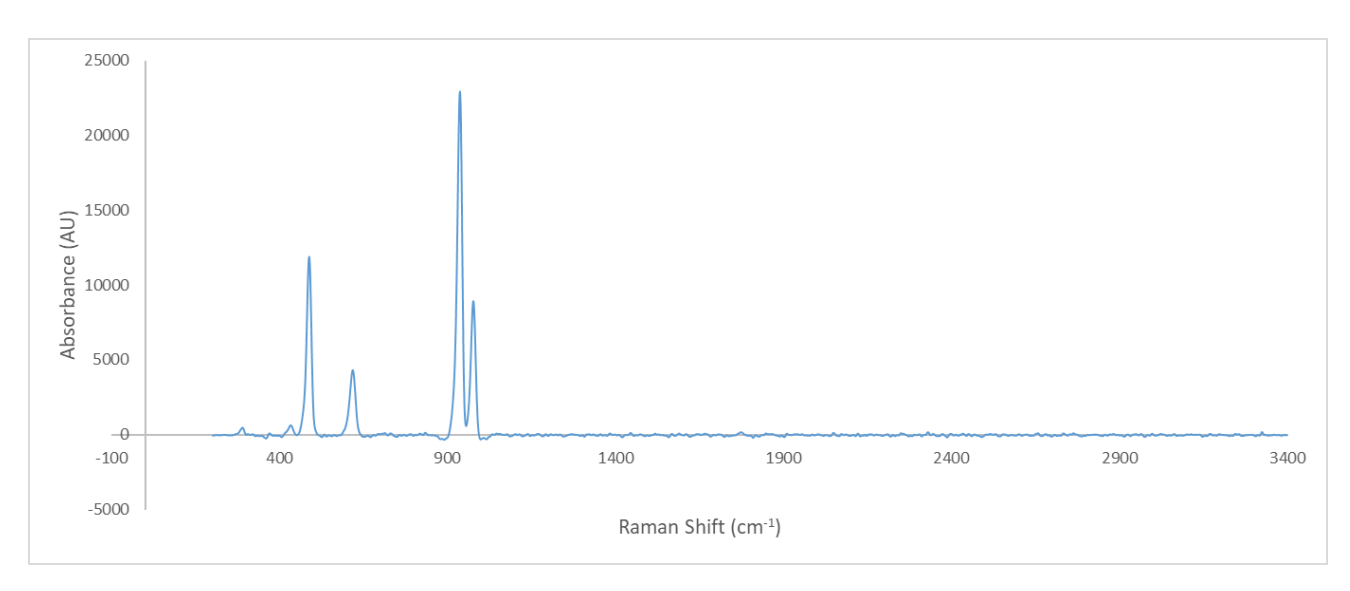


Figure 4.33: Raman spectrum of potassium chlorate sample DSTG1.

Peaks in a typical Raman spectrum of pure potassium chlorate include signals at approximately 280 cm<sup>-1</sup> (minor, combination of 2 peaks between 270-290 which sometimes become a single peak), 440 cm<sup>-1</sup> (minor, sharp and sometimes a shoulder), 490 cm<sup>-1</sup> (sharp), 620 cm<sup>-1</sup> (sharp), 940 cm<sup>-1</sup> (major, sharp) and 980 cm<sup>-1</sup> (sharp).

Raman spectra of all KClO<sub>3</sub> samples were pre-processed in the same manner as the previously discussed methodology used for IR spectra apart from the baseline correction, which was not required. All spectra were reduced to the range of 250-1100 cm<sup>-1</sup> as beyond 1100 cm<sup>-1</sup> no signals were present within any of the samples. This reduced the amount of data to be analysed by 70%, without losing any signals of interest. This would not always be possible especially when analysing KClO<sub>3</sub> HMEs with added fuels as additional signals may be present beyond 1100 cm<sup>-1</sup>. Samples with low signal and excessive fluorescence have been excluded and all remaining spectra were normalised to the major 940 cm<sup>-1</sup> peak. The final spectra in this dataset are displayed in Figure 4.34. Examining these spectra as a collective, visually, there is very little difference between them all. DSTG3 is the only sample to have an additional peak at 1050 cm<sup>-1</sup> setting it apart from the rest. The only other visible variation between spectra exist around the 280 cm<sup>-1</sup> region which may be enough for some level of discrimination between samples.

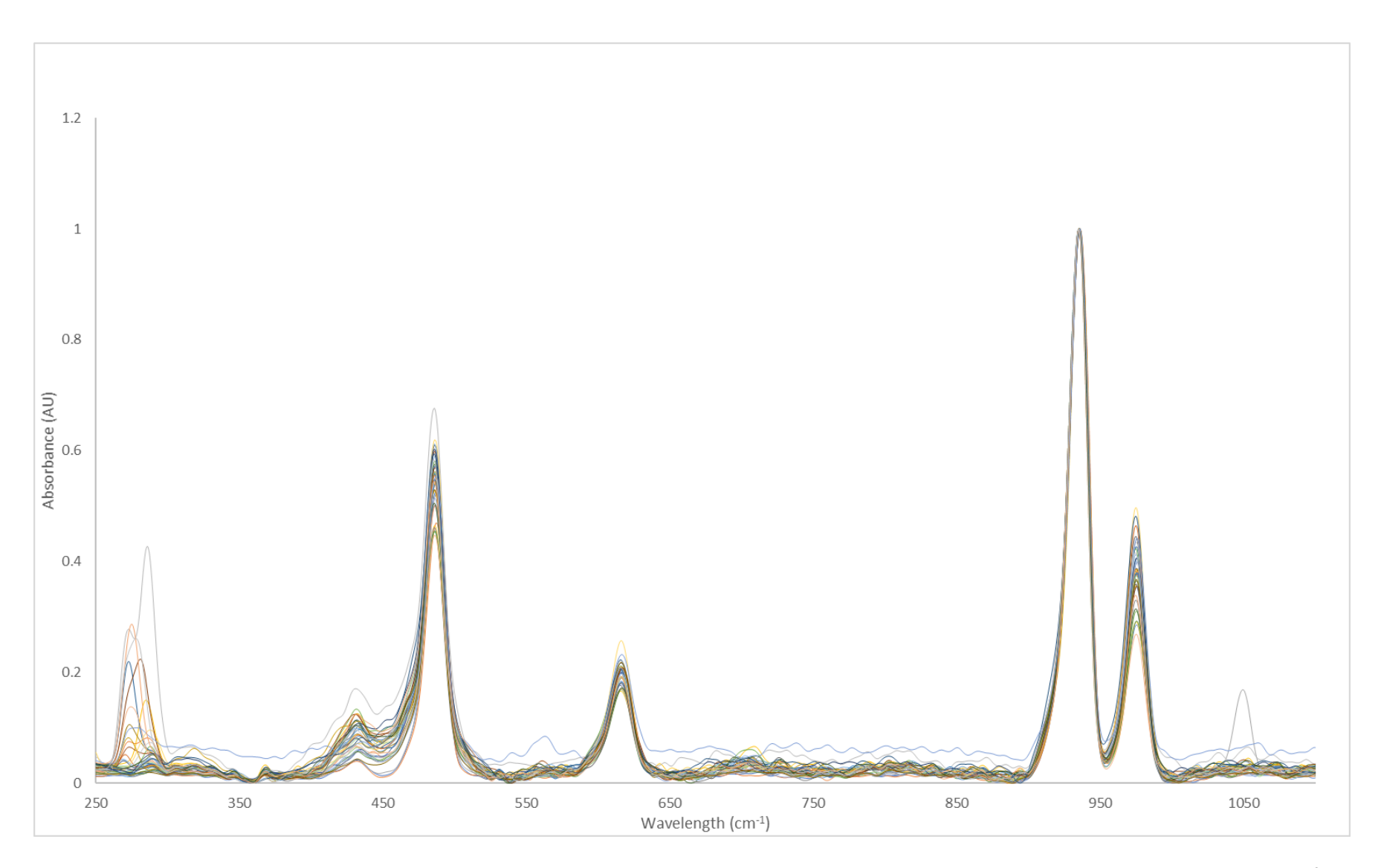


Figure 4.34: Normalised Raman spectra for all KClO<sub>3</sub> samples (excluding poor quality spectra) between 250 and 1100 cm<sup>-1</sup>.

To validate the preliminary assessment based on visual comparison of the IR spectra, HCA was performed on the IR dataset. The HCA does not show great potential in identifying clusters of samples as shown in Figure 4.35. The overall dataset is very similar as indicated by the Euclidean distance of the majority of samples being very minimal and there is very little distinct clustering.

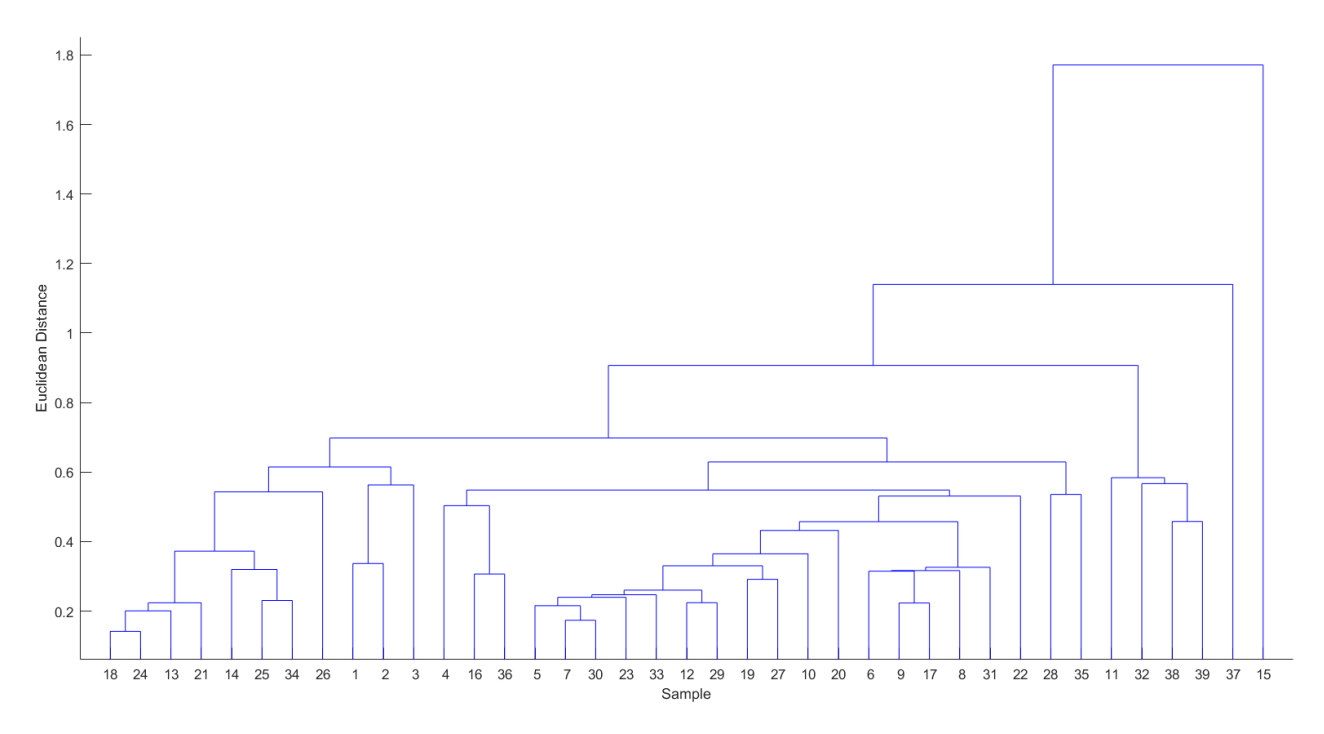


Figure 4.35: Resultant dendrogram from the hierarchical cluster analysis of normalised potassium chlorate Raman spectra.

Table 4.16: Sample correlation to number identifiers in HCA dendrogram in Figure 4.33.

Number	Sample	Number	Sample	Number	Sample	Number	Sample	Number	Sample
1	dstg1	9	KClO <sub>3</sub> 6	17	KClO₃ 15	25	KClO <sub>3</sub> 23	33	KClO <sub>3</sub> 32
2	dstg2	10	KClO <sub>3</sub> 7	18	KClO <sub>3</sub> 16	26	KCIO <sub>3</sub> 24	34	KClO <sub>3</sub> 33
3	dstg3	11	KClO <sub>3</sub> 8	19	KCIO <sub>3</sub> 17	27	KClO <sub>3</sub> 25	35	KClO <sub>3</sub> 36
4	E2	12	KClO <sub>3</sub> 9	20	KClO <sub>3</sub> 18	28	KClO <sub>3</sub> 26	36	KClO <sub>3</sub> 39
5	KClO₃ 1	13	KClO <sub>3</sub> 11	21	KClO <sub>3</sub> 19	29	KClO <sub>3</sub> 27	37	KClO <sub>3</sub> 41
6	KClO <sub>3</sub> 2	14	KClO <sub>3</sub> 12	22	KClO <sub>3</sub> 20	30	KClO <sub>3</sub> 28	38	KClO <sub>3</sub> 42
7	KClO <sub>3</sub> 4	15	KClO <sub>3</sub> 13	23	KClO <sub>3</sub> 21	31	KClO <sub>3</sub> 30	39	KClO <sub>3</sub> 43
8	KClO <sub>3</sub> 5	16	KClO <sub>3</sub> 14	24	KClO <sub>3</sub> 22	32	KClO <sub>3</sub> 31		

Regardless of the low probability of discriminatory value contained within this dataset, PCA was undertaken to test this hypothesis. In the following table of variance retention and accompanying scree plot, it is shown that the variance within the dataset was not well condensed by the PCA. The retention table shows that the variance is spread over many principal components with 95% accounted for at PC8 and 99% after an extreme 20 principal components. This is represented

graphically in the scree plot, where there is less of an obvious inflection point and more of a smooth curve.

Table 4.17: Variance retention of the PCA of normalised KClO₃ Raman data.

Component	Eigenvalue	Cumulative Percentage of Variance
PC1	0.1576	48%
PC2	0.0598	67%
PC3	0.0327	77%
PC4	0.0255	85%
PC5	0.0133	89%
PC6	0.0112	92%
PC7	0.0061	94%
PC8	0.0041	95%
	•••	
PC20	0.0004	99%

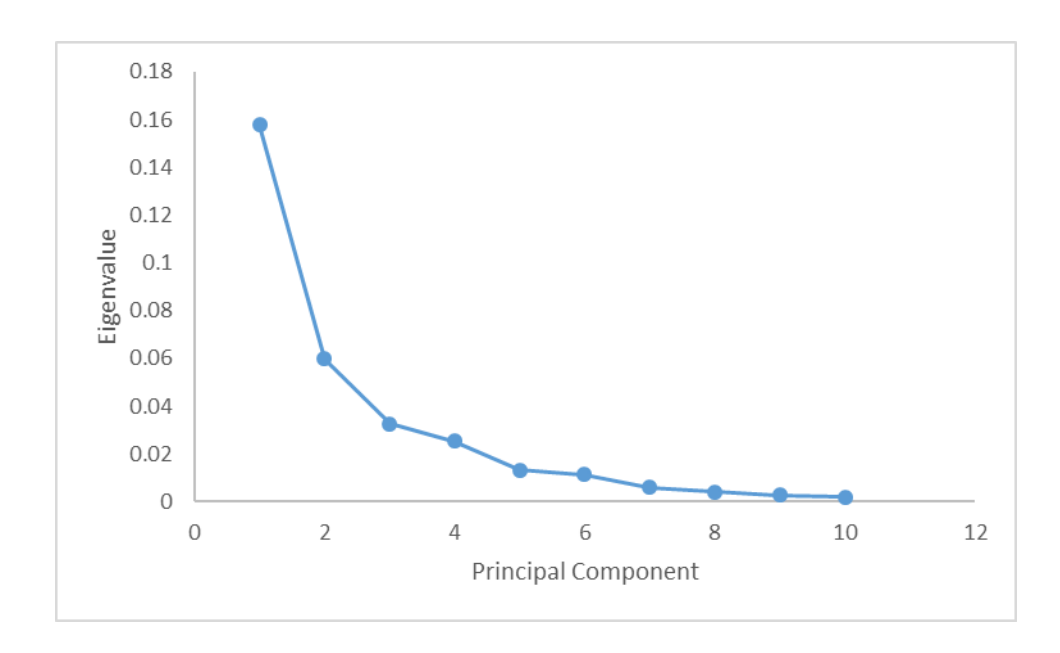


Figure 4.36: Scree plot for the PCA of normalised KClO<sub>3</sub> Raman data.

Another confirmation of a poor PCA can be seen from the loadings plots in Figure 4.37.

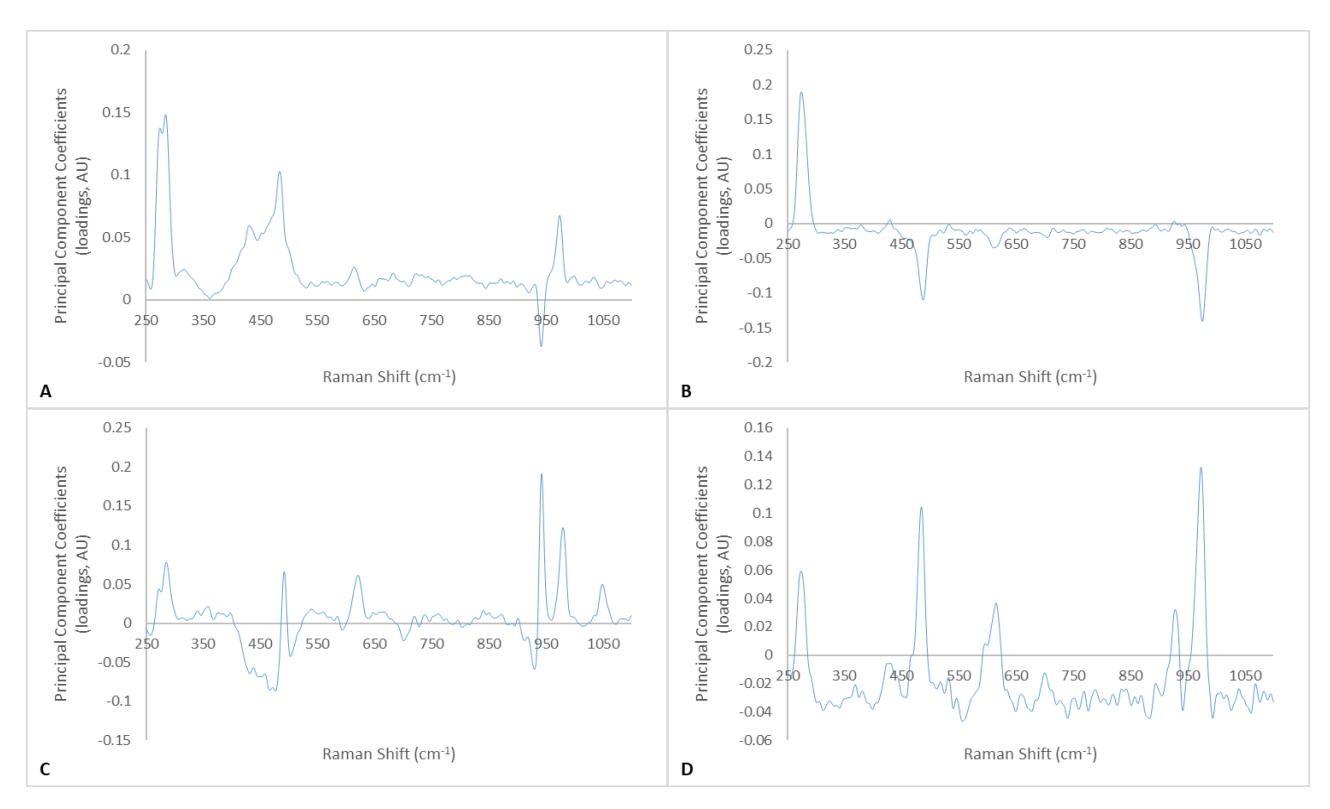


Figure 4.37: Spectrum loadings for A) PC1, B) PC2, C) PC3 and D) PC4 of the normalised KClO<sub>3</sub> Raman dataset.

Though the first and second principal components showed identifiable spectral features, by PC3 this had devolved into mainly background noise and sharp spikes rather than smooth peaks. This was yet another red flag that the analysis would provide little discrimination between samples within this dataset.

The final results were then examined to visualise exactly how little discriminatory value there was within the Raman spectra. In Figure 4.38 are two plots of PC1/PC2 and PC2/PC3 showing no clear clusters of samples as expected. Rather than identifiable groups of samples, the plots are just a nebulous cloud of data points. The only exception is sample KClO<sub>3</sub> 13, which was a slight outlier in PC1 due to an unusual signal at 208 cm<sup>-1</sup> and above average signal at 290 cm<sup>-1</sup>.

This analysis was an example where further analysis beyond a visual inspection of the original dataset does not yield any greater level of understanding. It also highlighted the various indicators that a PCA analysis was not going to achieve a great deal of discrimination. This included:

- a lack of separation between clusters in the HCA,
- the lack of successful variance condensation on examining the eigenvalues of the PCA,

- the lack of quality spectral loadings, and
- the principal component score plots which confirmed the lack of discriminatory value of the Raman dataset.

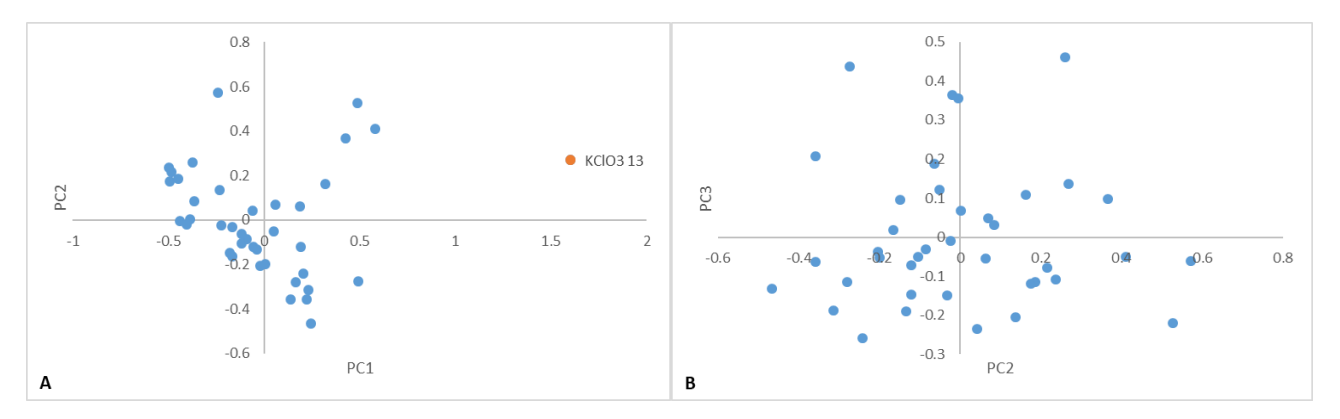


Figure 4.38: Score plots of A) PC2 vs PC1 and B) PC3 vs PC2 of normalised KClO₃ Raman dataset.

The lack of differences within Raman spectra stems from the lack of Raman active impurities within samples. This result highlights the complimentary nature or Raman and IR spectroscopy as IR active impurities were identified. The number of samples that data could be collected for in the Raman case was also reduced as some samples could not be recorded due to fluorescence and breakdown of equipment.

### 4.4 Combined IR and ICP-MS Data for Potassium Chlorate

The previous chapters analysed the FT-IR and ICP-MS datasets, which successfully identified discriminatory variance within each dataset individually. Here attempts are made to merge these datasets to interrogate whether, when combined, these datasets will allow better discrimination.

The first attempt involved the direct merging of the log transformed ICP-MS and the baseline corrected and normalised FT-IR transmittance datasets. In this case, the PCA score plots were first examined as the data has been previously investigated and shown to contain valuable discriminatory information.

PC1 (Figure 4.39) identifies two groupings of samples, with the higher score being the potassium chlorate samples synthesised from bleach and DST Group-obtained commercial samples and the lower score grouping being all potassium chlorate samples synthesised from pool chlorine. This was a grouping that could be established by both techniques individually. PC2 and onwards unfortunately

did not show any signs of discrimination between samples and instead was a single cloud of data points.

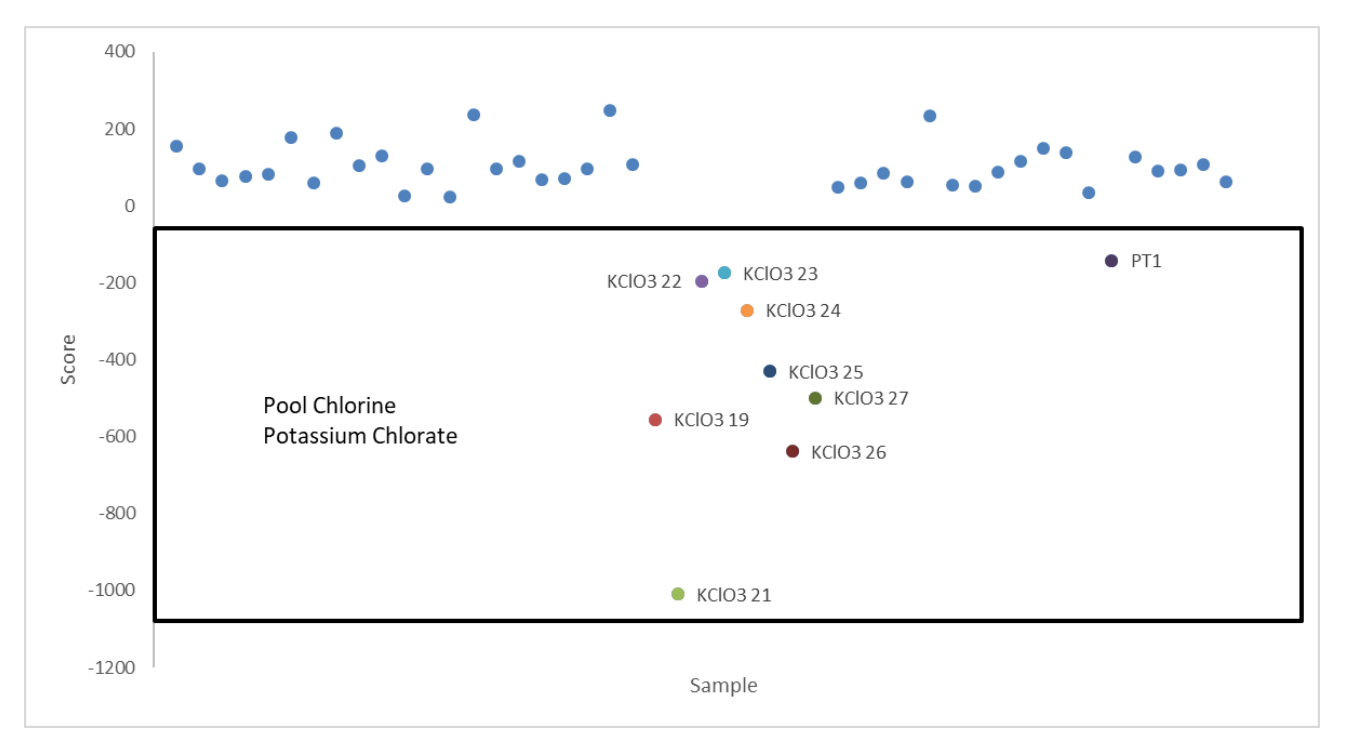


Figure 4.39: Score plot of PC1 for the combined raw FT-IR and log transformed ICP-MS datasets of KClO₃ samples.

This is quite a disappointing result as the PCA of the ICP-MS data alone highlighted a few additional groupings and so this was less successful than analysing each data set separately. One way to identify why there is a lesser degree of discriminatory variability is to examine the loadings/coefficients leading to the principal components. There is a difficulty in visualising this, as the FT-IR spectra have an independent variable (frequency in cm<sup>-1</sup>) and the ICP-MS data merely records the concentration of elements within a sample. They may be plotted as a scatter plot (Figure 4.40), however, this requires the ICP-MS data to be assigned arbitrary frequency values (in this case 25 cm<sup>-1</sup> apart) in order to plot all in the one chart.

When examining this plot of the coefficients for PC1, the issue becomes evident. The magnitude of variation within the spectral portion of the dataset is far greater than in the ICP-MS data, where only the variation in calcium content has any weight in the analysis. Hence a form of scaling needs to be implemented to even out the magnitudes of variation between the datasets. The optimisation of this scaling could be quite complicated; one possible method worth attempting is to normalise the largest variances in both the ICP-MS and FT-IR datasets. The elemental mass fraction which had the largest magnitude of variance in the ICP-MS data was identified as calcium (3 AU after log transformation)

and the peak in the FT-IR that had the greatest variation in %T values was at 3400 cm $^{-1}$  (40%). To equalise the magnitude of the variance at these two maximal positions the %T values of the FT-IR dataset were divided by 13 (approx. 40  $\div$  3). The resultant coefficient plot for PC1 (Figure 4.41) following PCA analysis of the transformed data shows a vast level of improvement with the coefficients between the ICP-MS and FT-IR portions of the data becoming more equal though the signs of the coefficients have reversed.

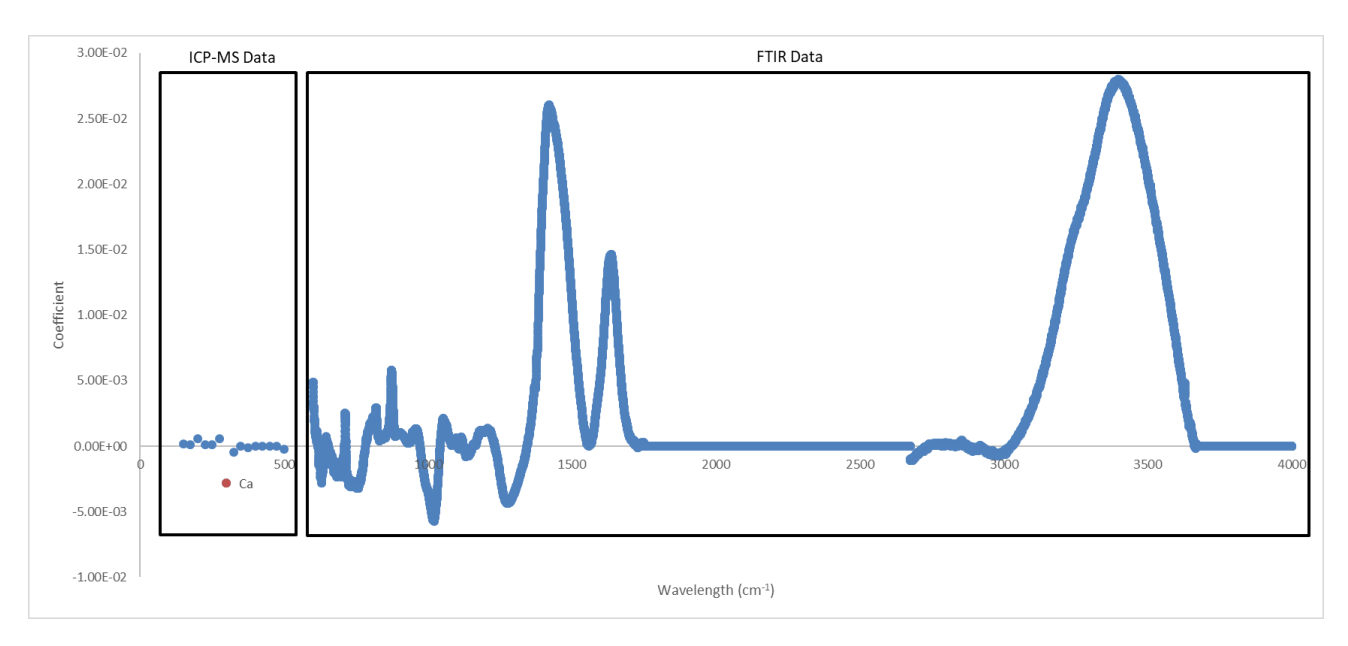


Figure 4.40: PC1 coefficient plot for the combined raw FTIR and log transformed ICP-MS datasets of KCIO<sub>3</sub> samples.

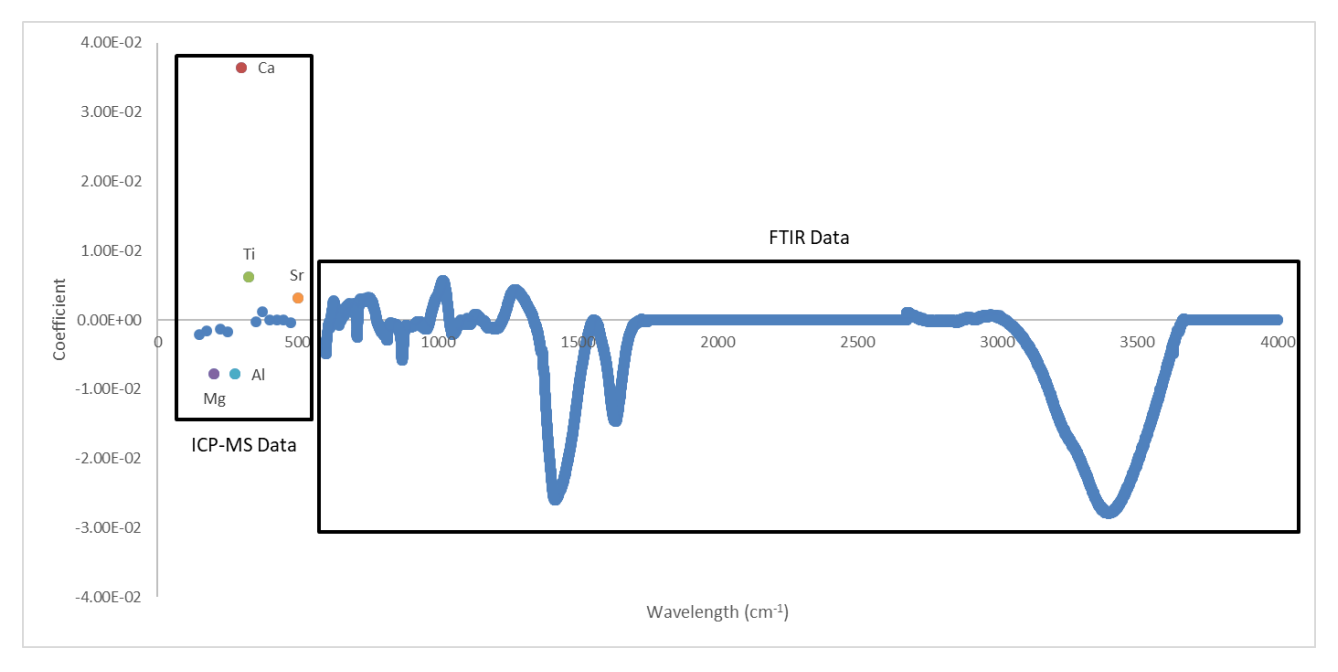


Figure 4.41: PC1 coefficient plot for the combined scaled FT-IR and log transformed ICP-MS datasets of KClO<sub>3</sub> samples.

The resultant score plots are significantly affected, with PC1 (Figure 4.42) still isolating all pool chlorine potassium chlorates from the household bleach and DSTG samples within this dataset, but with a greater score value than previously.

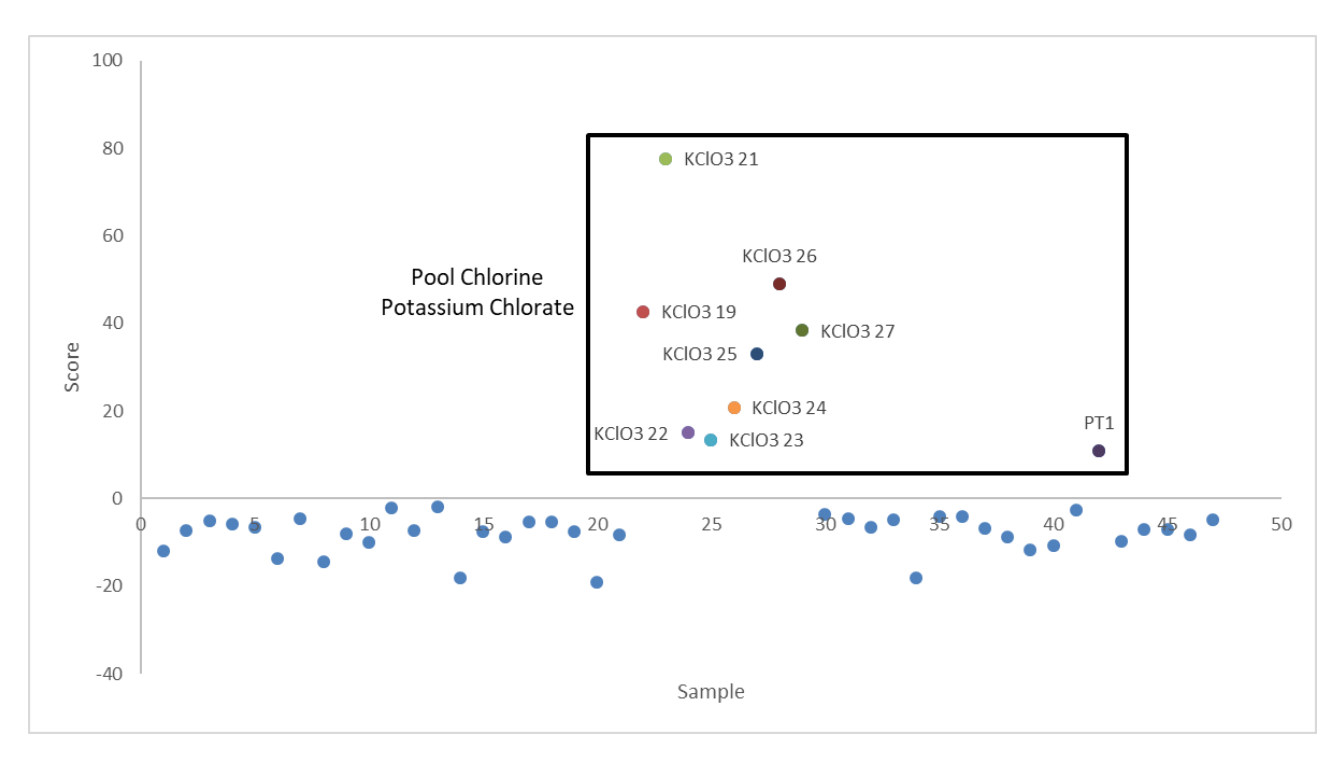


Figure 4.42: Score plot of PC1 for the combined scaled FT-IR and log transformed ICP-MS datasets of KClO<sub>3</sub> samples.

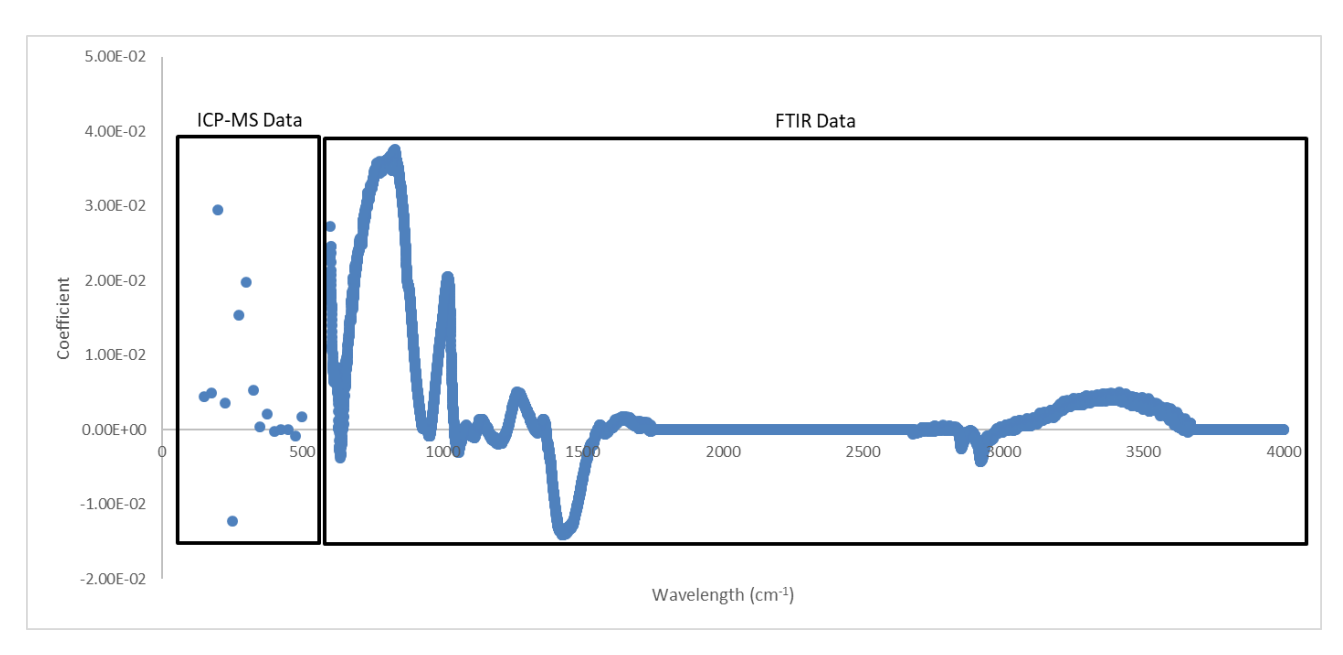


Figure 4.43: PC2 coefficient plot for the combined scaled FT-IR and log transformed ICP-MS datasets of KClO₃ samples.

Though this was promising, further PC score plots once again yielded no further discrimination. Examining the loading factors through coefficients (for example, PC2 coefficient plot in Figure 4.43) shows that this is no longer the issue as the two datasets are once again quite evenly matched in terms of relative magnitude of maximum contributions to the variance.

The only other point of interest that may be interrogated further is the variation retention (Table 4.18) and the corresponding scree plot (Figure 4.44).

Table 4.18: Variance retention table for the PCA of combined scaled FT-IR and log transformed ICP-MS datasets of KClO<sub>3</sub> samples.

Principal Component	PC Eigenvalues	Cumulative % of Variance Explained
PC1	366.9545	62%
PC2	115.0074	81%
PC3	68.41562	93%
PC4	14.59902	95%
PC5	8.135024	97%
PC6	5.689503	98%
PC7	3.256235	98%
PC8	2.257283	99%

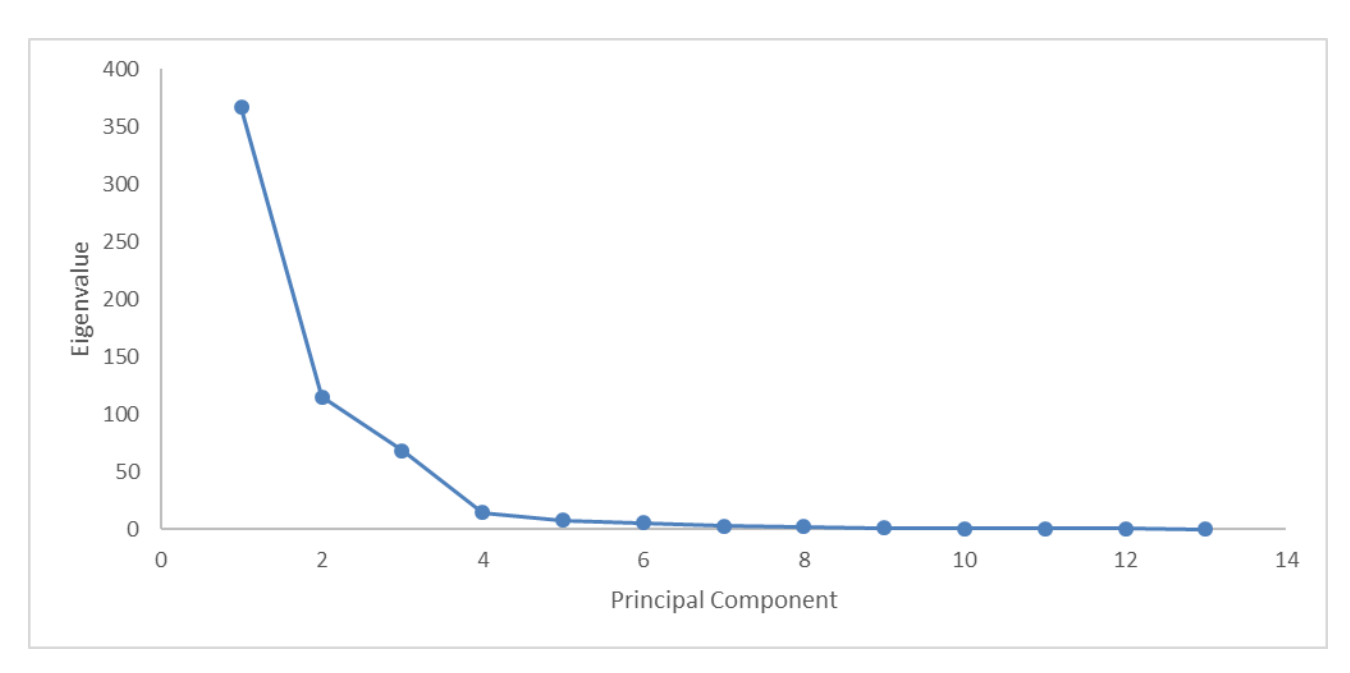


Figure 4.44: Scree plot for the PCA of combined scaled FT-IR and log transformed ICP-MS datasets of KClO<sub>3</sub> samples.

In examining the variance retention there are no red flags that would indicate an unsuccessful PCA. The variance is not solely resolved in PC1 and 93% is contained within the first three PCs resulting in a distinct inflection point at PC4 in the scree plot.

The PCA score plots were disappointing, with only the first principal component indicating any level of discrimination between samples. This indicates that the incorporation of multiple datasets in this case has not resulted in any benefit but has rather diluted the variance across a larger dataset which has negatively affected the discrimination between samples. Further optimisation of data preprocessing needs to be undertaken to resolve this issue; however, this could be quite a complex process requiring more sophisticated methods. One possible method would be to merge the datasets using a nonparametric regression, such as generalised regression neural network (GRNN). Though a very complex machine learning technique, which is computationally demanding, the rapid development of machine learning has made this a realistic technique. However, for this project GRNN was not possible with the computational equipment at hand, so this or similar nonparametric regression would be a very worthwhile future pursuit.

#### 4.5 Conclusions

The analysis of a representative set of potassium chlorates indicated some clear differences between samples based on their starting materials and synthetic procedures.

ICP-MS analysis could identify three different groups of potassium chlorate based on the synthetic procedure utilised i.e. household bleach, pool chlorine and electrochemical cell synthesis routes. This was primarily based on the trace metal concentrations of aluminium, calcium and magnesium as identified by PCA and confirmed by examining the raw data. Potentially an increase of the number of trace elements analysed could improve this level of discrimination. A preliminary investigation into the effect electrodes and electrolytes have on a final product's elemental profile showed that there is an identifiable link. This can help connect a sample of KClO<sub>3</sub> to its electrochemical cell make up including electrode metals and elevated trace elements in starting water. An aging study was undertaken to determine the potential to store digested samples for an extended period of time however many elements were too greatly affected over a 6-month period for this to be viable. This could potentially be investigated further by modifying storage conditions.

IR spectroscopy could identify two distinct groupings based on the presence of not entirely identified impurities present within KClO<sub>3</sub> samples produced from pool chlorine. The impurities were suspected to be as a result of the cyanuric acid, which was present as a chlorine stabiliser, however, not all the additional peaks in the spectra of these samples could be accounted for by cyanuric acid. Further investigation showed that other insoluble compound(s) such as calcium hydroxide may be present, or that the conditions in the electrolysis cell have effected a chemical reaction on the cyanuric acid.

Raman spectroscopy did not offer any discriminatory information between samples; however, this data was collected using a very basic Raman analyser used for field identification of hazardous substances which does not have the spectral fidelity of laboratory grade instruments.

ICP-MS and IR datasets for KClO<sub>3</sub> samples were quite difficult to merge effectively, in contrast to the IR-MS and ICP-MS datasets for AN samples investigated in the previous chapter. Multiple methods of data pre-processing prior to combination and multivariate analysis were attempted, however, all negatively affected the discriminatory information contained within each dataset individually. This could potentially be improved with a more complex non-linear multivariate analysis involving machine learning, such as general regression neural network or similar nonparametric analysis, which were beyond the data processing capabilities available in this project.

# 5. Analysis of Erythritol Tetranitrate Samples

In this chapter erythritol tetranitrate was analysed using IR-MS, ICP-MS, ATR-FTIR and Raman spectroscopy. Each dataset was interrogated individually to identify discriminatory information. The datasets proving to highlight discriminatory information were merged into a singular database and re-examined to determine the most successful pre-processing method of data integration. PCA of the combined dataset was undertaken to attempt to retain or enhance the original discrimination provided by the individual analytical techniques.

## 5.1 IR-MS of ETN

ETN is a member of the nitrate ester class of explosives and therefore contains significant amounts of both carbon and nitrogen. This allows for the IR-MS of samples as an additional analysis, in comparison to the inorganic oxidising agent and HME ingredient KClO<sub>3</sub> investigated in the previous chapter. This dataset is only two dimensional, comprising the carbon and nitrogen delta values for each sample. Therefore, PCA would not be able to provide any further dimensional reduction and so is not applied in this case. Instead the carbon and nitrogen values may be interrogated individually, as well as in combination.

To understand any changes in delta value, the reaction conditions leading to the products must be understood. The reaction equations are depicted in Equation 5.1, 5.2 and 5.3. Equation 5.1 clearly identifies that there is only one possible source of carbon (erythritol) and nitrogen (nitric acid) in the mixed acid method. Equation 5.2 only has one source of nitrogen and three carbon containing chemicals including the erythritol, acetic acid and acetic anhydride. The nitrate salt method in Equation 5.3 has only one source of carbon and one source of nitrogen, except in the ammonium nitrate case where two different nitrogen atoms are present, and one is not incorporated into the ETN product. This synthesis method produces nitric acid in-situ from a nitrate salt using sulfuric acid prior to the introduction of erythritol.

$$C_4H_{10}O_4 \xrightarrow{HNO_3/H_2SO_4} C_4H_6N_4O_{12}$$

Equation 5.1: Mixed acid nitration of erythritol to produce ETN.

$$C_4H_{10}O_4 \xrightarrow{HNO_3/AcOH/Ac_2O} C_4H_6N_4O_{12}$$

Equation 5.2: Acetyl nitrate nitration of erythritol to produce ETN.

$$C_4H_{10}O_4 + MNO_3 \xrightarrow{H_2SO_4} C_4H_6N_4O_{12} + MSO_4$$

Equation 5.3: Nitrate salt (potassium/ammonium/calcium nitrate) nitration of erythritol to produce ETN.

In all graphical representations of the data, each point is the mean value of a triplicate measurement and has error bars of one standard deviation.

#### 5.1.1 Carbon IR-MS Analysis

The carbon isotope ratios of the various ETN samples and their erythritol precursors were measured and displayed below in Figure 5.1, where they have been grouped into their methods of synthesis.

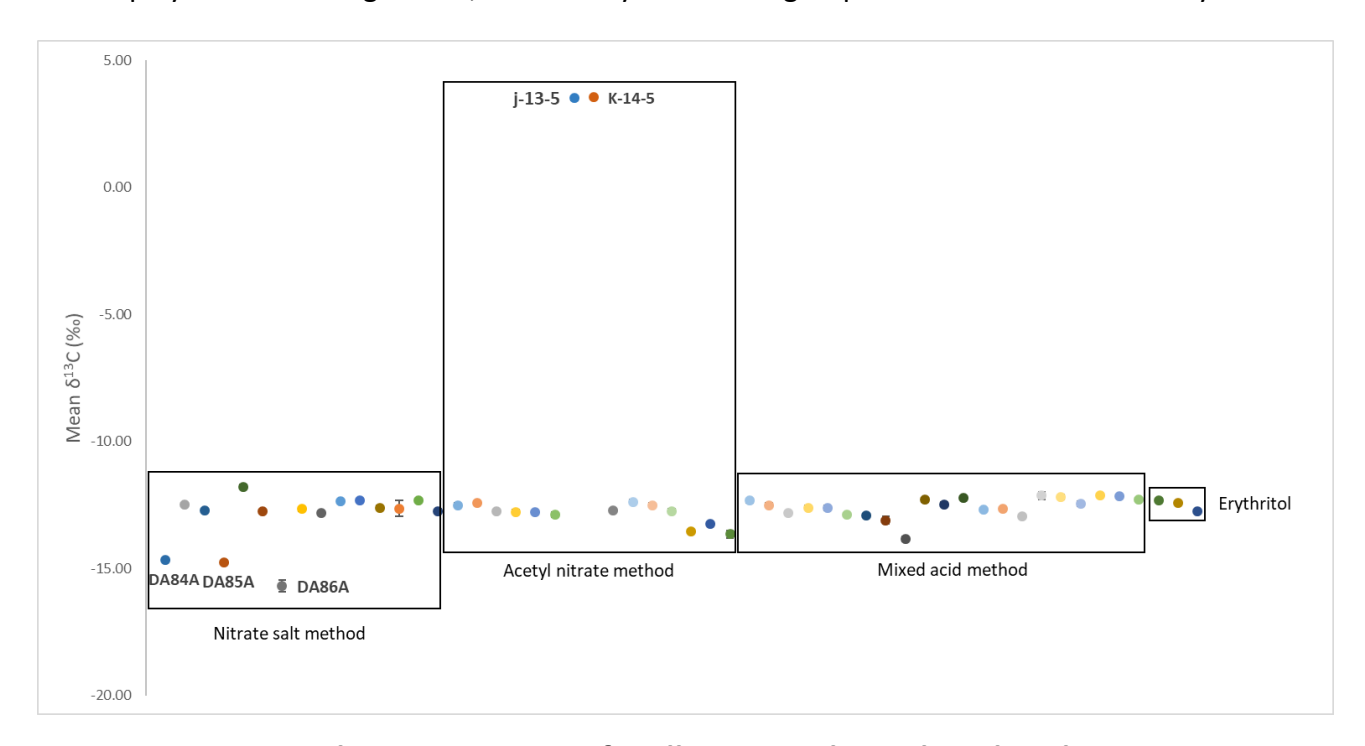


Figure 5.1: Carbon isotope ratios for all ETN samples and erythritol precursors.

The results clearly show that the three erythritol starting materials have very similar carbon isotope ratios of -12.3% to -12.77%, and that this has carried through to the final ETN product in the majority of cases. This is expected as the carbon backbone of the erythritol precursor does not take part in the nitration reactions of any of the three synthetic methods. However, there are a few anomalies, in particular j-13-5 and K-14-5 are distinctly separated from the rest at a  $\delta$  <sup>13</sup>C of +3.5%. Both samples were created using two different erythritols, however, they do share a common nitric acid precursor, DST NA3. This same batch of nitric acid was also used to prepare sample L-14-5 by the same method; L-14-5 does not follow this trend but rather falls in place with the main bulk of samples. Nitric acid also contains no carbon, and therefore should not have an effect on the final carbon delta value and

thus an explanation for the enrichment in the heavier <sup>13</sup>C isotope in these samples must be sought elsewhere. Many possible explanations may exist. Firstly, an incomplete purification of an ETN sample could result in AcOH and/or Ac<sub>2</sub>O being trapped within the ETN crystals. However, there are no signs of this in the IR spectra for the samples. Secondly, the potential conversion of one or more nitrate esters to acetate esters under the conditions of the reaction. However, once again the IR spectra for j-13-5 and K-14-5 do not show any acetate impurity signals. Both of these two possibilities could also be tested further using GC-MS and/or LC-MS and may be a worthwhile future direction. Thirdly, fractionation by a side reaction, such as the oxidation of the erythritol carbon backbone by the nitric acid. This is the least likely to be the cause however, as the shift would require the selective reaction of a significant amount of the erythritol, which would have a dramatic effect on the product yield if removed through recrystallisation. If not removed during purification, such a product would be identified by infrared spectroscopy. IR-MS analysis of AcOH and Ac<sub>2</sub>O for their carbon isotope ratios could also yield further insight, however, were not able to be measured due to instrument limitations.

There are also three other samples that break away from the main body of samples within the nitrate salt synthesis method. These are DA84A, DA85A and DA86A which were all created using Sigma-Aldrich erythritol and three differing nitrate salts. Once again, these samples are not the only samples to use these precursor materials and therefore it is unusual for these samples to separate from the others. However, there were some minor differences in the synthesis. Both DA84A and DA85A resulted in poor yields, much lower than the average yield using the same synthesis method. DA86A also had a minor adjustment during the synthesis with the addition of additional sulfuric acid to assist in stirring the reaction mixture. The only other difference common across these three samples were that they were synthesised by a different person to the rest of those produced by the nitrate salt method.

#### 5.1.2 Nitrogen IR-MS Analysis

The nitrogen isotope ratios of the ETN samples grouped by synthesis method are shown below in Figure 5.2.

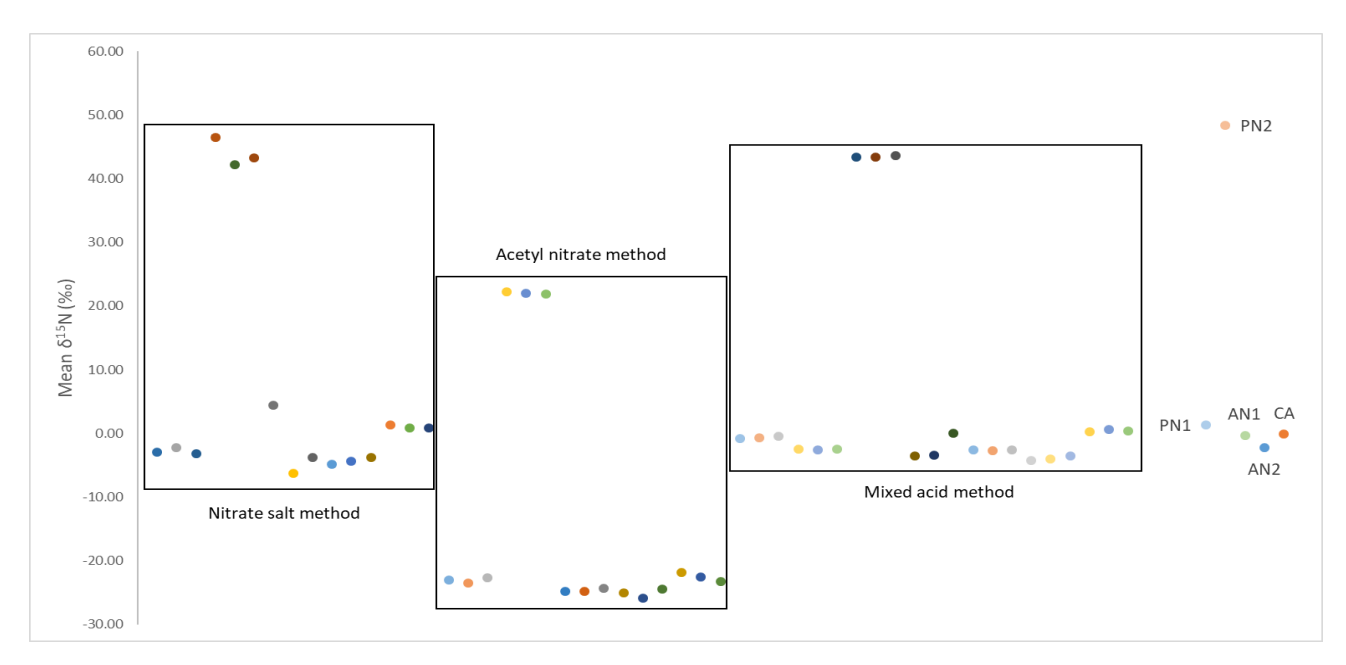


Figure 5.2: Nitrogen isotope ratio for all ETN samples and potassium nitrates.

The precursor nitrates have very similar nitrogen isotope ratios apart from potassium nitrate 2 (PN2). The nitrogen isotope ratio for both the nitrate salt and mixed acid methods closely resemble that of the starting nitrate salts. This suggests that little to no fractionation of nitrogen is occurring throughout the process of the synthesis, including the manufacture of the nitric acid reagent. This result means that the nitrogen isotope ratio of ETN produced could be linked to the precursor nitrate.

However, in samples resulting from the acetyl nitrate synthesis method, the nitrogen delta value is consistently lower, indicating significant fractionation due to the depletion of the heavier isotope, <sup>15</sup>N. This suggests that the acetyl nitrate nitration of erythritol has a preferential uptake of the lighter isotope, <sup>14</sup>N. Referring back to the reaction equation corresponding to this synthesis (Equation 5.2), the only source of nitrogen supplied is from the same nitric acid used in other syntheses. This supports the hypothesis that the action of this nitrating agent results in a differing reaction mechanism allowing for this preferential reactivity with the lighter isotope. This may be a result of the reaction proceeding under kinetic control, rather than thermodynamic control. The conditions of the reaction are not thermodynamically favoured as the solution is kept on ice throughout the reaction, whereas the other two methods involve a warming of the mixture to room temperature following the addition of all reagents. This strict restriction of temperature may be favouring the uptake of the lighter nitrogen isotope. However, more research would need to be undertaken to confirm this.

Another important note is although this synthesis is proposed to be an acetyl nitrate nitration, studies have shown that such a mixture of acetic anhydride and high concentration nitric acid actually forms nitrating species, including the desired acetyl nitrate ( $CH_3COONO_2$ ) but also ( $CH_3COHONO_2$ )<sup>+</sup>,  $N_2O_5$  and  $NO_2$ <sup>+</sup>. The latter two are believed to be most present at high concentrations of nitric acid and therefore the nitration may be much more complicated and involve dinitrogen pentoxide as the major nitrating agent, rather than acetyl nitrate<sup>139</sup>. As the two other synthesis pathways use  $NO_2$ <sup>+</sup> as the nitrating species, this difference in nitrating species within the reaction mixture may lead to differences in fractionation in the end product. Further investigations utilising isotopically labelled precursors could lead to the confirmation of such a hypothesis and a greater understanding of the specific reaction mechanism involved

#### 5.1.3 Combined IR-MS Analysis

The two previous sets of data can be combined to form a two-dimensional plot, represented in Figure 5.3 below.

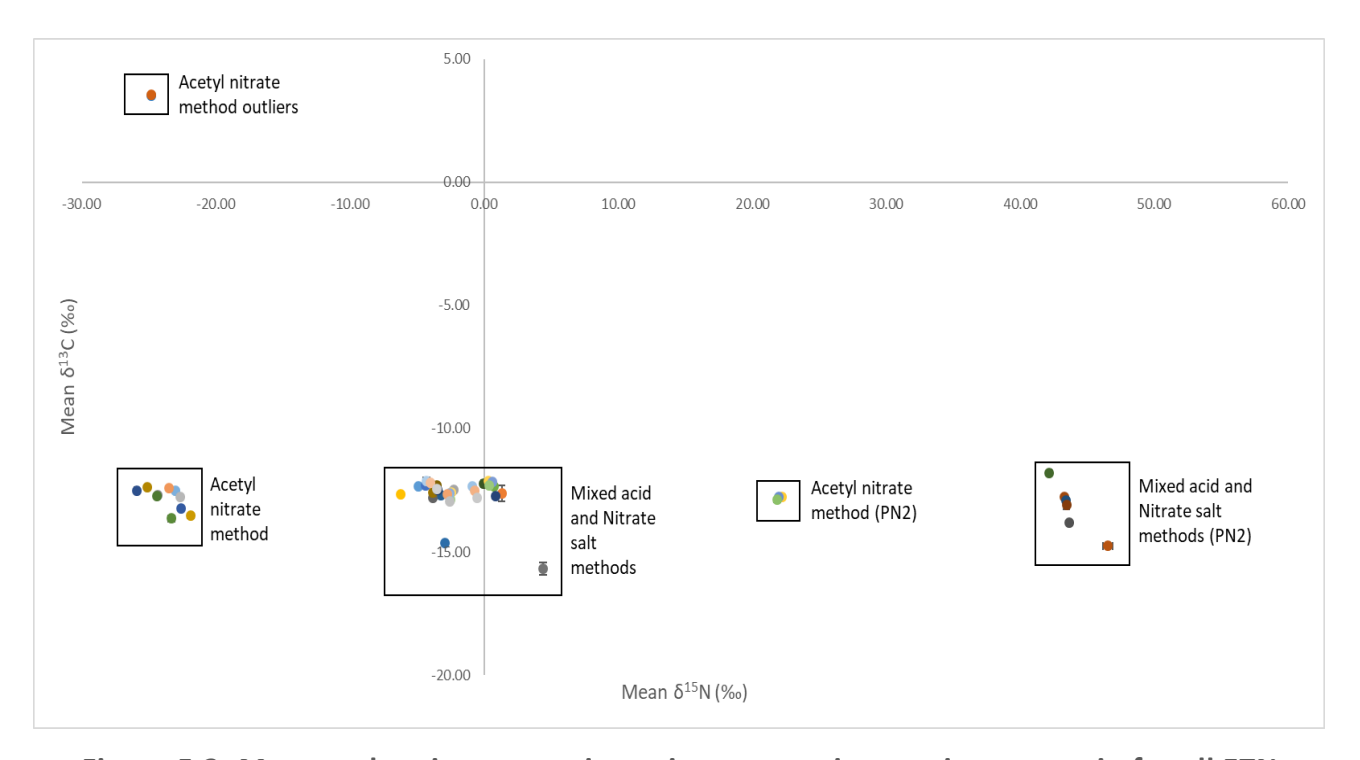


Figure 5.3: Mean carbon isotope ratio against mean nitrogen isotope ratio for all ETN samples.

This representation displays the entire dataset and therefore shows the maximal amount of discrimination possible. As a result, it is evident that there are differences between samples due to the starting material and synthesis methods used. Firstly, the samples cluster based on synthesis

methods with the acetyl nitrate method separating from the mixed acid and nitrate salt methods. Secondly, each synthesis method splits into two clusters due to samples involving the use of PN2, either directly in the synthesis, or as a source of nitric acid, having a much higher nitrogen-15 content than all other nitrogen containing precursors used.

#### 5.2 ICP-MS of ETN

The ICP-MS of ETN involved the analysis of the trace metals listed previously in Section 2.2.2. All samples, standards and controls for this analysis used 2% nitric acid as a matrix and were prepared gravimetrically for precision. As the aim of the analysis performed was quantitation, the following limits of quantification (LOQ) were obtained for each of the elements. This LOQ was calculated through the analysis of at least 5 blanks and taking ten times their standard deviation.

Table 5.1: Typical quantification limits for elements analysed in the ICP-MS of erythritol tetranitrate samples.

Element	Al	Ca	Со	Fe	K	Mg
LOQ (ppt)	374.1	821.5	4.3	179.3	3609.9	193.5
Element	Ni	Ru	Sr	U	Zn	
LOQ (ppt)	182.2	3.7	17.9	5.2	431.1	

The calibration of each element required fitting a linear line of best fit to the calibration data, using the best model of fit. This varied between the elements for the reasons discussed previously in the KClO<sub>3</sub> case. In Table 5.2, an example of a calibration used during this analysis is displayed.

Table 5.2: Example of calibration data for elements selected in the ICP-MS analysis of potassium chlorate.

Element	Mass	Linear Model	Coefficient of Correlation (R <sup>2</sup> )	Working Range (ppb)
Al	27	Simple Linear	0.999909	10-100
Ca	44	Simple Linear	0.99953	10-100
Со	59	Weighted Linear	0.999962	0.1-100
Fe	56	Simple Linear	0.99996	0.1-100
K	39	Simple Linear	0.99983	0.5-100
Mg	24	Weighted Linear	0.997829	0.1-100
Ni	60	Weighted Linear	0.999760	0.1-100
Ru	102	Weighted Linear	0.999674	0.1-100
Sr	88	Weighted Linear	0.999893	0.1-100
U	238	Weighted Linear	0.999861	0.01-10
Zn	66	Weighted Linear	0.996539	0.1-100

The amount of sample produced by DST Group was purposely kept minimal and therefore there was only enough sample for a single digestion for ICP-MS analysis. As a result, no duplicate or triplicate analysis was possible using ETN. Since the preparation of samples for analysis involved digesting the entirety of a sample, there is no question as to the accurate representation of the digested portion to the bulk material, minimising the need for random duplicates. There was, however, enough precursor material for triplicate analysis to measure the reliability of the sample preparation and analysis process. A triplicate of one ammonium nitrate and calcium nitrate precursor were analysed and percent coefficients of variation (%CV) were calculated; these results are displayed in Table 5.3. The %CV has been coloured green (0-10%), yellow (10.01-20%) and red (>20.01%) as in previous sections. These brackets have been designed to indicate the level of reliability in the measurements with green being ideal, yellow acceptable and red unacceptable.

The results show most of the elements are consistent across the triplicates with only two red values. The 141% coefficient of variation result for calcium was due to a carry-over effect. This was due to analysing the calcium nitrate replicates, which had a very high concentration of calcium prior to the first ammonium nitrate sample. This carry-over is due to either calcium not being cleared out of the sample introduction system or a build-up of calcium on the cones of the ICP-MS. For future analysis of such a material, a longer wash and/or rinse time should be implemented to minimise this effect. A blank analysis between samples could also be a reasonable precaution for samples with a high concentration of a single element. This is difficult to judge however, as sometimes estimated concentrations are not known.

Table 5.3: Percent coefficient of variation analysis of random triplicates.

Samples	Al (ppb)	Ca (ppb)	K (ppb)	Co (ppb)	Ni (ppb)	Ru (ppb)	U (ppb)	Sr (ppb)	Fe (ppb)	Mg (ppb)	Zn (ppb)
CN (1)	0.83	32690.68	5.01	0.01	0.00	0.00	0.00	24.36	0.48	88.03	1.51
CN (2)	0.99	26944.51	5.88	0.01	0.00	0.00	0.00	20.41	0.58	82.00	1.84
CN (3)	0.80	33834.55	6.14	0.01	0.00	0.00	0.00	23.20	0.64	86.02	1.58
%CV	9.67	9.68	8.56	8.66	0.00	0.00	0.00	7.31	11.90	2.94	8.73
AN (1)	345.62	2.68	0.00	0.03	0.00	0.00	0.00	0.00	0.73	0.54	1.66
AN1 (2)	365.32	0.00	0.00	0.03	0.00	0.00	0.00	0.00	3.41	0.42	2.24
AN1 (3)	323.50	0.00	0.00	0.02	0.00	0.00	0.00	0.00	0.63	0.42	1.63
%CV	4.95	141.42	0.00	9.19	0.00	0.00	0.00	0.00	80.87	12.52	15.29

#### 5.2.1 Exploratory Multivariate Data Analysis

The raw results of the analysis were transformed in the same manner as previously described in Chapter 3.3. This includes the NaN values being assigned zero values and the entire dataset undergoing a translation and logarithmic transformation. Exploratory analysis including HCA and PCA of the dataset was then undertaken.

HCA was performed to assess the potential of a PCA analysis and the resultant dendrogram and sample identity correlation table are displayed in Figure 5.4 and Table 5.4. This initial overview of the data shows potential for the data to be split into two clusters with one large and one smaller branching of samples within the dendrogram. There are also potentially 3-5 outliers in samples 55, 56 and 58 located to the extreme left and samples 52 and 54 to the extreme right with a large Euclidean distance between them and the remainder of samples.

Table 5.4: Sample correlation to number identifiers in HCA dendrogram in Figure 5.4.

Number	Sample	Number	Sample	Number	Sample	Number	Sample
1	BCH25	17	h 8 5	33	i 27 6	49	DA98A
2	BCH26	18	i 13 5	34	j 25 7	50	DA99A
3	BCH27	19	j 13 5	35	K 27 7	51	DA100A
4	BCH29	20	K 14 5	36	L78	52	unison
5	BHC30	21	L 14 5	37	M 5 12	53	natvia
6	BCH31	22	P 23 5	38	N 6 12	54	Sigald
7	BCH32	23	Q 22 5	39	O 7 12	55	CN (1)
8	всн33	24	R 27 5	40	P 25 3	56	CN (2)
9	BCH34	25	a 12 6	41	Q 37 3	57	CN (3)
10	BCH35	26	b 13 6	42	R 1 4	58	AN1 (1)
11	BCH36	27	c 15 6	43	DA84A	59	AN1 (2)
12	BCH37	28	d 18 6	44	DA85A	60	AN1 (3)
13	d 15 4	29	e 19 6	45	DA86A	61	AN2
14	e 16 4	30	f 20 6	46	DA95A		
15	f 17 4	31	g 25 6	47	DA96A		
16	g 8 5	32	h 26 6	48	DA97A		

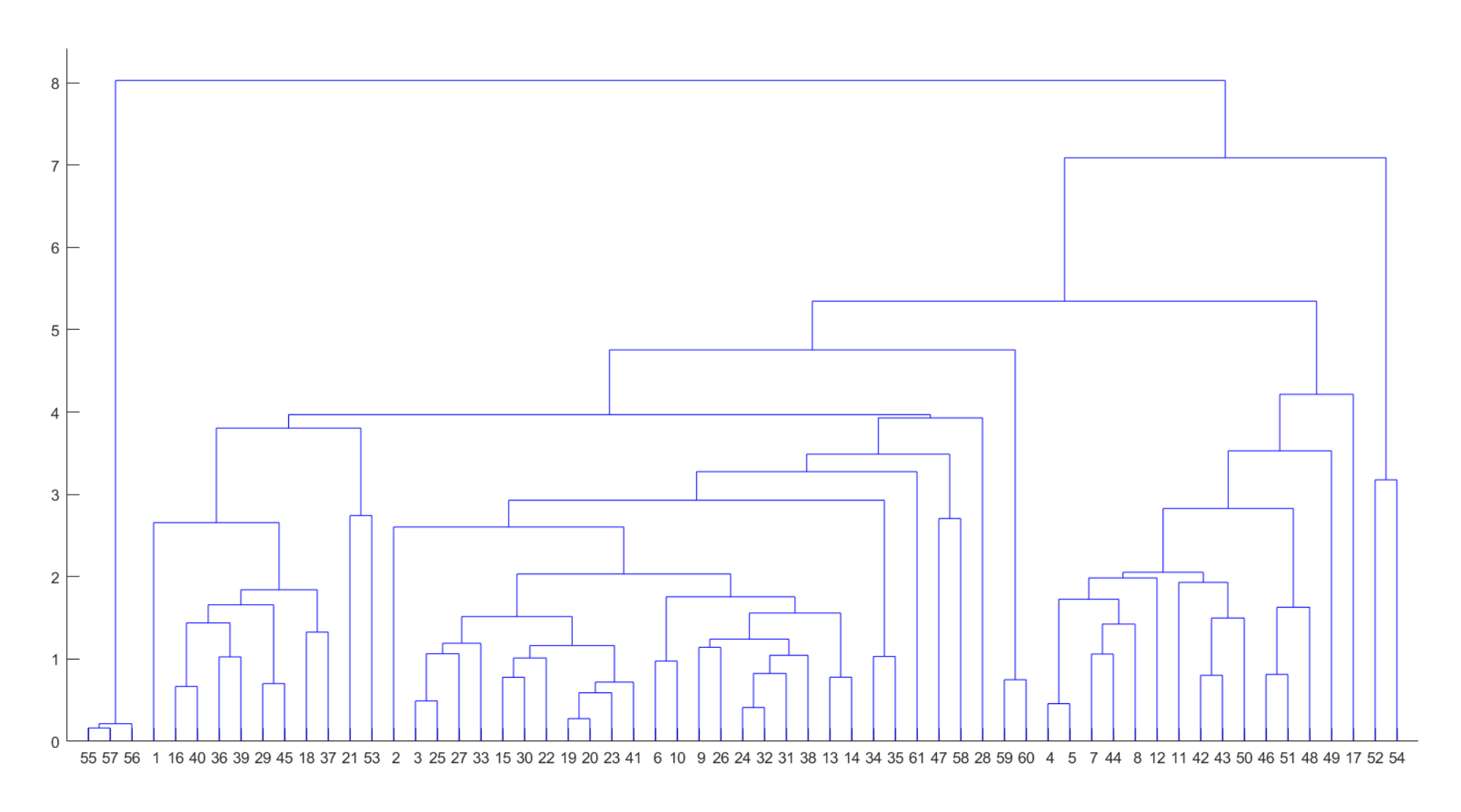


Figure 5.4: Resultant dendrogram from the hierarchical cluster analysis of erythritol tetranitrate ICP-MS data.

PCA analysis was undertaken and as always, the quality of the analysis was scrutinised. This began with breakdown of the percentage of variance retained by each principal component (Table 5.5) which may also be graphically displayed in a scree plot (Figure 5.5).

Table 5.5: Variance retention table for the PCA of ETN ICP-MS dataset.

Component	Principal Component Eigenvalues	Cumulative Percentage of Variance Explained
PC1	5.939349	44%
PC2	2.24841	65%
PC3	1.64934	85%
PC4	1.155819	92%
PC5	0.652899	96%
PC6	0.319539	97%
PC7	0.258544	98%
PC8	0.196207	99%

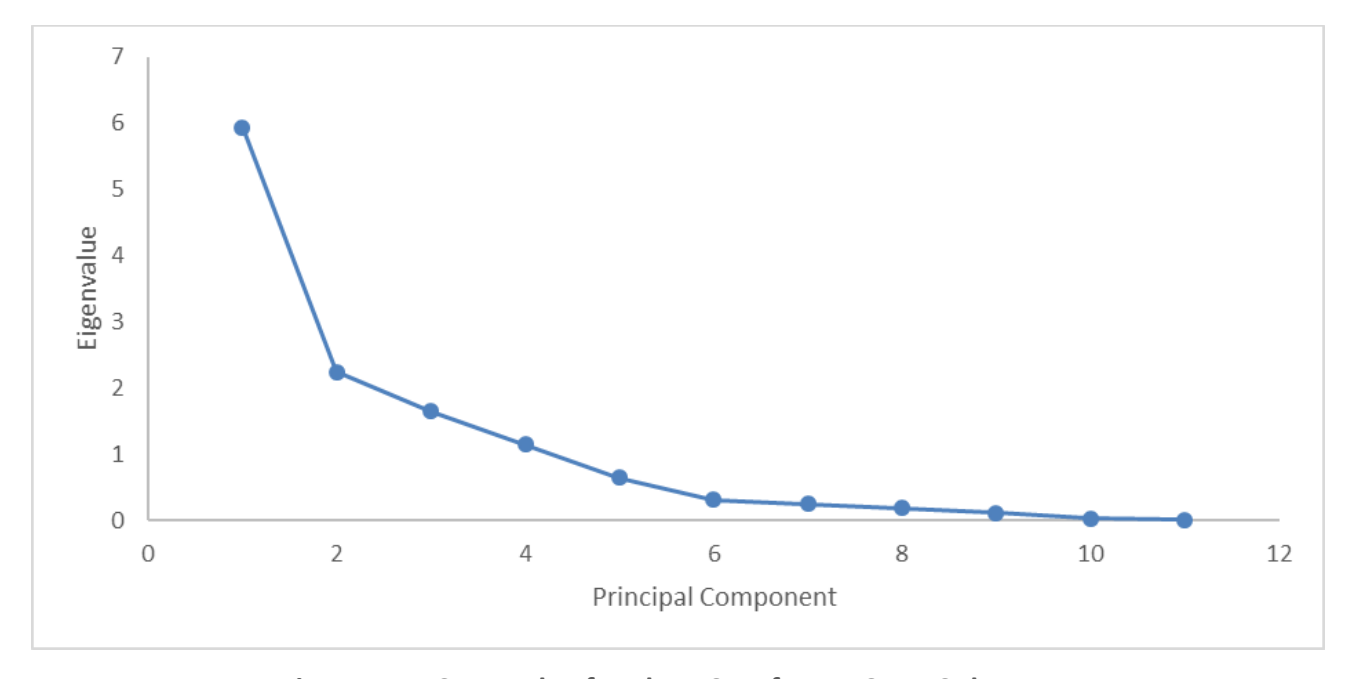


Figure 5.5: Scree plot for the PCA of ETN ICP-MS dataset.

The distribution of variance across the PCs is a little concerning, as the inflection point lies at PC2 and following this point there is still a significant gradient across PC2-6. This indicates that the variance is not heavily localised in a fewer number of variables, and typically means that there is little discriminatory data within the dataset.

The coefficient table (Table 5.6) reveals the key contributors of each of the principal components. Unfortunately, the coefficient table also supports the indications given by the scree plot with many elements contributing to each PC. Particularly concerning is the list of elements contributing to PC3, being almost identical to that of PC2, with only the minor addition of ruthenium and magnesium. Magnesium was already a significant variable contributing to PC1 and ruthenium is a very rare element that was not present in great amounts within the samples. All of this is a further indication that there is minimal discriminatory data within this ICP-MS dataset.

Table 5.6: Coefficient table for the first 8 PCs of the ETN ICP-MS dataset.

	PC1	PC2	PC3	PC4	PC5	PC6	PC7	PC8
Al		-0.3	-0.3	0.7			0.3	-0.2
Ca	0.6	0.6	-0.3		-0.4		0.2	
K	0.6	-0.5	0.6					
Со				0.2		0.6		0.5
Ni		-0.5	-0.5	-0.5	-0.2	0.3		
Ru			-0.2	-0.3	0.3	-0.2	0.8	0.3
U								
Sr	0.3	0.2	-0.2		0.7	0.2		-0.5
Fe		-0.3	-0.3			-0.5		-0.3
Mg	0.3		-0.3	0.2	0.3	-0.4	-0.4	0.6
Zn								

Table 5.7: Correlation coefficients for the PCA of the ETN ICP-MS dataset.

	Al	Ca	K	Со	Ni	Ru	U	Sr	Fe	Mg	Zn
Al									LEGEND	ı	
Ca				_					0.00-0.	25	
K					_				0.26-0.	50	
Со									0.51-0.	75	
Ni							_		0.76-0.	95	
Ru									0.96-1.	00	
U									_		
Sr										_	
Fe											_
Mg											
Zn											

The final aspect to consider was correlation between the elements as this can be the reason for a lack of discriminatory variance. The correlation coefficients have been calculated and the colour

coded version is displayed in Table 5.7. This does not identify any significant levels of correlation within the elements, so this was ruled out as an explanation for this lack of variance.

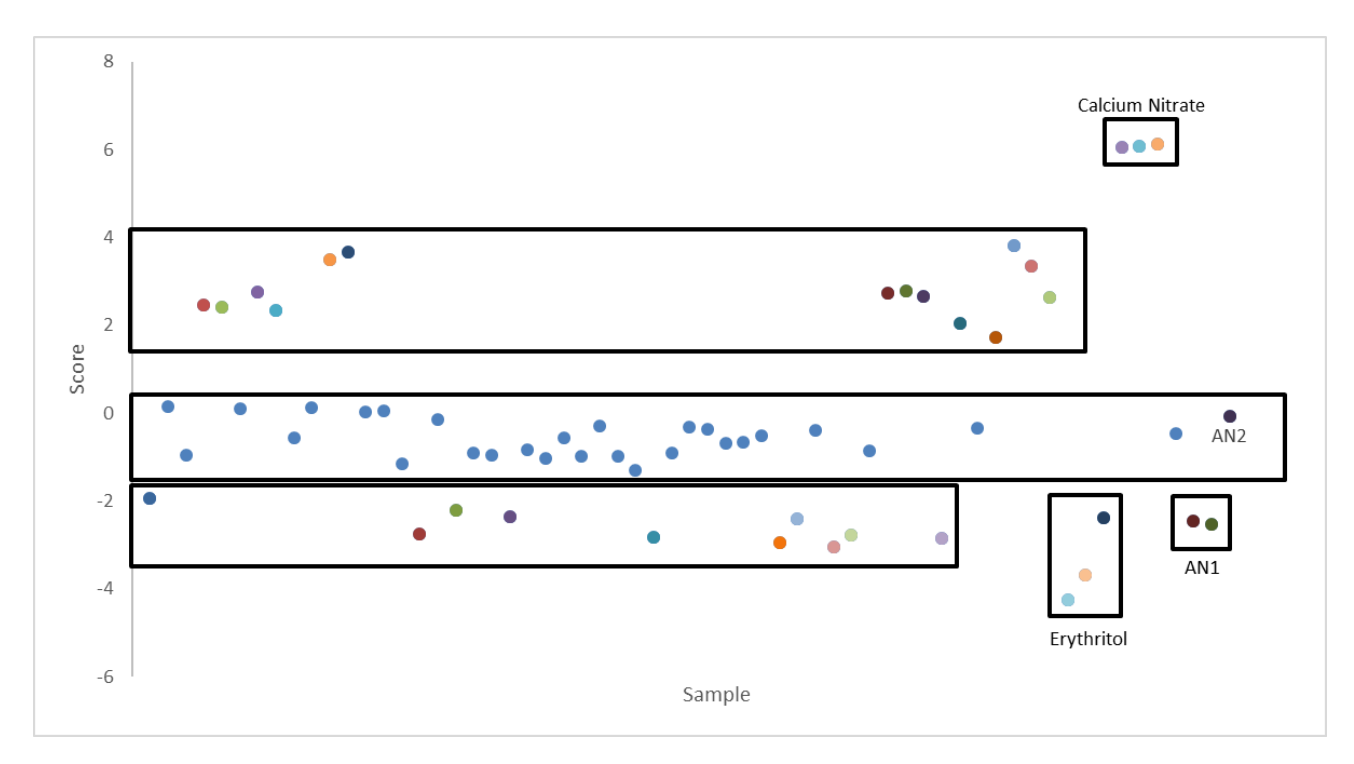


Figure 5.6: Score plot of PC1 from the PCA of ICP-MS data for ETN samples and precursors.

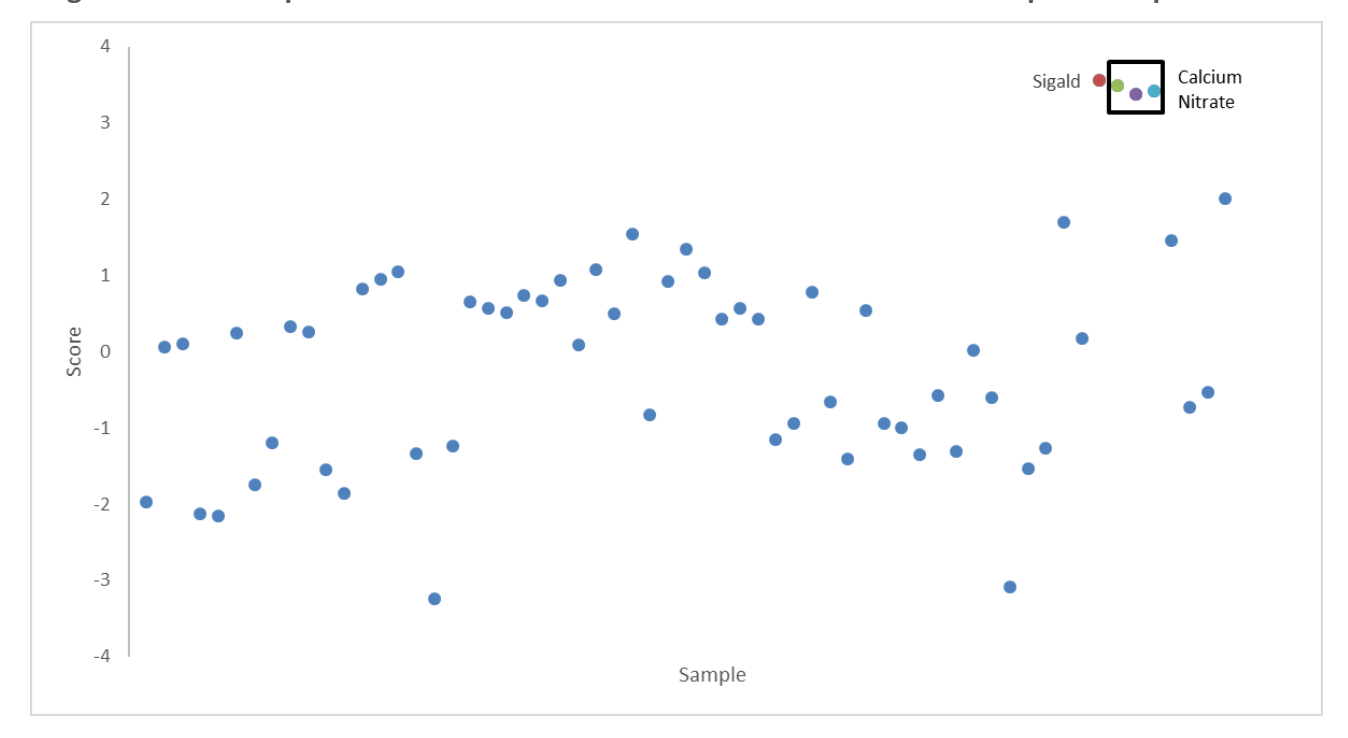


Figure 5.7: Score plot of PC2 from the PCA of ICP-MS data for ETN samples and precursors.

The results of the PCA in the form of individual score plots are plotted in Figures 5.6 and 5.7. Only PC1 showed clear groupings; PC2 indicated two possible groupings, however they are not distinctly

separated. PC3 and onwards showed no potential clustering of samples and were therefore of no interest.

PC1 shows that the dataset has some discriminatory information with three distinctly separated clusters of ETN. Many of the starting materials, however, are not distinctly separated with the three erythritols being in close proximity. One ammonium nitrate (AN1) is also similar to the erythritols, however, AN2 is contained within the central bracket of samples. Though 2 of the replicates of AN1 are positioned with the erythritols, the first of the triplicate has a higher score and is more in line with AN2. Examining the loadings in Figure 5.8, this can be attributed to an unusually high reading of calcium with the other replicate containing none. This is due to a shortcoming in the ICP-MS analysis, as the calcium nitrate caused a carryover effect to the first of the AN1 replicates. This could have been avoided by lengthening the rinse and flush time between these samples.

The final precursor, calcium nitrate, has a much greater score than the other precursors and samples. This is understandable as PC1 has been shown to include calcium content as a key factor in Table 5.6, and calcium nitrate contains far more than any other sample. It must be noted that the potassium nitrates (PN1 and PN2) were not included within this analysis, as potassium was included in the analysis and these samples contain percent levels of potassium making them very distinct outliers.

Interrogating the ETN samples initially revealed no pattern to explain the clustering as the scores relating to the synthesis method, erythritol and nitrate precursors are completely mixed. Initially these were the only variables that were considered during the synthesis of the ETN samples, however, there was one other factor that was overlooked and that was the person synthesising the material. This was the only factor that indicated a trend across the samples as detailed in Table 5.8. This result was different to the ICP-MS results in the previous KClO<sub>3</sub> analysis, where the precursors and synthesis methods utilised in the production of the samples could be linked to sample providing discriminatory data.

Table 5.8: Summary of variables for the high and low PC1 score clusters of ETN samples in Figure 5.6.

		High PC1 Score G	îroup	
Sample	Synthesis Method	Erythritol	Nitrate	Scientist
BCH 29	Nitrate Salt	Unison	Ammonium nitrate 1	Α
BCH 30	Nitrate Salt	Unison	Ammonium nitrate 2	Α
BCH 32	Nitrate Salt	Natvia	Potassium nitrate 1	А
BCH 33	Nitrate Salt	Natvia	Potassium nitrate 2	Α
BCH 36	Nitrate Salt	Natvia	Calcium nitrate	А
BCH 37	Nitrate Salt	Unison	Potassium nitrate 2	А
R 25 7	Acetyl Nitrate	Natvia	Calcium nitrate	В
DA 84A	Nitrate Salt	Sigma-Aldrich	Potassium nitrate 1	С
DA 85A	Nitrate Salt	Sigma-Aldrich	Potassium nitrate 2	С
DA 95A	Acetyl Nitrate	Sigma-Aldrich	Ammonium nitrate 2	С
DA 97A	Acetyl Nitrate	Natvia	Ammonium nitrate 2	С
DA 98A	Mixed Acid	Sigma-Aldrich	Ammonium nitrate 2	С
DA 99A	Mixed Acid	Unison	Ammonium nitrate 2	С
DA 100A	Mixed Acid	Natvia	Ammonium nitrate 2	С
		Low PC1 Score G	roup	
Sample	Synthesis Method	Erythritol	Nitrate	Scientist
BCH 25	Nitrate Salt	Sigma-Aldrich	Ammonium nitrate 2	Α
g 8 5	Acetyl Nitrate	Sigma-Aldrich	Potassium nitrate 2	В
i 13 5	Acetyl Nitrate	Natvia	Potassium nitrate 2	В
L 14 5	Acetyl Nitrate	Natvia	Ammonium nitrate 1	В
e 19 6	Mixed Acid	Unison	Potassium nitrate 1	В
L 7 8	Mixed Acid	Natvia	Ammonium nitrate 1	В
M 5 12	Mixed Acid	Sigma-Aldrich	Ammonium nitrate 2	В
0 7 12	Mixed Acid	Natvia	Ammonium nitrate 2	В
P 25 3	Mixed Acid	Sigma-Aldrich	Calcium nitrate	В
DA 86A	Nitrate Salt	Sigma-Aldrich	Ammonium nitrate 1	С

To better understand these results, the components having the greatest effect on PC1 were examined. In this case it is primarily the calcium and potassium (Figure 5.8), and to a lesser extent strontium and magnesium (Figure 5.9) content across the sample set.

Examining Figures 5.8 and 5.9, the low PC1 score samples can be identified as consisting of lower concentrations in up to three of the four elements, whereas the higher score grouping can be almost entirely explained by the concentration of potassium within a sample, with all samples apart from h-8-5 belonging to the high score group. This then raises the question of why it is that two of the three

chemists tended to introduce significant levels of potassium to the sample. Further information on the details of the synthesis revealed that the samples with elevated potassium concentrations were undertaken in a separate lab, and with different glassware and fume hood. This has potentially led to this level of discrimination between the samples, rather than any differing precursor or synthesis method. This would require further research, eliminating equipment and environmental factors before being certain of a link between sample and precursor or synthetic route, like in the previous KClO<sub>3</sub> research. A link between sample and synthetic environment or equipment could be useful in a real-world setting, as differences could lead to valuable information when gathering intelligence to focus an investigation or confirm linkages between a sample and manufacturer.

The score plot for PC2 (Figure 5.7) had far less distinct clustering with only the potential of two overlapping groups. PC2 incorporates the elemental mass fractions of aluminium, iron and nickel, however, calcium and potassium are still heavily factored into this principal component. Though this score plot does not permit an identification of clear groupings by itself, it may still be of use when a two-dimensional plot is formed from both PC1 and PC2 (Figure 5.10). This two-dimensional score plot with the sample manufacturer identified shows the extent of the trend with three identifiable groupings. Although this is the most identifiable trend across the variables, there is still a lot of cross over, with each grouping containing at least one sample made by each individual. This suggests that there is some level of discrimination, however, the reasoning for this discrimination is not easily explained. This requires further investigation before a confident conclusion could be drawn.

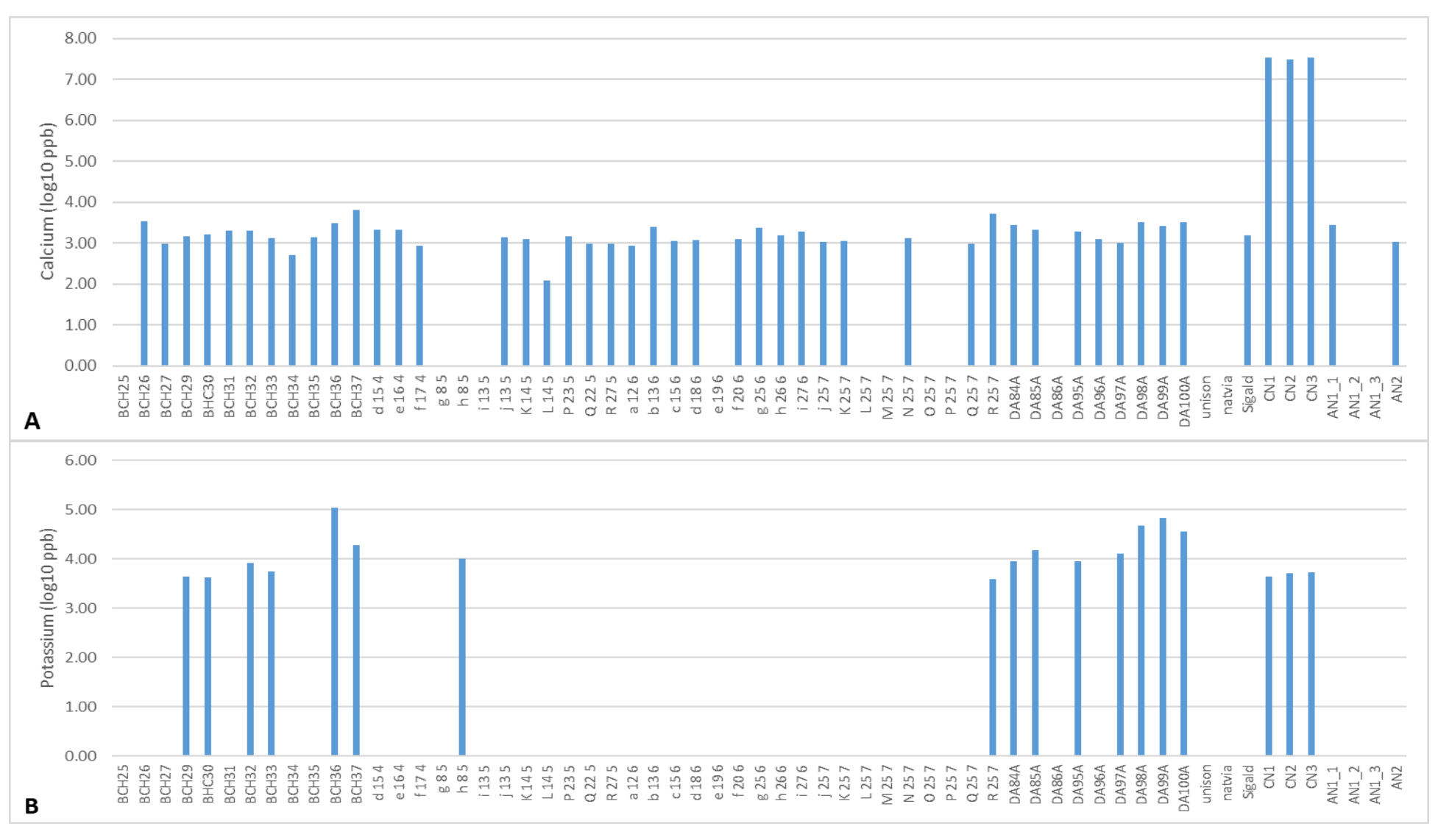


Figure 5.8: Bar charts for the ICP-MS analysis of A) calcium and B) potassium content for ETN samples and precursors.

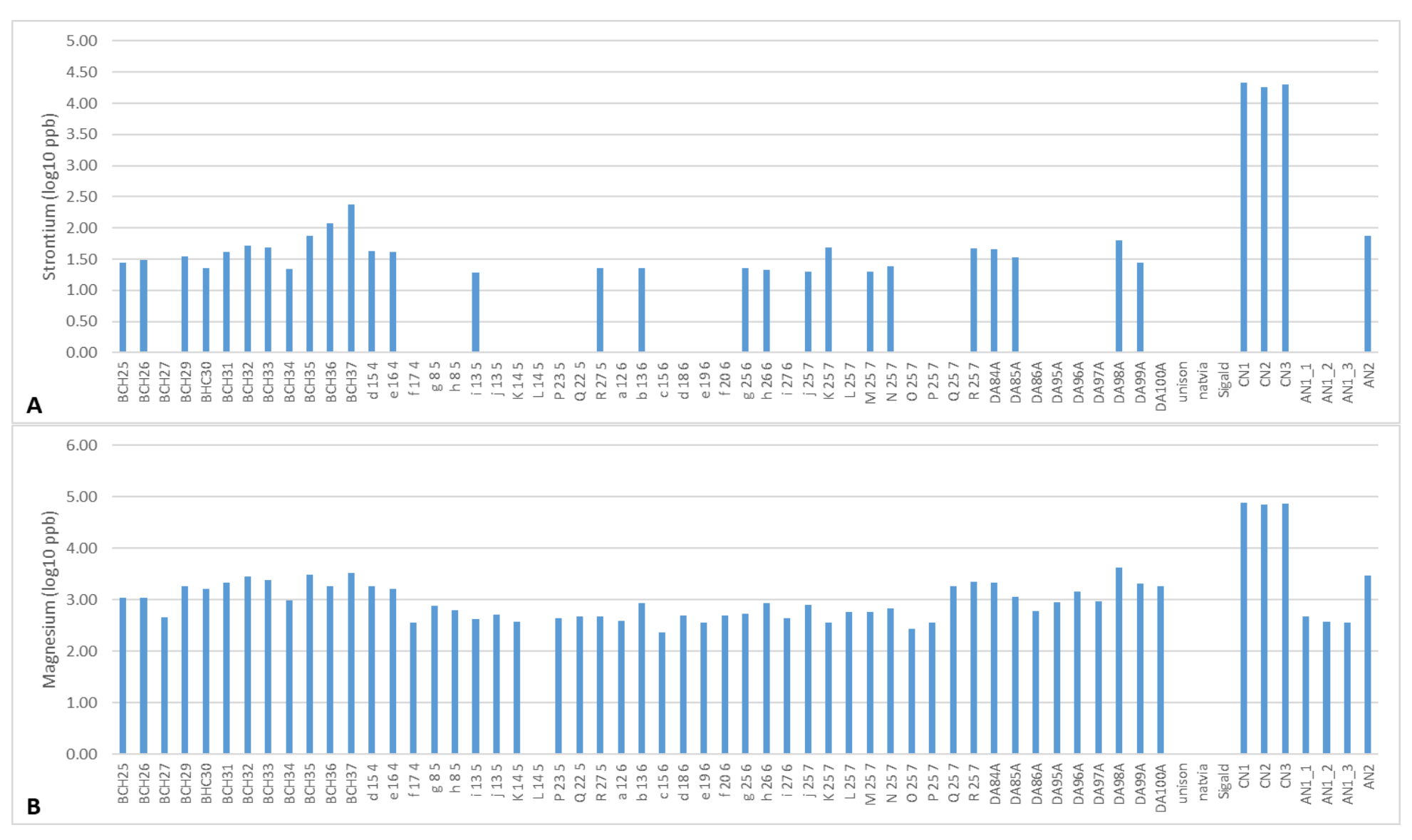


Figure 5.9: Bar charts for the ICP-MS analysis of A) strontium and B) magnesium content for ETN samples and precursors.

The synthesis of all samples involved a purification stage, including recrystallisation to remove residual acid to improve stability and to ensure small crystals were formed for safety reasons. This may also result in reduced levels of trace elemental content being present in the products, however, similar steps would be taken in clandestine labs for production of stable products.

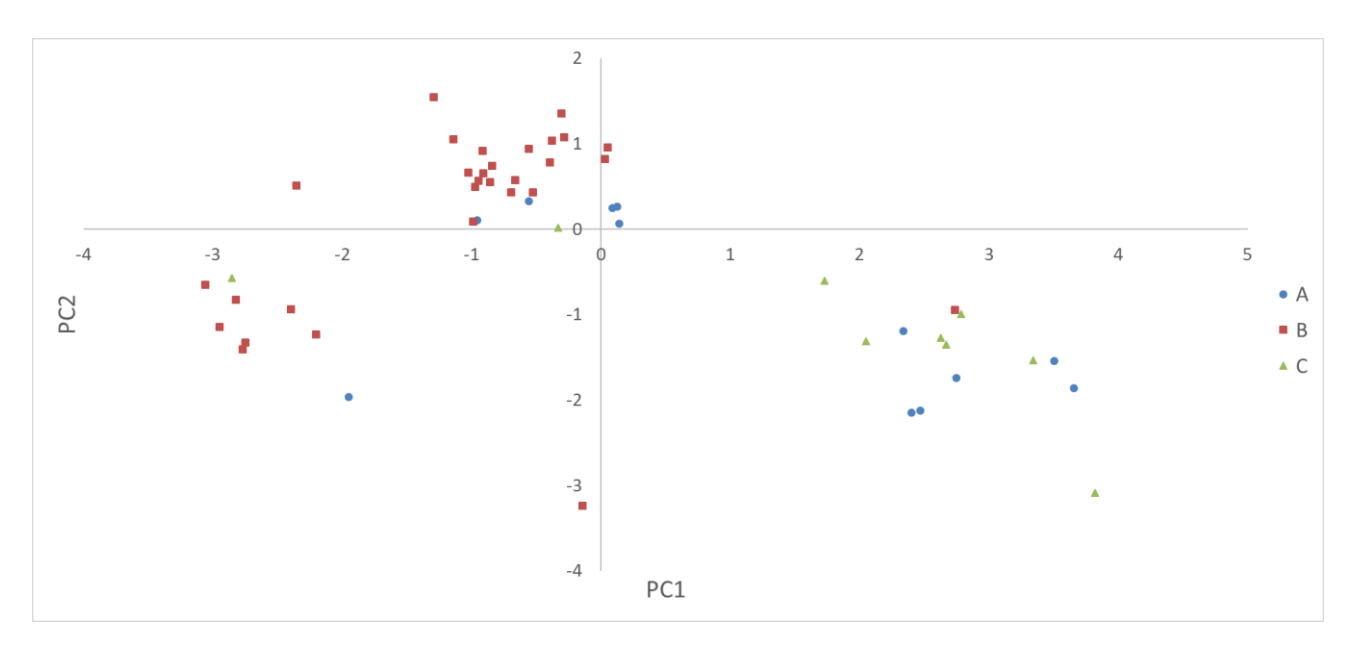


Figure 5.10: Two-dimensional score plot of PC1 and PC2 for the PCA of ICP-MS data for ETN samples.

In conclusion, unlike the case with potassium chlorate where the trace elemental profile revealed discriminatory information based on the synthesis pathways and precursors, the profiles of erythritol tetranitrate samples were more likely to have been influenced by environmental and human contamination. Though the trend was quite strong, there is a lot of crossover between clusters with at least one sample from each of the three chemists being present within each cluster. This information could be used to attribute a sample to an individual, especially if more unusual trace elements are found within the sample, which can be linked to either a location or synthesis equipment associated with that person. For example, someone synthesising samples in a corrugated iron shed could be found to introduce far more trace metals such as iron and tin, than someone performing a synthesis in the spare room of a house. An example of equipment differences could be the change in trace element profiles between plastic/glass/metal containers used for synthesis.

This study highlights the need to understand how the synthesis methods can affect a final product, and the factors that can influence the results obtained through various analytical techniques. It also stresses the importance of fusing various datasets from differing analytical techniques, as the additional data may provide the necessary variance to enable discrimination between samples of the

same substance. Data fusion can also identify different links between samples and increase confidence when matching precursors, synthetic methodologies and/or environments to a sample.

## 5.3 IR Spectrometry of ETN Samples

ETN samples were all created by DST Group and below in Figure 5.11 is an example of an infrared spectrum of a representative sample.

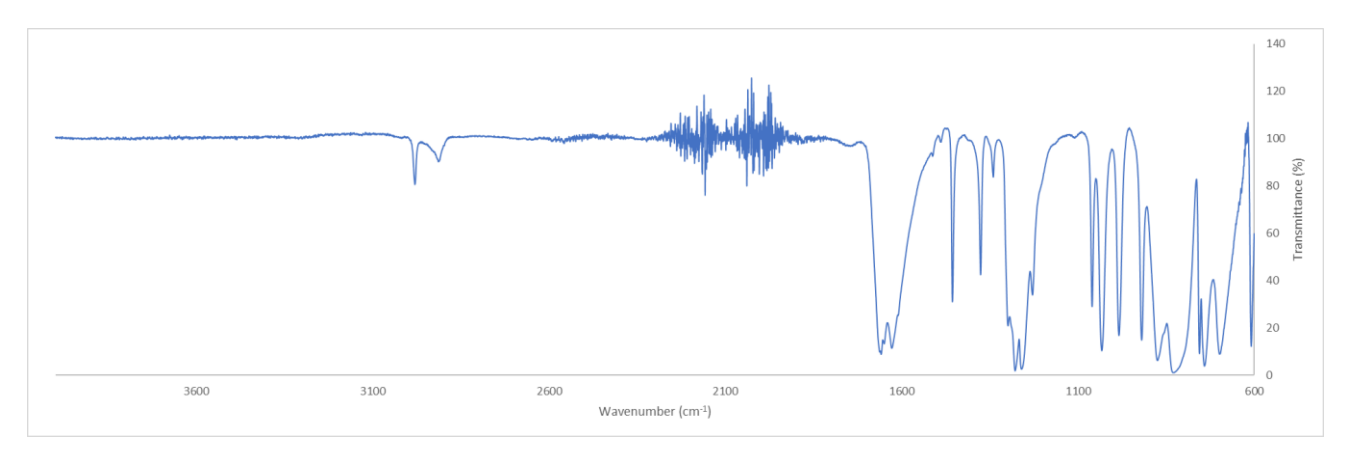


Figure 5.11: ATR IR spectrum of ETN sample BCH1-25.

There are many peaks in a typical infrared spectrum for ETN within the regions  $600-1700 \text{ cm}^{-1}$  and  $2900-3000 \text{ cm}^{-1}$  and this has been modelled and described in detail in other publications<sup>137</sup>. The area between 1950 and 2300 cm<sup>-1</sup> is once again noisy due to the diamond ATR crystal as described previously in the KClO<sub>3</sub> case.

Figure 5.12 plots the spectra of all samples together and highlights the similarity between all but one of the samples. All spectra have been pre-processed using the Spectrum software<sup>131</sup> to apply a polynomial baseline correction and normalisation. The baseline correction selected the points listed in Table 5.9 and the normalisation was done to 1 %T for the largest signal at 831 cm<sup>-1</sup>.

Figure 5.13 shows the spectra of all samples following both baseline correction and with the noisy ATR region removed, as for the  $KCIO_3$  FT-IR spectra.

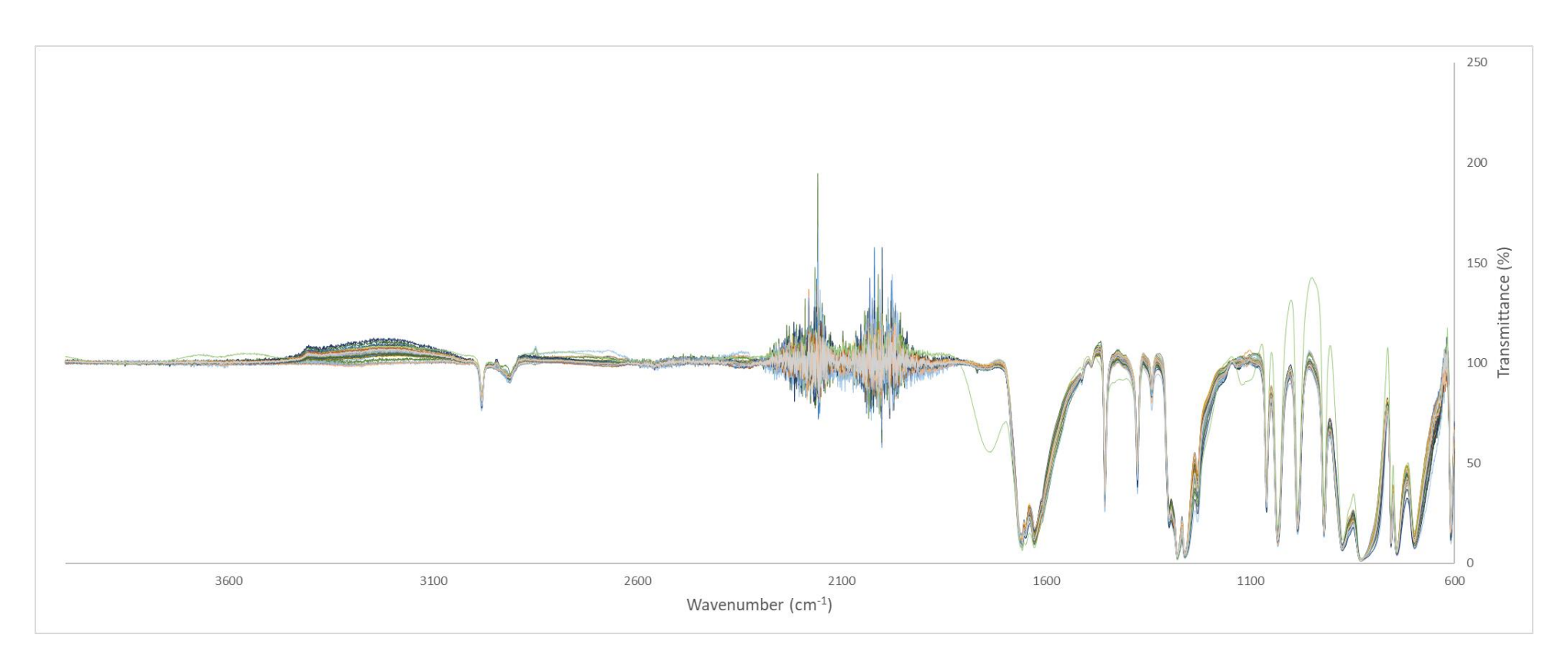


Figure 5.12: Baseline corrected and normalised infrared spectra of all erythritol tetranitrate samples.

Table 5.9: Polynomial baseline correction points for ETN FT-IR spectra.

Base Point	Position (cm <sup>-1</sup> )	Base Point	Position (cm <sup>-1</sup> )	Base Point	Position (cm <sup>-1</sup> )
1	4000	4	3000	7	1500
2	3700	5	2300	8	1146
3	3500	6	1829	9	620

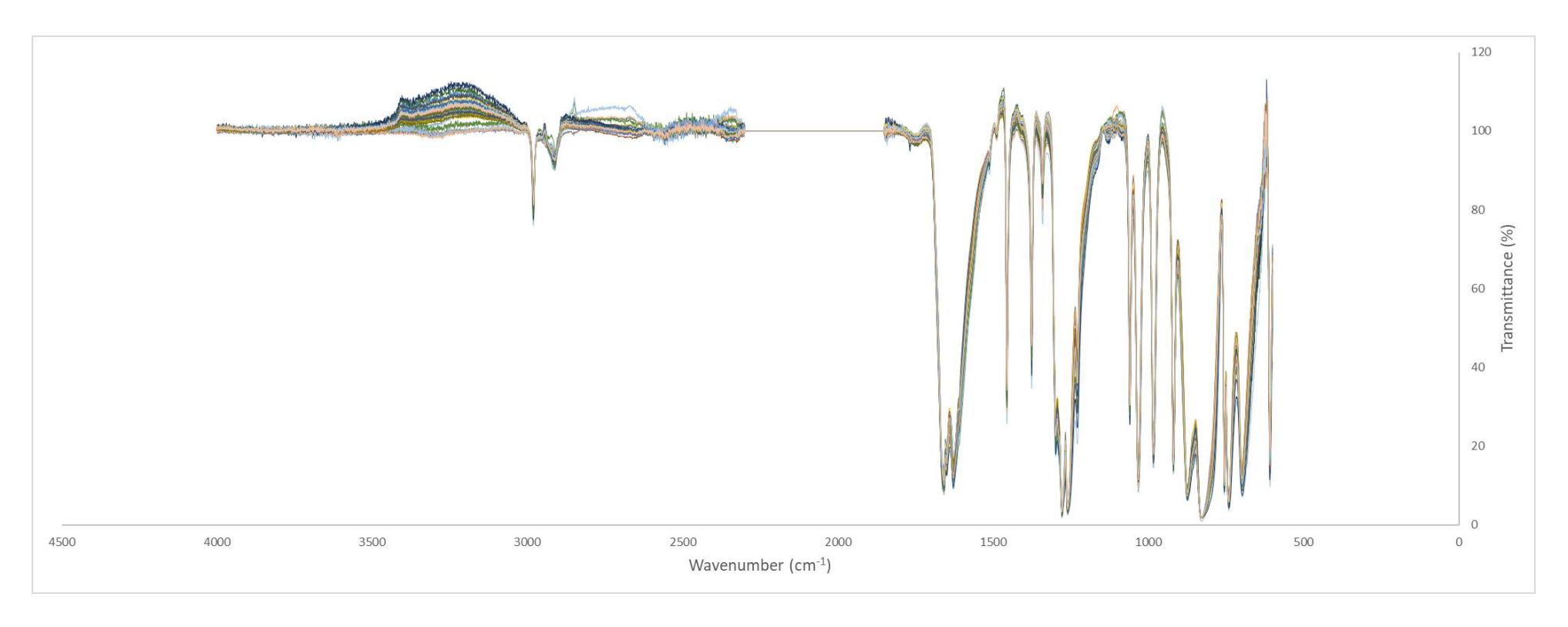


Figure 5.13: Baseline corrected and normalised IR spectra of ETN samples with outlier sample and ATR region removed.

In the outlier case of sample L-7-8 there is a distinct additional signal at 1743 cm<sup>-1</sup> and many of the other peak ratios are inconsistent with the rest of the samples after baseline correction and normalisation. This sample was unusual as there was a visible brown vapour forming within the headspace of the sample vial. Even when blown out with nitrogen gas, within 2 hours the vapour would once again fill the headspace of the vial. This indicates NO<sub>2</sub> gas formation due to the breakdown of the material and as a 1743 cm<sup>-1</sup> peak is detected, the possible formation of an aldehyde group within the molecule. This is most likely from the oxidation of a free primary hydroxyl group by the NO<sub>2</sub> gas suggesting that the synthesis of this sample was possibly only partially successful. Another possibility is that the purification process did not remove all residual acid or impurities leading to the additional 1743 cm<sup>-1</sup> signal and subsequent breakdown of the sample. From the laboratory notes there are no clear indicators of the synthesis not proceeding as per usual and resulted in a typical yield.

#### 5.3.1 Exploratory Multivariate Data Analysis

Prior to PCA this dataset requires the removal of the ATR intrinsic absorption region, which in this case was between 1850 and 2300 cm<sup>-1</sup>, and the previously mentioned outlier L-7-8 was removed as this would significantly hinder the effectiveness of the analysis. Examining the transformed dataset in Figure 5.13 there are no obvious identifiable signals separating samples as was the case in the potassium chlorate dataset. However, the exploratory data analysis can be used to confirm this.

First HCA was performed to identify any clear groupings within the dataset. This analysis is displayed in the dendrogram in Figure 5.14 with the sample identities presented in Table 5.10.

Table 5.10: Sample correlation to number identifiers in HCA dendrogram.

Number	Sample	Number	Sample	Number	Sample	Number	Sample	Number	Sample
1	a-12-6	11	BCH1-34	21	DA-95A	31	g-8-5	41	L-14-5
2	b-13-6	12	BCH1-35	22	DA-96A	32	g-25-6	42	M-5-12
3	BCH1-25	13	BCH1-36	23	DA-97A	33	h-8-5	43	N-6-12
4	BCH1-26	14	BCH1-37	24	DA-98A	34	h-26-6	44	0-7-12
5	BCH1-27	15	c-15-6	25	DA-99A	35	i-13-5	45	P-23-5
6	BCH1-29	16	d-15-4	26	DA-100A	36	i-27-6	46	P-25-3
7	BCH1-30	17	d-18-6	27	e-16-4	37	j-13-27	47	Q-22-5
8	BCH1-31	18	DA-84A	28	e-19-6	38	j-25-7	48	Q-27-3
9	BCH1-32	19	DA-85A	29	f-17-4	39	K-14-5	49	R-1-4
10	BCH1-33	20	DA-86A	30	f-20-6	40	K-27-7	50	R-27-5

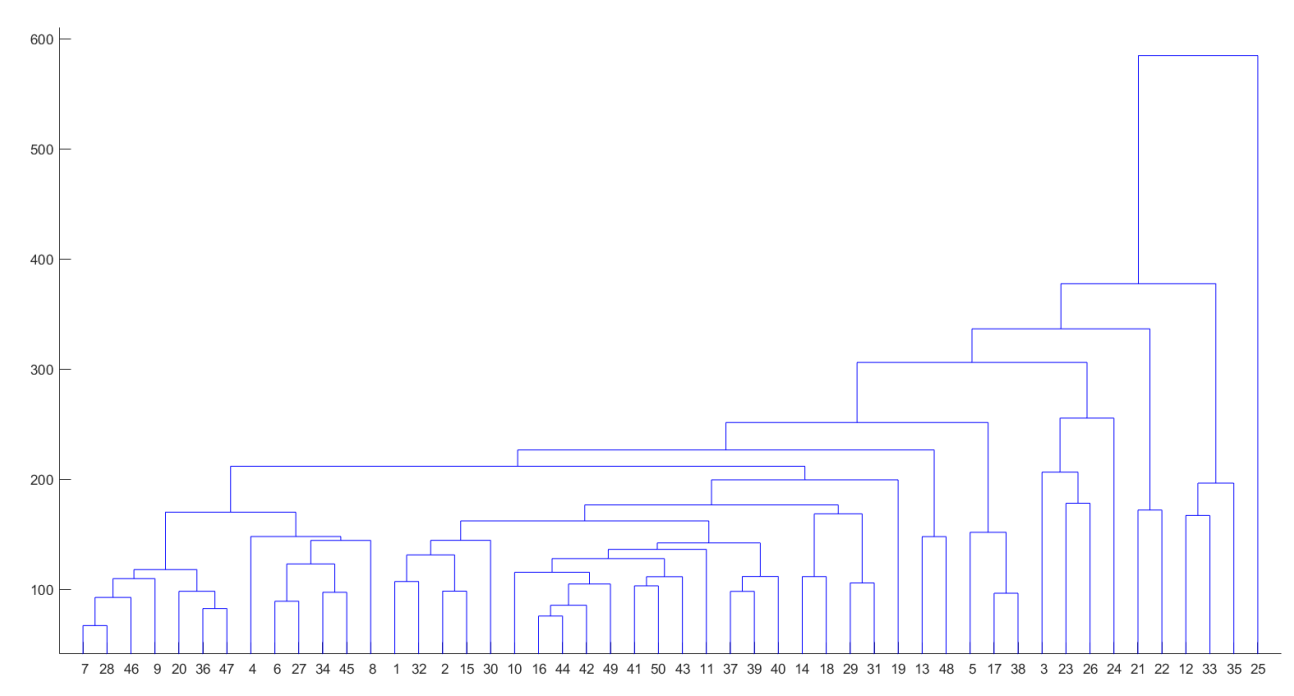


Figure 5.14: Resultant dendrogram from the hierarchical cluster analysis of IR data from erythritol tetranitrate samples.

This analysis indicates that there is very little clustering across the dataset with the Euclidean distances between samples being very low. The easiest way to visualise this is by comparing the most distant samples, i.e. BCH1-30 (#7) and DA-99A (#25). In Figure 5.15 the baseline corrected, and normalised spectra of both samples are plotted and there is very little difference between them. The peak signals are very close to identical apart from some minor differences in peak ratios. The baseline of DA-99A is also visually less stable, which is a result of the strength of absorption being weaker prior to normalisation.

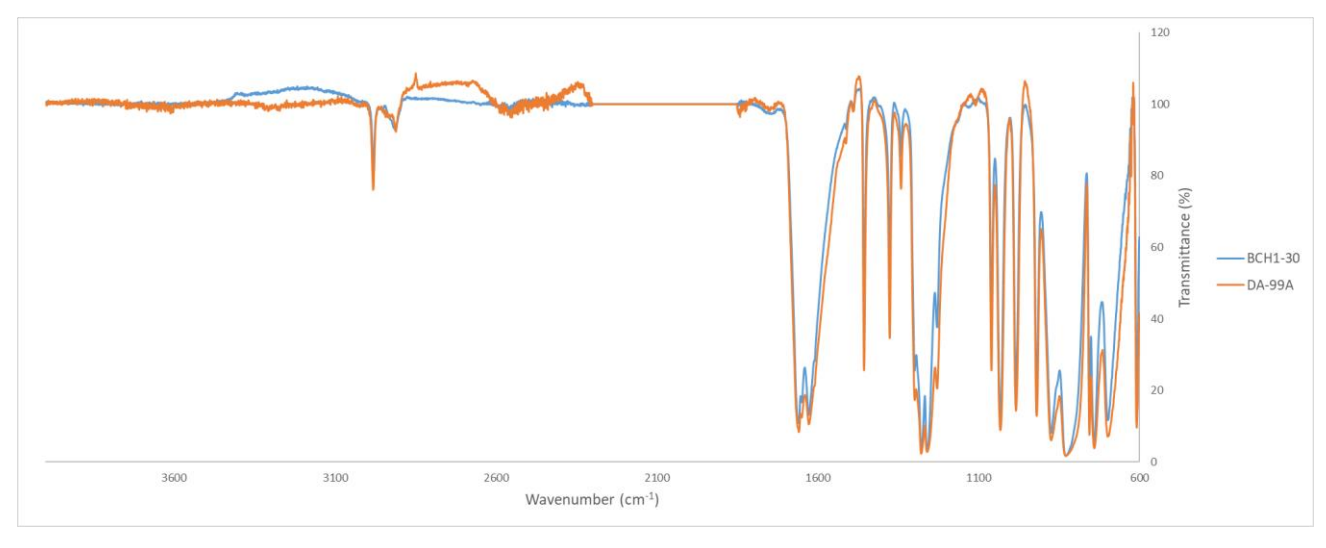


Figure 5.15: Comparative plotting of the pre-processed IR spectra of the most different ETN samples according to HCA.

With the lack of distinct differences within the dataset, the level of discrimination possible by PCA is very limited. However, this analysis was undertaken regardless. Firstly, the variance breakdown in Table 5.11 and scree plot in Figure 5.16 show that there is a much greater spread of variance over principal components than in the previous KClO<sub>3</sub> analysis.

Table 5.11: Variance retention table for the PCA of the pre-processed ETN IR dataset.

Component	PC Eigenvalues	Cumulative Percentage of Variance Explained
PC1	20475.49	51%
PC2	8922.3	74%
PC3	3062.754	81%
PC4	2495.883	87%
PC5	1061.96	90%
PC6	701.5402	91%
PC7	593.5788	93%

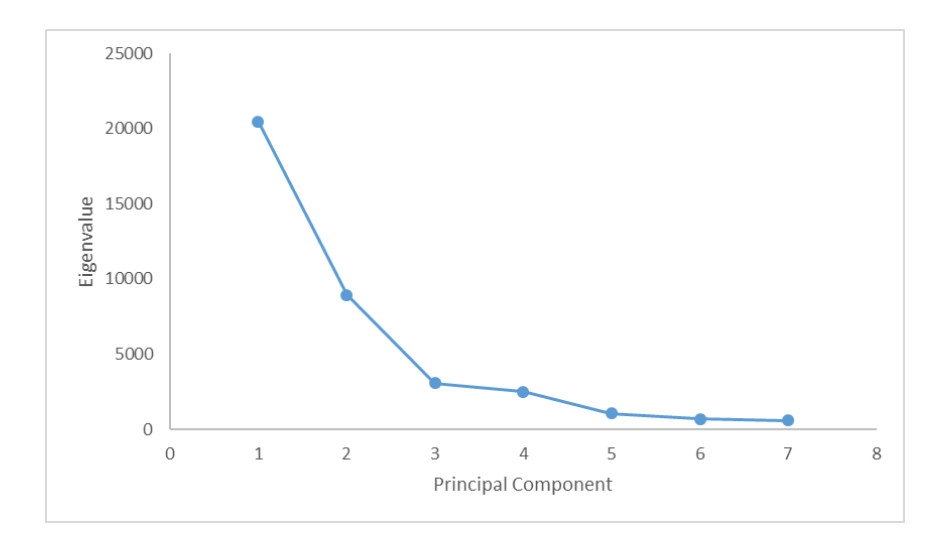


Figure 5.16: Scree plot for the PCA of the pre-processed ETN IR dataset.

This spread is an indication that the level of variance is quite minimal and distributed over a large number of variables, rather than there being clear regions of concentrated variance. PC1 contains 51% of the variance, however not until PC5 is 90% accounted. In contrast, 93% was accounted for by PC3 in the potassium chlorate case. The scree plot has an inflection point at PC3; however, the curve continues to significantly decrease when ideally there should be minimal variance contained in PCs after this inflection point. This lack of inflection point definition reiterates that the variance within the dataset is not significantly concentrated enough for highly successful PCA clustering.

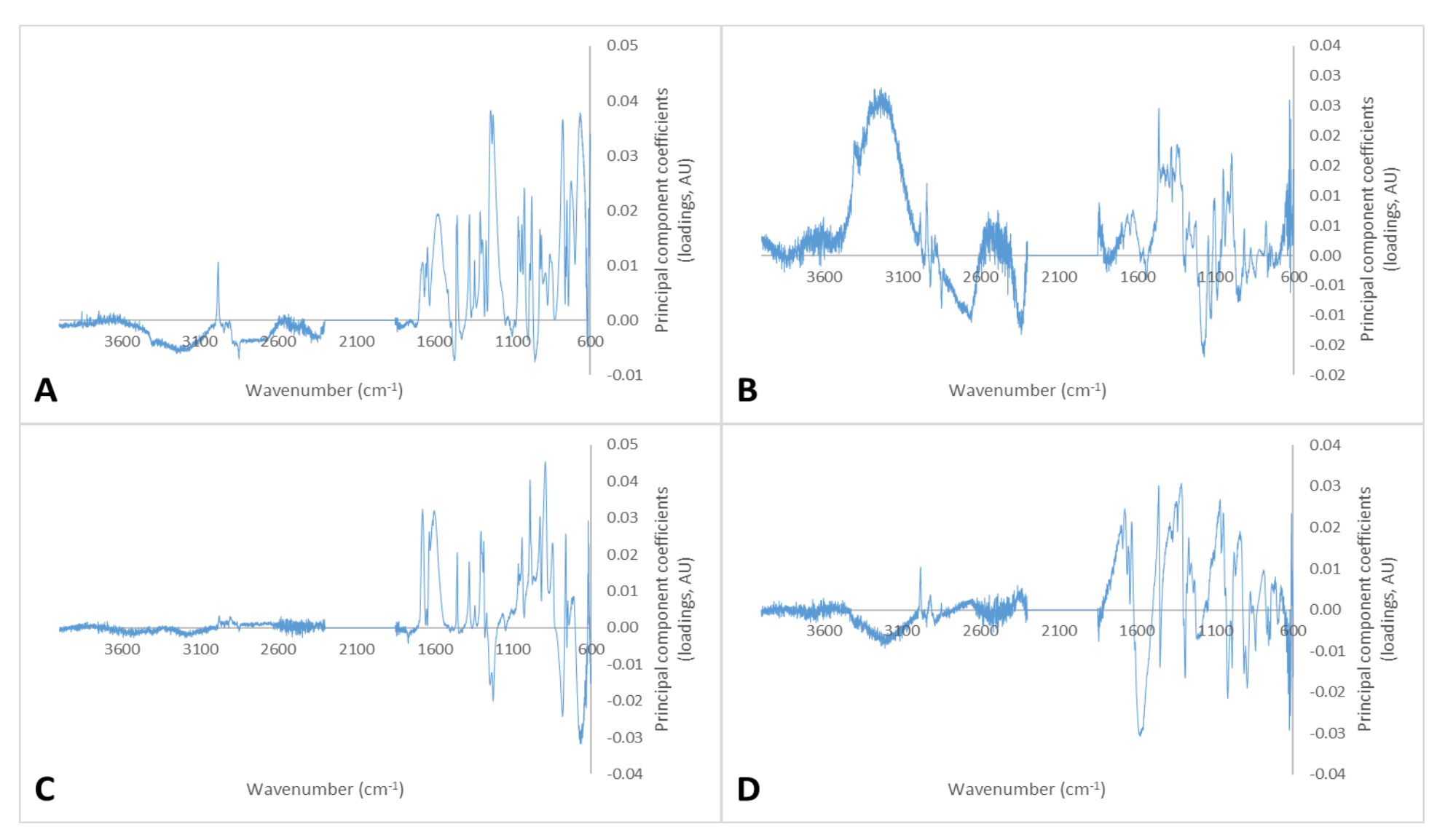


Figure 5.17: Spectrum loadings for A) PC1 B) PC2 C) PC3 and D) PC4 for the pre-processed ETN IR dataset.

This may be examined further by considering the loading factors of the dataset in Figure 5.17, which will help visualise this lack of variance. From examining these loadings, it is evident that after PC1, the loadings immediately lack the features from the original spectra such, as smooth curves and peak shapes but rather, become sharply jagged and ill-defined, noisy signals. This indicates that the level of variance is greatly uninformative; even in PC1, there are artefacts of background contribution in the 2300-4000 cm<sup>-1</sup> region.

With the variance between samples confirmed to be very minimal through both the variance breakdown, and loading factor plots, the PCA cannot be expected to identify distinct differences between samples. These expectations are realised when examining the principal component scores for PC1-PC4 in Figure 5.18.

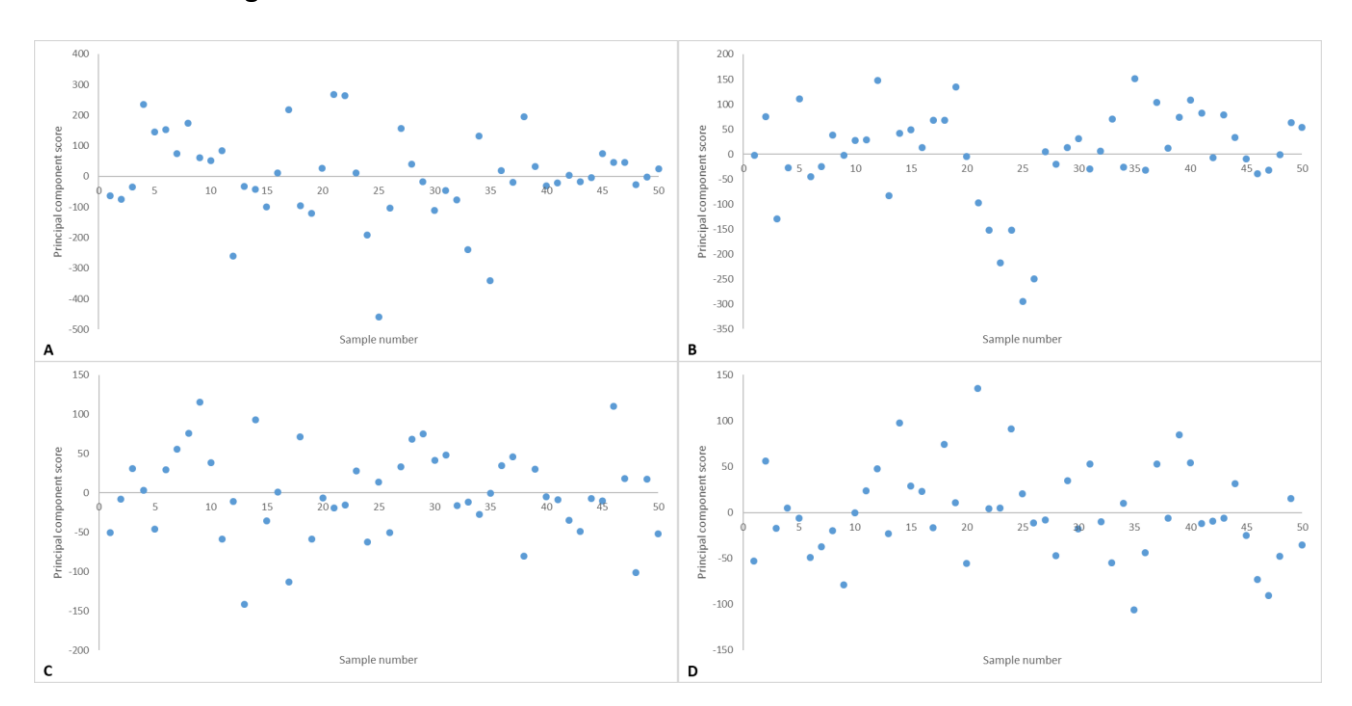


Figure 5.18: One dimensional score plots for A) PC1 B) PC2 C) PC3 and D) PC4 for the preprocessed ETN IR dataset.

The one-dimensional plots show very little distinguishable discriminatory clusters of samples other than a few samples in PC2 which slightly break away from the bulk. These samples are DA-96A, DA-97A, DA-98A, DA-99A and DA-100A and are separated only due to a minor difference in the shape of the baseline between 3000 and 3500 cm<sup>-1</sup>, which could be removed with a higher order polynomial correction, showing the lack of spectral differences between the spectra of this dataset. Combining any two or three of these plots to produce higher order two/three-dimension plots of principal components against one another is futile, as each on their own do not provide any substantial discriminatory power.

In the case of ETN, the ATR IR analysis and subsequent chemometric investigation has not resulted in discrimination between any of the samples. These samples did not contain any significant impurities from the precursor materials or synthetic method identifiable within the IR dataset. This may be a result of the ETN preparations being carried out by professionals using laboratory grade equipment and recrystallisation of the crude products. Both of these factors would reduce the chance of any impurities remaining in the final product. There was one outlier sample identified by ATR IR analysis, however this was due to deterioration of the sample.

## 5.4 Raman Spectroscopy of ETN

Originally this experimentation would have directly replicated the Raman analysis of potassium chlorate samples, using the DeltaNu Raman spectrometer. However, due to equipment failure this was not a possibility. Instead, a much higher resolution Raman spectrometer was used. A XploraRA Horiba Scientific Confocal Raman microscope was used. However, as the analysis of over 50 samples would require a large amount of time and cost, combined with the past lack of discriminatory power found for Raman spectra of KClO<sub>3</sub> samples, a scoping data collection was first taken of three different ETN samples produced by three different synthesis pathways and sets of starting material. These three samples are a good representation of the greatest possible amount of variation within the samples and if the results indicated some possible level of discrimination between samples, further investigations would be undertaken.

Although the spectra were collected over the range of -199 to 4000 cm<sup>-1</sup>, below 170 cm<sup>-1</sup> Rayleigh scattering artefacts dominate the spectrum and no signals exist over 3050 cm<sup>-1</sup>. Therefore, the results were plotted over the range of 170 to 3050 cm<sup>-1</sup> as depicted in Figure 5.19. These spectra do not reveal any clear signs of impurity or side product signals making the technique once again ineffective in discriminating between samples of like material. The same peaks are all present across each sample with the only difference being minor variances in peak ratio between some signals. This was determined not to be a significant enough difference to justify the testing of all samples, although it may be of interest for a future study.

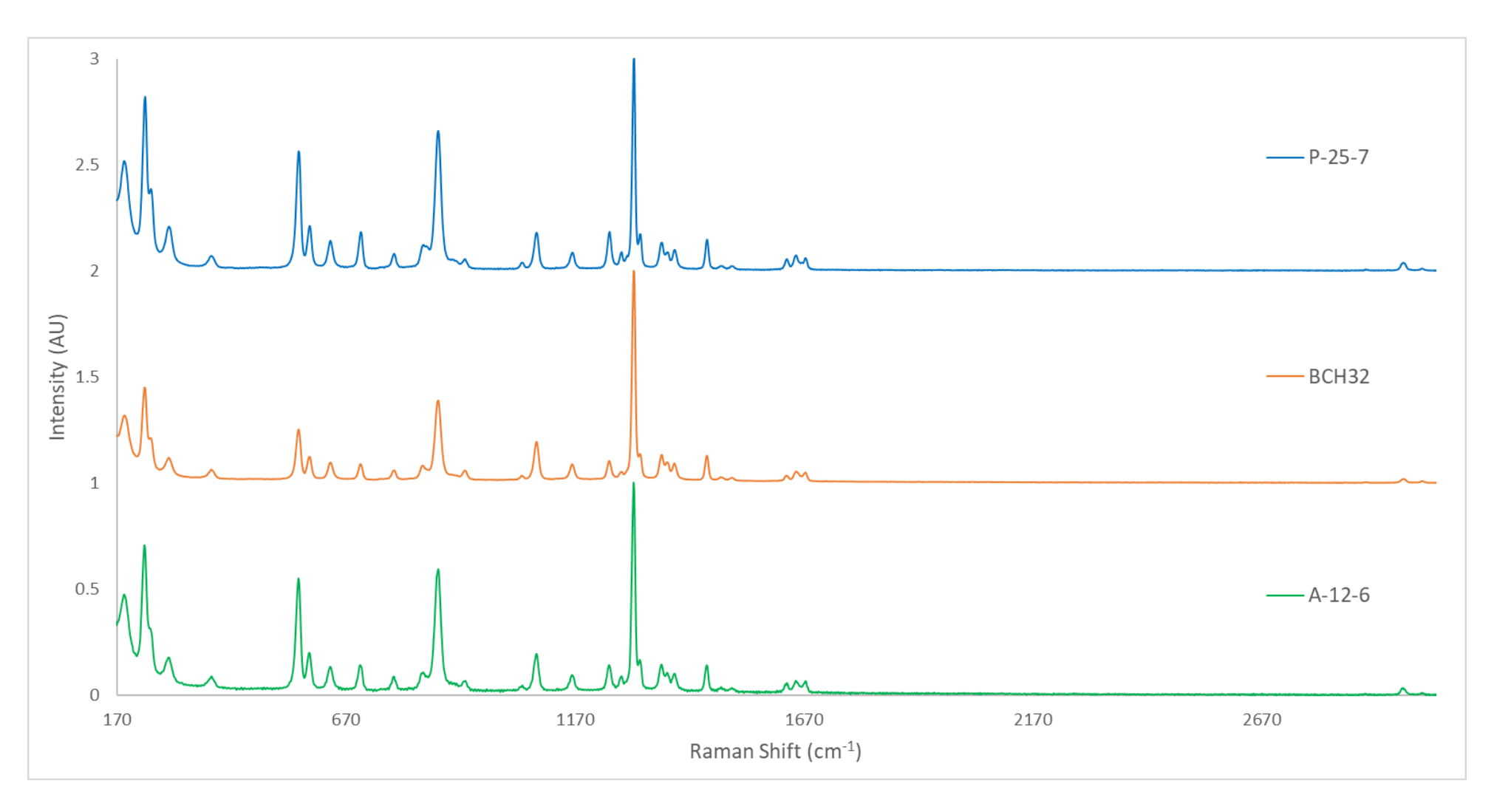


Figure 5.19: Raman spectra of three ETN samples made via differing synthesis methods (offset for clarity) showing all peaks are common.

Hence, the Raman spectra, even at this higher quality, did not yield any level of discrimination between the three samples of erythritol tetranitrate made by three different synthesis methods and from different precursors. This was, however, a very brief scoping investigation and there may be value for a future project to revisit higher resolution Raman spectroscopy to differentiate between ETN samples. This may be possible through the analysis of peak ratios, after ensuring that this is not simply an artefact of inconsistencies within a sample due to morphology, as this investigation did not collect spectra at numerous points on the surface of the sample. Taking survey scans at various locations on the sample was seen to change the spectrum, as the distance of the sample can change as the sample surface is not perfectly flat and even. For further analysis, various locations on each sample should be analysed and the spectra obtained averaged.

#### 5.5 Combined IR-MS and ICP-MS data for ETN

Previous sections presented the analysis of the IR-MS and ICP-MS datasets from the ETN samples and identified that discriminatory information was contained within the data. Not only did these datasets demonstrate a level of profiling between samples, but they did so based on different aspects of the data. IR-MS was able to discriminate between samples based on differences in precursors and synthesis routes, whereas ICP-MS identified trends based on the individuals synthesising the samples. Therefore, a combination of both datasets may bring together all three aspects and provide a greater level of discrimination for the samples.

A direct combination of the datasets resulted in very poor results, as was the case when merging FT-IR and ICP-MS datasets from the potassium chlorate samples. The first two principal components, rather than combining the datasets, simply used the nitrogen isotope ratio for PC1 and the carbon isotope ratio for PC2, then began using the ICP-MS data from PC3 onwards. This was easily identifiable using the coefficients (Table 5.12) and so steps were taken to allow a better merging of the datasets.

Table 5.12: Coefficient table of the first 4 PCs for the direct combination of the ETN IR-MS and ICP-MS datasets.

	PC1	PC2	PC3	PC4
Al			0.2	0.1
Ca			0.4	0.8
K		-0.1	0.9	-0.5
Со			0.1	
Ni			0.1	0.1
Ru			-0.1	
U				
Sr			0.2	0.2
Fe			0.1	0.1
Mg			0.1	0.1
Zn			0.1	
N ratio	1.0			
C ratio		1.0	0.1	-0.1

In Section 3.4, a similar combined dataset of AN and CAN samples was analysed, and a simple logarithmic transformation of both translated datasets allowed for a better merge. When the same process was applied to the combination of ETN datasets, however, the results were far from ideal. Rather than the IR-MS data heavily outweighing the ICP-MS data the opposite has occurred and now IR-MS data has not been incorporated into the early PCs (Table 5.13). In fact, the carbon IR-MS data is not accounted for until PC6 and even then, it is only a minor loading factor.

Table 5.13: Coefficient table of the first 6 PCs for the log transformed combined ETN IR-MS and ICP-MS datasets.

	PC1	PC2	PC3	PC4	PC5	PC6
Al	0.2	0.1	0.1	0.5	0.6	
Ca	0.3	0.9	-0.2	-0.2	-0.1	0.2
K	0.9	-0.4	-0.2	-0.1	-0.1	0.1
Со	0.1		0.2	0.4	0.1	0.4
Ni	0.1	0.1	0.7	0.3	-0.6	0.1
Ru	-0.1	-0.1	0.3	-0.5	0.3	0.7
U						
Sr	0.2	0.2	0.5	-0.4	0.3	-0.4
Fe	0.1	0.1	0.1		0.1	-0.1
Mg	0.1		0.2		0.2	-0.2
Zn	0.1		0.1		-0.1	
N ratio		-0.1	0.2	-0.3	-0.1	-0.3
C ratio						0.1

The final option was to calculate the greatest level of variance within the ICP-MS dataset and scale the IR-MS data to fit the same magnitude range, as previously used to merge the ICP-MS and IR data of the KClO<sub>3</sub> samples. The log transformed potassium mass fraction is the variable with the largest level of variance in the ETN ICP-MS data, with a maximum range of 5 AU, and so the translated nitrogen and carbon delta values were divided by 14 and 4, respectively, to also have a variance range of approximately 5‰. This resulted in a much better merging of the data as can be seen in Table 5.14. This method of pre-processing has many elements contributing to the PCs, though potassium is still dominant in PC1, and the IR-MS data is featured from the very first principal component.

Table 5.14: Coefficient table of the first 5 PCs for the combination of the ETN IR-MS (scaled) and log transformed ICP-MS datasets.

	PC1	PC2	PC3	PC4	PC5
Al	0.1	-0.1	0.1	0.2	-0.2
Са	0.3	-0.4	0.7	-0.4	
K	0.9	-0.1	-0.5	-0.1	0.1
Со	0.1			0.3	-0.1
Ni	0.1	0.1	0.2	0.6	0.3
Ru	-0.1	0.1		0.2	
U					
Sr	0.2	0.1	0.3	0.4	-0.2
Fe	0.1		0.1	0.1	
Mg	0.1		0.1	0.1	
Zn	0.1				0.1
N ratio	0.2	0.9	0.3	-0.3	0.2
C ratio	-0.1	-0.2			0.9

With so many variables contributing variance within the dataset, variance retention has been spread across a larger number of principal components as depicted in the scree plot (Figure 5.20). This means that more principal components must be examined to ensure that valuable information is not lost as there are still significant amounts of variance contained within later PCs.

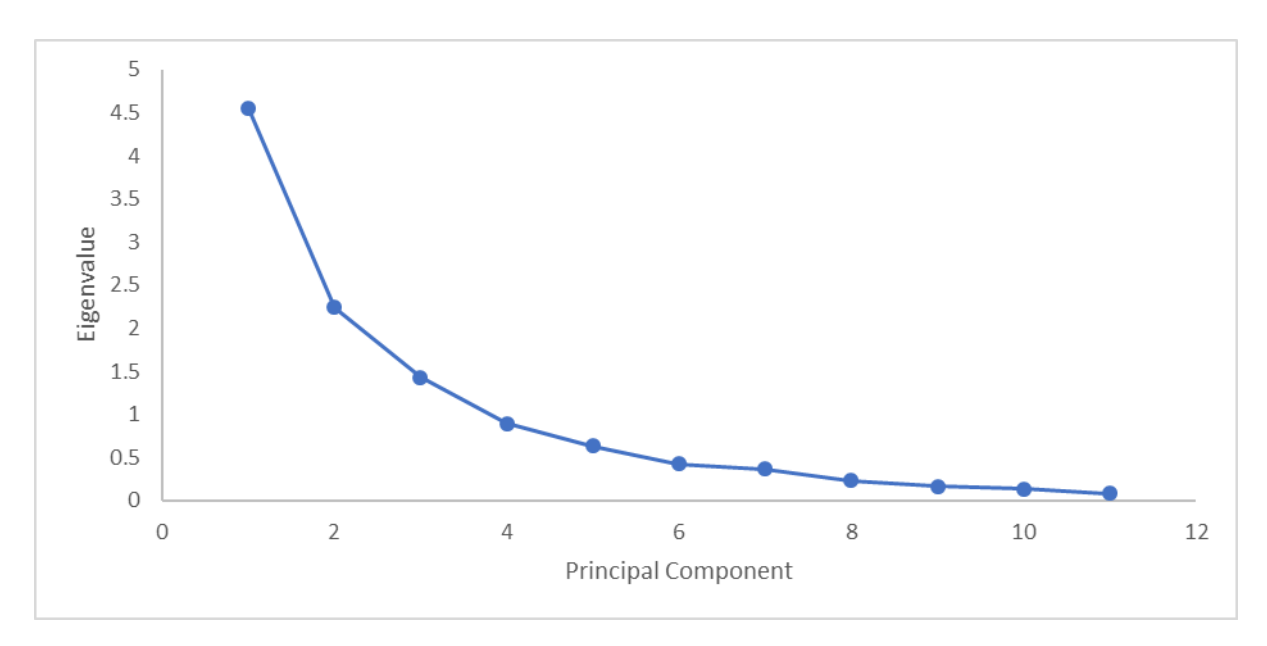


Figure 5.20: Scree plot for the PCA of the combined IR-MS and ICP-MS dataset for ETN.

Examining the score plots for individual PCs, however, reveal this not to be the case, with PC1 and PC2 being the only plots to reveal any separation between samples. Therefore, a two-dimensional plot of PC1 and PC2 (Figure 5.21) provided the best overview of this PCA. The samples have been plotted with colour coding based on the chemist it was synthesised by, as this was a key trend that cannot be mathematically represented.

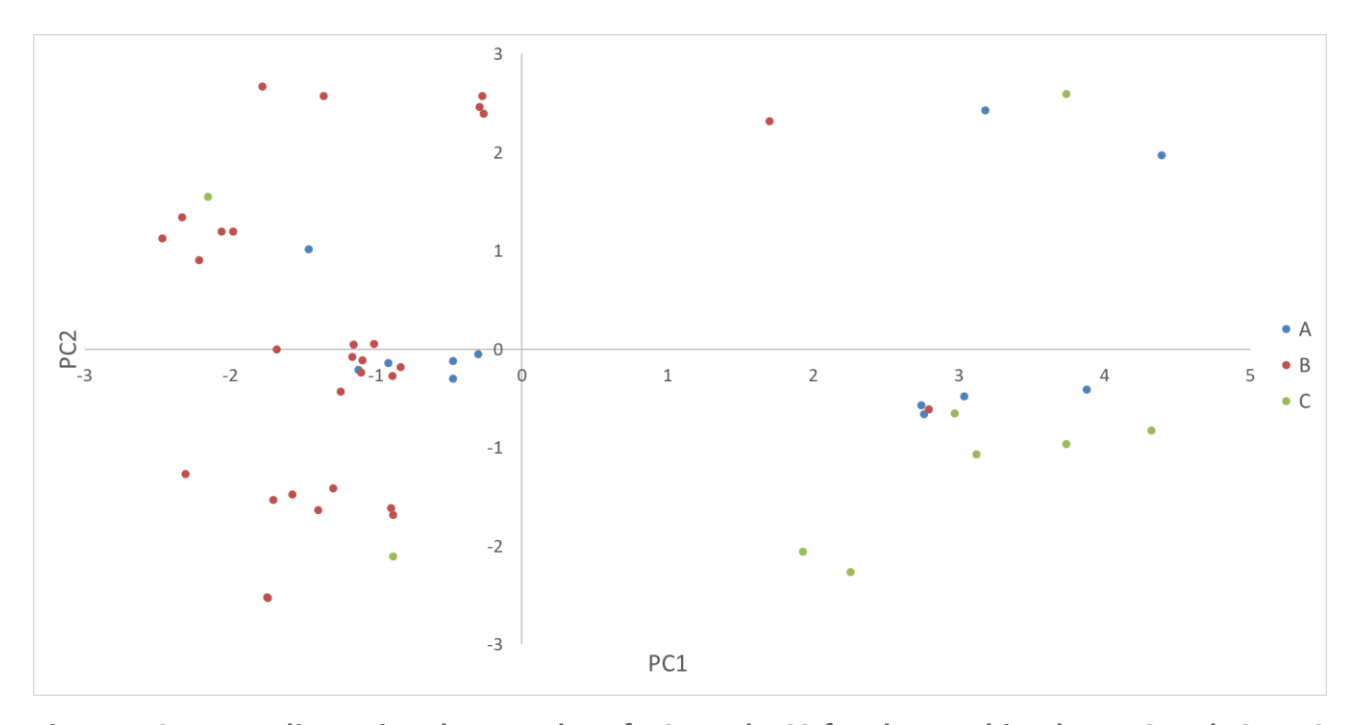


Figure 5.21: Two-dimensional score plot of PC1 and PC2 for the combined IR-MS and ICP-MS dataset for ETN (with chemist identity tag).

The plot still highlights the link between samples and the individual who made them, however, there is a lot of crossover and there are clearly more than three clusters within the resultant score plot. Another way to represent the data is by synthetic method, as this was a determining factor of discrimination within the IR-MS data alone. Figure 5.22 represents this visualisation and provides another perspective to the same plot. This perspective also shows successful clustering especially for the acetyl nitrate method, however, there is still significant crossover especially between the nitrate salt and mixed acid methods.

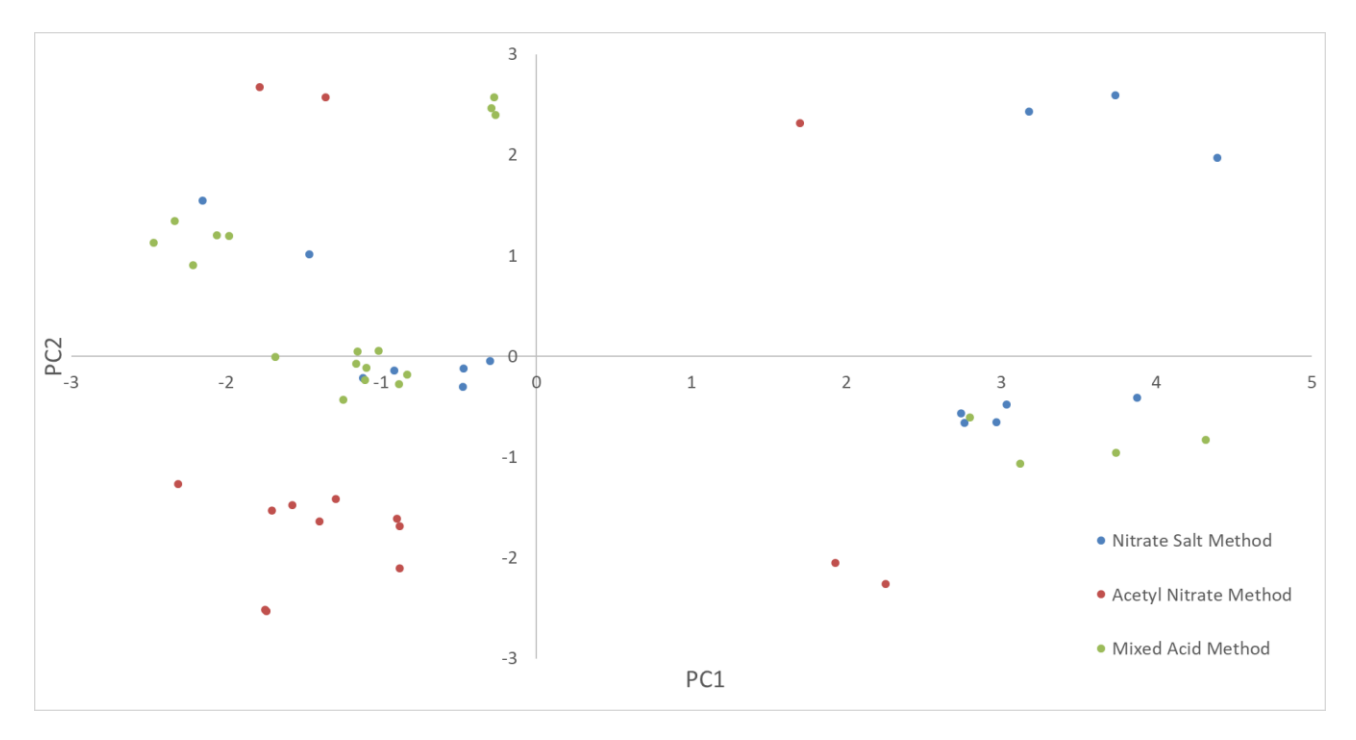


Figure 5.22: Two-dimensional score plot of PC1 and PC2 for the combined IR-MS and ICP-MS dataset for ETN (with synthesis method tag).

Both perspectives show clear clustering of like samples, with the chemist tag providing separation mainly across PC1 and the synthesis method tag separating more across PC2. Both plots also contain a significant number of outliers and so a representation containing both the method and chemist tags could improve cluster identification. This has been displayed in Figure 5.23, where points are coloured based on the synthesis method and shapes represent the chemist who synthesised the sample.

The plot now displays both the synthesis route and the creator's identity and how they affect the score of each of the samples. The PN2 samples are also labelled as these were also easily identifiable from the nitrogen isotope ratios originally and this is still the case after combining with the ICP-MS dataset. This combined tagging highlights the separation between chemist B and chemists A and C.

It also clearly depicts that the method of synthesis is not a great predictor on the clustering of samples.

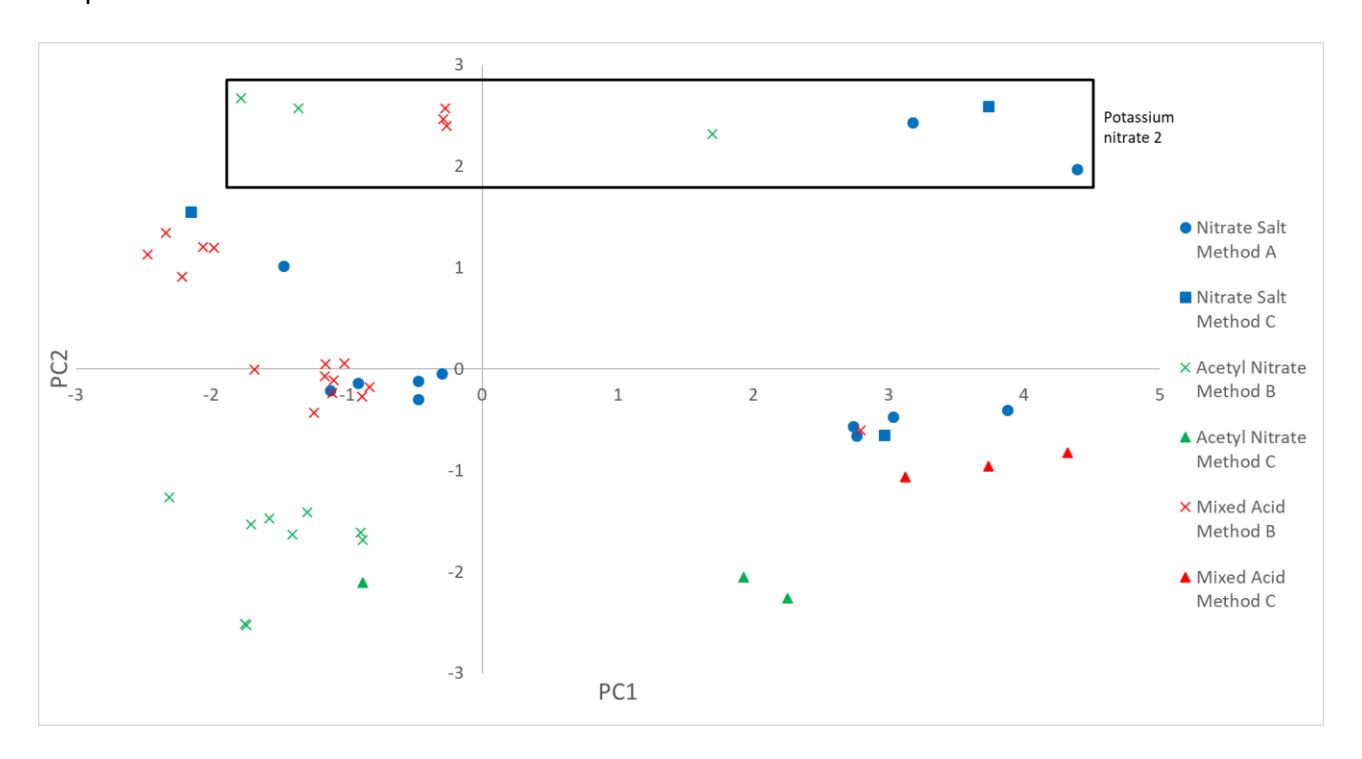


Figure 5.23: Two-dimensional score plot of PC1 and PC2 for the combined IR-MS and ICP-MS dataset for ETN (with chemist and synthesis method tags).

# 5.6 Chapter Conclusions

The analysis of erythritol tetranitrate identified some discriminatory data based on the synthesis method used and the chemist synthesising the material.

IR-MS could discriminate samples based on the nitrogen delta value, however, not via carbon delta value. The erythritol precursors had similar carbon isotope ratios and the nitration reaction conditions did not have an effect on these ratios. Nitrogen isotopic ratio, however, could be used to discriminate one nitrate salt (PN2) from the rest, due to its delta value and this carried through to the resultant material, even when first converted to nitric acid. This allows the nitrogen isotope ratio of the precursor to be directly linked to the final product, even after multiple synthesis stages. The acetyl nitrate nitration method also influenced the isotope ratio of the nitrate salt, consistently lowering the delta value and thus distinguishing samples synthesised by this method.

ICP-MS identified that samples could be discriminated, not due to the starting material but rather the chemist producing the material. Further investigation into the possible causes for this variation suggested it may have been due to the use of a different set of equipment used in the synthesis. The

samples produced by one chemist resulted in differing levels of calcium, potassium and strontium from two other chemists following the same procedures and using the same precursors.

Unfortunately, both IR and Raman spectroscopy could not identify any discriminatory information within the spectra due to the lack of identifiable impurities.

Analysis of a combined dataset of IR-MS and ICP-MS data was undertaken and successful in retaining the information identified by each dataset individually. The combination required the normalisation of the magnitudes of variance across the two datasets prior to combination, in order to prevent one set of data overriding the other. Without this additional normalisation, effectively the weighting of the datasets becomes highly uneven favouring one dramatically. This highlights the importance of developing a suitable preparation of the data, especially when combining two different datasets such as a spectrum and an elemental profile. The validation of any dataset merging methodology can only be accomplished through the understanding of the multivariate data analysis. In the case of PCA, this comes through the interrogation of the loading factors and principal component variance retention.

# 6. THz/Far-IR Spectroscopic Analysis of Explosives

In this chapter research into the rapidly developing analytical technique THz/Far-IR spectroscopy was undertaken, to assess its potential for identifying a range of energetic materials. This technique extends the fingerprint region of a standard IR spectrum to yield more signals, which may be used to detect and identify explosives and potentially impurities if present. This could potentially allow for the discrimination of samples of like material, based on impurities and additives, like fuels or stabilisers.

The potential for the use of the technique to identify materials within different packaging was also investigated. A wide range of plastics and paper were investigated to determine the level of transparency across these materials.

## 6.1 Analysis of Pelletised Explosives

Initial investigations involved collecting the spectra of pelletised materials in either polyethylene (PE) or paraffin wax matrices. Both materials produced pellets of great transparency in the THz/Far-IR wavelengths through to a typical IR region as shown in Figures 6.1 and 6.2.

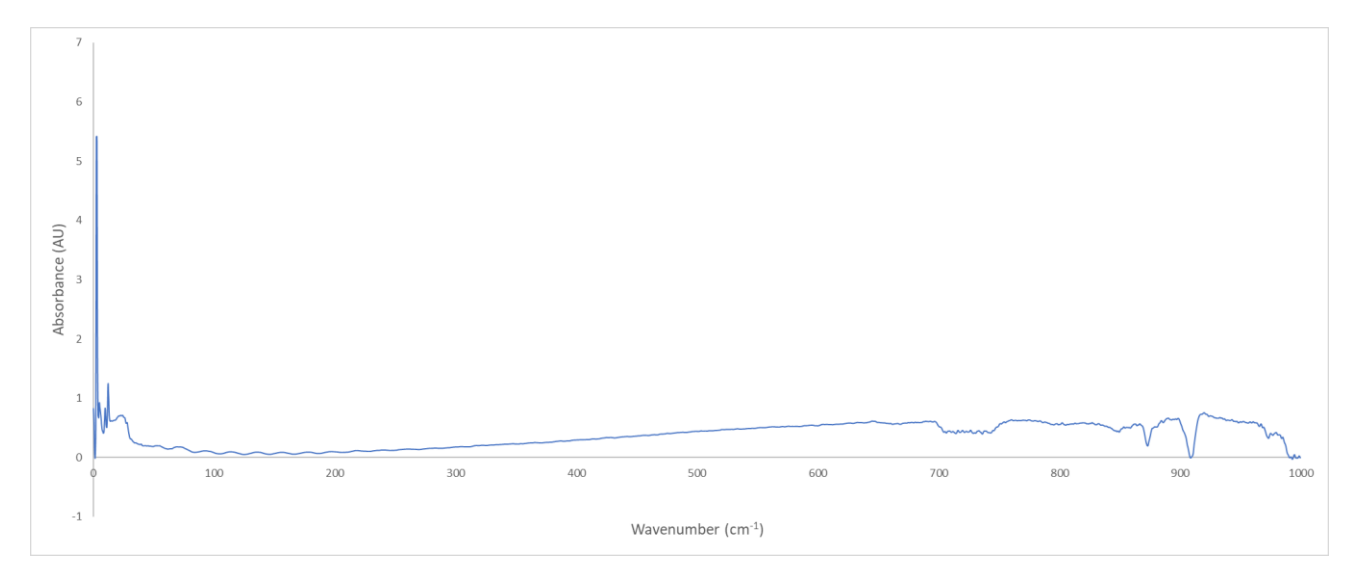


Figure 6.1: THz/Far-IR spectrum of a polyethylene pellet showing great transparency in the frequency range of 30-1000 cm<sup>-1</sup>.

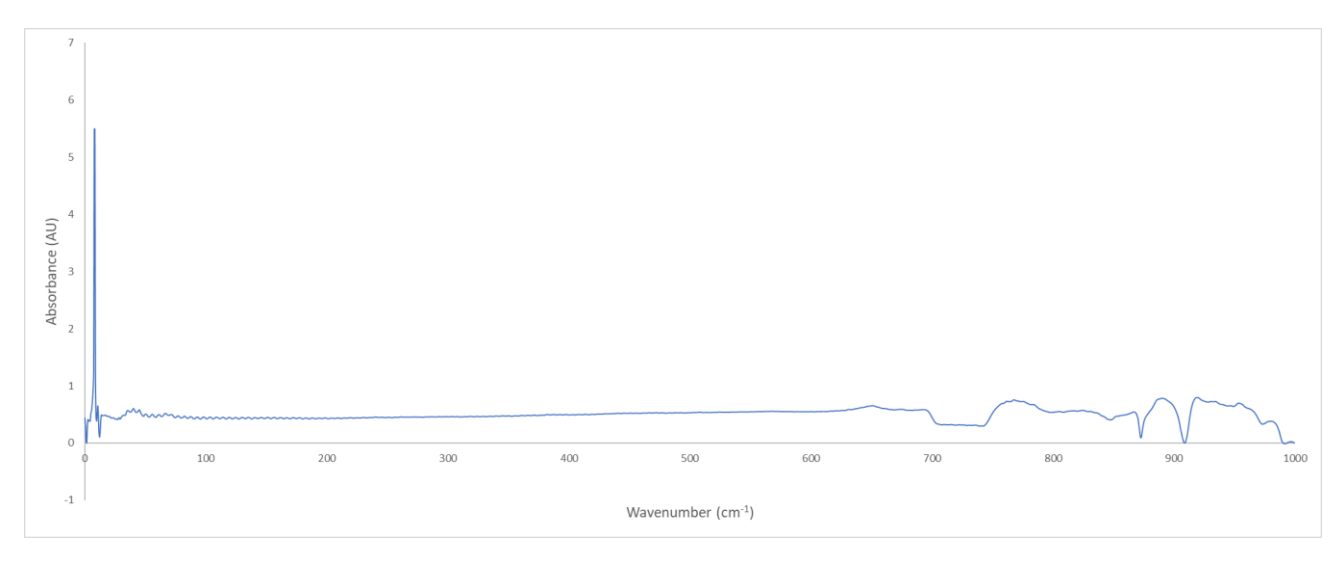


Figure 6.2: THz/Far-IR spectrum of a paraffin wax pellet showing great transparency in the frequency range of 30-1000 cm<sup>-1</sup>.

Although similar transparencies could be obtained using either matrix, there were preparation differences. The PE method involved mixing the sample with the PE at a desired ratio in a mortar and pestle, then pressing this using a hand press. The wax method on the other hand, required the sample to be coated on the wax through the shaking of wax and sample in an Eppendorf tube and then lightly pressed by hand as the hand press applied too much pressure to generate acceptable pellets. This method was much more difficult than expected as the coating of materials was only effective when the wax was softened through heating. This could easily be done within a warm oven at 30°C, however, upon pressing the wax would then become slightly adhesive to the die set, making the removal of a pellet difficult. An additional issue with the wax was that the pellet would commonly break under the vacuum of the sample compartment when loaded into the cryostat, whereas the PE pellets would not. For these reasons, PE was favoured for the analysis of all samples, even though its transparency was slightly less than the wax below 40 cm<sup>-1</sup>.

The samples of explosives studied throughout this THz/Far-IR research were provided by Victoria Police from their storage of samples collected from old explosives factories, seized, salvaged from detonation cords or manufactured by the Victoria Police Forensic Services Department. This included samples of RDX, HMX, PETN, AN, KCIO<sub>3</sub>, HMTD, UN and NU.

Pellets of sample mixed with PE were prepared, and their spectra collected as depicted in the following Figures 6.3-6.7. The spectra range between 30-650 cm<sup>-1</sup> as both the pelletising material and detector did not allow recording of wavenumbers below 30 cm<sup>-1</sup>.

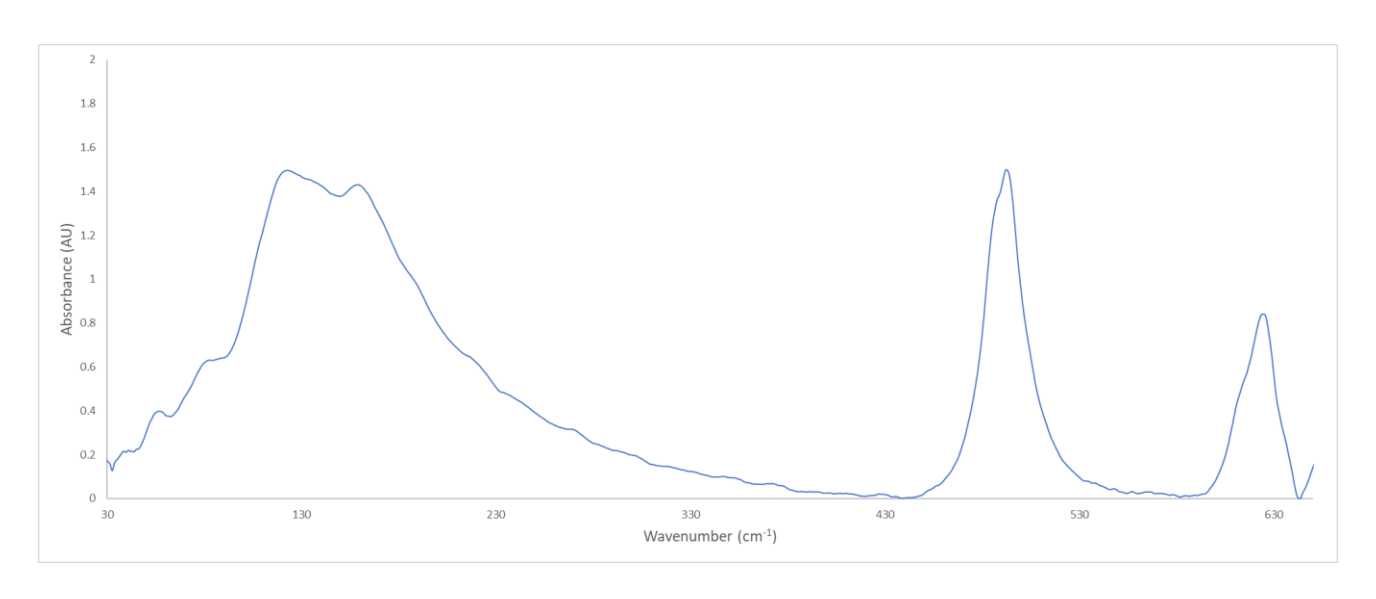


Figure 6.3: THz/Far-IR spectrum of potassium chlorate (25% in PE) in the frequency range of 30-650 cm<sup>-1</sup>.

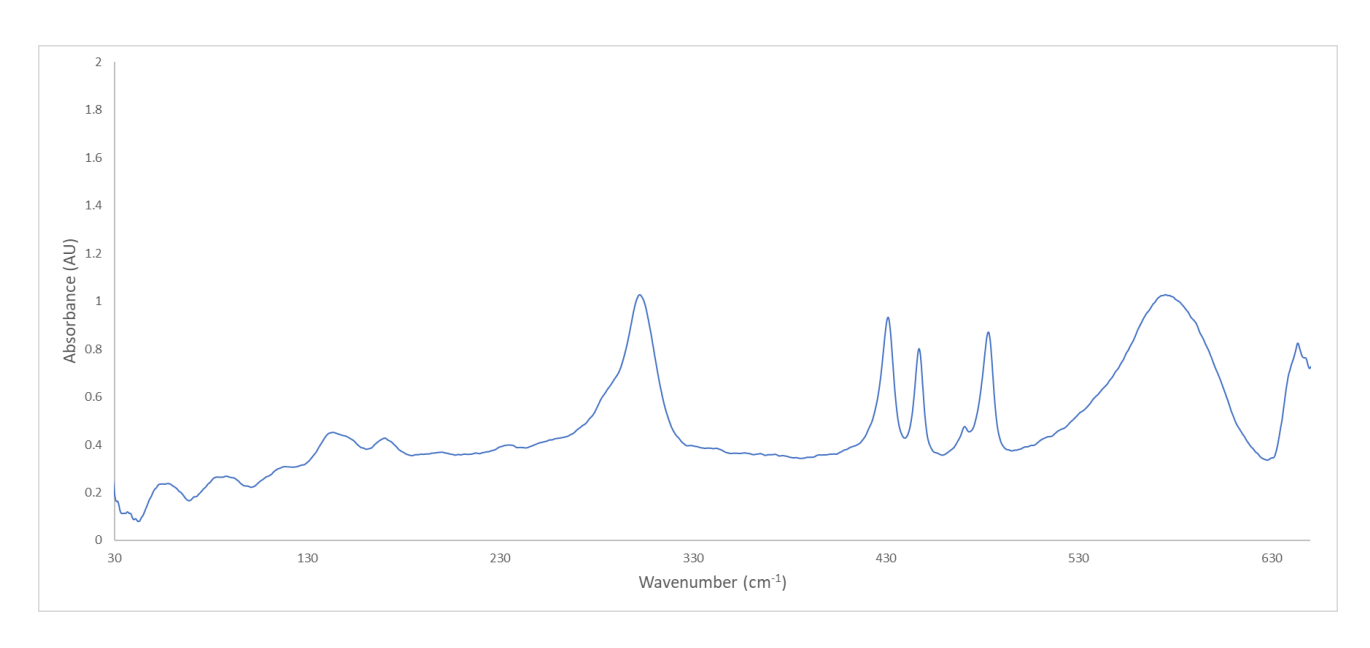


Figure 6.4: THz/Far-IR spectrum of nitrourea (25% in PE) in the frequency range of 30-650 cm<sup>-1</sup>.

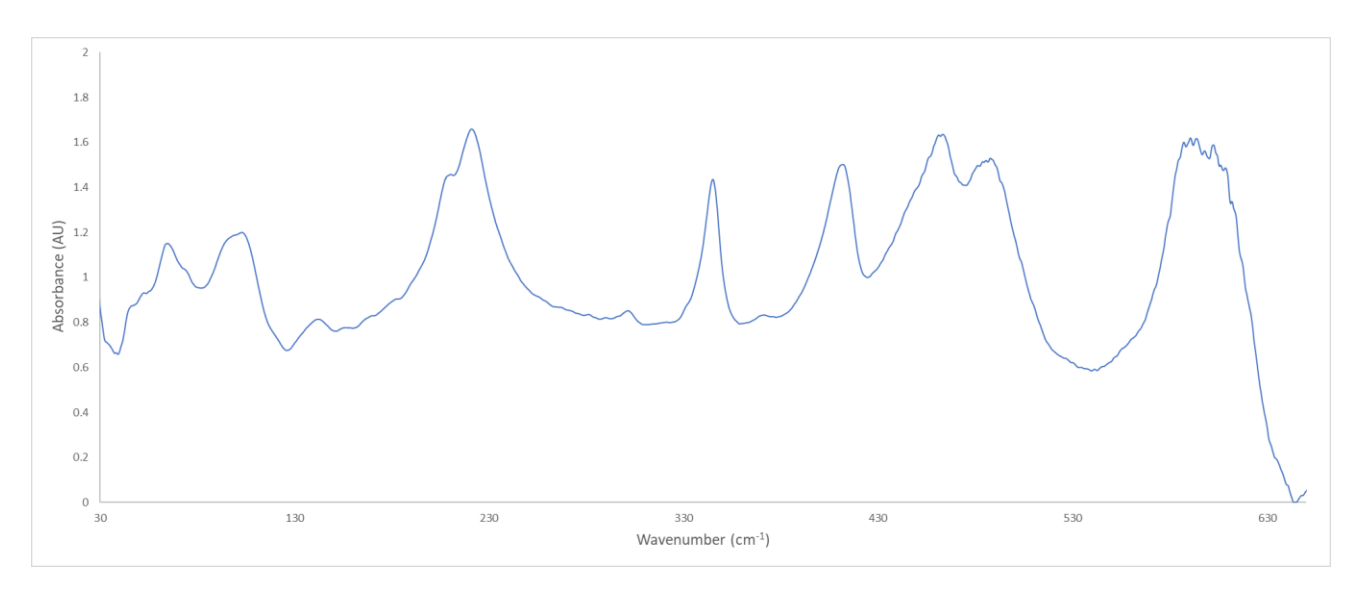


Figure 6.5: THz/Far-IR spectrum of RDX (50% in PE) in the frequency range of 30-650 cm<sup>-1</sup>.

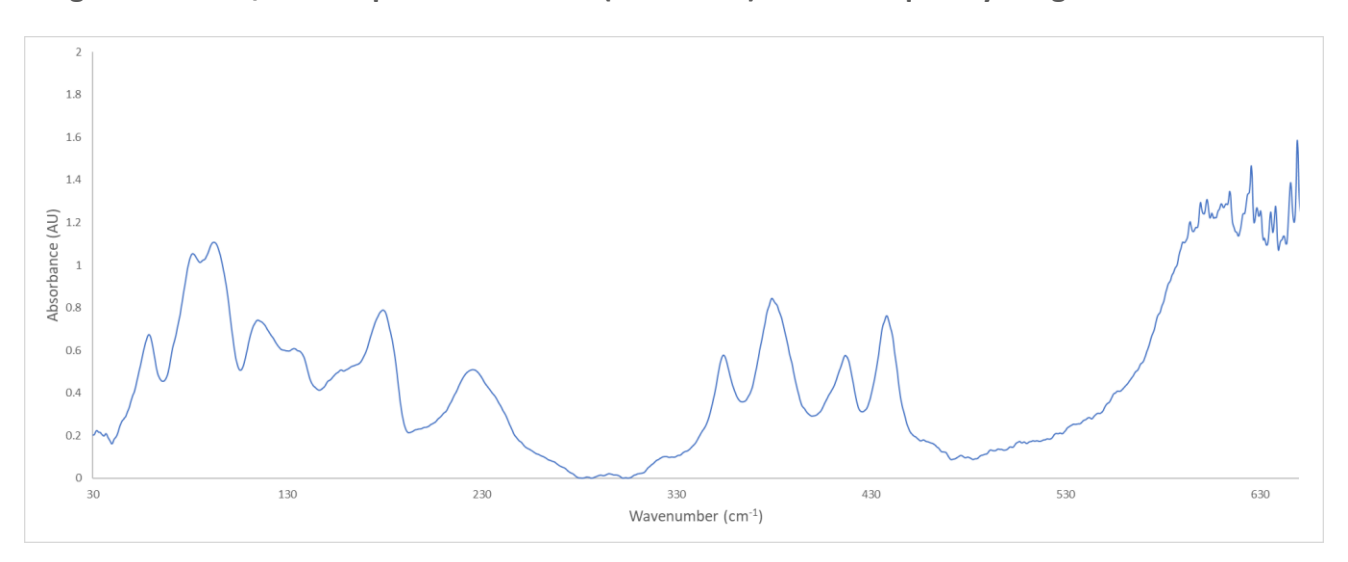


Figure 6.6: THz/Far-IR spectrum of HMX (50% in PE) in the frequency range of 30-650 cm<sup>-1</sup>.

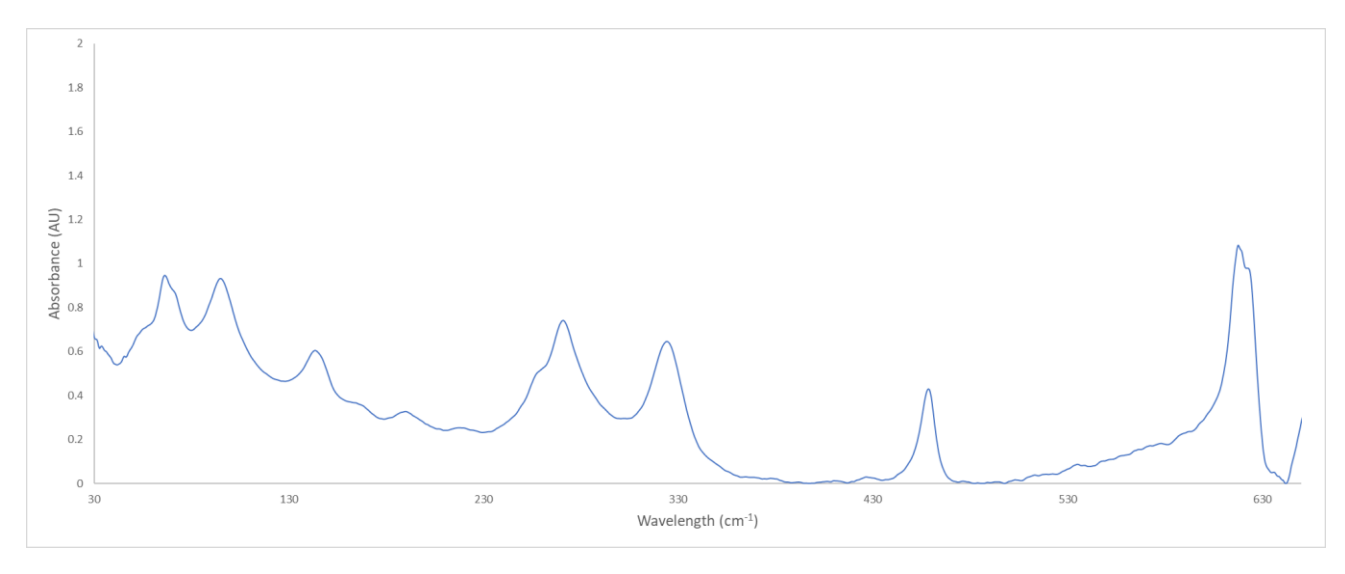


Figure 6.7: THz/Far-IR spectrum of PETN (50% in PE) in the frequency range of 30-650 cm<sup>-1</sup>.

These materials contain distinct signature peaks in the THz/Far-IR region, highlighting the potential for such a technique to be utilised in the identification of materials. This also indicates that if any impurity signals were present within this region, the analysis would be able to identify them so long as concentrations of the impurities were high enough. If this could identify impurities, there is a possibility of linking samples to precursors, as was the case in the FTIR studies on KCIO<sub>3</sub>.

#### 6.2 Analysis of Samples Through Packaging Materials

Though the identification ability of the THz/Far-IR is a useful result, standard IR can already clearly determine the identification of many materials, including explosives, and is also portable. Where the true potential lies in this technique is in the ability to see through packaging materials. To investigate this, a range of materials, including plastics and paper, were cut into 1 cm<sup>2</sup> squares loaded onto the cryostat in the same way as the pellets. A summary of the results are as follows in Table 6.1 broken down into 3 categories.

Table 6.1: Summary of THz/Far-IR absorbance results for various materials.

Little/no significant absorbance	Significant absorbance peaks	Significant areas of non- transparency
<ul> <li>Cling film/wrap</li> <li>Zip-lock clear bag</li> <li>Zip-lock red bag</li> <li>Paraffin wax paper</li> <li>Black garbage bag</li> <li>Bubble wrap</li> <li>Bubble wrap</li> <li>(popped)</li> <li>Plastic folder sleeve</li> <li>Packaging plastic</li> <li>Non-transparent purple postage bag</li> </ul>	<ul> <li>Overhead projector slide</li> <li>Target shopping bag</li> </ul>	<ul> <li>Soft drink bottle</li> <li>McDonalds cup lid</li> <li>Kimwipe</li> <li>Paper towel</li> <li>Lens wipes</li> <li>Post-It note</li> <li>Printer paper</li> <li>Paper Envelope</li> </ul>

The materials listed in the "little/no significant absorbance" category were highly transparent, similar to the polyethylene used to pelletise materials. One difference was that some of the spectra contained an oscillation across the spectrum. An example spectrum showing an extreme version of this oscillation is shown in Figure 6.8. This is proposed to be a result of the materials boundaries causing the partial reflection of the light at each boundary.

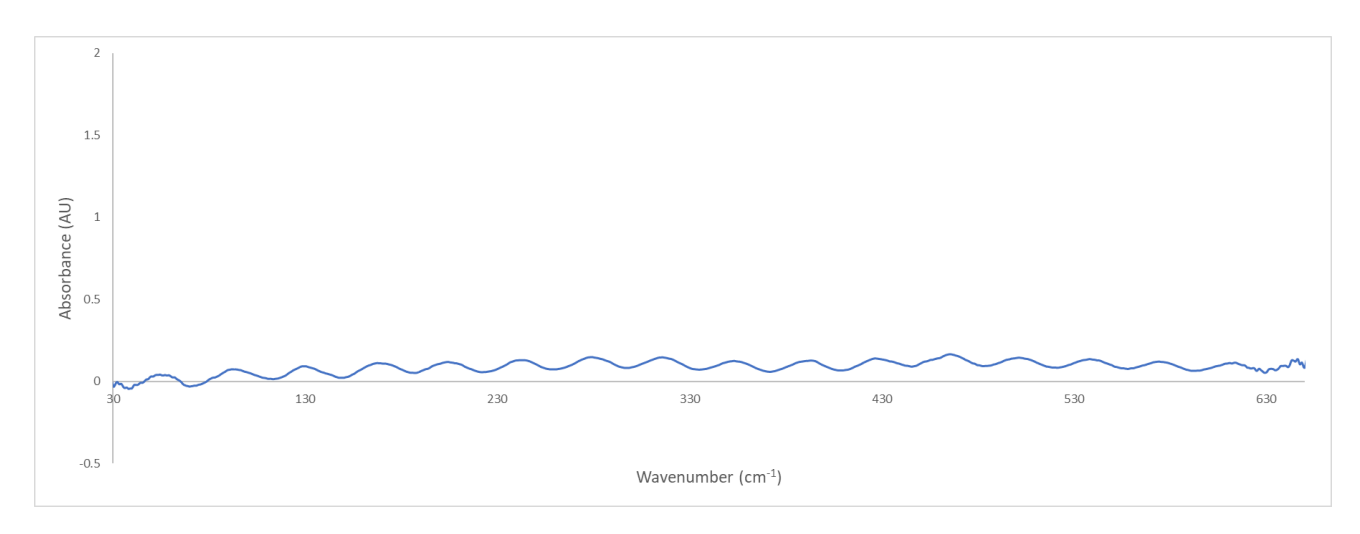


Figure 6.8: THz/Far-IR spectrum of a red Zip-Lock bag between the frequency range of 30-650 cm<sup>-1</sup> showing very little absorbance and clear oscillation.

In the second category of material significant absorbance peaks are found within the wavelength range restricting the transparency to smaller windows. This can hamper the identification of some chemicals with signature peaks, coinciding with those in the packaging material. As an example, the spectrum of an overhead projector slide is shown in Figure 6.9 below. Small oscillation artefacts are also seen with these samples due to the same reflection of light at material boundaries.

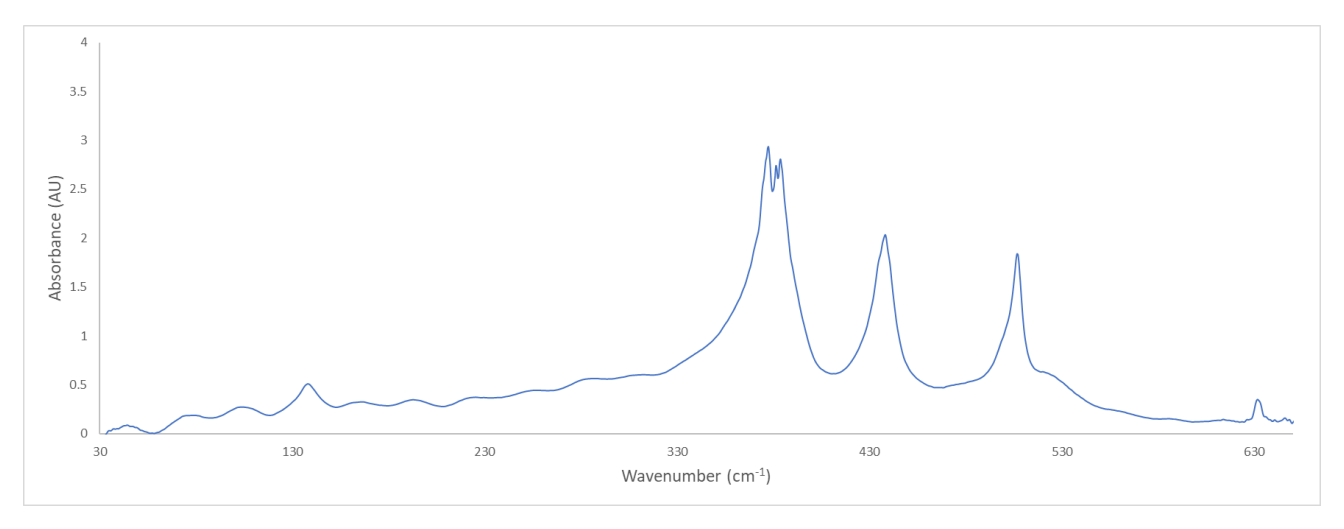


Figure 6.9: THz/Far-IR spectrum of an overhead projector slide between the frequency range of 30-650 cm<sup>-1</sup> showing strong absorbances at 380, 438 and 507 cm<sup>-1</sup>.

The spectra of materials in the final category have significant regions of non-transparency within the wavelength range making chemicals contained within these packaging materials difficult to identify. These materials include papers and higher density plastics. As an example, the spectrum of a Post-It note is shown in Figure 6.10 below.

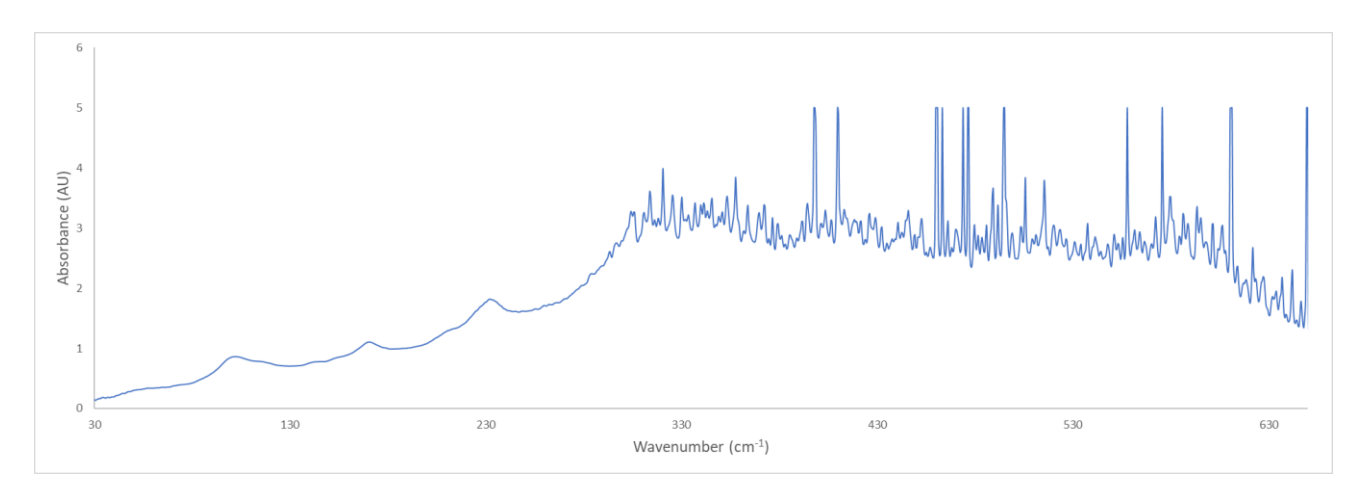


Figure 6.10: THz/Far-IR spectrum of a Post-It note between the frequency range of 30-650 cm<sup>-1</sup> showing a sloping absorption, peaks at 104, 173 and 234 cm<sup>-1</sup> and saturation beyond 300 cm<sup>-1</sup>.

These results are very interesting as it highlights the potential for THz/Far-IR analysis to identify chemicals within some packaging materials. A study was then conducted to mimic a real-world scenario with an explosive sample placed within a postage bag. The measurement was taken using two configurations, one where the explosive is in direct contact with the bag as would be the case of a heavily packed parcel. The second where there is an air gap between the postage bag and the explosive as would be the case when the parcel is not packed to its full potential. The results are summarised in Figure 6.11 with a normalisation at the 458 cm<sup>-1</sup> peak and an offset of +2 AU between each spectrum.

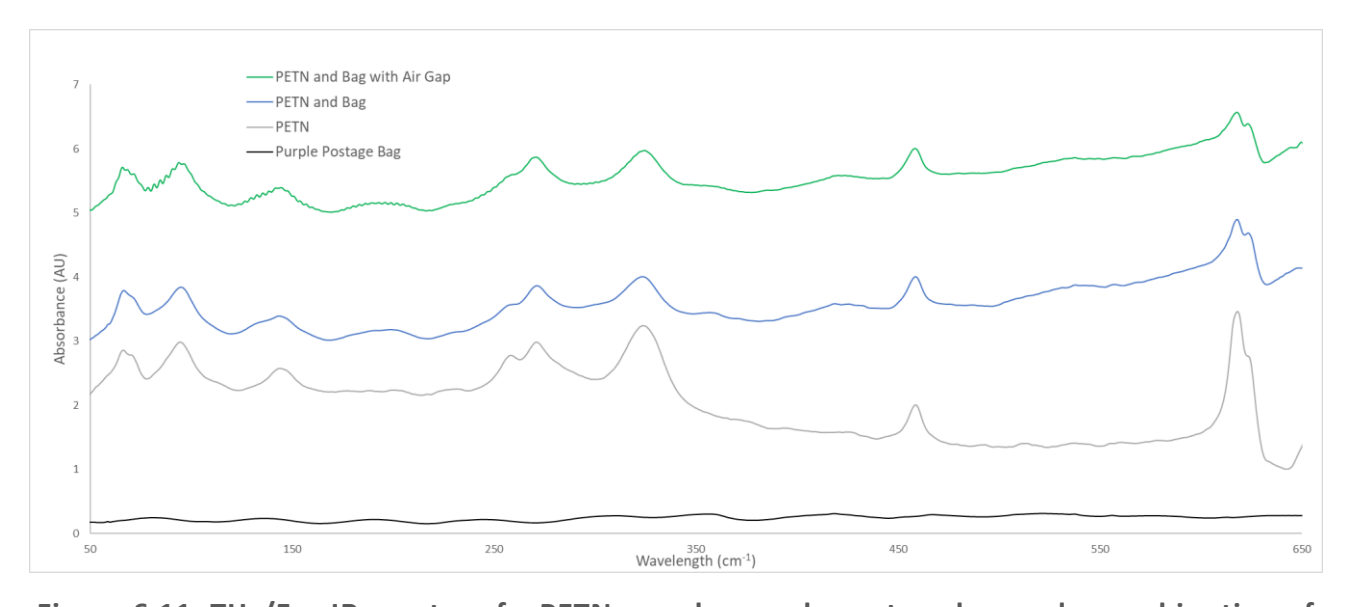


Figure 6.11: THz/Far-IR spectra of a PETN sample, purple postage bag and a combination of the two with and without air between them.

The results show that the packaging material is quite transparent within the THz/Far-IR region. The difference between the PETN alone, and that of the bag and sample, is quite minimal. The intensity of the peaks has been diminished slightly and some features are less prevalent. The double peak at around 270 cm<sup>-1</sup> has become more of a shoulder, however, the opposite effect has occurred for the 620 cm<sup>-1</sup> peak where a shoulder has become more prominent. The addition of an air gap between sample and packaging has had even less effect, simply introducing a minor amount of oscillation to the signal, more so towards the lower wavenumbers.

#### 6.3 ATR THz/Far-IR Spectroscopy

The THz/Far-IR beamline recently acquired an ATR accessory allowing for materials to be directly analysed and so the same explosives were investigated. The resultant spectra (Figures 6.12-6.17) are not greatly different to the transmission spectra previously recorded in Figures 6.3-6.7. Many do have sharper signals and a lower, more stable baseline; however, the primary benefit of the analysis is the removal of the sample preparation steps. A small amount of sample can be placed directly on to the ATR diamond and analysed, instead of the previous sample preparation, saving approximately 30 minutes per sample.

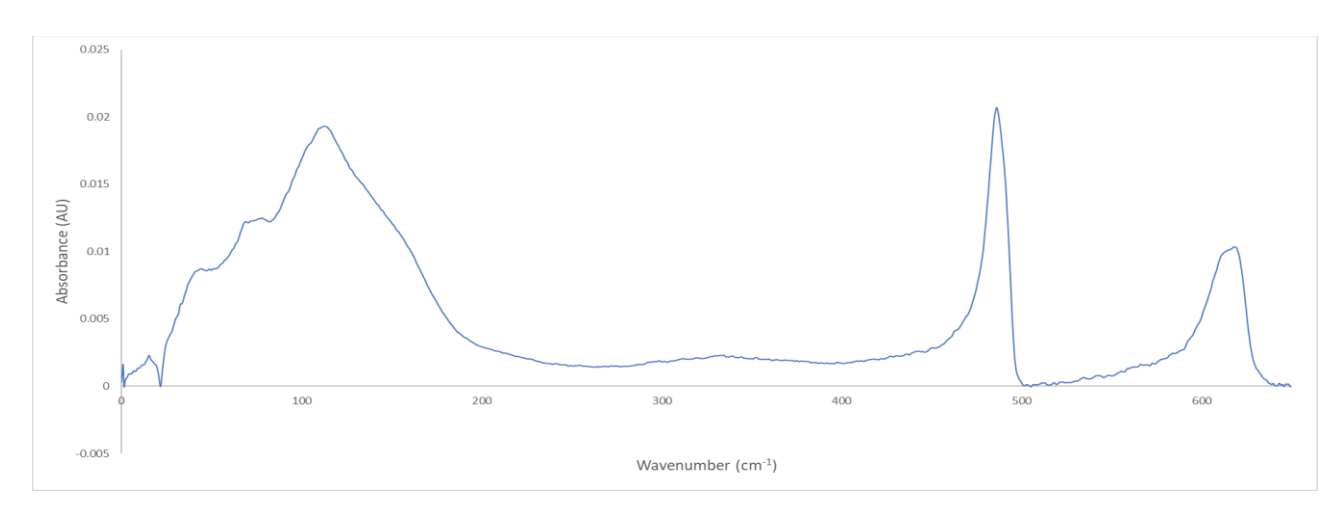


Figure 6.12: ATR THz/Far-IR spectrum of KClO<sub>3</sub> (bleach precursor) in the frequency range of 0-650 cm<sup>-1</sup>.

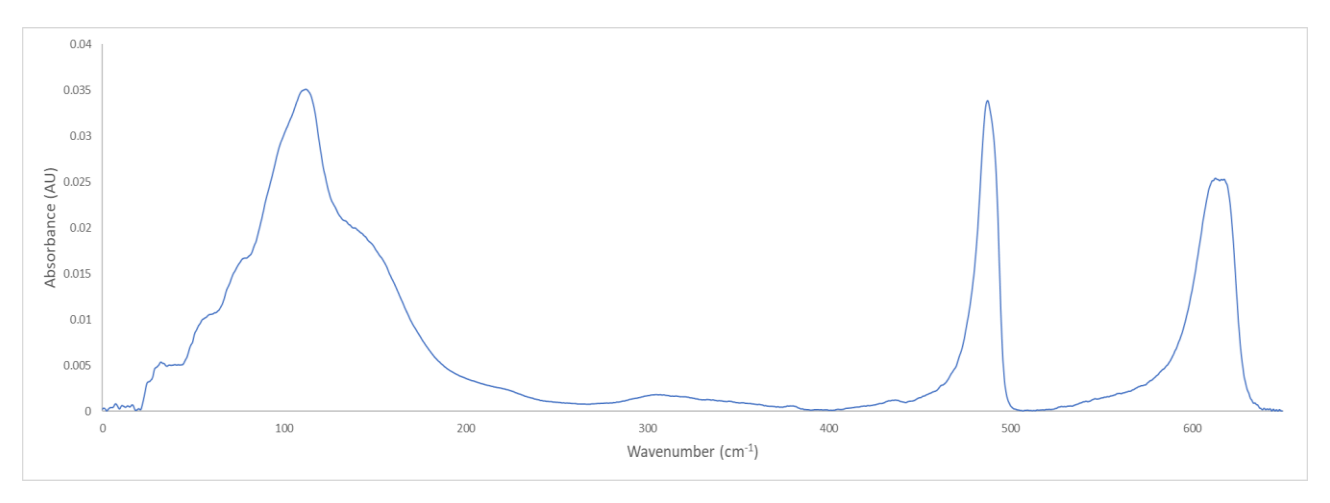


Figure 6.13: ATR THz/Far-IR spectrum of KClO<sub>3</sub> (pool chlorine precursor) in the frequency range of 0-650 cm<sup>-1</sup>.

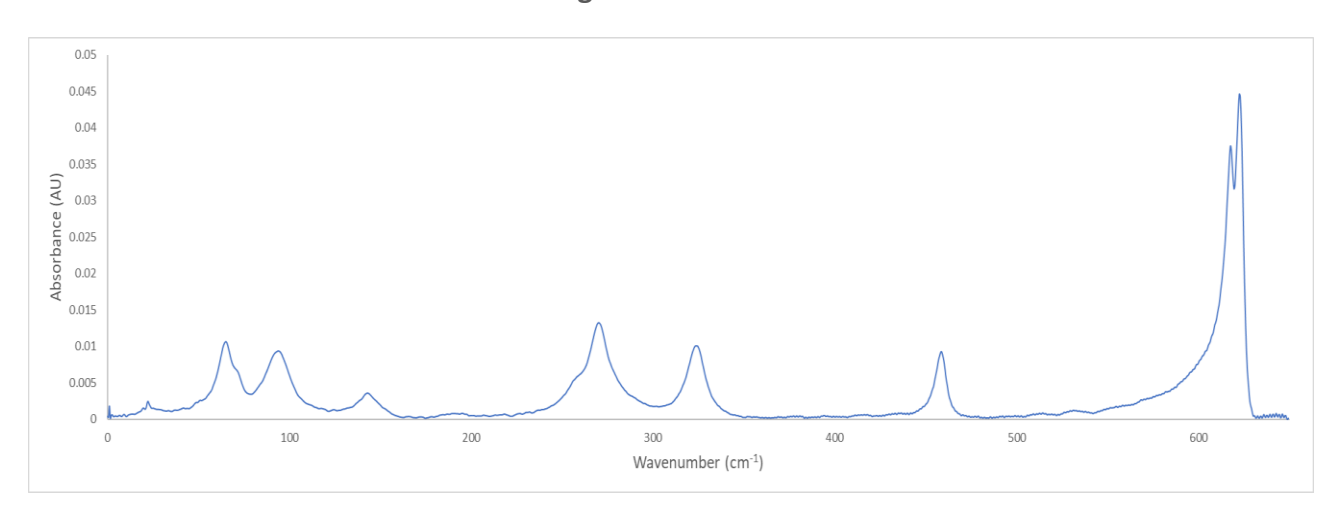


Figure 6.14: ATR THz/Far-IR spectrum of PETN in the frequency range of 0-650 cm<sup>-1</sup>.

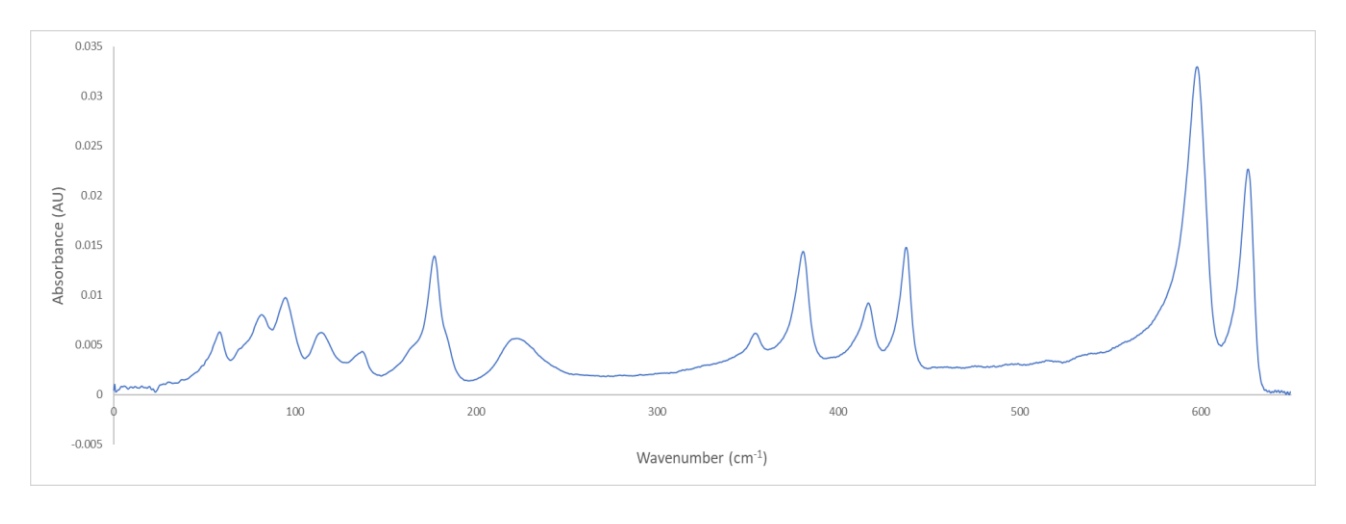


Figure 6.15: ATR THz/Far-IR spectrum of HMX in the frequency range of 0-650 cm<sup>-1</sup>.

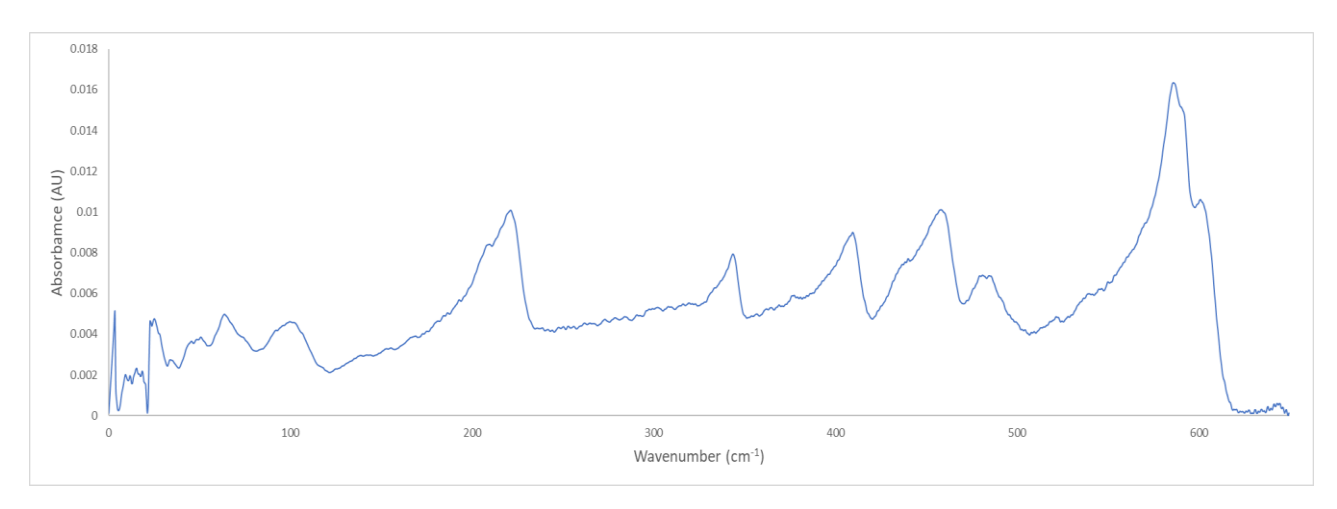


Figure 6.16: ATR THz/Far-IR spectrum of RDX (Type I) in the frequency range of 0-650 cm<sup>-1</sup>.

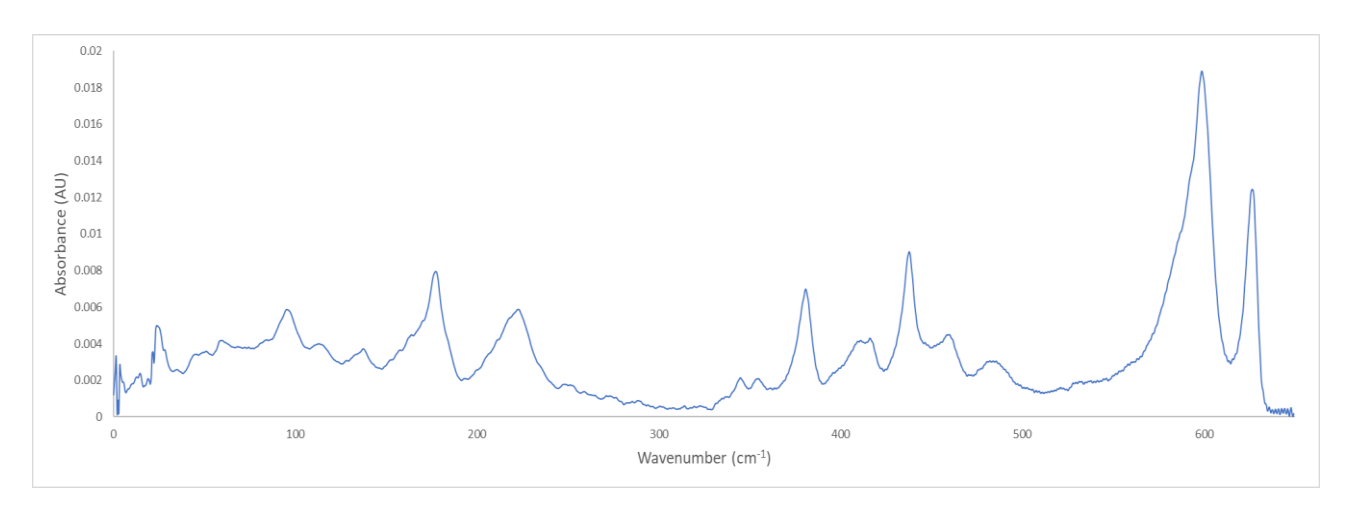


Figure 6.17: ATR THz/Far-IR spectrum of RDX (Type II) in the frequency range of 0-650 cm<sup>-1</sup>.

All of the spectra identify clear signature peaks for each of the materials making them all easily identifiable. The spectra have lower baselines with sharper signals in comparison to their pelletised counterparts, however, the number and position of signals is the same. The peak shapes of the two KClO<sub>3</sub> samples (Figures 6.12 and 6.13) are slightly different especially the shouldering on the 100 cm<sup>-1</sup> peak. The ratios are also different between the signature peaks leading to the potential to discriminate between the two synthesis methods; however, more research is required to confirm this. The spectra obtained are of high enough quality to be highly useful in developing a library of these types of materials.

# 6.4 Full Range Infrared Spectra

With the successful collection of THz/Far-IR ATR spectra, four of the materials were then analysed in the Mid-Near-IR region using a Perkin-Elmer Frontier FTIR with an ATR accessory. The two sets of data were then combined to make a single Far to Near-IR spectrum for each material. The largest

peak in the overlapping 600-650 cm<sup>-1</sup> region between the two spectra was normalised, enabling the two halves of the spectrum to be comparable.

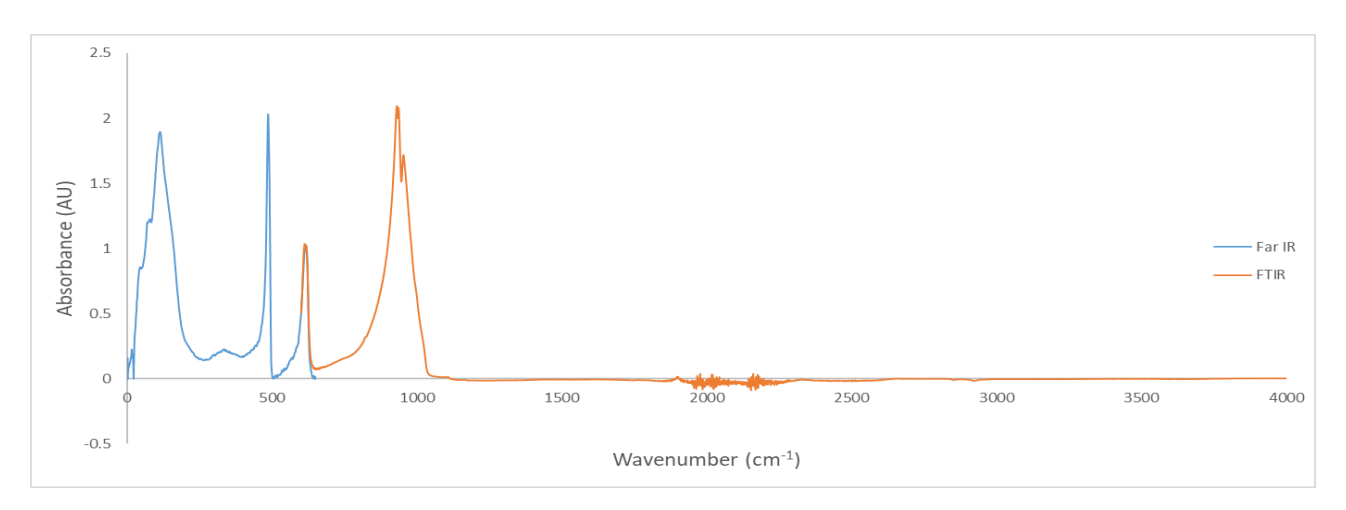


Figure 6.18: Combined THz/Far-IR and FTIR ATR spectrum of KClO₃ (bleach precursor).

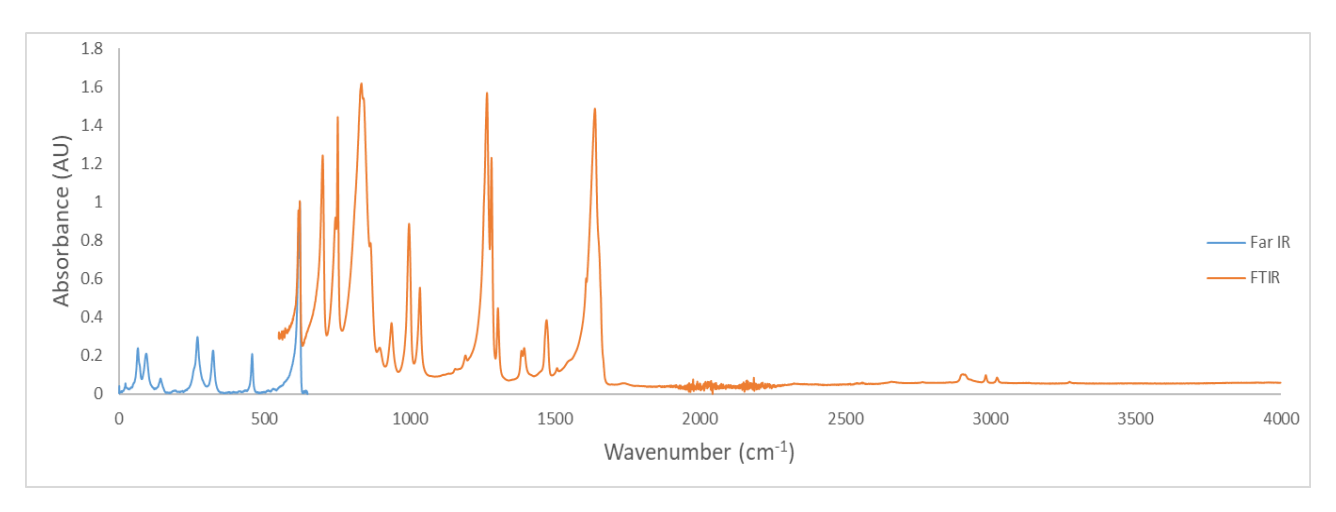


Figure 6.19: Combined THz/Far-IR and FTIR ATR spectrum of PETN.

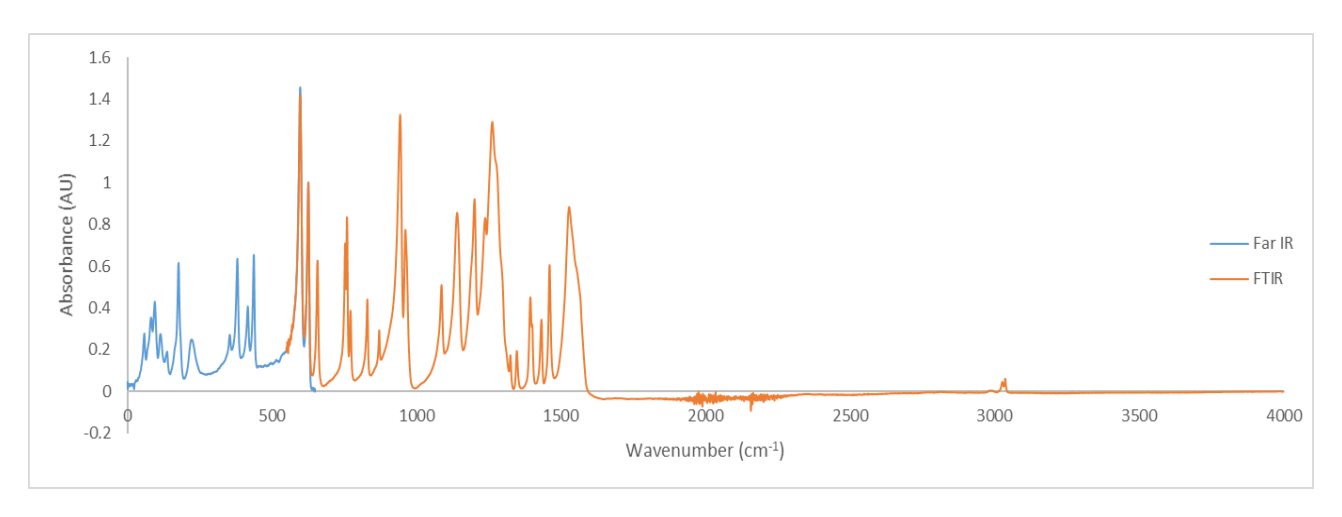


Figure 6.20: Combined THz/Far-IR and FTIR ATR spectrum of HMX.

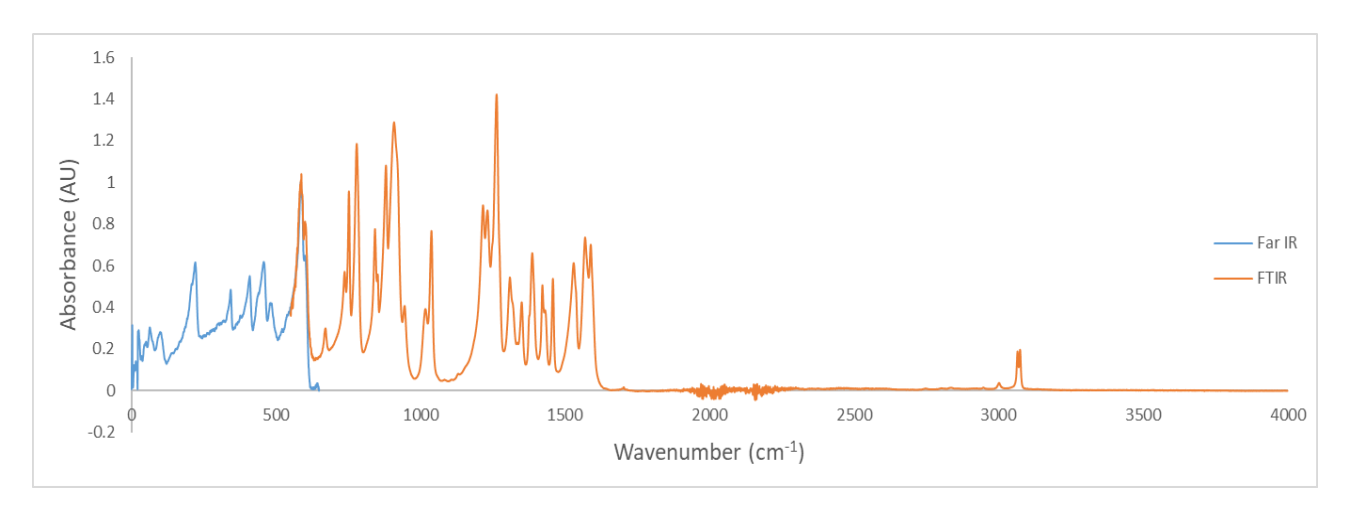


Figure 6.21: Combined THz/Far-IR and FTIR ATR spectrum of RDX (type I).

These combined spectra (Figures 6.18-6.21) show that there are more signals that may be used to identify material. This extra region could potentially be used to detect additional peaks from impurities, which would allow discrimination between samples of like material. Future work should be undertaken, investigating the potential for this technology to detect impurities by analysing multiple samples of an energetic material or ingredient, as for the other analytical techniques in this research. This data could then be processed using the exploratory data analysis methodologies employed for other spectral data in this research to reveal any potential discrimination as was the case for the infrared spectroscopy of potassium chlorate.

## 6.5 Chapter Conclusions

The field of THz/Far-IR spectroscopy is rapidly advancing and the potential of the technology to be used as a standoff detection method is of great interest for the identification of explosives. Here it has been shown to clearly identify a range of explosives and even identify materials through some packaging materials. This technique also extends the fingerprint region of an infrared spectrum, allowing for a greater level of identification and potentially highlighting additional impurities within this region. All of the THz/Far-IR research within this project was undertaken at the ANSTO Australian Synchrotron facility resulting in high resolution spectra. The current portable systems do not yield the same quality of data without further developments. This may result in poorer levels of impurity detection; more research is required to assess this source attribution and sample discrimination potential. Firstly, the detection of discriminatory impurities due to differing starting materials with the high-resolution THz/Far-IR beamline should be investigated. Secondly, similar testing would then

be undertaken with the current portable system in development at the French-German Research Institute of Saint-Louis.

### 7. Conclusions and Future Directions

This project has successfully investigated the potential of multiple analytical techniques to discriminate between samples of like material for the two explosives related materials studied, potassium chlorate and erythritol tetranitrate.

Erythritol tetranitrate samples were provided by DST Group however, clandestine methods from various online sources were successfully modified and optimised to safely and reliably produce potassium chlorate samples.

In the analysis of potassium chlorate, ICP-MS and IR spectroscopy proved useful in discriminating between samples based on their synthesis method and differences in precursor materials. ICP-MS identified links between product and precursor through trace elemental profiles and FT-IR found impurities originating from precursors. Principal component analysis managed to condense the discriminatory information within not only each dataset individually, but also a combination of both datasets. The analysis not only condenses the discriminatory data but also identifies exactly what parts of the dataset contribute to the discrimination, including the elements and ranges of wavenumbers that provide the valuable data. These results highlight the potential of such an analysis to link a material to a precursor based on differences in trace elemental profile or the presence of impurities. There is potential to improve the level of discrimination obtained through the inclusion of additional elements. Further analytical techniques could be used to investigate differences between samples to increase the amount of discriminatory data. Examples include chromatographic techniques such as liquid chromatography or an electrokinetic separation method like capillary electrophoresis. Both would provide another perspective on differences between samples.

Erythritol tetranitrate was found to be at least partially discriminated through IR-MS and ICP-MS analysis. The IR-MS data was shown to discriminate between samples based on differences in nitrate salt precursors that carried through to the final product, including via a nitric acid intermediary, and fractionation based on differing synthesis pathways. More research into the reaction mechanism could identify the exact reasoning for the fractionation identified using the acetyl nitrate synthesis pathway. ICP-MS resulted in discrimination, not due to differences in trace metal concentrations in precursors but from the difference in laboratory environment and equipment used in the synthesis of the ETN samples. This result indicates that in some cases, different equipment or locations used for synthesis could be identified as they may introduce different levels of trace elements into the

product. This could lead to highly valuable information useful in directing investigations, to find more concrete evidence of a link. Further studies surrounding the effects of equipment and environmental effects on synthesis should be undertaken to validate this hypothesis. PCA once again assisted in distilling the dataset and highlighting the discriminatory information within the dataset using the same data pre-processing as the KClO<sub>3</sub> datasets. This suggests that the pre-processing of elemental and spectral datasets is quite robust. As in the case of potassium chlorate, an increase in the number of measured trace elements and additional analytical techniques including liquid chromatography and capillary electrophoresis could provide further discriminatory data. This additional perspective on the differences between samples could magnify the separation leading to more concrete discrimination.

Although discriminatory data could be identified within both materials datasets, the merging of data collected from different analytical techniques proved to be a significant issue. This was a major limitation of the use of PCA as an exploratory data analysis tool. The purely mathematical approach highlights issues surrounding the differences in the magnitudes of variation of different variables. This results in the weighting of the variables with a greater magnitude of variation and more work needs to be done into solving this issue. A suggested direction for future work to resolve this would be to employ the use of a non-parametric regression, such as generalised regression neural network. This is a machine learning technique that can be used for the classification and prediction of samples. Though quite advanced and computationally demanding, with modern technology and advances in machine learning, this technique is becoming much more achievable.

The investigation into the potential of THz/Far-IR to identify materials using only the extended fingerprint region of standard IR spectroscopy was also highly successful. A range of materials were clearly identified with many signals outside the standard range of FT-IR analysis, which could also be effective at identifying impurities within this region. The technique also showed the potential to identify materials through a range of non-transparent plastic-based packaging materials including postage bags and black garbage bags. With the current development of a portable THz/Far-IR system capable of standoff analysis, much more research can be undertaken in future to investigate the discriminatory ability of the technique.

The aim of this project was to analyse samples via multiple analytical techniques then use a subsequent chemometric analysis to both individual and combined datasets to identify linkages between samples of like material. The analysis of the material was successful with methods

developed for the safe acid digestion of materials for elemental analysis. The methodologies developed for the chemometric analysis of individual datasets was successful however, more research should be taken into the merging of data from various analytical techniques. Specifically, harnessing more modern data analysis techniques in the field of machine learning could prove very effective in analysing such a nonparametric dataset. The PCA analysis of collected data was successful in discriminating between samples of like material providing links between samples, precursor materials, synthetic pathways and possibly equipment.

## 8. References

- [1] Schmidt, E.E., et al. (2014). "The Future of Internet Freedom." New York Times. Retrieved 11 March 2014. <a href="https://www.nytimes.com/2014/03/12/opinion/the-future-of-internet-freedom.html">https://www.nytimes.com/2014/03/12/opinion/the-future-of-internet-freedom.html</a>
- [2] Unlisted Author. (13 June 2016). "Shanghai airport rocked by homemade bomb blast." The Strait Times. Retrieved 20 November 2019. <a href="https://www.straitstimes.com/asia/east-asia/homemade-bombs-thrown-at-shanghai-airport">https://www.straitstimes.com/asia/east-asia/homemade-bombs-thrown-at-shanghai-airport</a>
- [3] The Internet Society. (2012). "Global Internet User Survey 2012." Archived 14 March 2013 at the Wayback Machine. Retrieved 11 March 2014. <a href="http://wayback.archiveit.org/9367/20170911022514/https://www.internetsociety.org/internet/global-internet-user-survey-2012">http://wayback.archiveit.org/9367/20170911022514/https://www.internetsociety.org/internet/global-internet-user-survey-2012</a>
- [4] GlobalWebIndex. (2019). "VPN Users Around the World." Retrieved 15 December 2019. https://www.globalwebindex.com/reports/vpn-usage-around-the-world
- [5] Cullison, A., et al. (2012). "Karzai Bans Ingredient of Taliban's Roadside Bombs." <u>The Wall Street Journal</u>.
- [6] GAO. (2012). "Counterterrorism U.S. Agencies Face Challenges Countering the Use of Improvised Explosive Devices in the Afghanistan/Pakistan Region." GAO, Editor.
- [7] GAO. (2012). "Combating Terrorism State Should Enhance Its Performance Measures for Assessing Efforts in Pakistan to Counter Improvised Explosive Devices." GAO, Editor.
- [8] United States Department of Defense. (May 2019). "Dictionary of Military and Associated Terms."

  <u>Joint Publication 1 (JP1).</u>
- [9] McCurry, P. M., (2015). "The Use of Advanced Analytical Techniques to Enable Batch and Source Matching of Homemade Explosives." Doctor of Philosophy Thesis: Flinders University.
- [10] Lehmann, R. O. Y., (2014). "Comparison and discrimination of energetic materials via multiple analytical techniques and chemometrics." Honours Thesis: Flinders University.
- [11] Brust, H., et al. (2015). "Isotopic and elemental profiling of ammonium nitrate in forensic explosives investigations." Forensic Science International **248**: 101-112.

- [12] Tauler, R., (2020). "Chemometrics and Intelligent Laboratory Systems." <u>Chemometrics Society</u>. Retrieved 23 January 2020. <a href="https://www.journals.elsevier.com/chemometrics-and-intelligent-laboratory-systems/">https://www.journals.elsevier.com/chemometrics-and-intelligent-laboratory-systems/</a>
- [13] Trejos, T., et al. (2016). "A Novel Forensic Tool for the Characterization and Comparison of Printing Ink Evidence: Development and Evaluation of a Searchable Database Using Data Fusion of Spectrochemical Methods." <u>Journal of Forensic Sciences</u> **61**(3): 715-724.
- [14] Davies, P. (2014). "Energetic Materials Safety and Awareness Course." Defence Science and Technology Organisation: Adelaide.
- [15] Beveridge, A. (1998). "Forensic Investigation of Explosions." Taylor & Francis Ltd: London.
- [16] Berwick, G. (2007). "The Executive's Guide to Insurance and Risk Management." (2nd ed.). Balmain, Australia: QR Consulting.
- [17] Akhavan, J. (2004). "The Chemistry of Explosives." (2nd ed.). Royal Society of Chemistry: Cambridge.
- [18] Oxley, J. C., et al. (2009). "Decompositions of urea and guanidine nitrates." <u>Journal of Energetic</u>

  <u>Materials</u> **27**(1): 17-39.
- [19] Almog, J., et al. (2005). "A field diagnostic test for the improvised explosive urea nitrate." <u>Journal of Forensic Sciences</u> **50**(3): 582-586.
- [20] Tamiri, T., et al. (2009). "Urea nitrate, an exceptionally easy-to-make improvised explosive: Studies towards trace characterization." <u>Analytical and Bioanalytical Chemistry</u> **395**(2): 421-428.
- [21] Oxley, J. C., et al. (2013). "Synthesis and characterization of urea nitrate and nitrourea." <u>Propellants, Explosives, Pyrotechnics</u> **38**(3): 335-344.
- [22] Aranda, R., et al. (2011). "Forensic utility of isotope ratio analysis of the explosive urea nitrate and its precursors." <u>Forensic Science International</u> **206**(1-3): 143-149.
- [23] Chirico, R., et al. (2014). "Proximal detection of energetic materials on fabrics by UV-Raman spectroscopy". Proceedings of SPIE 9073, Chemical, Biological, Radiological, Nuclear, and Explosives (CBRNE) Sensing XV, 90730F.
- [24] FBI. "Oklahoma City Bombing." Retrieved 15 December 2019. https://www.fbi.gov/history/famous-cases/oklahoma-city-bombing

- [25] NaCTSO, "The Threat", Retrieved 11 March 2014. <a href="http://www.secureyourfertiliser.gov.uk/threat.htm">http://www.secureyourfertiliser.gov.uk/threat.htm</a>
- [26] COAG. (2014) "Meeting Outcomes 25th June 2004." Council of Australian Governments.
- [27] EPA. (1995). "Inorganic Chemical Industry." U.S. Environmental Protection Agency: North Carolina.
- [28] Benson, S. J., et al. (2009). "Forensic analysis of explosives using isotope ratio mass spectrometry (IR-MS) Discrimination of ammonium nitrate sources." Science and Justice **49**(2): 73-80.
- [29] Meyer, R., et al. (2007) "Explosives." Wiley-VCH Verlag GmbH: Weinheim.
- [30] Almeida, M. R., et al. (2015). "Detection of explosives on the surface of banknotes by Raman hyperspectral imaging and independent component analysis." <u>Analytica Chimica Acta **860**(0): 15-22.</u>
- [31] Howa, J. D., et al. (2014). "Isolation and stable nitrogen isotope analysis of ammonium ions in ammonium nitrate prills using sodium tetraphenylborate." Rapid Communications in Mass Spectrometry 28(13): 1530-1534.
- [32] Benson, S. J., et al. (2010). "Forensic analysis of explosives using isotope ratio mass spectrometry (IR-MS) Part 1: Instrument validation of the DELTAplusXP IR-MS for bulk nitrogen isotope ratio measurements." <u>Journal of Forensic Sciences</u> **55**(1): 193-204.
- [33] Benson, S. J., et al. (2010). "Forensic analysis of explosives using isotope ratio mass spectrometry (IR-MS) Part 2: Forensic inter-laboratory trial: Bulk carbon and nitrogen stable isotopes in a range of chemical compounds (Australia and New Zealand)." <u>Journal of Forensic Sciences</u> **55**(1): 205-212.
- [34] Brust, H., et al. (2015). "Isotopic and elemental profiling of ammonium nitrate in forensic explosives investigations." Forensic Science International **248**: 101-112.
- [35] Widory, D., et al. (2009). "Sourcing explosives: A multi-isotope approach." <u>Science and Justice</u> **49**(2): 62-72.
- [36] Bauer, A. J. R., et al. (2014). "Laser-induced breakdown spectroscopy and spectral analysis of improvised explosive materials." <u>Proceedings of SPIE 9101</u>, <u>Next-Generation Spectroscopic</u> Technologies VII, 91010M.

- [37] Singh, A. (2006). "Small, logical steps cracked case: Roy." <u>The Times of India</u>. Retrieved 06 April 2015. <a href="http://timesofindia.indiatimes.com/city/mumbai/Small-logical-steps-cracked-case-Roy/articleshow/2062187.cms?referral=PM">http://timesofindia.indiatimes.com/city/mumbai/Small-logical-steps-cracked-case-Roy/articleshow/2062187.cms?referral=PM</a>
- [38] Anonymous. (2008). "Jaipur blasts: RDX used, HuJI suspected." The Times of India. Retrieved 06

  April 2015. <a href="http://timesofindia.indiatimes.com/india/Jaipur-blasts-RDX-used-HuJI-suspected/articleshow/3038962.cms?referral=PM">http://timesofindia.indiatimes.com/india/Jaipur-blasts-RDX-used-HuJI-suspected/articleshow/3038962.cms?referral=PM</a>
- [39] Wines, M. (1999). "Debate on Cause of Moscow Blast Heats Up." <u>The New York Times</u>. Retrieved 06 April 2015. <a href="http://www.nytimes.com/1999/09/10/world/debate-on-cause-of-moscow-blast-heats-up.html">http://www.nytimes.com/1999/09/10/world/debate-on-cause-of-moscow-blast-heats-up.html</a>
- [40] Myers, S.L. (2004). "Explosive Suggests Terrorists Downed Plane, Russia Says." <u>The New York Times</u>. Retrieved 06 April 2015. <a href="http://www.nytimes.com/2004/08/28/world/explosive-suggests-terrorists-downed-plane-russia-says.html">http://www.nytimes.com/2004/08/28/world/explosive-suggests-terrorists-downed-plane-russia-says.html</a>
- [41] Urbanski, T. (1967). "Chemistry and Technology of Explosives Vol. III." <u>PWN-Polish Scientific</u> Publishers: Warszawa.
- [42] Bachmann, W. E., et al. (1949). "A new method of preparing the high explosive RDX." <u>Journal of the American Chemical Society</u> **71**(5): 1842-1845.
- [43] Spyckerelle, C., et al. (2008). "Reduced Sensitivity RDX Obtained from Bachmann RDX." <u>Propellants, Explosives, Pyrotechnics</u> **33**(1): 14-19.
- [44] Zhang, W., et al. (2014). "Progress on laser-induced decomposition of explosives investigated by spectroscopic methods." <u>Applied Spectroscopy Reviews</u> **49**(7): 550-563.
- [45] Botti, S., et al. (2013). "Trace level detection and identification of nitro-based explosives by surface-enhanced Raman spectroscopy." <u>Journal of Raman Spectroscopy</u> **44**(3): 463-468.
- [46] Lock, C. M., et al. (2008). "Investigation of isotopic linkage between precursor and product in the synthesis of a high explosive." <u>Forensic Science International</u> **179**(2-3): 157-162.
- [47] Gelman, F., et al. (2011). "Precise and accurate compound-specific carbon and nitrogen isotope analysis of RDX by GC-IR-MS." <u>International Journal of Environmental Analytical Chemistry</u> **91**(14): 1392-1400.

- [48] Künzel, M., et al. (2014). "Thermal behavior and decomposition kinetics of ETN and its mixtures with PETN and RDX." <u>Journal of Thermal Analysis and Calorimetry</u> **115**(1): 289-299.
- [49] Miller, G. R., et al. (2001). "A Review of the Crystal Structures of Common Explosives, Part I: RDX, HMX, TNT, PETN, and Tetryl." U. S. N. R., Ed. United States Navy: Washington DC.
- [50] Tyrrell, É., et al. (2011). "Coupled reversed-phase and ion chromatographic system for the simultaneous identification of inorganic and organic explosives." <u>Journal of Chromatography A</u> **1218**(20): 3007-3012.
- [51] Stenhouse, J. (1849). "Nachtrag zu der Abhandlung über die stickstoffhaltigen Bestandtheile der Vegetabilien, als die Quellen von künstlichen Alkaloïden." <u>Justus LiebigsAnnalen der Chemie</u> **72**: 86–88.
- [52] Brady, J. E., Smith, J. L., Hart, C. E. and Oxley, J. (2012), "Estimating Ambient Vapor Pressures of Low Volatility Explosives by Rising-Temperature Thermogravimetry." <u>Propellants, Explosives, Pyrotechnics</u> **37**(2): 215–222.
- [53] Charles, P. S. (1942). "Nitration of alcohols", <u>U.S. Patent 2301231</u>.
- [54] Yan, Q.-L., et al. (2013). "The effect of molecular structure on thermal stability, decomposition kinetics and reaction models of nitric esters." <u>Thermochimica Acta</u> **566**(0): 137-148.
- [55] Johnsson, G., et al. (1965). "Rate of onset of vasodilator effect of glyceryl trinitrate, propatylnitrate and erythrityl tetranitrate in man." <u>Scandinavian Journal of Clinical and Laboratory Investigation</u> **17**(6): 600-606.
- [56] Weitzman, D. (1953). "Penta-erythritol Tetranitrate in Treatment of Angina." <u>British Medical</u> Journal **2**(4851): 1409-1412.
- [57] Oxley, J., et al. (2008). "Characterization and Analysis of Tetranitrate Esters." <u>Propellants, Explosives, Pyrotechnics</u> **37**: 24-39.
- [58] Künzel, M., et al. (2017). "Explosive Properties of Melt Cast Erythritol Tetranitrate (ETN)." <u>Central European Journal of Energetic Materials</u> **14**: 418-429.
- [59] Künzel, M., et al. (2014). "Thermal behavior and decomposition kinetics of ETN and its mixtures with PETN and RDX." Journal of Thermal Analysis and Calorimetry **115**(1): 289-299.

- [60] Yan, Q.-L., et al. (2013). "The Effect of Molecular Structure on Thermal Stability, Decomposition Kinetics and Reaction Models of Nitric Esters." Thermochimica Acta **566**: 137-148.
- [61] Oxley, J.C., et al. (2017). "Thermal Decomposition of Erythritol Tetranitrate: A Joint Experimental and Computational Study." <u>Journal of Physical Chemistry C</u> **121**: 16145-16157.
- [62] Oxley, J.C., et al. (2017). "Eutectics of Erythritol Tetranitrate." <u>Journal of Physical Chemistry C</u> **121**: 16137-16144.
- [63] Selesovsky, J., et al. (2015). "Accelerating Rate Calorimetry Decomposition of Nitroesters." <u>Proceedings of the 18th Seminar on New Trends in Research of Energetic Materials, Pardubice, Czech</u>
  <u>Republic</u> 1: 789-793.
- [64] Manner, V.W., et al. (2015). "Explosive Performance Properties of Erythritol Tetranitrate (ETN)." <u>Propellants, Explosives, Pyrotechnics</u> **40**: 460-462.
- [65] Matyáš, R., et al. (2015). "Characterization of Erythritol Tetranitrate. Physical Properties." <u>Propellants, Explosives, Pyrotechnics</u> **40**: 185-188.
- [66] Song, X.-L., et al. (2014). "Synthesis, Characterization of 1,2,3,4-Erythrityl Tetranitrate." <u>Hanneng</u> <u>Cailiao</u> **22**: 458-461.
- [67] Matyáš, R., et al. (2016). "Analytical Characterization of Erythritol Tetranitrate, an Improvised Explosive." <u>Journal of Forensic Sciences</u> **61**: 759-764.
- [68] Oleske, J.B., et al. (2015). "Identifying Raman and Infrared Vibrational Motions of Erythritol Tetranitrate." <u>Applied Spectroscopy</u> **69**: 1397-1402.
- [69] Carol, J., (1960). "Infrared Analysis of Erythritol Tetranitrate, Pentaerythritol Tetranitrate, and Mannitol Hexanitrate." <u>Journal of the Association of Official Agricultural Chemists</u> **43**: 259-261.
- [70] Urbanski, T. et al, (1963). "Infrared Spectra of Nitric Esters. Part 2. Rotational Isomerism of Some Esters." Transactions of the Faraday Society **59**: 1046-1054.
- [71] Cruse, C.A., et al. (2019). "Generating Highly Specific Spectra and Identifying Thermal Decomposition Products via Gas Chromatography/Vacuum Ultraviolet Spectroscopy (GC/VUV): Application to Nitrate Ester Explosives." <u>Talanta</u> **195**: 580-586.
- [72] Forbes, T.P., et al. (2015). "Trace Detection and Competitive Ionization of Erythritol Tetranitrate in Mixtures Using Direct Analysis in Real Time Mass Spectrometry." <u>Analytical Methods</u> **7**: 3632-3636.

- [73] Hagan, N., et al. (2017). "Ion Mobility Spectrometry High Resolution LTQ-Orbitrap Mass Spectrometry for Analysis of Homemade Explosives." <u>Journal of the American Society for Mass Spectrometry</u> **28**: 1531-1539.
- [74] Ostrinskaya, A., et al. (2017). "Characterization of Nitrated Sugar Alcohols by Atmospheric-Pressure Chemical-Ionization Mass Spectrometry." Rapid Communications in Mass Spectrometry 31: 333-343.
- [75] Dong, X.-F., et al. (2012). "Effect of potassium chlorate on thermal decomposition of cyclotrimethylenetrinitramine (RDX)." <u>Journal of Analytical and Applied Pyrolysis</u> **93**(0): 160-164.
- [76] Australian National Security. "Overseas terrorist attacks." Retrieved 5 July 2015. <a href="http://www.nationalsecurity.gov.au/Securityandyourcommunity/Pages/Overseasterroristattacks.as">http://www.nationalsecurity.gov.au/Securityandyourcommunity/Pages/Overseasterroristattacks.as</a>
- [77] Ropp, R. C. (2013). "Encyclopedia of the Alkaline Earth Compounds." Vol 1, pp. 79-83. Elsevier: Oxford.
- [78] Helmenstiene, A.M. "Potassium Chlorate from Bleach and Salt Substitute." Retrieved 5 July 2015. http://chemistry.about.com/od/makechemicalsyourself/a/Potassium-Chlorate-From-Bleach-And-Salt-Substitute.htm
- [79] Berger, B., et al. (1995). "Quantitative studies on the zirconium potassium perchlorate nitrocellulose pyrotechnic system using differential scanning calorimetry and chemical analysis." Thermochimica Acta **255**(0): 227-239.
- [80] Dong, X.-F., et al. (2012). "Effect of potassium chlorate on thermal decomposition of cyclotrimethylenetrinitramine (RDX)." <u>Journal of Analytical and Applied Pyrolysis</u> **93**(0): 160-164.
- [81] Fathollahi, M., et al. (2004). "The effect of the particle size of potassium chlorate in pyrotechnic compositions." <u>Combustion and Flame</u> **138**(3): 304-306.
- [82] Pourmortazavi, S. M., et al. (2006). "Thermal behavior of aluminium powder and potassium perchlorate mixtures by DTA and TG." <u>Thermochimica Acta 443(1)</u>: 129-131.
- [86] Anan'ev, V., et al. (2014). "Reactions of atomic oxygen with the chlorate ion and the perchlorate ion." <u>Chemical Physics Letters</u> **607**(0): 39-42.

- [83] Shimada, S. (1995). "Thermosonimetry and microscopic observation of the thermal decomposition of potassium chlorate." <u>Thermochimica Acta</u> **255**(0): 341-345.
- [84] Berger, B., et al. (1995). "Thermal analysis studies on the zirconium/nickel alloy-potassium perchlorate-nitrocellulose pyrotechnic system." Thermochimica Acta 269–270(0): 687-696.
- [85] Berger, B., et al. (1995). "Thermomicroscopy studies on the zirconium-potassium perchlorate-nitrocellulose pyrotechnic system." <u>Thermochimica Acta</u> **269–270**(0): 639-648.
- [87] Johns, C., et al. (2008). "Identification of homemade inorganic explosives by ion chromatographic analysis of post-blast residues." Journal of Chromatography A **1182**(2): 205-214.
- [88] Benson, S., et al. (2006). "Forensic Applications of Isotope Ratio Mass Spectrometry—A Review." <u>Forensic Science International</u> **157**(1): 1-22.
- [89] Pierrini, G., et al. (2007). "Evaluation of preliminary isotopic analysis (13C and 15N) of explosives.

  A likelihood ratio approach to assess the links between Semtex samples." Forensic Science International 167: 43-48.
- [90] Coleman, D.C., et al. (1991). "Carbon Isotope Techniques." Academic Press: San Diego.
- [91] Meier-Augenstein, W. (2010). "Stable Isotope Forensics: An Introduction to the Forensic Application of Stable Isotope Analysis." (1st ed.). John Wiley and Sons: Hoboken, NJ.
- [92] Forensic Isotope Ratio Mass Spectrometry- The IR-MS Technique. Retrieved 2 October 2014 <a href="http://forensic-isotopes.org/irms2.html">http://forensic-isotopes.org/irms2.html</a>
- [93] West, J.B., et al. (2009). "Isoscapes: Understanding Movement, Pattern, and Process on Earth Through Isotope Mapping." (1st Ed.). Springer Science+Business Media B.V: Dordrecht.
- [94] Beauchemin, D. (2008). "Inductively Coupled Plasma Mass Spectrometry." <u>Analytical Chemistry</u> **80**: 4455-4486.
- [95] Forsgard, N. (2007). "Inductively Coupled Plasma Spectrometry for Speciation Analysis: Development and Applications." Doctor of Philosophy Dissertation, Uppsala University. Retrieved 2 October 2014. http://www.diva-portal.org/smash/get/diva2:170564/FULLTEXT01.pdf.
- [96] IUPAC. (1991). "Isotopic composition of the elements." Pure Applied Chemistry 63(7): 991-1002.
- [97] Thomas, R. (2002). "A beginner's guide to ICP-MS: Part XII-A review of Interferences." Spectroscopy **17**(10): 24-31.

- [98] McCurdy, E., et al. (2006). "Unmatched removal of spectral interferences in ICP-MS using Agilent octopole reaction system with helium collision mode: Application-metal analysis." <u>Agilent Technologies:</u> 1-8.
- [99] Suzuki, E.M. (1999). "Infrared spectra of U.S. automobile original topcoats (1974-1989): VI. Identification and analysis of yellow organic automotive paint pigments—isoindolinone yellow 3R, isoindoline yellow, anthrapyrimidine yellow, and miscellaneous yellows." <u>Journal of Forensic Science</u> **44**(6): 1151-1175.
- [100] Chappell, J.S., et al. (2004). "The extraction and infrared identification of gamma-hydroxybutyric acid (GHB) from aqueous solutions." <u>Journal of Forensic Science</u> **49**(1): 52-59.
- [101] Ryland, S., et al. (2001). "Discrimination of 1990s original automotive paint systems: a collaborative study of black non-metallic base coat/clear finishes using infrared spectroscopy." Journal of Forensic Science **46**(1): 31-45.
- [102] Lopez-Artiguez, M., et al. (1995). "Unequivocal Identification of Several Common Adulterants and Diluents in Street Samples of Cocaine by Infrared Spectroscopy." <u>Journal of Forensic Science</u> **40**(4): 602-610.
- [103] Oxley, J., et al. (2008). "Raman and Infrared Fingerprint Spectroscopy of Peroxide-Based Explosives." Society for Applied Spectroscopy **62**(8): 906-915.
- [104] Pristera, F., et al. (1960). "Analysis of Explosives Using Infrared Spectroscopy." <u>Analytical</u> <u>Chemistry</u> **32**(4): 495-508.
- [105] Department of CC Technology. (2003). "Discover the Raman Advantage." DeltaNu: Wyoming. Retrieved February 2004. <a href="http://www.deltanu.com">http://www.deltanu.com</a>
- [106] Thermo Fisher Scientific Inc. (2014). FirstDefender RM. Retrieved November 2014. http://www.ahurascientific.com/chemical-explosives-id/products/firstdefenderrm/index.php
- [107] Eckenrode, B.A., et al. (2001). "Portable Raman spectroscopy systems for field analysis.(Research and Technology)" <u>Forensic Science Communications</u> **3(**4): 1-10.
- [108] Tracy, N.S.H., et al. (2003). "Forensic Applications of Raman Spectroscopy in the Identification of Car Paints." Retrieved August 2014. <a href="http://staff.science.nus.edu.sg/~scilooe/srp">http://staff.science.nus.edu.sg/~scilooe/srp</a> 2003/sci paper/phy/research paper/ng see hwai tracy.pdf

- [109] Sands, H.S., et al. (1998). "UV-excited resonance Raman spectroscopy of narcotics and explosives." <u>Journal of Forensic Science</u> **43**(3): 509-513.
- [110] Ryder, A.G. (2002). "Classification of Narcotics in Solid Mixtures Using Principal Component Analysis and Raman Spectroscopy." <u>Journal of Forensic Science</u> **47**(2): 275-284.
- [111] Ryder, A.G., et al. (1999). "Identifications and Quantitative Measurements of Narcotics in Solid Mixtures Using Near-IR Raman Spectroscopy and Multivariate Analysis." <u>Journal of Forensic Science</u> **44**(5): 1013-1019.
- [112] Suzuki, E.M., et al. (2001). "In Situ Identification and Analysis of Automotive Paint Pigments Using Line Segment Excitation Raman Spectroscopy: Inorganic Topcoat Pigments." <u>Journal of Forensic Science</u> **46**(5): 1053-1069.
- [113] Tukhvatullin, F.H., et al. (1998). "The Shape and Width of the 818 cm<sup>-1</sup> Raman Band of Propan-2-ol in Solutions." Journal of Raman Spectroscopy **29**: 1027-1029.
- [114] Tonouchi, M. (2007). "Cutting-edge terahertz technology." Nature Photonics 1(2): 97-105.
- [115] Bergé, L., et al. (2019). "Terahertz spectroscopy from air plasmas created by two-color femtosecond laser pulses: The ALTESSE project." <u>EPL Europhysics Letters</u> **126**(24001).
- [116] Chen, J., et al. (2007). "Absorption coefficients of selected explosives and related compounds in the range of 0.1-2.8 THz." Optics Express 15(19): 12060-12067.
- [117] Leahy-Hoppa, M.R., et al. (2007). "Wideband terahertz spectroscopy of explosives." <u>Chemical Physics Letters</u> **434**(4): 227-230.
- [118] Federici, J., et al. (2005). "THz imaging and sensing for security applications explosives, weapons and drugs." <u>Semiconductor Science and Technology</u> **20**(7): S266-S280.
- [119] Kemp, M.C., et al. (2003). "Security applications of terahertz technology." <u>Proc. SPIE 5070,</u> Terahertz for Military and Security Applications.
- [120] Shen, Y., et al. (2005). "Detection and identification of explosives using terahertz pulsed spectroscopic imaging." Applied Physics Letters 86(24): 1-3.
- [121] Pereira, M., et al. (2017). "THz for CBRN and Explosives Detection and Diagnosis." <u>NATO Science</u> for Peace and Security Series B: Physics and Biophysics.

- [122] Liu, J., et al. (2016). "Identification of high explosive RDX using terahertz imaging and spectral fingerprints." <u>Journal of Physics: Conference Series</u> **680**(1).
- [123] IonVantage for Isoprime V1.6.1.0 [Software Package]. (2014). Elementar Analysensysteme GmbH: Hanau.
- [124] varioISOTOPE cube V3.0.4 [Software Package]. (2014). Elementar Analysensysteme GmbH: Hanau.
- [125] Syngistix<sup>™</sup> V1.1 [Software Package]. (2015). PerkinElmer Inc.: Waltham.
- [126] Perkin-Elmer Inc. (2019). NexION 350D ICP-MS Product Brochure. Available at https://www.perkinelmer.com/pdfs/downloads/bro\_nexion350icpmsbrochure.pdf
- [127] Ródenas de La Rocha, S., et al. (2009). "Trace elements determination in edible seaweeds by an optimized and validated ICP-MS method." <u>Journal of Food Composition and Analysis</u> **22**(4): 330-336.
- [128] Winderbaum, L., et al. (2012). "Multivariate Analysis of an LA-ICP-MS Trace Element Dataset for Pyrite." Mathematical Geosciences **44**(7): 823-842.
- [129] Wold, S., et al. (1987). "Principal component analysis." <u>Chemometrics and Intelligent Laboratory Systems</u> **2**(1): 37-52.
- [130] Biswal, P. C. (2007). "Probability and Statistics." (1st ed.) Phi Learning: Delhi.
- [131] Spectrum V10.4.00.0190 [Software Package]. (2013). PerkinElmer Inc.: Waltham.
- [132] Rinnan, A., et al. (2009). "Review of the most common pre-processing techniques for near-infrared spectra." Trends in Analytical Chemistry **28**(10): 1201-1222.
- [133] NuSpec<sup>™</sup> [Software Package]. (2009). DeltaNu: Laramie.
- [134] OPUS V7.2 [Computer software]. (2012). Bruker Optik GmbH: Ettlingen.
- [135] Yang, C., et al. (2014). "Spectral Characterisation of RDX, ETN, PETN, TATP, HMTD, HMX, and C-4 in the Mid-Infrared Region." Technical Report. Battelle Eastern Science and Technology Center: Aberdeen.
- [136] Mildren, R. (2013). "Intrinsic Optical Properties of Diamond" in "Optical Engineering of Diamond." pp. 1-34. Wiley-VCH Verlag GmbH: Weinheim.

[137] Oleske, J., et al. (2015). "Identifying Raman and Infrared Vibrational Motions of Erythritol Tetranitrate." Applied Spectroscopy, **69**(12): 1397-1402.

[138] Manner, V., et al. (2014). "Crystal Structure, Packing Analysis, and Structural-Sensitivity Correlations of Erythritol Tetranitrate." <u>Crystal Growth & Design</u>, **14**(11): 6154-6160.

[139] Novikov, S., et al. (1965). "New possibilities in nitration with a mixture of nitric acid and acetic anhydride." <u>Bulletin of the Academy of Sciences of the USSR, Division of Chemical Science</u>, **14**(1): 90-95.